

General Disclaimer

One or more of the Following Statements may affect this Document

- This document has been reproduced from the best copy furnished by the organizational source. It is being released in the interest of making available as much information as possible.
- This document may contain data, which exceeds the sheet parameters. It was furnished in this condition by the organizational source and is the best copy available.
- This document may contain tone-on-tone or color graphs, charts and/or pictures, which have been reproduced in black and white.
- This document is paginated as submitted by the original source.
- Portions of this document are not fully legible due to the historical nature of some of the material. However, it is the best reproduction available from the original submission.

SECOND ANNUAL REPORT ON
THERMAL SCALE MODELING OF A SPACECRAFT RADIATOR
WITH COUPLED
FORCED CONVECTION-CONDUCTION-RADIATION HEAT TRANSFER

National Aeronautics and Space Administration
Marshall Space Flight Center

Multidisciplinary Research Grant

NGR-19-001-068

David P. Colvin

Dupree Maples

Department of Mechanical, Aerospace, & Industrial Engineering
College of Engineering
Louisiana State University
Baton Rouge, Louisiana 70803

ACKNOWLEDGMENT

The author would like to express his sincere appreciation and extend his gratitude to the following individuals who provided help during his graduate program.

Dr. Dupree Maples, who served as major advisor and committee chairman. His interest, encouragement, and guidance were invaluable during my graduate study at Louisiana State University.

My graduate committee, composed of Dr. David Thompson, Prof. E. S. Adler, Jr., Dr. Gerald Whitehouse, and Dr. Roy Goodrich.

Mr. Bill George, Mr. Jack Hughes, Mr. Dennis Gilbert, Mr. John Schweinberg, and Mr. Berdell Pearson of the Component Test Facility of the General Electric Company at the National Aeronautics and Space Administration's Mississippi Test Facility for their assistance during the experimental investigation.

Mrs. Sandra Vanselous for assistance and typing, and Mrs. Genelle Montgomery for advice in preparation of the manuscript.

My Mother and Father, whose influence and encouragement have guided me from the beginning of my education.

My wife, Virginia, for her many years of encouragement and sacrifice during my graduate study. Also my daughter, Polly Bee, and son, Mark David, for their patience and periods of relaxation.

In addition, I would like to thank the National Aeronautics and Space Administration for their financial and facility support during this investigation.

TABLE OF CONTENTS

<u>Chapter</u>	<u>Page</u>
I. INTRODUCTION	1
II. LITERATURE SURVEY	4
III. MODELING CRITERIA	17
IV. THERMAL ANALYSIS	28
V. TEST SPECIMENS	47
VI. EXPERIMENTAL APPARATUS	61
VII. EXPERIMENTAL PROCEDURE	84
VIII. RESULTS AND DISCUSSION	100
IX. CONCLUSIONS AND RECOMMENDATIONS	148
BIBLIOGRAPHY	151
APPENDIX A - LIST OF EXPERIMENTAL EQUIPMENT	154
APPENDIX B - VACUUM SYSTEM DESCRIPTION AND OPERATION	160
APPENDIX C - FLOW RATES VERSUS REYNOLDS NUMBERS	170
APPENDIX D - LEAK DETECTOR DESCRIPTION	180
APPENDIX E - CALIBRATION OF FLOW METER AND BALANCE	187
APPENDIX F - THERMOCOUPLE LEAD WIRE TEST	192
APPENDIX G - STRIP-CHART RECORDER CALIBRATION	194
APPENDIX H - CONDUCTION ERROR TEST	199
APPENDIX I - ERROR ANALYSIS	203
APPENDIX J - LINER TEMPERATURE DISTRIBUTION	206

LIST OF TABLES

<u>Table</u>	<u>Page</u>
1. Stainless Steel Specimen Tube Dimensions	50
2. Aluminum Specimen Tube Dimensions	51
3. Modeling Error	101
4. Calculation of Re^* and D^*	103
5. Experiment Sheet for 1" Stainless Steel Tube - January 8, 1971	105
6. Measured Temperatures at Designated Locations for 1" Stainless Steel Tube - January 8, 1971	106
7. Experiment Sheet for 1" Stainless Steel Tube - January 11, 1971	108
8. Measured Temperatures at Designated Locations for 1" Stainless Steel Tube - January 11, 1971	109
9. Experiment Sheet for 3/4" Stainless Steel Tube - February 8, 1971	111
10. Measured Temperatures at Designated Locations for 3/4" Stainless Steel Tube - February 8, 1971	112
11. Experiment Sheet for 1/2" Stainless Steel Tube - December 15, 1970	114
12. Measured Temperatures at Designated Locations for 1/2" Stainless Steel Tube - December 15, 1970	115
13. Experiment Sheet for 1/4" Stainless Steel Tube - January 14, 1971	117
14. Measured Temperatures at Designated Locations for 1/4" Stainless Steel Tube - January 14, 1971	118
15. Experiment Sheet for 1" Aluminum Tube - February 26, 1971 ...	121
16. Measured Temperatures at Designated Locations for 1" Aluminum Tube - February 26, 1971	122
17. Experiment Sheet for 3/4" Aluminum Tube - February 12, 1971	124

Table

Page

18.	Measured Temperatures at Designated Locations for 3/4" Aluminum Tube - February 12, 1971	125
19.	Experiment Sheet for 1/2" Aluminum Tube - February 2, 1971 ..	127
20.	Measured Temperatures at Designated Locations for 1/2" Aluminum Tube - February 2, 1971	128
21.	Experiment Sheet for 1/4" Aluminum Tube - January 27, 1971 ..	130
22.	Measured Temperatures at Designated Locations for 1/4" Aluminum Tube - January 27, 1971	131
H-1.	Experiment Sheet for Conduction Error Tests on 3/4" and 1" Aluminum Tubes	200
H-2.	Measured Temperatures at Designated Locations for Conduction Error Tests on 3/4" and 1" Aluminum Tubes	201

LIST OF FIGURES

<u>Figure</u>	<u>Page</u>
1. Specimen Tube End	49
2. Thermocouple Locations on Specimen Tube	54
3. Welding Station with Specimen Tube	55
4. Thermocouple Attachment to Stainless Steel Specimen Tube	56
5. Thermocouple Attachment to Aluminum Specimen Tube	57
6. Unpainted Stainless Steel Specimen Tubes	58
7. Stainless Steel Test Specimen Tubes and Plug Gages	59
8. Aluminum Test Specimen Tubes and Plug Gages	60
9. Experimental Systems Block Diagram	62
10. Pressurization and Flow Systems Schematic Diagram	63
11. Vacuum Chamber	64
12. Cryogenic Liner	65
13. Specimen Tube Suspended within Vacuum Chamber	68
14. Thermocouple Vacuum Feedthroughs	70
15. Multipoint Strip-chart Data Recorder	71
16. Strip-chart Data Recorders	73
17. Inlet Fluid Temperature Control System	74
18. Temperature Control System Components	75
19. Pressurization Control System	77
20. Flow Evacuation System	78
21. Flow Control System	81
22. Flow Collection System	83
23. Entrance Tube to Specimen Tube Connection	86

<u>Figure</u>	<u>Page</u>
24. Assembled Tubular System and Transition Junction Heat Sink ..	87
25. Tubular System in Vacuum Chamber	88
26. Tubular System Viewed Through Cryogenic Liner Cover	89
27. Suspended Entrance Tube with Door Flange	91
28. Attachment of Flange to Chamber Door	92
29. Experimental Test Setup (Right Side View)	93
30. Experimental Test Setup (Left Side View)	94
31. Water Collection for Flow Rate Determination	96
32. Weighing of Water for Flow Rate Determination	97
33. Flow Control Adjustment by Author During Experiment	98
34. Graphical Relationship Between Re^* and D^*	104
35. Temperature Versus Length for Various Re on 1" Stainless Steel Tube - January 8, 1971	107
36. Temperature Versus Length for Various Re on 1" Stainless Steel Tube - January 11, 1971	110
37. Temperature Versus Length for Various Re on 3/4" Stainless Steel Tube - February 8, 1971	113
38. Temperature Versus Length for Various Re on 1/2" Stainless Steel Tube - December 15, 1970	116
39. Temperature Versus Length for Various Re on 1/4" Stainless Steel Tube - January 14, 1971	119
40. Temperature Versus Length for Various Re on 1/4" Stainless Steel Tube - January 15, 1971	120
41. Temperature Versus Length for Various Re on 1" Aluminum Tube - February 26, 1971	123
42. Temperature Versus Length for Various Re on 3/4" Aluminum Tube - February 12, 1971	126
43. Temperature Versus Length for Various Re on 1/2" Aluminum Tube - February 2, 1971	129
44. Temperature Versus Length for Various Re on 1/4" Aluminum Tube - January 27, 1971	132

<u>Figure</u>	<u>Page</u>
45. Temperature Versus Length for Various Stainless Steel Tubes at Re = 45	133
46. Temperature Versus Length for Various Stainless Steel Tubes at Re = 40	134
47. Temperature Versus Length for Various Stainless Steel Tubes at Re = 35	135
48. Temperature Versus Length for Various Stainless Steel Tubes at Re = 30	136
49. Temperature Versus Length for Various Stainless Steel Tubes at Re = 25	137
50. Temperature Versus Length for Various Stainless Steel Tubes at Re = 20	138
51. Temperature Versus Length for Various Aluminum Tubes at Re = 45	139
52. Temperature Versus Length for Various Aluminum Tubes at Re = 40	140
53. Temperature Versus Length for Various Aluminum Tubes at Re = 35	141
54. Temperature Versus Length for Various Aluminum Tubes at Re = 30	142
55. Temperature Versus Length for Various Aluminum Tubes at Re = 25	143
56. Temperature Versus Length for Various Aluminum Tubes at Re = 20	144
57. Temperature Versus Length for Various Stainless Steel Tubes	145
58. Temperature Versus Length for Various Aluminum Tubes	146
59. Temperature Versus Length for Various Aluminum and Stainless Steel Tubes	147
A-1. Schematic Diagram for Equipment Listing	155
B-1. Overall View of Vacuum System	161
B-2. Vacuum System Control Console	162
B-3. Vacuum Pumping System	163

<u>Figure</u>	<u>Page</u>
B-4. Multiple-jet Metal-diffusion Pump With Ejector Stage	165
D-1. CEC Vacuum Leak Detector	181
D-2. Leak Detector Block Diagram	182
D-3. Diatron Ionization Chamber	183
D-4. Ion Paths from Exit Slit	184
D-5. Diatron Ion Path	185
E-1. Calibration Curve for Flowmeter, Shunt Valve = 0	188
E-2. Calibration Curve for Flowmeter, Shunt Valve ≠ 0	189
G-1. Calibration Curve for Strip-chart Recorder, Thermocouples 1 - 11, 14	195
G-2. Calibration Curve for Strip-chart Recorder, Thermocouples 12, 13, 16	196
G-3. Calibration Curve for Strip-chart Recorder, Thermocouple 15	197
G-4. Calibration Curve for Strip-chart Recorder, Thermocouple 17	198
H-1. Temperature Versus Length for Conduction Error Tests	202
J-1. Liner Section Key	207
J-2. Liner Temperature Distribution Layout	208

NOMENCLATURE

A	Area for heat transfer
A_c	Cross-sectional area
A_n	Normal area
A_s	Surface area
A_1	Area of surface 1
A_2	Area of surface 2
C	Contact conductance
C_j	Total heat capacity
C_{kj}	Conduction exchange coefficient between regions k and j
C_p	Specific heat at constant pressure
D	Diameter
D_h	Hydraulic diameter
D_i	Inside diameter
D_o	Outside diameter
E	Energy emitted
F	Shape factor
F_e	Configuration factor for emitted earth energy
F_{kj}	Configuration factor = the fraction of energy directly incident on the surface k , from surface j , which is emitting diffusely
F_r	Configuration factor for albedo absorption
F_s	Configuration factor for absorbed solar energy
Gr	Grashof number
h	Convective film coefficient

I	Intensity of radiation
J_0	Bessel function of the first kind of zeroth order
L	Length
l	Length of tube
n	Arbitrary constant
Nu	Nusselt number
Nu_z	Local Nusselt number
P	Pressure
Δp	Pressure drop
Pr	Prandtl number
Q	Total heat input
q	Heat transfer rate
q''	Heat transfer rate per unit area
q'''	Heat transfer rate per unit volume
q_j	Internal power dissipation in the j^{th} region
R	Radius
R'	Albedo energy
R_{kj}	Overall radiant coefficient for non radiative transfer from region k to j
Re	Reynolds number
r	Radial direction in cylindrical coordinates
\bar{r}	Dimensionless radius
r_i	Inside radius
r_o	Outside radius
S	Solar Intensity
T	Temperature
T_f	Fluid temperature

T_m	Mean fluid temperature
T_o	Characteristic temperature
T_r	Reference temperature
T_s	Surface temperature
\bar{T}	Dimensionless temperature
\bar{T}_o	Dimensionless characteristic temperature
\bar{T}_r	Dimensionless reference temperature
\bar{T}_s	Dimensionless surface temperature
ΔT	Temperature difference
t	Thickness
u	Fluid velocity in z direction
u_m	Mean fluid velocity in z direction
V	Volume
v	Fluid velocity in radial direction
x, y, z	Orthogonal coordinates
$\bar{x}, \bar{y}, \bar{z}$	Dimensionless orthogonal coordinates
Y_o	Bessel function of the second kind of zeroth order
z	Characteristic length in axial direction

GREEK

α	Thermal diffusivity
α	Absorptance, the fraction of energy absorbed from the total energy incoming to a surface element
α_{kj}	Absorptance for radiation interchange between the k and j surfaces
β	Volumetric coefficient of expansion
γ_m	Arbitrary constant
ϵ	Emittance

κ	Thermal conductivity
θ	Time
λ	Mean free path
μ	Dynamic viscosity
ν	Kinematic viscosity
ρ	Density
σ	Stefan-Boltzmann Constant
ϕ	Angular variation in cylindrical coordinates
$\phi_{\kappa j}$	$\epsilon_j A_j F_{j\kappa} \sigma T_j^4 / A_\kappa$ in which $F_{j\kappa}$ is the configuration factor and the A's are surface area for energy leaving surface κ and arriving at surface j .
ω	Fluid flow rate

SUBSCRIPTS

c	Cross-sectional
f	Fluid
i, j, k	Regions of uniform temperature
m	Model
n	Normal
o	Characteristic
p	Prototype
s	Surface
1	Surface 1
2	Surface 2

SUPERSCRIPTS

*	Ratio of model property to prototype property
n	Arbitrary constant
s	Constant for solar absorptance

ABSTRACT

A thermal model of a spacecraft radiator has been designed and tested at the National Aeronautics and Space Administration's Mississippi Test Facility. The unique feature of this model is that all three modes of heat transfer--forced convection, conduction, and radiation--are utilized simultaneously under steady-state conditions. A fluid is forced under pressure using similar flow conditions through both prototype and model which are suspended within a cryogenic vacuum chamber. Heat is transferred from the fluid to the tube's inside wall, which then conducts the energy to its outer surface where it is radiated to the surrounding shell that is maintained at a cryogenic temperature with liquid nitrogen. A high vacuum chamber at the facility is used to house the experiment. Both prototypes and models take the form of long tubes with thermocouples welded to the exterior surface to determine the effectiveness of the modeling criteria. Special precautions have been taken to isolate thermally the specimen and to establish a hydrodynamic boundary layer before specimen entry. The wall thickness of the models has been sized to permit both temperature and material preservation. The effects of physical size and fluid flow parameters on the modeling criteria for both low and high thermal conductivity materials are presented.

CHAPTER I.

INTRODUCTION

Measurement of temperature plays an important role in design and development of objects or systems which are exposed to hostile environments. An environment such as outer space with its high vacuum and low temperature may be simulated, for test purposes, with a cryogenic vacuum chamber. These space chambers are limited in size and may require extensive supporting facilities. For these and other reasons, use of scale models for test purposes has become expedient and sometimes necessary.

A thermal model may be defined as a model, different and usually smaller in size than its prototype, that will accurately predict the thermal behavior of its prototype under suitable conditions.

A radiator will be used to control the environment within the spacecraft during such extended missions as that proposed for Skylab. These radiators will transfer heat energy from a fluid which has been circulated through the living quarters and electronic equipment. This energy will then be radiated in a controlled manner to deep space so that a suitable environment can be maintained within the spacecraft. Space radiators will be used on Skylab's Apollo Telescope Mount and the 14-foot-diameter Space Station Module. Future radiators such as those for a Space Shuttle Vehicle may be extensive in size and could require elaborate test facilities.

In order to model thermally a given object or system accurately, the scale factors or ratios of model-to-prototype parameters must be

determined. Thus, one may observe the behavior of the parameter of interest--for example, temperature--on the model; and by application of the scale factor, he may determine what the parameter would be in a corresponding location on the prototype or full-scale specimen.

The period of time during which the parameter of interest is observed is important for analysis purposes. Equilibrium conditions which may occur during long periods of space travel may be successfully modeled as steady-state conditions. Time periods during which parameters may vary, such as launch, mid-course correction, and reentry, involve transient conditions.

Thermal energy or heat is transferred due to a difference in temperature and depends upon the nature of the surrounding medium. Heat may be transferred by conduction through solids or fluids due to direct contact of mass. Convective heat transfer occurs between a fluid and a surface and depends upon the motion; e.g., velocity of the fluid relative to the surface. Free or natural convection involves fluid flow due to a density gradient whereas forced convection occurs when the fluid is forced to flow because of a difference in pressure. Radiation heat transfer or infrared electromagnetic radiation does not require an intermediary medium and becomes increasingly important with large temperature differences.

Previous work in thermal modeling has involved mainly steady-state conduction and conduction-radiation coupled systems such as may be found in the walls of an unmanned spacecraft during a long interplanetary voyage. Some investigations into transient modeling of these systems have also been accomplished. Convection-conduction-radiation coupled systems as encountered in fluid systems and manned spacecraft

have only recently and partly been investigated. Steady state and transient analyses on a system of concentric cylinders with free convection within an annulus was completed in 1969; but, to date, no work has been published on convection-conduction-radiation coupled systems involving forced convection.

The purpose of this research was to investigate the applicability of thermal modeling under steady-state conditions for a single material system involving forced convection from a flowing fluid in a tube, conduction through and down the tube, and radiation to a cryogenic vacuum environment.

CHAPTER II.

LITERATURE SURVEY

Investigations into thermal modeling of spacecraft and their components began less than 10 years ago. Some of the studies included experimental programs, while others were theoretical. Numerical analysis has been frequently used to verify proposed modeling criteria. Most of the studies involved coupled conduction and radiation systems under steady-state and transient conditions.

Dimensional analyses have been discussed by Langhaar [1] and used successfully in wind tunnel testing for years. The Buckingham π -theorem has been used to determine the number of independent dimensionless groups required to express the relation describing a phenomenon. Determination of these groups involved manipulation of a product of the variables, each raised to an unknown power, and equating the sum of the exponents of each primary dimension making up the variable to zero. Some exponent values are then chosen to permit simultaneous solution of the resulting algebraic equations which results in the determination of the dimensionless groups.

Dimensional analysis was used by Gabron and Fowle [2] and derived dimensionless groups of thermal modeling parameters for testing reduced-scale thermal models. Conduction by solids and joints, internal heat generation, and radiation were used in the study. It was concluded that precise thermal modeling was inherently limited by the size of the smallest scaled model (as measured by the input power per unit volume).

Clark and Laband [3] investigated the temperature history of a manned spacecraft in earth orbit. By dimensional analysis they used the modeling criteria

$$\frac{\sigma T^4}{q''} \quad \frac{\kappa T}{Lq''} \quad \frac{\kappa \theta}{CpL^2}$$

to fabricate and test a cylindrical model. Although test results were not presented, a theoretical analysis indicated that a 43 F change in exterior wall temperature would result in a 6 F variation at the inner wall. Calculations for thermal stress indicated that they were smaller than load stresses during launch. It was also found that 84 percent of the heat generated internally by six men and three kw of internal power was rejected from the spacecraft's exterior skin, while 16 percent was emitted through spacecraft radiators.

Katz [4] briefly discussed thermal criteria and its associated problems with choice of materials. The modeling ratios presented were:

$$\frac{\kappa T}{q''L^2}, \quad \frac{\sigma LT^3}{\kappa}, \quad \frac{\kappa \theta}{CpL^2}$$

Katzoff [5] discussed the scaling criteria for the design and testing of thermal models of spacecraft. Four dimensionless similitude parameters given below were derived using dimensional analysis concerning radiation, internal heat generation, thermal conductivities of materials, and heat capacities of materials

$$\frac{\sigma T^4}{q''} \quad \frac{q'''L}{q''} \quad \frac{q''L}{\kappa T} \quad \frac{CpLT}{q''\theta}$$

Test facility criteria were discussed, and the difficulties of the accurate scaling of thermal conductivity and heat capacity were pointed

out. Similarity criteria for convective heat transfer with gases in spacecraft was also discussed. In the absence of a gravitational field, the Nusselt number is a function of the Reynolds and Prandtl numbers; but gravitational free convection requires that the Grashof number also be considered. Relationships involving these quantities and experimental evidence was not presented.

Wainwright, Kelley, and Keese [6] presented the modeling criteria and scaling techniques as applied to the thermal modeling of spacecraft. Discussion included the Buckingham π -theorem, thermal energy balance on a thin plate, and environmental simulation facilities. The similitude approach was used to reduce the energy differential equation to obtain the following modeling criteria for mutually reflecting elements of a thin model.

$$\frac{\alpha E}{T_0^4}, \quad \frac{\sigma \epsilon T_0^3 L^2}{\kappa_0 t}, \quad \frac{\rho C_p L^2}{\kappa_0 \theta_0}$$

Dimensionless groups for thermal scale modeling of coupled radiation and conduction systems were presented by Vickers [7] and are given below.

$$\frac{\rho C_p L^2}{\kappa \theta}, \quad \frac{\epsilon \sigma T^3 L}{\kappa}, \quad \frac{C_p L}{\kappa}, \quad \frac{\alpha_k j \phi_k j L}{\kappa T}, \quad \frac{\alpha_s S L}{\kappa T}, \quad \frac{q}{L \kappa T}, \quad \frac{q''}{\kappa T}, \quad \frac{q''' L}{\kappa T}$$

He then concluded that temperature preservation offered many advantages for steady-state conditions, but material preservation techniques appeared to be more useful for slow transient conditions.

Jones [8] used the similitude method to reduce a set of simultaneous, first-order differential equations which described the thermal behavior of spacecraft to a group of 28 ratios that were required to

remain constant. These ratios were not all independent but contained six independent sets:

$$\frac{T_j^*}{T^*}, \frac{E_{kj}^* F_{kj}^* A_k^*}{\epsilon_j^* A_j^*}, \frac{\alpha_j^* \delta A_j^* S^* \theta^*}{C_j^* T_j^*}$$

$$\frac{\epsilon_j^* \sigma A_j^* T_j^{*3} \theta^*}{C_j^*}, \frac{C_{kj}^* \theta^*}{C_j^*}, \frac{q_j^* \theta^*}{C_j^* T_j^*}$$

where j and k refers to the j th and k th regions, respectively. These similarity parameters were compared to those of other investigators to show that the results are the same.

Chao and Wedekind [9] used the similitude approach to analyze mathematically the criteria for temperature preservation and material preservation. Analysis was for two- and three-dimensional walls and included property variations of thermal conductivities and heat capacities. Distorted thickness was discussed as a compromise to facilitate modeling.

Vickers [10] authored a comprehensive review of the literature which discussed the general problems of thermal modeling, the reasons for improving the state-of-the-art, and the resulting advantages. He stated that temperature and materials preservation were mutually exclusive using an assumption of perfect geometric similarity and that the laws controlling thermal scale modeling of spacecraft for steady-state conditions were well understood.

An investigation of coupled radiation and conduction thermal modeling was made by Matheny [11] using similarity ratios described by Watkins. The tests involved two discs connected by a solid member within a cryogenic vacuum environment and provided close agreement between prototype and model.

Folkman, Baldwin, and Wainwright [12] applied the modeling criteria

$$\frac{\kappa_0 \theta_0^*}{\rho_0^* C_p^* L^{*2}}, \quad \frac{\sigma^* \epsilon^* L^{*2} T_0^{*3}}{\kappa_0^* \tau^*}, \quad \frac{q''^*}{\sigma^* \epsilon^* T_0^{*4}}, \quad \frac{\alpha^* I^*}{\sigma^* \epsilon^* T_0^{*4}}$$

to a conceptual cylindrical space station. A 8:1 scale model was fabricated for coupled radiation and conduction testing in a space simulation chamber. Results showed agreement within a 25 F for steady-state conditions on the meteoroid shield, and 5 F on the cabin wall.

Rolling [13] used the similitude approach to develop the modeling criteria for space vehicles. The general differential equation for an energy balance on an elemental volume was given by

$$\rho V C_p \frac{dT}{d\theta} = A_s S F_s + A_r R F_r + A_e E F_e + q''' + \sum_{n=1}^n \kappa_n A_n \frac{dT}{dL} + \sum_{j=1}^J \sigma A_j F_j (T_j^4 - T^4)$$

where $\rho V C_p (dT/d\theta)$ was the rate of change in sensible heat of the element, $A_s S F_s$ was the total absorbed solar energy, $A_r R F_r$ was the energy transfer due to albedo absorption, $A_e E F_e$ was the emission due to earth emission absorption, and q''' was the internal heat generation. $\sum_{n=1}^n \kappa_n A_n (dT/dL)$ was the heat conducted between the element and its surroundings, and $\sum_{j=1}^J \sigma A_j F_j (T_j^4 - T^4)$ represents all energy transfer along radiative paths. Substitution for the model-to-prototype ratios using material preservation, $A_s^* = L^{*2}$, and no albedo or earth emission absorption gave:

$$\frac{V^* T^*}{\theta^*} = L^{*2} S^* = Q^* = \frac{A_n^* T^*}{L^*} = L^{*2} T^{*4}$$

These ratios were the governing similitude criteria. Experimental studies were conducted on full-scale, half-scale, and quarter-scale models of two opposed, flat discs connected by four tubular legs. The half-scale model was designed using material preservation, while the quarter-scale model was designed on the basis of temperature preservation. Although the tube diameter was designed to $D^* = L^*$, the availability of stock material necessitated some geometrical distortion of this criteria. Experimental results gave agreement between prototype and models to within 15 F, or three percent error, based on the absolute temperature.

Adkins [14] introduced a method of geometric scaling that allowed thermal modeling while preserving both material and temperature. He utilized similitude to develop modeling criteria for a thin-walled cylinder.

$$\theta^* = L^{*2} \quad R^* = L^{*2}$$

A hollow cylinder and sphere, heated by radiation from a plate heater, were used in one test configuration. A dumbbell-shaped model consisting of two hollow spheres connected by a copper rod and heated by a bird cage in one sphere served as another configuration. Wall thickness was modeled with a thin wall approximation, and both steady-state and transient conditions were studied. Results of testing in a cryogenic vacuum chamber showed a maximum discrepancy of less than 10 percent of the maximum temperature measured at any location and time.

Jones and Harrison [15] presented the analysis and results for two sets of experiments in thermal scale modeling. The modeling criteria were

$$\frac{T_j^*}{T_k^*}, \frac{R_{kj}^* T^{*3} \theta^*}{C_{pj}^*}, \frac{q_j^* \theta^*}{C_{pj}^* T_j^*} \quad (j, k=1, \dots, 4)$$

where R_{kj} is the overall radiant coefficient for net radiative transfer from region k to j , and q_j is the internal power dissipation in the j th region. The prototype and model consisted of a plate, cylinder, and sphere exchanging thermal energy only by radiation and located relative to one another in an unsymmetrical arrangement. Experimental results showed agreement on a half-scale model to within 8 K.

Gabron, Johnson, Vickers, and Lucas [16] performed thermal modeling experiments on the Mariner IV spacecraft. The spacecraft's mission took it into deep space at a fixed altitude to the sun so that its temperatures satisfied steady-state requirements. A half-scale model was constructed using temperature preservation techniques and tested in a space simulation chamber. The modeling criteria are given below.

$$T^*, \frac{L^*}{\kappa^*}, C^*, \frac{q^*}{L^2}, \frac{L^{*2}}{\kappa^* t^*}$$

Comparison of the model temperatures to those of the actual spacecraft showed agreement of most of the measurements within 25 F, and some within 10 F.

Shih [17] presented a discussion of similitude criteria which included the relationship $R^* = t^* = L^{*2}$ for preserving both material and temperature in model and prototype. Also considered were changes in thermal conductivity and specific heat with temperature. Two types of spacecraft were discussed: the gravitationless type and the type with artificial gravity of some magnitude. Free convection was considered in

a state of artificial gravity, but no experimental work was presented or planned.

Barcus [18] used dimensional analysis to develop modeling criteria for a radiation-conduction, steady-state computer investigation. A cubical box which received solar radiation while it emitted to space was modeled with a length scale of 1/10. Results using distortion factors and distorted geometry yielded temperature differences between prototype and model from 0 to 80 F. He concluded that the best features of temperature and material preservation could be retained by using geometric distortion techniques.

Young and Shanklin [19] applied the similitude technique to a set of differential equations that described the thermal behavior of a prototype and model with a configuration similar to a spool. The two flat ends were a heater plate and a cold plate, respectively, with a cylindrical rod connecting them at their central axis. Temperature and material preservation were accomplished using geometrical distortion during steady-state and transient conditions. Results were accurate to within five percent, utilizing both radiation and conduction heat transfer.

Miller [20] investigated the application of thermal modeling to steady-state and transient conduction in cylindrical solid rods for both single and multiple material systems. He obtained the following relationships using dimensional analysis:

$$q'''^* = L^{*-2} \quad q''^* = L^{*-1} \quad q^* = L^{*3}$$

$$T^* = 1 \quad \theta^* = L^{*2}, \quad R^* = L^{*2}$$

Miller used simultaneous temperature and material preservation. Prototype and model temperatures in corresponding locations were no more than 13 F apart, and the majority of data was less than 5 F in error.

A computer program was used by Watkins [21] to derive sets of independent similarity ratios by dimensional analysis. Forty-nine groups containing seven independent similarity ratios were developed for the general case of coupled radiation and conduction thermal modeling.

Hsia and van der Blik [22] investigated the effect of internal convection in space vehicular models with a numerical computation. Results for gases were presented, but it was considered uncertain whether or not the technique could be applied to liquids in thin-walled containers.

Thermal scale modeling without thermal similitude has also been mathematically investigated by Doenecke [23]. Results indicated that the skin may be anisotropically scaled, but the materials and thermal contact coefficients could be preserved. The resulting thermal analysis was more complicated, but the construction or testing of the model was simplified.

Buna [24] mathematically studied the criteria of thermally matching interfacing scale models constructed by the use of different scale modeling techniques. His investigation included an analysis of the conditions of similarity, the techniques of radiation and conduction modeling, and the thermal matching of radiation and conduction models. Applications were made to the scaling of multilayer insulations, the scaling of cabin atmospheric convection, and the scale modeling of docking ports. Cabin convection was briefly examined for zero-g forced convection and

forced convection with superimposed natural convection, but the analysis was chiefly concerned with gases.

Rolling, Marshall, and Murray [25] discussed thermal modeling of a space telescope using a length scale ratio of 1/6.43 and material preservation for coupled radiation and conduction. The limiting scale ratio appeared to be 1/7, and multilayer insulation limited accurate simulation of thermal conductivity. Results generally agreed within one percent of the absolute temperature of the prototype.

Maples [26] was evidently the first to investigate thermal modeling with all three modes of heat transfer simultaneously. He analyzed the problem of free or natural convection in the annulus of a concentric cylinder system. The similitude approach was applied to the energy differential equation to obtain the modeling criteria. Both temperature and material preservation were employed, and the diameter was scaled as $D^* = L^{*2}$. Thermal energy was conducted radially from a heater within the inner cylinder through the wall to dry air within the annulus. Following the free convection across the annulus, the heat was conducted through the outer cylinder and radiated to the cryogenic liner surrounding the inside of the vacuum chamber. Lexan end flanges and guard heaters were used to insure a constant radial heat flux and isothermal surfaces. Prototype and half-scale models were fabricated from 6061-T6 aluminum tubing, and thermocouples along the surfaces recorded the temperature distribution under steady-state conditions. Results indicated modeling for $h^* = 1$ with a difference between prototype and model of about 4 F.

Klockzien and Shannon [27] discussed thermal modeling of spacecraft using both temperature preservation and material preservation. Results

of full-scale, half-scale, and 0.285-scale tests on double-walled specimens suspended within a space simulation chamber and subjected to combined radiation and conduction heat transfer were reported. Steady-state and transient tests yielded close agreement between full- and half-scale specimens. The 0.285-scale model differed in temperature by 15 F and was attributed largely to the use of aluminum tape which caused a change in the effective thermal conductivity. Similitude criteria for combined radiation-conduction-convection heat transfer were suggested for laminar flow over flat plates, but laboratory verification was not attempted.

MacGregor [28] at Boeing analyzed the limitations associated with thermal modeling. An understanding of errors resulting from uncertainties in the thermophysical properties, geometric dimensions, and the test environment was the primary objective of this study. Secondary objectives of the program were the development of additional scaling criteria or compromise techniques applicable to special problem areas in thermal modeling such as transient response, thermal control coatings, multilayer insulation, thermal gradient effects, and test environment effects. An experimental program was conducted on a prototype and half-scale vehicle for a number of combinations of solar illumination and internal power dissipation under a simulated space environment. It was concluded that thermal modeling of multilayer insulation was the major problem area and that numerical analysis can be used to improve experimental modeling results for known compromises of modeling criteria. It was also concluded that a 1/10 scale appeared to be a practical lower limit on thermal modeling.

Rolling, Murray, and Marshall [29] at Lockheed also discussed the limitations associated with thermal scale modeling at length. It was

concluded that the problems regarding model construction, instrumentation, and materials selection become increasingly difficult at the smaller scale ratios. Temperature preservation was preferred over material preservation, and the use of both techniques simultaneously required geometric distortion of all components which could become difficult in most complex systems. Modeling of multilayer insulation could be accomplished with temperature preservation using $k^*/t^* = 1$ for the same blanket material with fewer layers. The modeling of common joints with any degree of acceptable accuracy was concluded to be a major problem.

Holm and Miller [30] used similitude to develop modeling criteria for a heat pipe from the governing differential equations. Two modeling techniques were considered: material preservation and heat flux preservation. Heat flux preservation yielded temperature preservation, but it did not allow material preservation. The similarity relations were found to be:

$$(T_v - T_o)^* = \left\{ \frac{q}{L} \left[\frac{\ln(r_2/r_1)}{\kappa_1} + \frac{\ln(r_3/r_2)}{\kappa_2} \right] \right\}^*$$

$$T_o^* = \frac{(q^*/\varepsilon^*)^{1/2}}{(L^*)^{1/2}} \quad \text{and} \quad q^* = \left(\frac{\kappa NL}{R_m} \right)^*$$

where T_v = temperature of the vapor

T_o = temperature of the condenser outer wall

r_1 = inside wick radius

r_2 = outside wick radius

r_3 = outside wall radius

κ_1 = thermal conductivity of the wick

κ_2 = thermal conductivity of the wall

N = water parameter

h_{fg} = latent heat of vaporization

σ = surface tension

R_m = minimum radius of curvature of the liquid-vapor interface

A unique test apparatus was built using a coiled copper coil as the cryogenic cold wall. This assembly was placed within an 18-inch-diameter bell jar to simulate the high vacuum environment. Tests were run to determine the steady-state modeling capability and certain wick characteristics. Results showed good agreement with no predicted temperature more than 10 F in error. The heat flux preservation technique was not experimentally verified.

CHAPTER III.

MODELING CRITERIA

Thermal modeling has been divided into two categories: temperature preservation and material preservation. Temperature preservation required that temperatures at analogous locations on the prototype and model be equal. In some cases this may require that a different material be used for the model than for the prototype. Material preservation permits the use of the same material for both prototype and model, but predicts a scaled difference in temperature at analogous locations. Most researchers prefer to maintain thermal similitude between prototype and model, but it would also be desirable to use the same material for both objects. This combination of criteria has been used by Miller [20], Adkins [14], and Maples [26]; and appears to be satisfactory under certain circumstances. The restriction involves the use of a thin-wall approximation which may be acceptable depending upon the object being modeled. For the case of a thin-walled tube or chamber such as a spacecraft wall, this approximation may be used to develop certain modeling criteria.

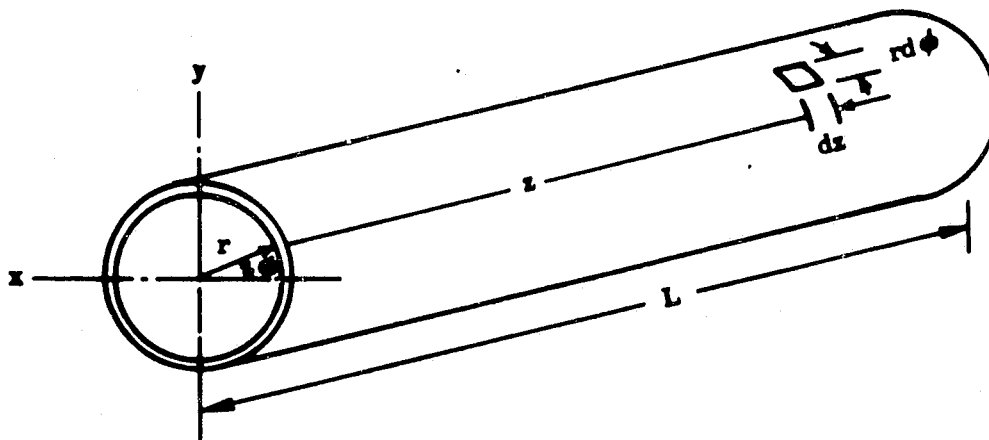
Further, thermal modeling may be approached in two ways: dimensional analysis or similitude. Dimensional analysis requires knowledge of all parameters associated with the problem, but can lead to useful results. The similitude approach involves the use of the governing differential equations and boundary conditions and offers a distinct advantage to the inexperienced. Either method results in the same set of similarity parameters, but the similitude approach will be used here.

Before deriving the similarity parameters, the constraints imposed upon the problem will be discussed. The first restriction involved the use of homogeneous and isotropic materials. The second required that there be perfect geometric similarity between prototype and model. Thirdly, the model and prototype must have the same uniform and constant surface characteristics. This was achieved by coating the surfaces of both the prototype and model with a highly absorptive flat black paint. The fourth requirement was that the radiant heat flux from the simulated environment was approximately zero. This approximation was achieved by using a cryogenic liner cooled to liquid nitrogen temperature to simulate the environment. It was also assumed that all energy radiated from the prototypes and models was absorbed by the cryogenic liner. The fifth restriction was that the properties of the prototype and model were constant and invariable during testing. Use of a small temperature range of approximately 30 F to 80 F insured this approximation. A sixth constraint was that heat transfer by convection and conduction external to the specimen was negligible. This criteria was satisfied by a vacuum environment, the suspension of the test element on nonconducting threads, and its connection to adjacent tubing with insulated fittings.

With these constraints it was decided to test a low and a high thermal conductivity material to verify the modeling criteria for the forced convection-conduction-radiation problem. A fluid at room temperature with a fully developed velocity boundary layer was introduced to a tubular specimen with a large length-to-diameter ratio. Heat was then transferred from the water to the inner surface of the tube by forced convection. This energy was then transferred through the tube to its outer surface and along its length by conduction. Because the specimen

tube was thermally insulated from its connecting members and surrounded by a vacuum environment, the only avenue remaining for heat transfer from the outer surface was radiation to the cryogenic liner. This exchange completed the desired chain of energy transport involving all three modes of heat transfer: conduction, convection, and radiation. The specimen tube was allowed to achieve thermal equilibrium, thereby satisfying the steady-state criteria.

Similarity parameters may be derived from the conduction equation for temperature distribution in a pipe as shown below.



The partial differential conduction equation in cylindrical coordinates may be written

$$\frac{\partial T}{\partial \theta} = \alpha \left[\frac{\partial^2 T}{\partial r^2} + \frac{1}{r} \frac{\partial T}{\partial r} + \frac{1}{r^2} \frac{\partial^2 T}{\partial \phi^2} + \frac{\partial^2 T}{\partial z^2} \right] \quad (1)$$

where T is the temperature at any time t and at any radius r , angular displacement ϕ , and distance z down the tube. The parameter α is a property of the tube material called the thermal diffusivity and is equal to a ratio of its thermal conductivity κ to a product of the material's density ρ , and specific heat, C_p , as

$$\alpha = \frac{\kappa}{\rho C_p}$$

Temperature within the tube no longer changes with time under steady-state conditions; thus, $\frac{\partial T}{\partial \theta} = 0$ and equation (1) reduces to

$$\frac{\partial^2 T}{\partial r^2} + \frac{1}{r} \frac{\partial T}{\partial r} + \frac{1}{r^2} \frac{\partial^2 T}{\partial \phi^2} + \frac{\partial^2 T}{\partial z^2} = 0 \quad (2)$$

For a uniform specimen surrounded by an isothermal environment, the angular distribution of temperature around the tube is equal; thus

$$\frac{\partial^2 T}{\partial \phi^2} = 0$$

Equation (2) then becomes

$$\frac{\partial^2 T}{\partial r^2} + \frac{1}{r} \frac{\partial T}{\partial r} + \frac{\partial^2 T}{\partial z^2} = 0 \quad (3)$$

The boundary condition at the inside surface of the tube is

$$h(T_f - T) = -\kappa \left. \frac{\partial T}{\partial r} \right]_r = \frac{D_i}{2} \quad (4)$$

where h is the convective heat transfer coefficient, T_f is the temperature of the fluid, T is the temperature of the tube at the point in question, κ is the tube's thermal conductivity, r is a displacement in the radial direction, and D_i is the inside diameter of the tube.

The boundary condition at the outside surface of the tube is

$$-\sigma \epsilon (T^4 - T_o^4) = -\kappa \left. \frac{\partial T}{\partial r} \right]_r = \frac{D_o}{2} \quad (5)$$

where σ is the Stefan-Boltzmann constant equal to 1713×10^{-12} Btu per hr.-sq. ft.- $^{\circ}R^4$, ϵ is the emittance of the surface, T_0 is the temperature of the cryogenic liner to which the tube is radiating, and D_0 is the outside diameter of the tube.

The conduction equation (3) may be non-dimensionalized by choosing

$$\bar{r} = \frac{r}{D_0} \quad \bar{T} = \frac{T}{T_r} \quad \bar{z} = \frac{z}{L} \quad (6)$$

where T_r is an arbitrary reference temperature, and L is the length of the tube. Introduction of these quantities yields

$$\frac{T_r}{D_0^2} \frac{\partial^2}{\partial \bar{r}^2} (T/T_r) + \frac{1}{D_0} \frac{T_r}{r} \frac{\partial}{\partial \bar{r}} (T/T_r) + \frac{T_r}{L^2} \frac{\partial^2}{\partial \bar{z}^2} (T/T_r) = 0$$

or

$$\frac{T_r}{D_0^2} \frac{\partial^2 \bar{T}}{\partial \bar{r}^2} + \frac{T_r}{D_0^2} \frac{1}{\bar{r}} \frac{\partial \bar{T}}{\partial \bar{r}} + \frac{T_r}{L^2} \frac{\partial^2 \bar{T}}{\partial \bar{z}^2} = 0$$

Dividing the above equation by T_r/D_0^2 yields

$$\frac{\partial^2 \bar{T}}{\partial \bar{r}^2} + \frac{1}{\bar{r}} \frac{\partial \bar{T}}{\partial \bar{r}} + \frac{D_0^2}{L^2} \frac{\partial^2 \bar{T}}{\partial \bar{z}^2} = 0 \quad (7)$$

The inside condition, equation (4), may also be non-dimensionalized.

$$h(T_f - T) = -\kappa \left. \frac{\partial T}{\partial r} \right|_r = \frac{D_i}{2}$$

$$h T_r \left(\frac{T_f}{T_r} - \frac{T}{T_r} \right) = \left. \frac{-\kappa T_r}{D_0} \frac{\partial}{\partial \bar{r}} \left(\frac{T}{T_r} \right) \right|_{\bar{r} = \frac{D_i}{D_0}} = \frac{D_i}{2 D_0}$$

Letting $\bar{T}_f = \frac{T_f}{T_r}$, $\bar{T} = \frac{T}{T_r}$, and $\bar{r} = \frac{r}{D_o}$

results in
$$hT_r (\bar{T}_f - \bar{T}) = - \left. \frac{\kappa T_r}{D_o} \frac{\partial \bar{T}}{\partial \bar{r}} \right]_{\bar{r} = \frac{D_i}{2D_o}}$$

It would be desirable to utilize the Nusselt number or non-dimensionalized heat transfer coefficient which may be written

$$Nu = \frac{hD_i}{\kappa_f}$$

where Nu is the non-dimensional Nusselt number, h is the heat transfer coefficient, D_i is the tube's inside diameter, and κ_f is the fluid's thermal conductivity. Introducing the necessary parameters and dividing both sides by T_r yields

$$\frac{hD_i}{\kappa_f} \frac{\kappa_f}{D_i} (\bar{T}_f - \bar{T}) = - \left. \frac{\kappa}{D_o} \frac{\partial \bar{T}}{\partial \bar{r}} \right]_{\bar{r} = \frac{D_i}{2D_o}}$$

or
$$\frac{\kappa_f}{D_i} Nu (\bar{T}_f - \bar{T}) = - \left. \frac{\kappa}{D_o} \frac{\partial \bar{T}}{\partial \bar{r}} \right]_{\bar{r} = \frac{D_i}{2D_o}}$$

Solving for $\left. \frac{\partial \bar{T}}{\partial \bar{r}} \right]_{\bar{r} = \frac{D_i}{2D_o}}$ yields

$$\left. \frac{\partial \bar{T}}{\partial \bar{r}} \right]_{\bar{r} = \frac{D_i}{2D_o}} = \frac{D_i}{2D_o} = \frac{-\kappa_f}{\kappa} \frac{D_o}{D_i} Nu (\bar{T}_f - \bar{T}) \quad (8)$$

The boundary condition at the outside surface was

$$\sigma \epsilon (T^4 - T_0^4) = -\kappa \left. \frac{\partial T}{\partial r} \right]_{\bar{r}} = \frac{D_0}{2}$$

Non-dimensionalizing as before,

$$\sigma \epsilon T_r^4 \left(\frac{T^4}{T_r^4} - \frac{T_0^4}{T_r^4} \right) = \frac{-\kappa T_r}{D_0} \left. \frac{\partial}{\partial r/D_0} (T/T_r) \right]_{\frac{r}{D_0}} = \frac{D_0}{2D_0}$$

or introducing $\bar{T}_0 = \frac{T_0}{T_r}$ gives

$$\sigma \epsilon T_r^3 (\bar{T}^4 - \bar{T}_0^4) = \frac{-\kappa}{D_0} \left. \frac{\partial \bar{T}}{\partial \bar{r}} \right]_{\bar{r}} = \frac{D_0}{2D_0}$$

Solving for $\left. \frac{\partial \bar{T}}{\partial \bar{r}} \right]_{\bar{r}} = \frac{D_0}{2D_0}$ yields

$$\left. \frac{\partial \bar{T}}{\partial \bar{r}} \right]_{\bar{r}} = \frac{D_0}{2D_0} = \frac{-\sigma \epsilon D_0 T_r^3}{\kappa} (\bar{T}^4 - \bar{T}_0^4) \quad (9)$$

A thin wall approximation is used where $D_i = D_o = D$; and the second order temperature variation with the radius, r , is negligible, or

$$\frac{\partial^2 \bar{T}}{\partial \bar{r}^2} = 0 \quad (10)$$

The first order gradient may be written as the average of the gradient at the inside and outside surfaces, or

$$\frac{1}{\bar{r}} \frac{\partial \bar{T}}{\partial \bar{r}} = \frac{1}{\bar{r}} \frac{1}{2} \left[\left. \frac{\partial \bar{T}}{\partial \bar{r}} \right]_{\bar{r}} = \frac{D_i}{2D_0} + \left. \frac{\partial \bar{T}}{\partial \bar{r}} \right]_{\bar{r}} = \frac{D_o}{2D_0} \right] \quad (11)$$

Utilizing the thin wall approximation and substituting (8) and (9) into (11) gives

$$\frac{1}{\bar{r}} \frac{\partial \bar{T}}{\partial \bar{r}} = \frac{-1}{2\bar{r}} \left[\frac{\kappa_f D}{\kappa} \text{Nu} (\bar{T}_f - \bar{T}) + \frac{\sigma \epsilon D T_r^3}{\kappa} (\bar{T}^4 - \bar{T}_0^4) \right] \quad (12)$$

Substitution of equations (10) and (12) into (7) yields, for $D_0 = D$,

$$\frac{-D}{2\bar{r}} \left[\frac{\kappa_f \text{Nu}}{\kappa D} (\bar{T}_f - \bar{T}) + \frac{\sigma \epsilon T_r^3}{\kappa} (\bar{T}^4 - \bar{T}_0^4) \right] + \frac{D^2}{L^2} \frac{\partial^2 \bar{T}}{\partial \bar{z}^2} = 0$$

Division by D gives the desired non-dimensionalized differential equation

$$\frac{-\kappa_f \text{Nu}}{2\kappa D} \left(\frac{\bar{T}_f - \bar{T}}{\bar{r}} \right) - \frac{\sigma \epsilon T_r^3}{2\kappa} \left(\frac{\bar{T}^4 - \bar{T}_0^4}{\bar{r}} \right) + \frac{D}{L^2} \frac{\partial^2 \bar{T}}{\partial \bar{z}^2} = 0 \quad (13)$$

In order to model a system, the differential equation must satisfy both the prototype and its model. Dimensionless terms present no problem since by definition their dimensionless nature is universally applicable. The only terms remaining in the differential equation that must satisfy both prototype and model are the coefficients of the non-dimensionalized terms. These, then, must be equal for both model and prototype and are listed below.

$$\frac{\kappa_f \text{Nu}}{2\kappa D}, \quad \frac{\sigma \epsilon T_r^3}{\kappa}, \quad \frac{D}{L^2} \quad (14)$$

Writing the coefficient for the prototype with subscripts p , and for the model with subscripts m , yields

$$\left(\frac{\kappa_f \text{Nu}}{2\kappa D} \right)_p = \left(\frac{\kappa_f \text{Nu}}{2\kappa D} \right)_m$$

Dividing both sides by $\left(\frac{\kappa_f \text{Nu}}{2\kappa D} \right)_p$ yields

$$1 = \frac{\left(\frac{\kappa_f Nu}{\kappa D}\right)_m}{\left(\frac{\kappa_f Nu}{\kappa D}\right)_p}$$

Defining

$$\left(\frac{\kappa_f Nu}{\kappa D}\right)^* = \frac{\left(\frac{\kappa_f Nu}{\kappa D}\right)_m}{\left(\frac{\kappa_f Nu}{\kappa D}\right)_p}$$

the first modeling criteria becomes

$$\left(\frac{\kappa_f Nu}{\kappa D}\right)^* = 1 \quad (15)$$

The * thus indicates a scaled quantity of model-to-prototype ratio.

Likewise, the two remaining coefficients become

$$\left(\frac{\sigma \epsilon T_r^3}{\kappa}\right)^* = 1 \quad (16)$$

and

$$\left(\frac{D}{L^2}\right)^* = 1 \quad (17)$$

Equation (17) may be written

$$D^* = L^{*2} \quad (18)$$

which states that the diameter scales as the square of the length. It

is also possible to write

$$L^* = \sqrt{D^*} \quad (19)$$

Thus, for a model of one-half the diameter of the prototype, it can be written

$$D^* = \frac{D_m}{D_p} = \frac{1}{2}$$

and,

$$L^* = \frac{L_m}{L_p} = \sqrt{\frac{1}{2}} = 0.707$$

Therefore, the length, L_m , of the model is 0.707 the length of prototype, L_p . If the prototype were, say, 48 inches long, the half-size model would be $0.707 \times 48 = 33.936$ inches.

For materials preservation, the same material is in both prototype and model, or

$$\kappa_f^* = \kappa^* = 1 \quad (20)$$

Use of this fact in equation (15) yields a particularly interesting relationship:

$$\frac{Nu^*}{D^*} = 1$$

or

$$Nu^* = D^* \quad (21)$$

Since σ , the Stefan Boltzmann constant, and ϵ , the emittance, are the same for prototype and model, equation (16) gives

$$\frac{T_r^{*3}}{\kappa^*} = 1$$

for materials preservation, $\kappa^* = 1$; therefore, temperature preservation is also implied as

$$T_r^* = 1 \quad (22)$$

If equation (3) was non-dimensionalized by choosing $\bar{r} = \frac{r}{t_w}$ where t_w was the wall thickness of the tubing, there would have resulted in an identical manner

$$t_w^* = L^{*2} \quad (23)$$

The modeling criteria may then be summarized as

$$D^* = t_w^* = Nu^* = L^{*2} \quad (24)$$

and

$$T^* = \kappa^* = 1 \quad (25)$$

which implies both temperature and materials preservation.

CHAPTER IV.

THERMAL ANALYSIS

Thermal analysis of this experiment is complex since three simultaneous modes of heat transfer are involved. Furthermore, temperature dependence of fluid properties must be considered during the convective part of the energy transfer. As pointed out in Chapter I, energy transfer is initially from the fluid to the tube's inner wall by convection. Conduction then transfers the heat radially as well as longitudinally down the tube to its outer surface where the energy is radiated to the cryogenic liner. For convenience, each mode of heat transfer will be considered separately.

CONVECTION

In laminar or smooth flow through a tube, heat transfer takes place solely by conduction within the fluid. Heat transfer analysis is facilitated by a discussion of fluid phenomena and properties.

Poiseuille's law, derived by Maxwell, relates the pressure drop down a tube to the tube diameter, fluid flow rate-- ω , and dynamic viscosity-- μ [31].

$$\frac{\Delta P}{l} = \frac{128\mu}{\pi D_1^4} \omega$$

Dimensional analysis has been used to yield pressure drop per unit length for laminar, incompressible flow [31], as

$$\frac{\Delta P}{l} = \frac{4}{D_1} \left(\frac{16}{Re} \right) \frac{\rho u m^2}{2}$$

where Re is the dimensionless Reynolds number and u_m is the mean fluid velocity. The term $16/Re$ is also the friction factor--a measure of the effects of Reynolds number and surface roughness.

The Reynolds number, a dimensionless ratio, relates the inertial to the viscous forces

$$Re = \frac{\rho V D_H}{\mu} \quad (26)$$

For flow within tubes, the hydraulic diameter is equal to the inside diameter. For $Re < 2300$, the flow is laminar or smooth. The Reynolds number is also temperature dependent; i.e., its determination involves dynamic fluid viscosity which varies from 2.36 lbm/ft.hr. at 70 F to 4.32 lbm/ft.hr. at 32 F.

Fluid properties can be described by the Prandtl number, which is a dimensionless ratio involving viscosity, specific heat, and thermal conductivity.

$$Pr = \frac{\mu C_p}{k_f} \quad (27)$$

The Prandtl number essentially relates the momentum diffusivity to the thermal diffusivity of the fluid. For $Pr < 1$, the momentum function prevails. The Pr number for distilled water increases with decreasing temperature from 6.82 at 80 F to 13.7 at 32 F due primarily to the temperature dependence of fluid viscosity. Thermal conductivity of water varies from 0.347 Btu/hr.-ft.-F at 70 F to 0.319 Btu/hr.-ft.-F at 32 F.

The Nusselt number is essentially a non-dimensionalized heat transfer coefficient:

$$\text{Nu} = \frac{hD_1}{\kappa_f} \quad (28)$$

where D_1 is the inside diameter of the tube and h is the convective heat transfer coefficient. For water in forced convection, h normally has a range of 50 to 2000 Btu/hr.-sq.ft. F. The convective heat transfer coefficient is best defined by Newton's Law of Cooling, which states:

$$q = hA(T_o - T_m) \quad (29)$$

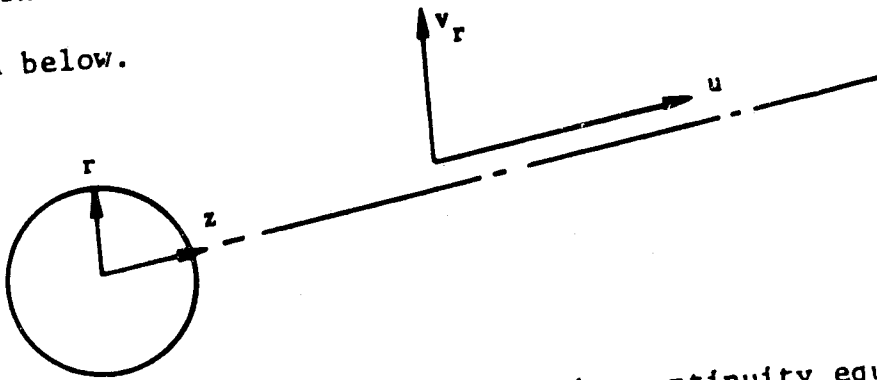
where A is the surface area, T_o is the surface temperature, and T_m is the bulk fluid temperature. The Nusselt number is seen to vary with the diameter for constant h . For laminar flow in tubes and ducts, the Nusselt number can be written as some function of the Reynolds and Prandtl numbers.

$$\text{Nu} = f(\text{Re}, \text{Pr})$$

A complete viscous fluid solution for flow within a tube poses mathematical difficulty for all but the most simple flow geometries. Prandtl's discovery of the hydrodynamic boundary layer adjacent to a surface--where most of the change in velocity takes place--greatly simplified analysis of the flow field. Flow within a tube is a boundary layer problem in which the boundary layer grows near the tube entrance until its growth is stopped by symmetry at the center line of the tube. The tube radius then becomes the ultimate boundary layer thickness. When heat transfer exists between the fluid and the surface, a thermal boundary layer will also be found where the major temperature changes occur. The hydrodynamic boundary layer does not necessarily coincide

with the thermal boundary layer unless the $Pr = 1$. For $Pr > 1$, the predominating influence of the viscosity causes a rapid development of fully developed hydrodynamic flow; while the temperature distribution changes more slowly, attaining a fully developed profile much further along the tube.

The mathematical equations that describe the flow and temperature distributions within the fluid are the continuity, momentum, and energy equations. The continuity equation may be derived using the coordinate system shown below.



For constant density flow within a tube, the continuity equation may be written:

$$\frac{\partial u}{\partial z} + \frac{\partial v_r}{\partial r} + \frac{v_r}{r} = 0 \quad (30)$$

For axisymmetric flow in a circular tube, the momentum equation of the boundary layer becomes:

$$\rho u \frac{\partial u}{\partial z} + \rho v_r \frac{\partial u}{\partial r} + \rho c \frac{dP}{dz} = \frac{1}{r} \frac{\partial}{\partial r} \left(r \mu \frac{\partial u}{\partial r} \right) \quad (31)$$

Note that this equation is valid for variable properties ρ and μ .

The energy equation for steady flow in a circular tube may be written:

$$\rho u c_p \frac{\partial T}{\partial z} + \rho v_r c_p \frac{\partial T}{\partial r} - \left[\frac{\kappa}{r} \frac{\partial}{\partial r} \left(r \frac{\partial T}{\partial r} \right) + \frac{\kappa}{r^2} \frac{\partial}{\partial \phi} \left(\frac{\partial T}{\partial \phi} \right) + \kappa \frac{\partial}{\partial z} \left(\frac{\partial T}{\partial z} \right) \right] = 0 \quad (32)$$

where the dissipation function and the pressure gradient have been neglected. Note that this equation contains a conduction term in the z direction.

For fully established flow within circular tubes, the momentum equation yields the parabolic velocity distribution.

$$u = \frac{r_0^2 g_c}{4 \mu} \left(\frac{-dP}{dx} \right) \left(1 - \frac{r^2}{r_0^2} \right) \quad (33)$$

or

$$u = 2V \left(1 - \frac{r^2}{r_0^2} \right) \quad (34)$$

where V is the mean velocity defined by

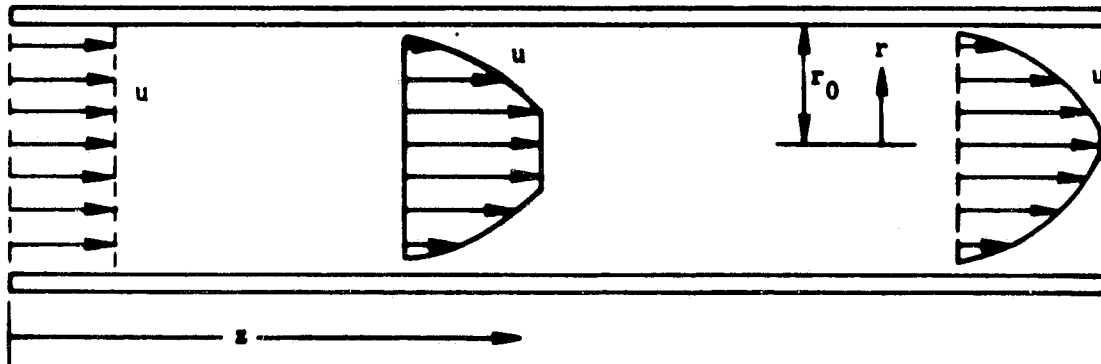
$$V = \frac{1}{A_c} \int_{A_c} u dA_c$$

and A_c is the cross-sectional area.

The velocity distribution change in the entrance region of a tube has been analyzed by Langhaar [32] where the results are expressed in dimensionless form. The length necessary to develop the parabolic velocity distribution varies with the Reynolds number approximately as

$$l = \frac{Re}{20} D \quad (35)$$

where D_i denotes the inside tube diameter. The development of the velocity profile in the hydrodynamic entry region of a tube is shown as follows:



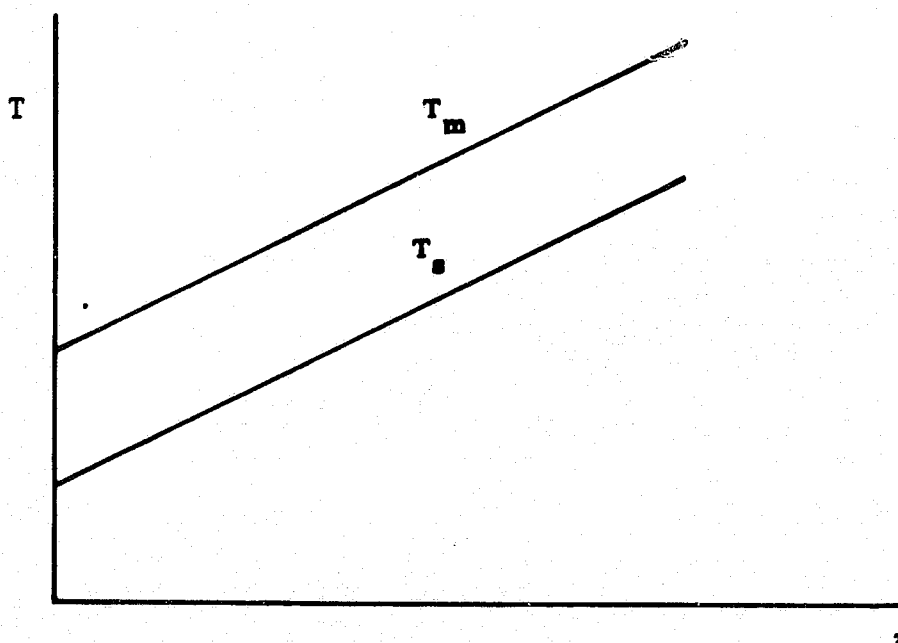
For symmetric heat transfer, negligible axial conduction, and fully developed flow, the energy equation reduces to

$$\frac{1}{r} \frac{\partial}{\partial r} \left(r \frac{\partial T}{\partial r} \right) = \frac{u}{\alpha} \frac{\partial T_m}{\partial z}$$

where $\alpha = k_f / \rho C_p$, the thermal diffusivity. One of the solutions to this equation assumes a constant heat rate per unit of tube length. In this case, the energy equation becomes

$$\frac{1}{r} \frac{\partial}{\partial r} \left(r \frac{\partial T}{\partial r} \right) = \frac{u}{\alpha} \frac{dT_m}{dz} \quad (36)$$

The temperature variation with tube length is shown below.



Applicable boundary conditions are:

$$T = T_0 \text{ at } r = r_0$$

$$\frac{\partial T}{\partial r} = 0 \text{ at } r = 0$$

Substituting the parabolic velocity profile, equation (34) into (36) gives

$$\frac{1}{r} \frac{\partial}{\partial r} \left(r \frac{\partial T}{\partial r} \right) = \frac{\partial V}{\alpha} \left(1 - \frac{r^2}{r_0^2} \right) \frac{dT_m}{dz}$$

Integrating twice with respect to r , and evaluation at the boundary conditions, results in the temperature profile

$$T = T_0 - \left(\frac{2V}{\alpha} \right) \left(\frac{dT_m}{dz} \right) \left(\frac{3}{16} r_0^2 + \frac{r^4}{16r_0^2} - \frac{r^2}{4} \right)$$

Mixed mean fluid temperature or bulk fluid temperature is defined by Kays (33) to be

$$T_m = \frac{1}{A_c V} \int_{A_c} u T dA_c$$

or

$$T_m = \frac{2}{r_0^2 V} \int_0^r u T r dr$$

Substitution for u and T and integration yields

$$T_m = T_0 - \frac{11}{96} \left(\frac{2V}{\alpha} \right) \left(\frac{dT_m}{dz} \right) r_0^2$$

At this point, the convective heat transfer coefficient may be evaluated using equation (29).

$$q_0'' = h (T_0 - T_m) = h \left(\frac{11}{96} \right) \left(\frac{2V}{\alpha} \right) \left(\frac{dT_m}{dz} \right) r_0^2 \quad (37)$$

Conservation of thermal energy at the wall gives the wall surface heat flux as

$$q_0'' = \frac{r_0 V \rho C_p}{2} \left(\frac{dT_m}{dz} \right) \quad (38)$$

Equating (37) and (38) gives

$$h = \frac{48}{11} \frac{\kappa_f}{D_1} = 4.364 \frac{\kappa_f}{D_1} \quad (39)$$

where $D_1 = 2r_0$. This relation holds for fully developed temperature and velocity profiles, and results from the fact that the energy transport is a purely molecular conduction problem under these conditions.

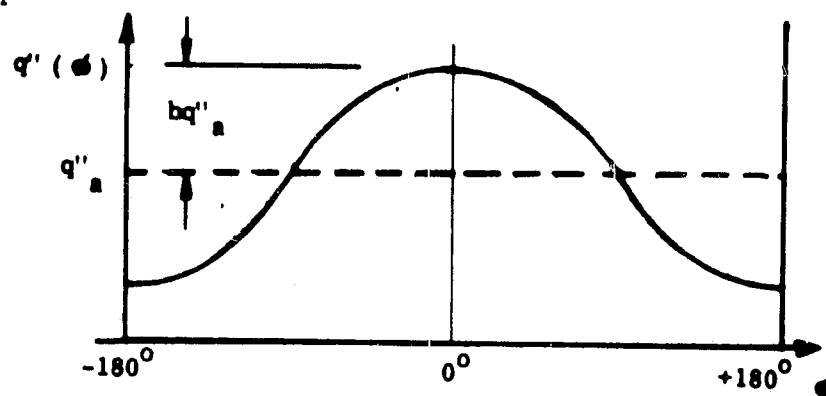
Equation (39) may also be written:

$$Nu = \frac{hD_1}{\kappa_f} = 4.364 \quad (40)$$

Reynolds investigated the problem of laminar flow in a circular tube with fully developed constant heat rate conditions axially, but with a cosine peripheral variation of heat flux

$$q''(\phi) = q''_a (1 + b \cos \phi)$$

as shown in



The local Nusselt number was found to be

$$\text{Nu}(\phi) = \frac{1 + b \cos \phi}{\frac{11}{48} + \frac{b \cos \phi}{2}}$$

which was found to behave strangely depending upon the choice of b .

The thermal entry length must be considered where the temperature of the fluid is uniform over the flow cross section where heat transfer begins and the velocity profile is already fully established and invariant. Consideration is restricted to laminar, incompressible, low-velocity flow. The energy equation (32) is written

$$\frac{\partial^2 T}{\partial r^2} + \frac{1}{r} \frac{\partial T}{\partial r} = \frac{u}{\alpha} \frac{\partial T}{\partial z} - \frac{\partial^2 T}{\partial z^2} \quad (41)$$

and non-dimensionalized using

$$\bar{T}_0 = \frac{T_0 - T}{T_0 - T_e}, \quad \bar{r} = \frac{r}{r_0}, \quad \bar{u} = \frac{u}{V}, \quad \bar{z} = \frac{z/r_0}{\text{RePr}}$$

where T_e is the uniform entering fluid temperature and Z is the axial distance from where heat transfer starts. Substitution of these relations into equation (41) results in

$$\frac{\partial^2 \bar{T}_0}{\partial \bar{r}^2} + \frac{1}{\bar{r}} \frac{\partial \bar{T}_0}{\partial \bar{r}} = \frac{\bar{u}}{2} \frac{\partial \bar{T}_0}{\partial \bar{z}} - \frac{1}{(\text{RePr})^2} \frac{\partial^2 \bar{T}_0}{\partial \bar{z}^2} \quad (42)$$

The last term in equation (41) considers heat conduction in the axial direction. Singh [34] found that as a general rule this term is negligible for $RePr > 100$ and will be dropped with this reservation.

The parabolic velocity profile is applicable for fully developed laminar flow

$$u = 2V \left(1 - \frac{r^2}{r_0^2}\right) \quad \bar{u} = 2 \left(1 - \bar{r}^2\right) \quad (43)$$

Substitution of (43) into (42) gives the desired equation

$$\frac{\partial^2 \bar{T}_0}{\partial \bar{r}^2} + \frac{1}{\bar{r}} \frac{\partial \bar{T}_0}{\partial \bar{r}} = \left(1 - \bar{r}^2\right) \frac{\partial \bar{T}_0}{\partial \bar{z}}$$

The solution $\bar{T}_0 = \bar{T}_0(\bar{z}, r)$ is then found for a uniform heat flux using the boundary conditions

$$T_0(0, \bar{r}) = 1, \quad \left. \frac{\partial \bar{T}_0}{\partial \bar{r}} \right|_{\bar{r}=1} = \left. \frac{\partial \bar{T}_0}{\partial \bar{r}} \right|_{\bar{r}=0} = 0$$

Kays [33] presented the results in terms of the local Nusselt number, Nu_z .

$$Nu_z = \left[\frac{1}{Nu_\infty} - \frac{1}{2} \sum \frac{e^{-\delta m^2 \bar{z}}}{Am \delta m^4} \right]^{-1}$$

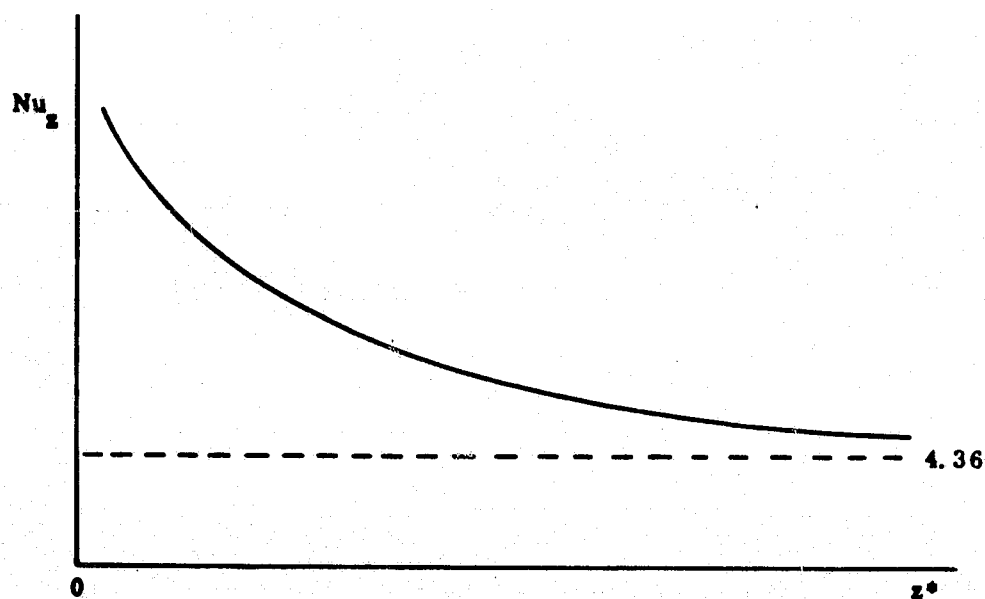
The necessary eigenvalues and constants are given below.

\underline{M}	$\underline{\gamma m^2}$	\underline{Am}
1	25.68	7.630×10^{-3}
2	83.86	2.058×10^{-3}
3	174.2	0.901×10^{-3}
4	296.5	0.487×10^{-3}
5	450.9	0.297×10^{-3}

A tabulation of Nu_z as a function of \bar{Z} is given below.

\bar{Z}	Nu_z
0	∞
0.002	12.00
0.004	9.93
0.010	7.49
0.020	6.14
0.040	5.19
0.100	4.51
∞	4.36

and is plotted as



Specific heat and thermal conductivity of water are relatively independent of temperature, but viscosity decreases markedly with temperature. Density of water, however, varies little with temperature. The Prandtl number varies with temperature in much the same manner as the viscosity. The general effect of property variation with temperature is to change the velocity and temperature profiles, thus yielding different friction and heat transfer coefficients than would be obtained if the properties were constant.

It has been found convenient to apply some correction to account for property variation to the constant property solutions or experimental data for engineering applications. Two schemes popular for correction of constant-property results are the reference temperature method and the property ratio method. The reference temperature method utilizes a characteristic temperature chosen for evaluation of the non-dimensional groups and presents certain awkwardness in internal flow applications [33]. The property ratio method for liquids involves the dimensionless ratios raised to a power such as

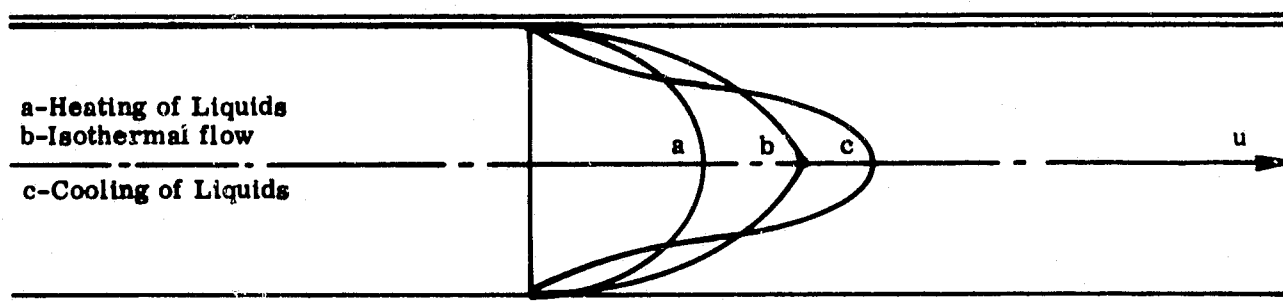
$$\frac{Nu}{Nu_{cp}} = \left(\frac{\mu_0}{\mu_m} \right)^n \quad (45)$$

Properties in the non-dimensional parameters are evaluated at local mixed mean fluid temperature, and the subscript cp refers to the constant-property solution or small temperature difference experimental result. The viscosity μ_0 is evaluated at the surface temperature, and μ_m is evaluated at the mixed mean temperature. The exponent n is a function of geometry and type of flow.

Yang [35] considered the laminar thermal-entry-length problem in a circular tube for both constant surface temperature and constant heat rate. He found that

$$n = -0.11 \quad (46)$$

was a good approximation for both cases. In either case, it is noted that the influence of viscosity ratio on the dimensionless ratios is not very great. The influence of large temperature differences on flow parameters results in the velocity distribution within a tube as shown below [36].



When flow velocity is very low, buoyancy forces may be on the same order of magnitude as the external forces due to forced circulation. Free convection may then result in mixed flow within the tube. Eckert [37] studied heat transfer in mixed flow with air in a vertical pipe, but the results were qualitative and presented primarily to call attention to the existence of phenomena of mixed flow.

The Grashof number is a dimensionless quantity used in free convection studies in relating buoyant effects to heat transfer, and is written:

$$Gr = \frac{\rho^2 \beta g D^3 \Delta T}{\mu^2} \quad (47)$$

where D is the inside diameter and ΔT is the temperature gradient.

For mixed flow within a horizontal tube, free convection would increase the heat transfer to the upper surface and decrease the heat transfer to the lower surface [38].

CONDUCTION

The general heat conduction equation in a cylindrical coordinate system is

$$\frac{\partial^2 T}{\partial r^2} + \frac{1}{r} \frac{\partial T}{\partial r} + \frac{1}{r^2} \frac{\partial^2 T}{\partial \phi^2} + \frac{\partial^2 T}{\partial z^2} + \frac{q'''}{\kappa} = \frac{1}{\alpha} \frac{\partial T}{\partial \theta} \quad (48)$$

For steady state conditions and no heat generation, we obtain the Laplace equation:

$$\frac{\partial^2 T}{\partial r^2} + \frac{1}{r} \frac{\partial T}{\partial r} + \frac{1}{r^2} \frac{\partial^2 T}{\partial \phi^2} + \frac{\partial^2 T}{\partial z^2} = 0 \quad (49)$$

Two simple solutions will be presented first: one for a radial temperature distribution only, and another for an axial temperature distribution. For a radial variation only in a hollow tube of inner radius r_1 and outer radius r_2 , we can set

$$\frac{\partial^2 T}{\partial \phi^2} = \frac{\partial^2 T}{\partial z^2} = 0$$

in equation (49) and obtain

$$\frac{d^2T}{dr^2} + \frac{1}{r} \frac{dT}{dr} = 0$$

or

$$\frac{1}{r} \frac{d}{dr} \left(r \frac{dT}{dr} \right) = 0$$

Integration gives

$$T = T_1 - \frac{T_1 - T_2}{\ln r_2/r_1} \ln \frac{r}{r_1} \quad (50)$$

Thus, the temperature in a hollow circular cylinder is a logarithmic function of the radius.

For an axial temperature distribution only, we obtain

$$\frac{d^2T}{dz^2} = 0$$

which integrates to

$$\frac{dT}{dz} = \text{constant} \quad (51)$$

and

$$T = \left(\frac{T_2 - T_1}{L} \right) z + T_1 \quad (52)$$

RADIATION

The emittance of the tube surface and the liner surface was uniform and high due to the use of a highly emissive black paint which was sprayed evenly onto the materials. The spectral emittance of the paint was approximately 0.90 for all relevant wavelengths. Since the emittance is relatively independent of wavelength, the surface may be considered to be gray. The nature of the paint and the technique of

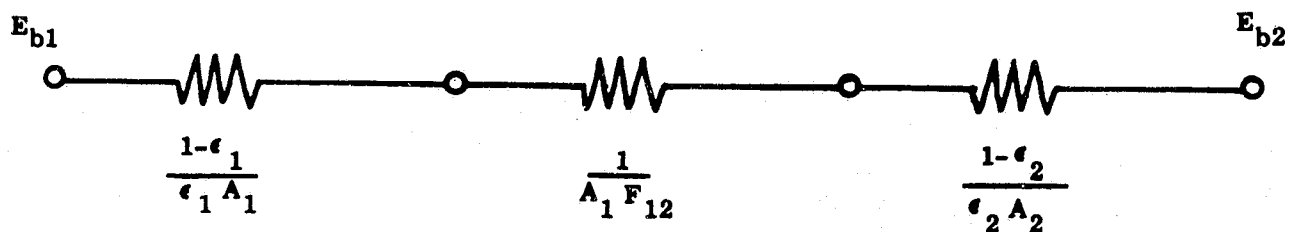
application combined to give what is assumed to be a diffuse surface. Temperature dependence is minimal, although most paints show a decrease in emittance with an increase in temperature [39].

For a steady-state condition, the rate of energy loss by radiation in this experiment is equal to the energy gain by conduction and convection.

$$q''_{\text{Rad.}} = q''_{\text{cond.}} + q''_{\text{conv.}} \quad (53)$$

The radiation will then become the governing mode of heat transfer since it is the primary means by which energy can be transferred from the tube.

Radiation heat transfer from the tube to the surrounding liner may be calculated using the network representation described by Wiebelt [39] and shown below.



The net heat exchange may be written

$$q_{1 \rightarrow 2} = \frac{\sigma(T_1^4 - T_2^4)}{\frac{1-\epsilon_1}{\epsilon_1 A_1} + \frac{1}{A_1 F_{12}} + \frac{1-\epsilon_2}{\epsilon_2 A_2}} \quad (54)$$

where F_{12} is the configuration factor or view factor. A heat transfer rate of 108 Btu/hr. was calculated for the exchange between a 1-inch-diameter tube, four feet in length, at 50 F to the cryogenic liner at

-300 F with a configuration factor of 1.0 and a 0.9 emittance for both surfaces.

Radiation shielding may be provided by insertion of multiple layers of highly reflective material between the radiating members. Aluminized mylar foil with a thickness of 0.0005 inch was crinkled to reduce heat conduction and wrapped around the radiating item. Calculations showed that radiation was reduced to 0.1 percent when 50 layers of crinkled foil was used.

The determination of the configuration factor can be a difficult and complex problem. If, however, the radiating object cannot see itself and is completely surrounded by a surface at a much lower temperature, the configuration factor approaches unity. Surfaces at higher temperatures which are viewed by the test specimen must be highly reflective to reduce their effect.

Radiant exchange between the elements of a pair of concentric cylinders of equal length L , and inner and outer radii r and R , is obtainable from the relation giving the configuration factor from the inner surface of the outer cylinder to the inner cylinder [40].

$$F_{21} = \frac{r}{R} - \frac{1}{\pi} \frac{r}{R} \cos^{-1} \left[\frac{(L/R)^2 + (r/R)^2 - 1}{(L/R)^2 - (r/R)^2 + 1} \right] + \quad (55)$$

$$\frac{1}{2\pi} \left[\left(\frac{L}{R} + \frac{R}{L} + \frac{r^2}{RL} \right)^2 - \left(\frac{2r}{L} \right)^2 \right]^{1/2} \cos^{-1} \left[\frac{(L/R)^2 + (r/R)^2 - 1}{(L/R)^2 - (r/R)^2 + 1} \cdot \frac{r}{R} \right] +$$

$$\frac{1}{2\pi} \left(\frac{L}{R} - \frac{R}{L} + \frac{r^2}{RL} \right) \sin^{-1} \frac{r}{R} - \frac{1}{4} \left(\frac{L}{R} + \frac{R}{L} - \frac{r^2}{RL} \right)$$

The reciprocity theorem states that

$$A_1 F_{12} = A_2 F_{21} \quad (56)$$

where A_1 and A_2 are the surface areas of the tube and liner respectively, and F_{12} is the configuration factor from the tube to the liner. Substitution of appropriate surface areas yields a numerical value for F_{12} .

CHAPTER V.

TEST SPECIMENS

In order to verify the modeling criteria developed in Chapter III, a series of test models were fabricated of both high and low thermal conductivity materials. A 1.0-inch outside diameter (O.D.) type 304 stainless steel tube 48 inches in length was used as the prototype or full-size low thermal conductivity specimen. Three scale models were then fabricated from 0.75-inch O.D., 0.50-inch O.D., and 0.25-inch O.D. type 304 stainless steel tubing. Their scale lengths were 41.568 inches, 33.936 inches, and 24.000 inches, respectively. A 1.0-inch O.D. type 6061 aluminum tube 48 inches in length was used as the prototype high thermal conductivity specimen. Three scale models were also fabricated from 0.75-inch O.D., 0.50-inch O.D., and 0.25-inch O.D. type 6061 aluminum tubing to the same lengths as those of the stainless steel models.

The scale models were fabricated on a lathe by turning down the O.D. of the tube to the desired wall thickness based upon the modeling criteria given in Chapter III and the average wall thickness of the 1.0-inch O.D. prototype. According to the criteria, the wall thickness scales as the diameter. Thus, the wall thickness of the 0.75-inch O.D. model must be 0.75 the wall thickness of the 1.0-inch O.D. prototype. Likewise, wall thickness of the 0.50-inch model must be 0.50 the wall thickness of the 1.0-inch O.D. specimen, and 0.25-inch O.D. model must have a wall thickness that is 0.25 the wall thickness of the 1.0-inch O.D. prototype. Necessarily then, the first step was to measure

accurately the wall thickness of the 1.0-inch O.D. at several points to obtain an average dimension. This was done with a telescoping gage and a micrometer with accuracy certified by NASA. Scaled wall thicknesses were then calculated as described above. The wall thickness of each size tubing was selected from available sizes to be slightly larger than the desired wall thickness that was anticipated. For example, the stainless steel tubing was ordered with 0.120-inch wall thickness for the 1.0-inch O.D. specimen, and a wall thickness of 0.65 inch was ordered for the 0.50-inch O.D. tubing. The outside diameter of the models was then turned down on a lathe to yield the desired wall thickness. A short lip of material (Figure 1) was left to the original O.D. to facilitate machinability and allow connection of the model with common fittings during testing. Because of the selection of nearest largest-size tubing, this lip was usually only 0.010 inch larger than the turned-down dimension and thus can be considered to contribute little, if any, thermal effect to the temperature measurement near the ends of the tubing. Dimensions of the eight specimen tubes are given in Tables 1 and 2.

In order to insulate thermally the specimen tube from the tubing before and after itself, nylon Swagelok unions were used as connections on each end. Teflon front ferrules were used in each fitting to achieve better sealing characteristics of the connection. Additionally, to insure a smooth flow within the tube at the leading end, a teflon insert was fitted within the nylon union and its inside diameter was matched to the inside diameter of the respective tubing.

It was then necessary to fabricate an entrance tube of proper length from the same stock as that of the test specimen so a desirable

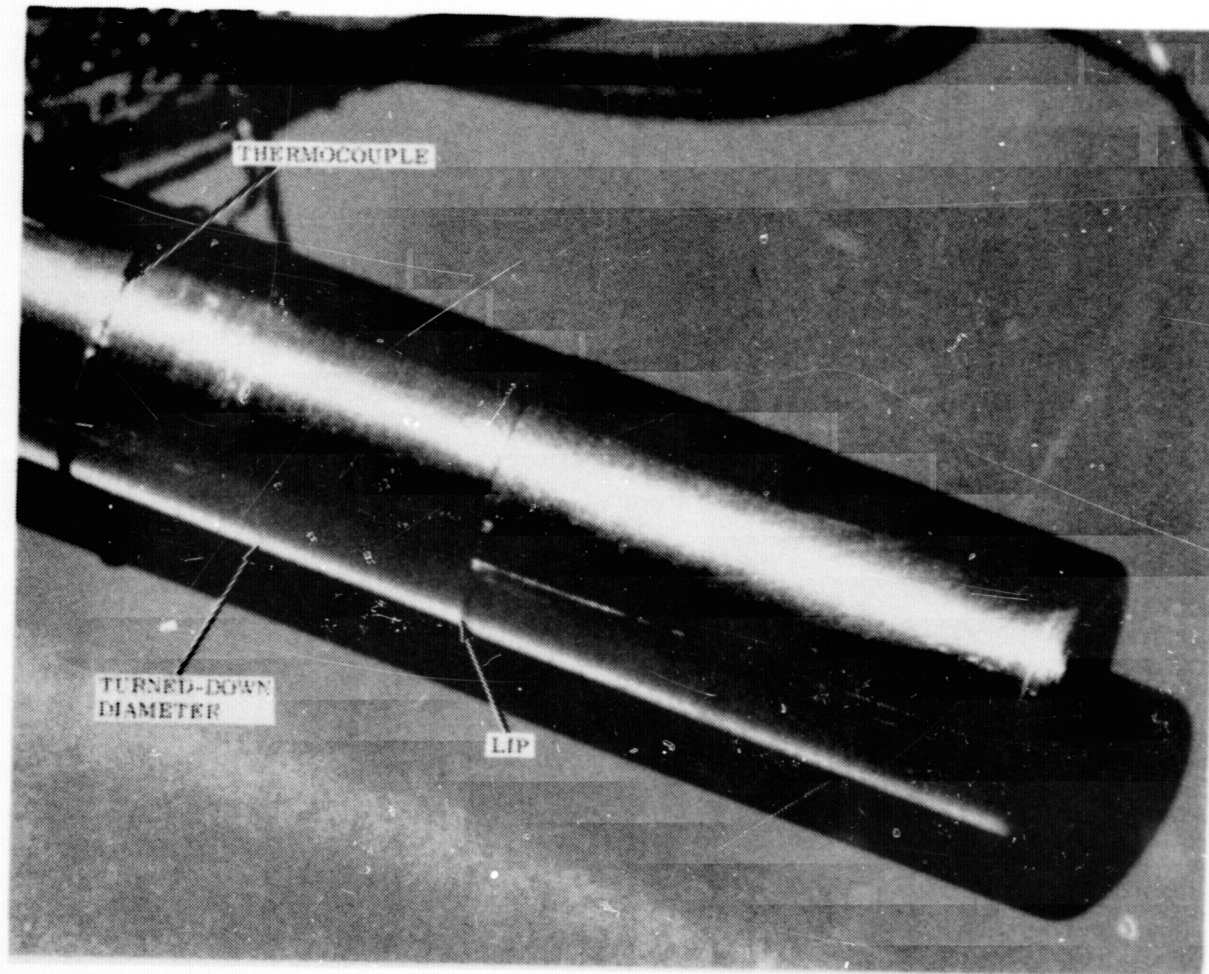


Figure 1. Specimen Tube End

TABLE 1
STAINLESS STEEL SPECIMEN TUBE DIMENSIONS*

<u>Nominal O.D.</u>	<u>Actual O.D.</u>	<u>Actual I.D.</u>	<u>Nominal Wall Thickness</u>	<u>Turn-Down Wall Thickness</u>	<u>Overall Length</u>	<u>Lip Length</u>
1.000	0.9985	0.7629	0.120	0.1178	48.000	1.250
0.750	0.7524	0.5625	0.095	0.0884	41.568	1.000
0.500	0.5030	0.3852	0.065	0.0589	33.936	1.000
0.250	0.2502	0.1913	0.035	0.0295	24.000	0.750

* All dimensions are shown in inches.

TABLE 2
ALUMINUM SPECIMEN TUBE DIMENSIONS*

<u>Nominal O.D.</u>	<u>Actual O.D.</u>	<u>Actual I.D.</u>	<u>Nominal Wall Thickness</u>	<u>Turn-Down Wall Thickness</u>	<u>Overall Length</u>	<u>Lip Length</u>
1.000	1.001	0.8365	0.083	0.082	48.000	1.250
0.750	0.750	0.622	0.065	0.0615	41.568	1.000
0.500	0.502	0.4045	0.049	0.0410	33.936	1.000
0.250	0.2505	0.1945	0.028	0.0205	24.000	0.750

* All dimensions are shown in inches.

fluid flow profile or velocity boundary layer within the tube could be established before entry into the test specimen. The inside diameter of the entrance tube, front fitting, and test specimen were then the same; thus avoiding any discontinuities that could induce undesirable turbulence or mixing within the flowing fluid. The length of the entrance tube for the establishment of laminar flow is a function of both Reynolds number and tubing size according to the relation

$$l = \left(\frac{d}{20} \right) Re$$

where l was the required tube length, d was the tube diameter, and Re was the dimensionless Reynolds number. The Reynolds number could be written

$$Re = \frac{\rho V d}{\mu}$$

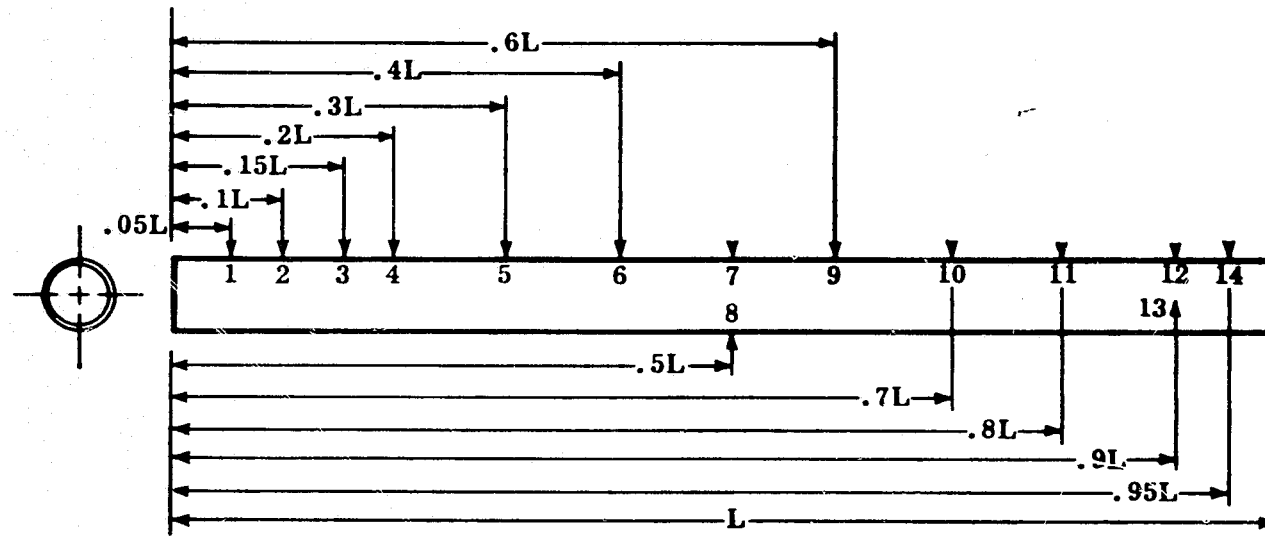
where ρ was the fluid density, V was the velocity, d was the tube's inside diameter, and μ was the fluid viscosity.

To be conservative, this length was determined for a Reynolds number of 2000 although it was anticipated that flow rates would be considerably lower. The 1.0-inch O.D. tubing had an entrance tube length of 100 inches. The 0.75-inch O.D. entrance tube was 75 inches in length. Similarly, the 0.50-inch O.D. entrance tube was 50 inches long, while the 0.25-inch entrance tube was 25 inches in length. Plug gages were fabricated from brass or nylon rods and used to insure alignment.

It was necessary to attach thermocouples to the exterior surface of the specimen tube in order to determine thermal similarity between prototype and model. Fourteen 30-gage, copper-constantan thermocouples were fabricated and spot welded to each specimen tube at certain

locations (Figure 2). Leads to each thermocouple were wrapped circumferentially around the specimen to minimize lead wire measurement error. The tubes were then spray painted with two thin coats of flat black paint (Velvet coating 101-C10 by 3M) to insure uniform and efficient radiative heat transfer. Thermocouple lead wires were then painted with a bright aluminum paint to a distance at least six inches from the tube to reduce lead wire radiation loss and subsequent measurement error.

Energy necessary to spot weld thermocouples to the stainless steel tube was considerably less than that required for the aluminum tube. In addition, constantan wire required less power than copper. Copper wire required 12 to 15 watt-seconds for stainless tubes, while constantan wire needed only four to five watt-seconds for a satisfactory weld. Copper wire on aluminum tubes required 80 to 95 watt-seconds, and the constantan wire used 15 to 25 watt-seconds of energy for a good weld. It was also noted that the smaller diameter tubes required slightly more energy for a satisfactory spot weld than did the larger diameter tubes. The small welder and setup used on the stainless steel tubes and the welding station for the 1-inch tube is shown in Figure 3. Attachment of thermocouples to the 1-inch stainless steel tube is shown in Figure 4. A larger welder was used to attach the thermocouples to the aluminum tubes. Use of this equipment for the attachment of thermocouples to the 1-inch aluminum tube is shown in Figure 5. Three unpainted stainless steel specimens and their plug gages are shown in Figure 6, The four prepared stainless steel specimen tubes are depicted in Figure 7, and the four prepared aluminum specimen tubes and their plug gages are shown in Figure 8.



Thermocouple Number	TUBE LENGTH DIMENSION*												
	L	.05L	.10L	.15L	.2L	.3L	.4L	.5L	.6L	.7L	.8L	.9L	.95L
		1	2	3	4	5	6	7 & 8	9	10	11	12 & 13	14
Tube Diameter													
1.0	48.000	2.40	4.80	7.20	9.60	14.40	19.20	24.0	28.8	33.6	38.4	43.2	45.6
.75	41.568	2.078	4.157	6.235	8.314	12.470	16.627	20.784	24.941	29.098	33.254	37.411	39.490
.50	33.936	1.697	3.394	5.090	6.787	10.181	13.574	16.968	20.362	23.755	27.149	30.542	32.239
.25	24.000	1.20	2.40	3.60	4.80	7.20	9.60	12.00	14.40	16.80	19.20	21.60	22.80

* All dimensions are shown in inches.

Figure 2. THERMOCOUPLE LAYOUT ON SPECIMEN

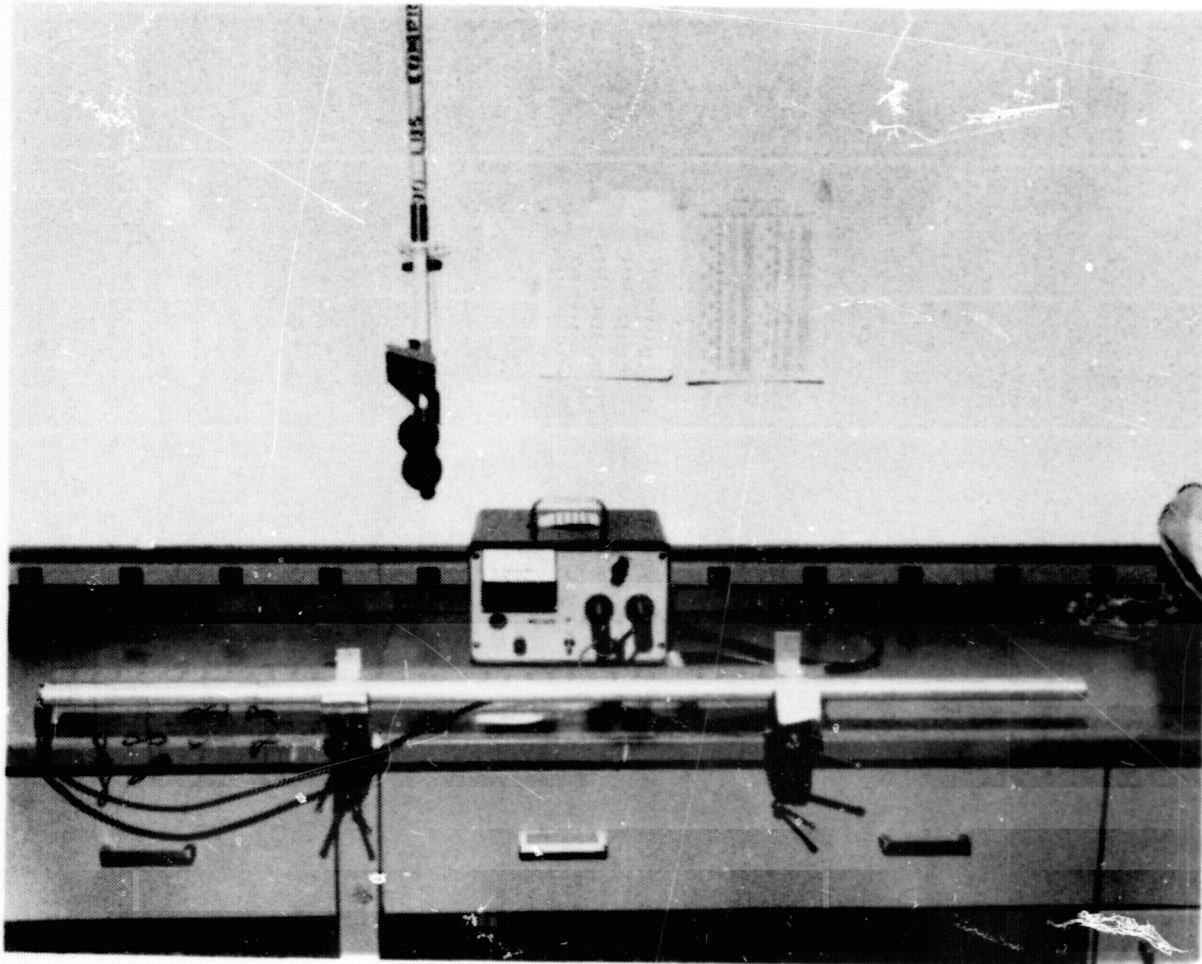


Figure 3. Welding Station with Specimen Tube

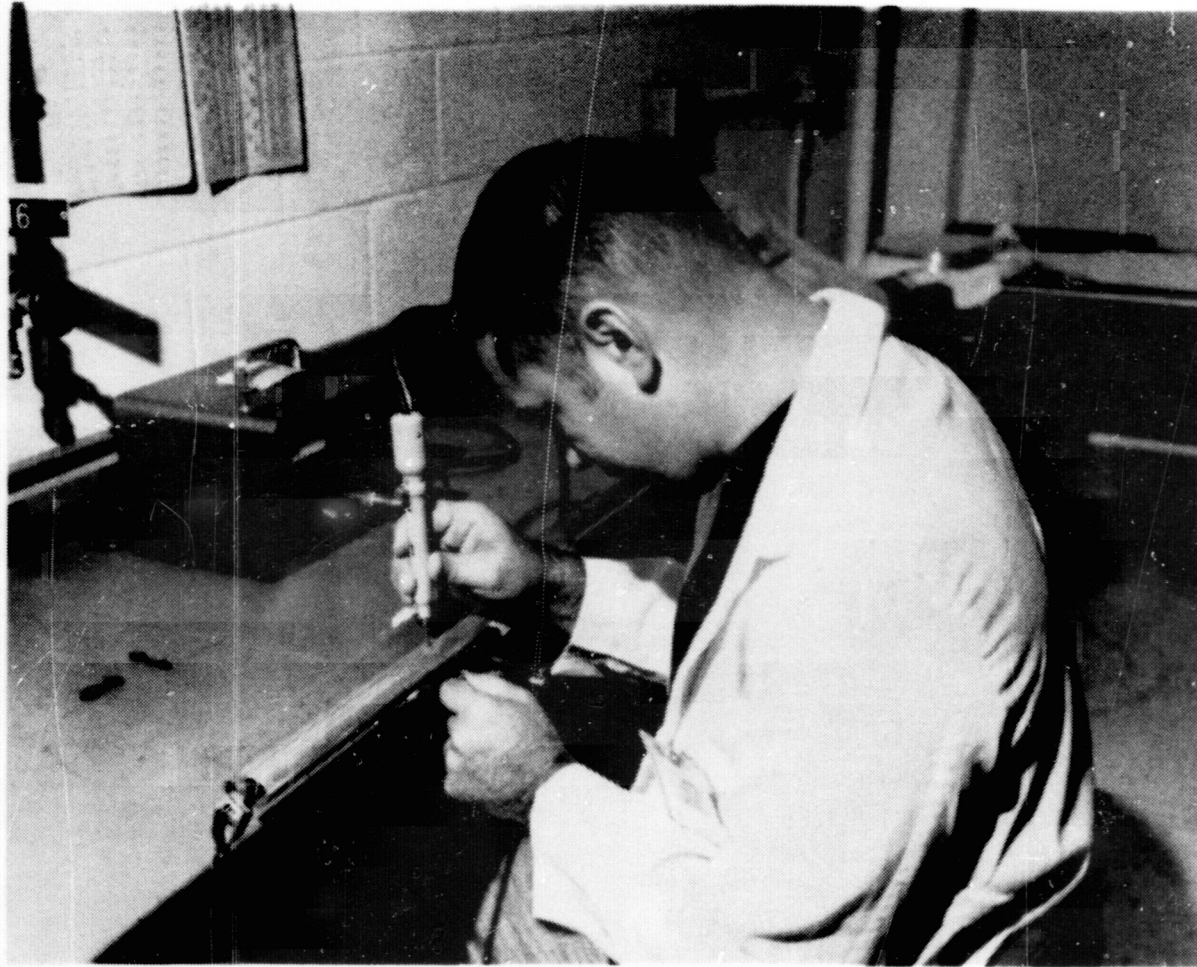


Figure 4. Thermocouple Attachment to Stainless Steel Specimen Tube

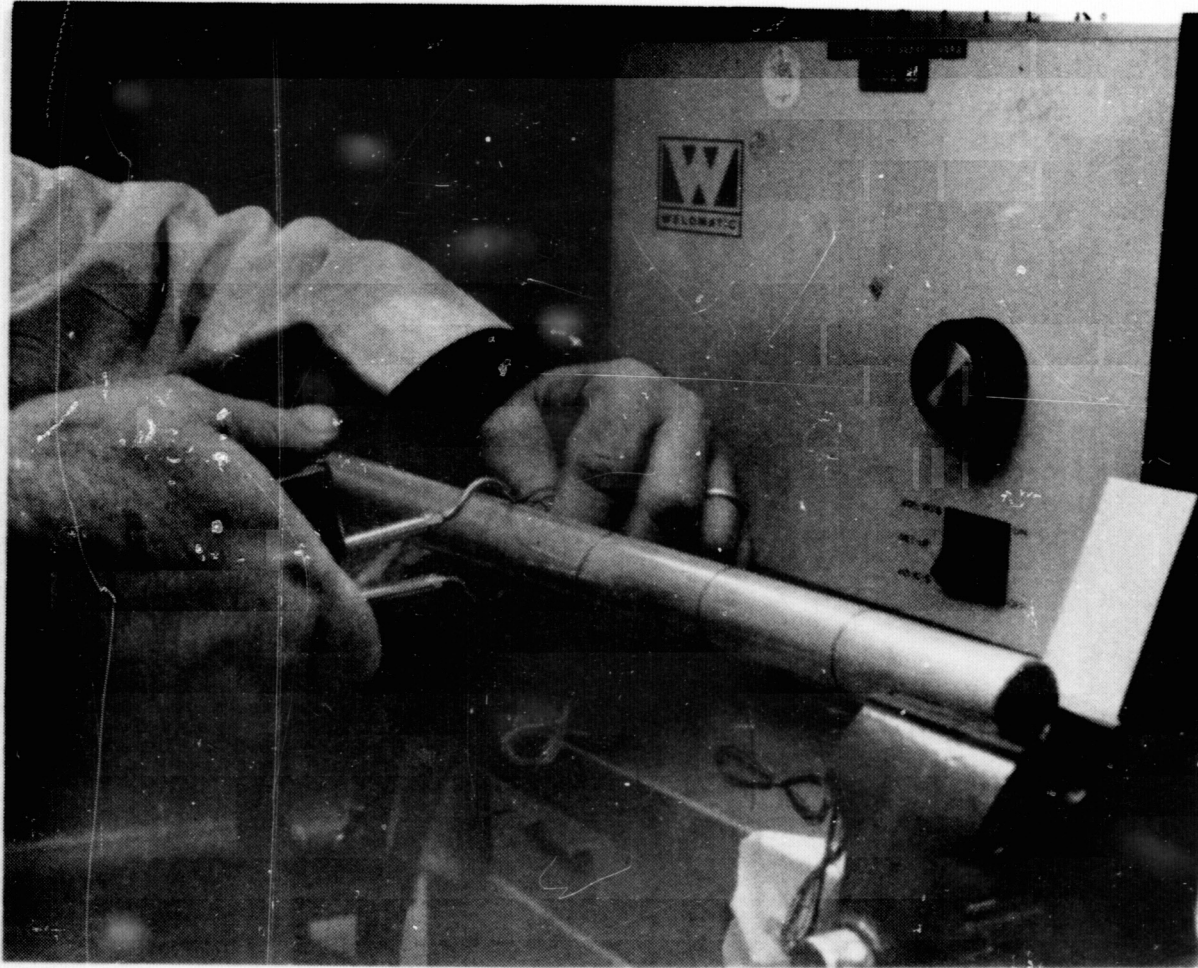


Figure 5. Thermocouple Attachment to Aluminum Specimen Tube

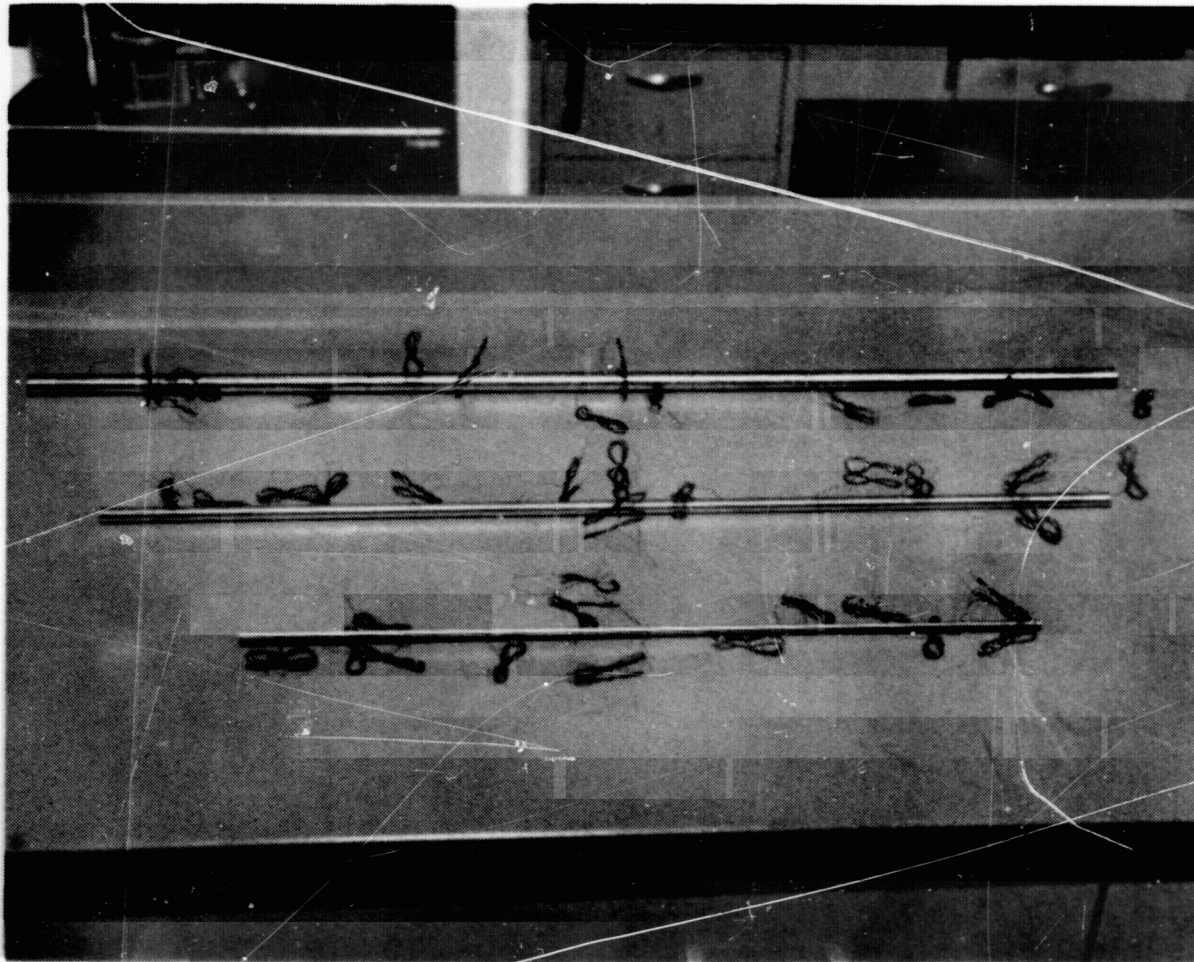


Figure 6. Unpainted Stainless Steel Specimen Tubes



Figure 7. Stainless Steel Test Specimen Tubes and Plug Gages

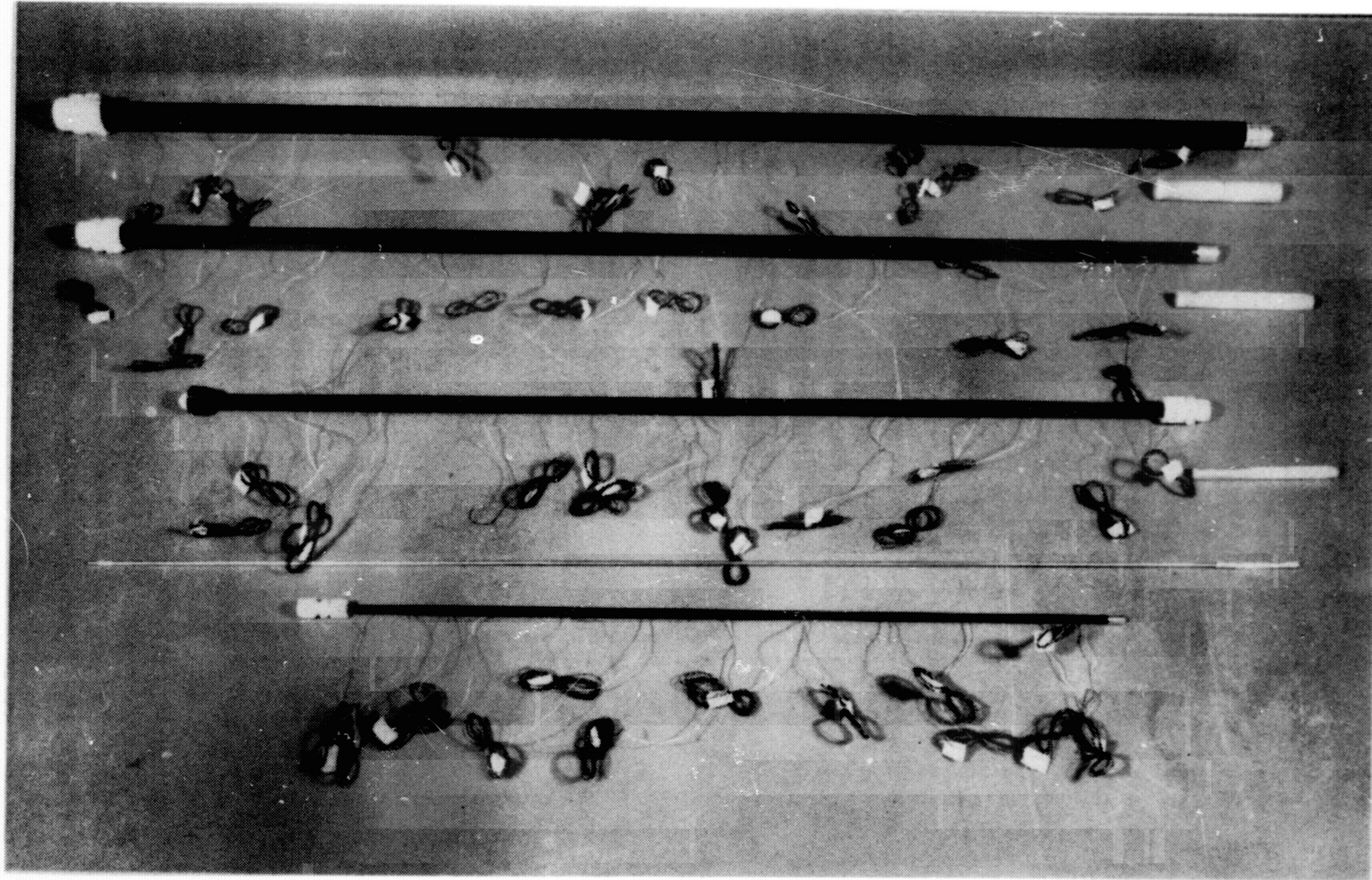


Figure 8. Aluminum Test Specimen Tubes and Plug Gages

CHAPTER VI.

EXPERIMENTAL APPARATUS

The experimental apparatus can be divided into eight basic sections: the vacuum and cryogenic system, the tubular system, the instrumentation and recording system, the inlet temperature control system, the flow pressurization system, the flow evacuation system, the flow measuring and control system, and the flow collection system. A block diagram of these systems is shown in Figure 9, and a schematic diagram of the pressurization and flow systems is given in Figure 10. A complete list of all experimental equipment is presented in Appendix A.

VACUUM AND CRYOGENIC SYSTEM

Prototypes and models described in Chapter V were fabricated for test inside a space simulation chamber that provided the necessary low temperature, high vacuum environment for accurate simulation of energy exchange between the tubes and their surroundings. The Murphy-Miller high altitude test chamber (Figure 11) is a standard piece of test equipment located at the National Aeronautics and Space Administration's (NASA) Mississippi Test Facility. This chamber was constructed of carbon steel with an interior 48 inches in diameter, 60 inches long, and had a raised shelf four inches above the bottom. The chamber was evacuated through one end, and a full-width door across its opposite end provided easy access to the interior. Instrumentation feedthroughs in the chamber wall permitted direct connection to the 16 thermocouples; fluid feedthroughs introduced liquid nitrogen to the cryogenic liner which is shown in Figure 12.

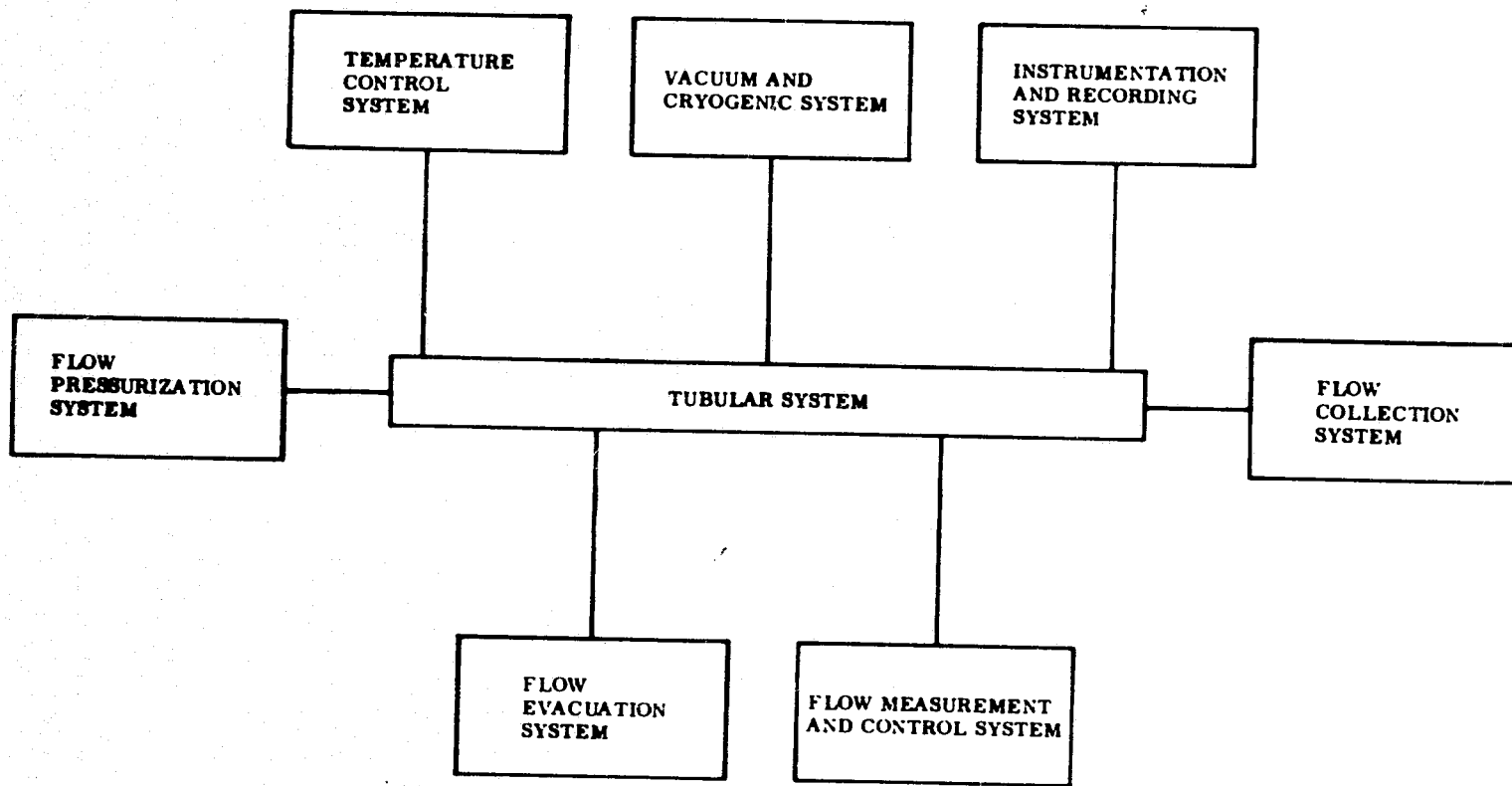


Figure 9. Experimental Systems Block Diagram

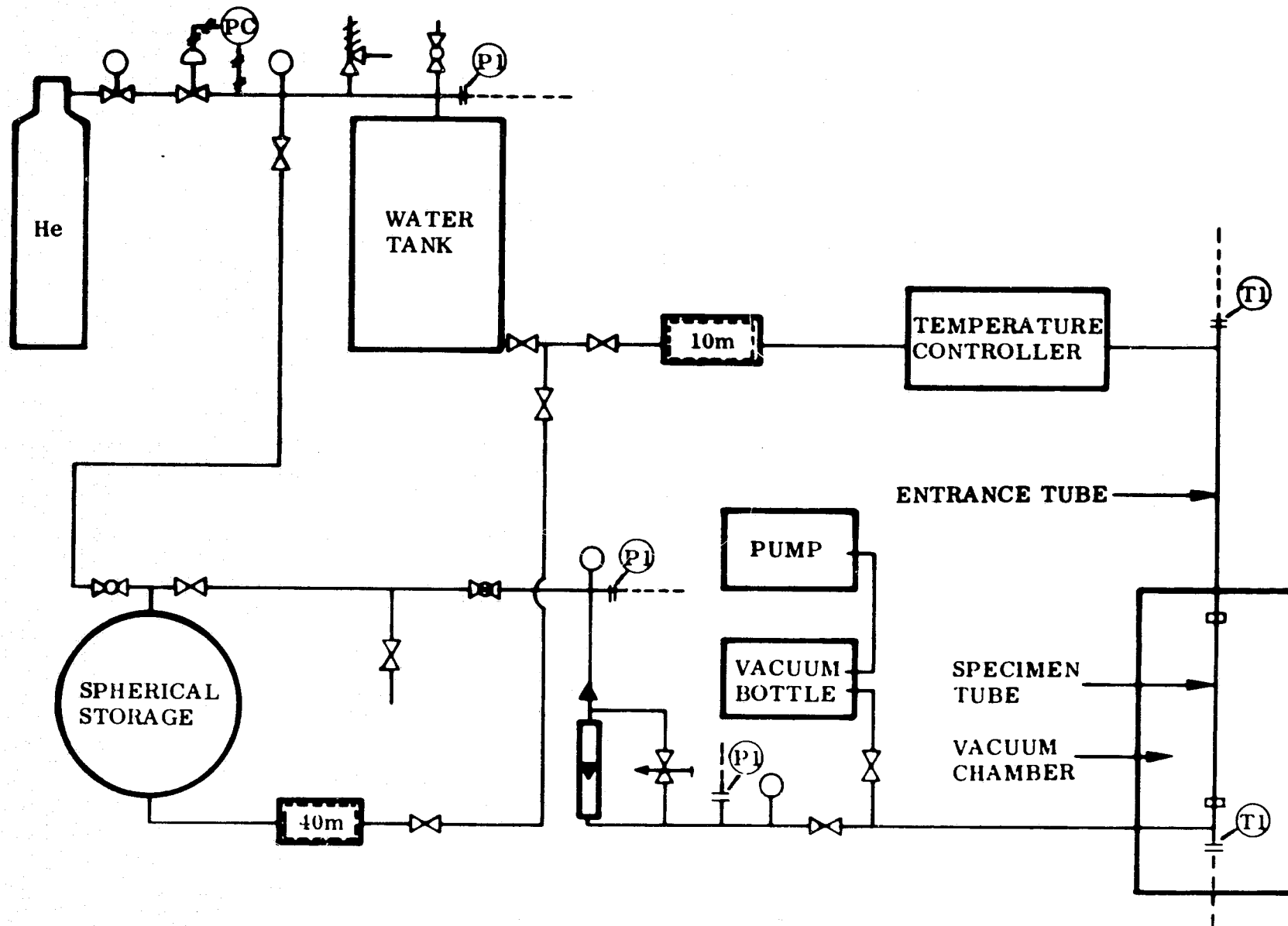


Figure 10. Pressurization and Flow Systems Schematic Diagram

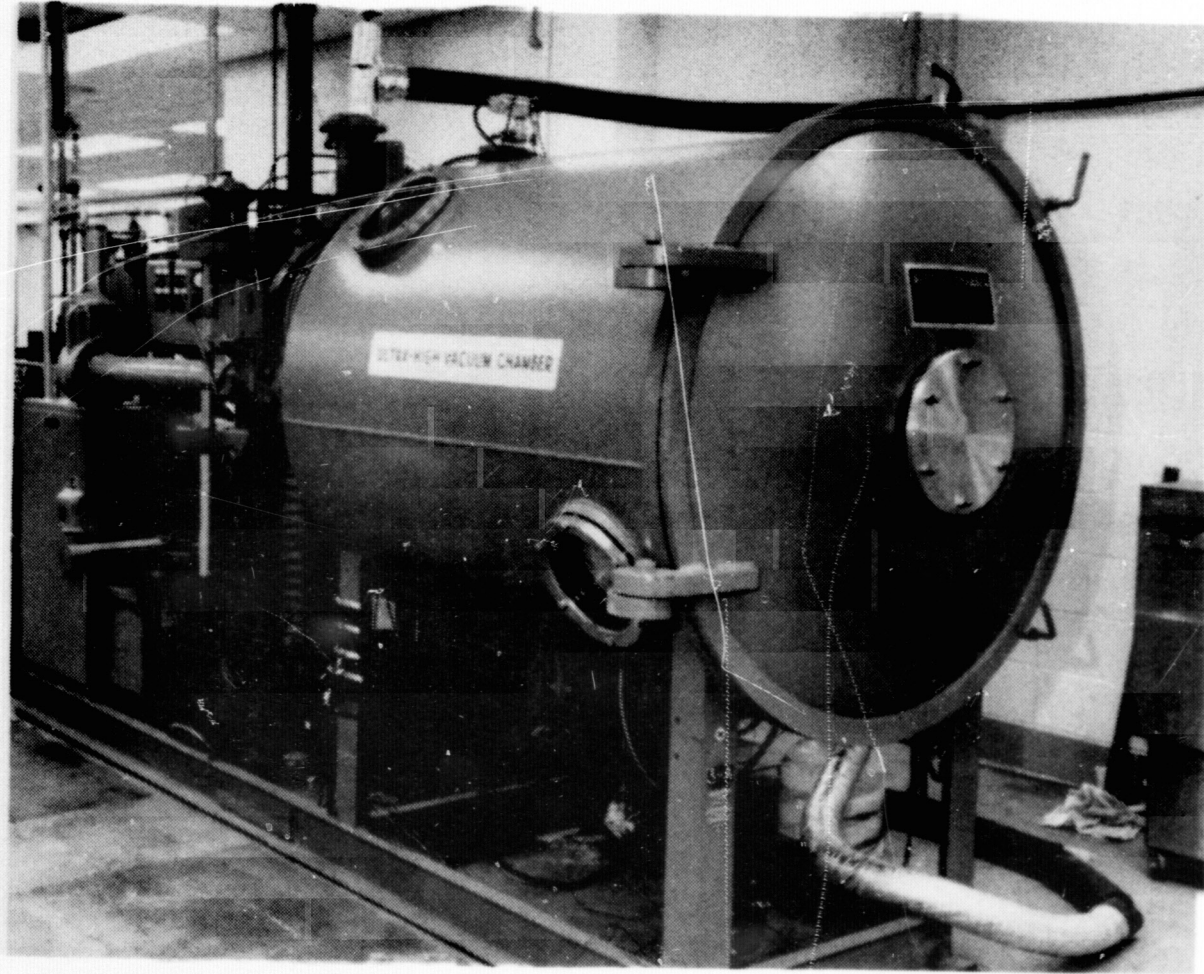


Figure 11. Vacuum Chamber

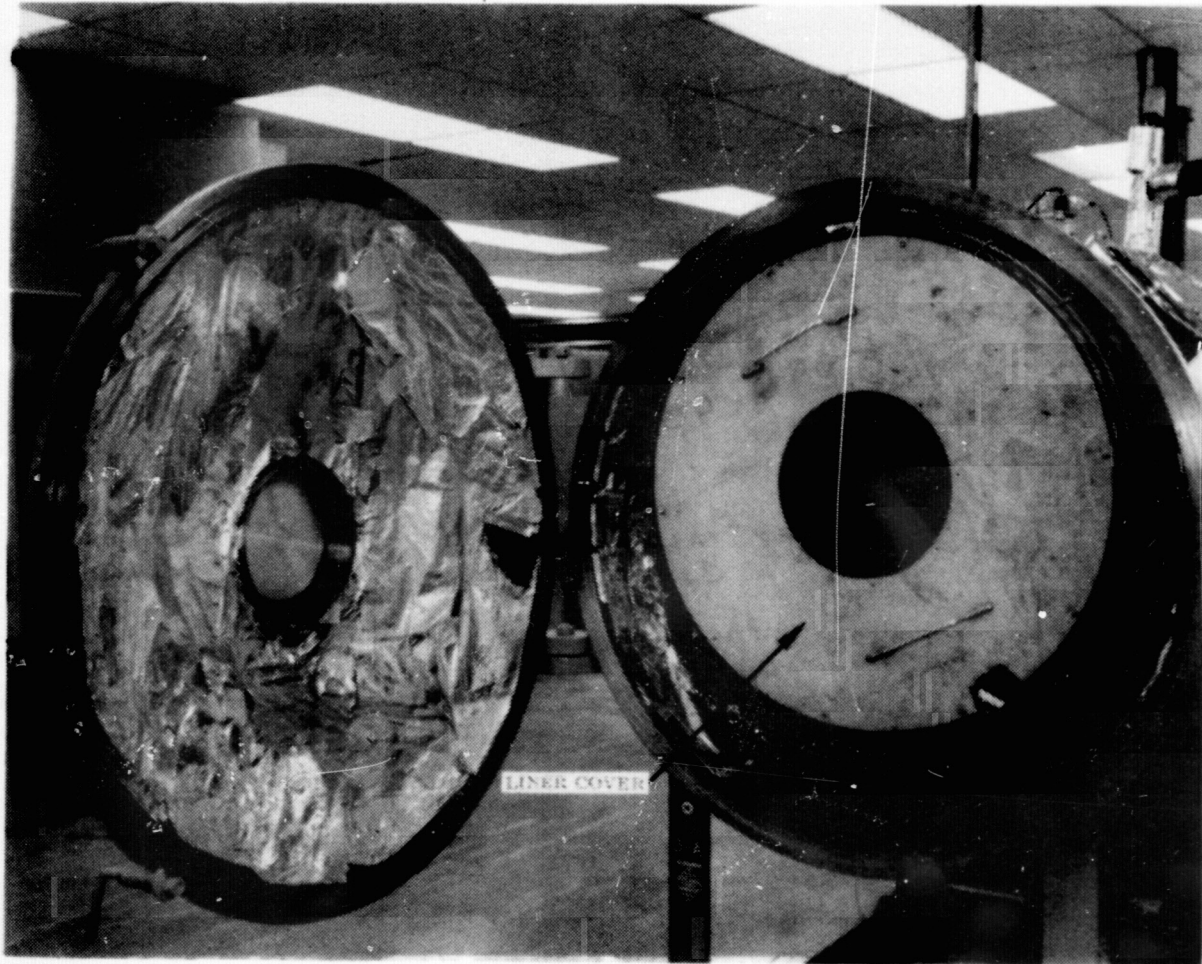


Figure 12. Cryogenic Liner

This liner was designed to fit within the chamber like a sleeve and simulate the low temperature environment of outer space. The liner shell was constructed of stainless steel with interior dimensions 54 inches long and 38 inches in diameter. The shell which carried the liquid nitrogen was spirally wrapped with 0.625-inch outside diameter (O.D.) copper tubing held to the outside liner surface with threaded rod. At one end of the liner was an optically tight baffle, and at the other was a removable flange. A Cenco liquid level controller was used in conjunction with a solenoid valve to control nitrogen flow and maintain the necessary level of liquid nitrogen within the liner tubing. The inner wall of the liner was coated with 3M Velvet Coating 101-C10 black paint to insure a surface with high and uniform values of emittance. The outer wall of the liner and the inner wall of the chamber were covered with aluminum foil to reduce the heat transfer between the two surfaces. The liner was supported on four adjustable legs to minimize heat conduction from the outer chamber wall to the liner. Installation of fitted covers to the liner wall reduced heat transfer through the chamber port-holes. During operation the inner wall of the liner normally reached -290 F, while its outer wall read -275 F. The vacuum system is described in more detail in Appendix B.

Two 100-gallon insulated dewars filled with liquid nitrogen from an outside storage facility supplied the cryogenic system. External to each dewar, a heat exchanger provided the necessary pressure to force the liquid nitrogen into the cryogenic liner. Pressure was normally maintained at 20 to 40 psig during the experiment.

TUBULAR SYSTEM

The tubular system consisted of the specimen tube, its entrance tube, and the flex hoses used to connect the tubes to the other systems in this experiment. Dimensions and fabrication of the specimen and entrance tubes were discussed in Chapter V. Flexible hoses used to connect the systems were made of stainless steel lined with teflon and had an inside diameter of 0.5 inch.

The specimen tube under test was suspended horizontally from the top of the chamber liner on two thin nylon cords very long in comparison to their diameter to minimize conduction losses. Figure 13 shows the specimen tube suspended within the chamber. Fluid flow was into the exposed end of the tube and out of the opposite end at the far end of the chamber. A short fitting at the exit end of the tubing permitted a thermocouple measurement of the fluid temperature as it left the instrumented specimen tube. Here fluid flowed through a flexible hose insulated with radiation shielding made of 40 wraps of crinkled 0.001-inch aluminized mylar to the exit port on the chamber. A similar radiation shield was placed around the entrance tube between the chamber door and the front nylon coupling to the specimen tube. Cajon Ultra-Torr fittings were used to vacuum seal entrance and exit tubes at the chamber flanges on the door and exit port. These fittings contained an o-ring that was squeezed around the tube when the fitting was tightened. A thermocouple gland and stainless steel tee were attached to the front of the entrance tube to permit a fluid temperature measurement before the working fluid entered the specimen tube. A metal Swagelok union fitting with nylon ferrules at the front end of the entrance tube facilitated introduction of the plug gage into the tubes for alignment purposes.

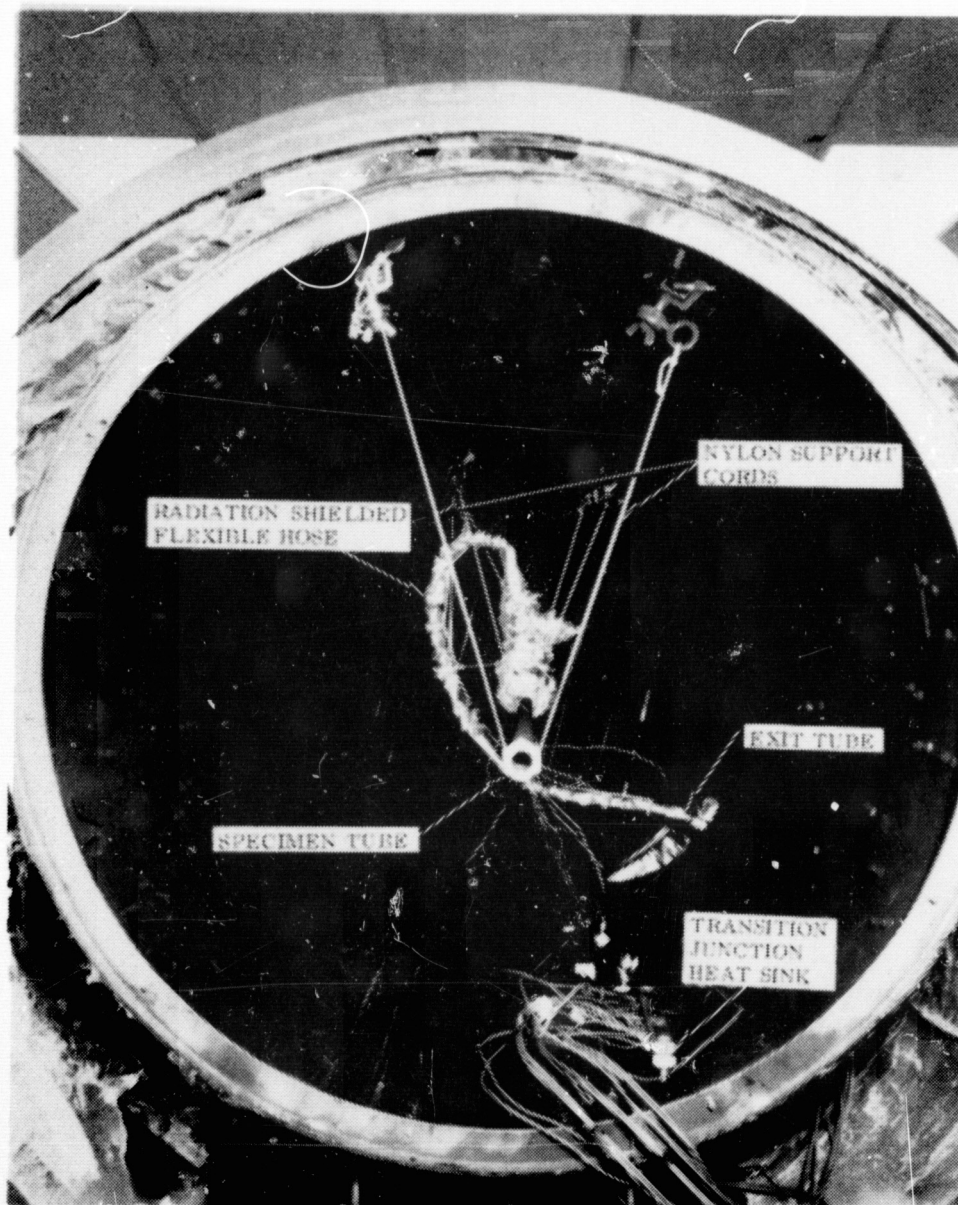


Figure 13. Specimen Tube Suspended
within Vacuum Chamber

INSTRUMENTATION AND RECORDING SYSTEM

Fourteen 30-gage copper-constantan thermocouples were used to measure the temperature distribution along the specimen tube. Additionally, one was used to measure the temperature on the inside wall of the cryogenic liner, and another one was used to measure the exit fluid temperature as previously described.

These 16 thermocouples were connected to 12-gage thermocouple lead wires with transition junctions where the larger thermocouple lead wire was inserted through the vacuum chamber wall by means of four vacuum feedthroughs. Glyptol, an insulating varnish manufactured by General Electric, was used to seal around the lead wires within and outside the vacuum feedthroughs. The vacuum feedthroughs are shown in Figure 14. Outside the chamber, thermocouple lead wires were connected from the feedthroughs to an ice-bath reference junction and then to strip-chart recorders located in an adjacent recording room. Constantan thermocouple lead wires were connected to copper wires, insulated with General Electric RTV silicone sealant at the reference junction, and placed inside an insulated dewar filled with a crushed ice and water mixture.

Figure 15 shows the Leeds and Northrup multipoint strip-chart recorder which was well suited to this experiment. This recorder sampled each of 12 thermocouples for 10 seconds, amplified its signal through one common amplifier, and printed the appropriate thermocouple number at the temperature location on the continuously moving strip chart. These features permitted fast calibration, easy monitoring, and simple data reduction. The 10-second sampling time presented no problem to a steady-state analysis since the recorder cycled through all 12 thermocouples every two minutes.

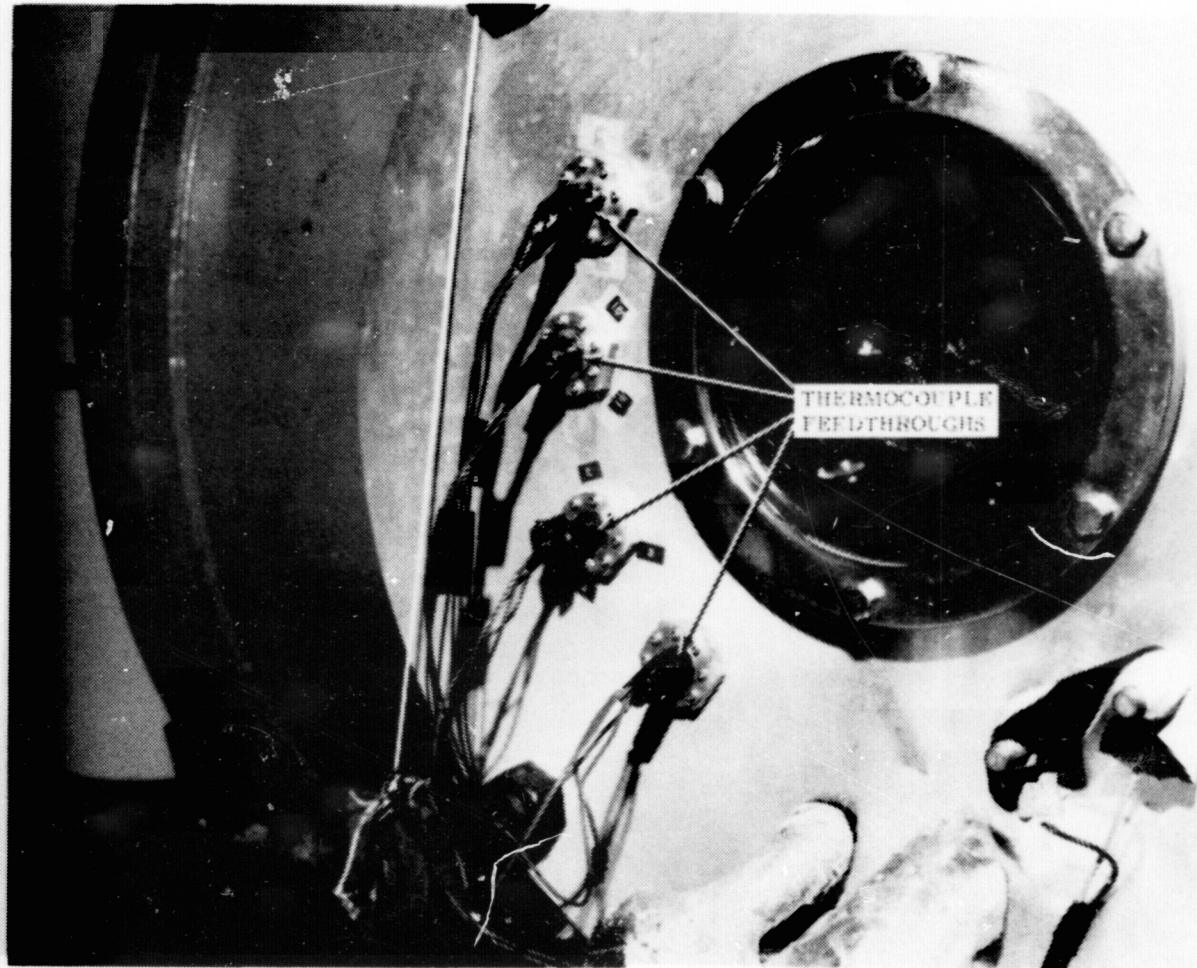


Figure 14. Thermocouple Vacuum Feedthroughs

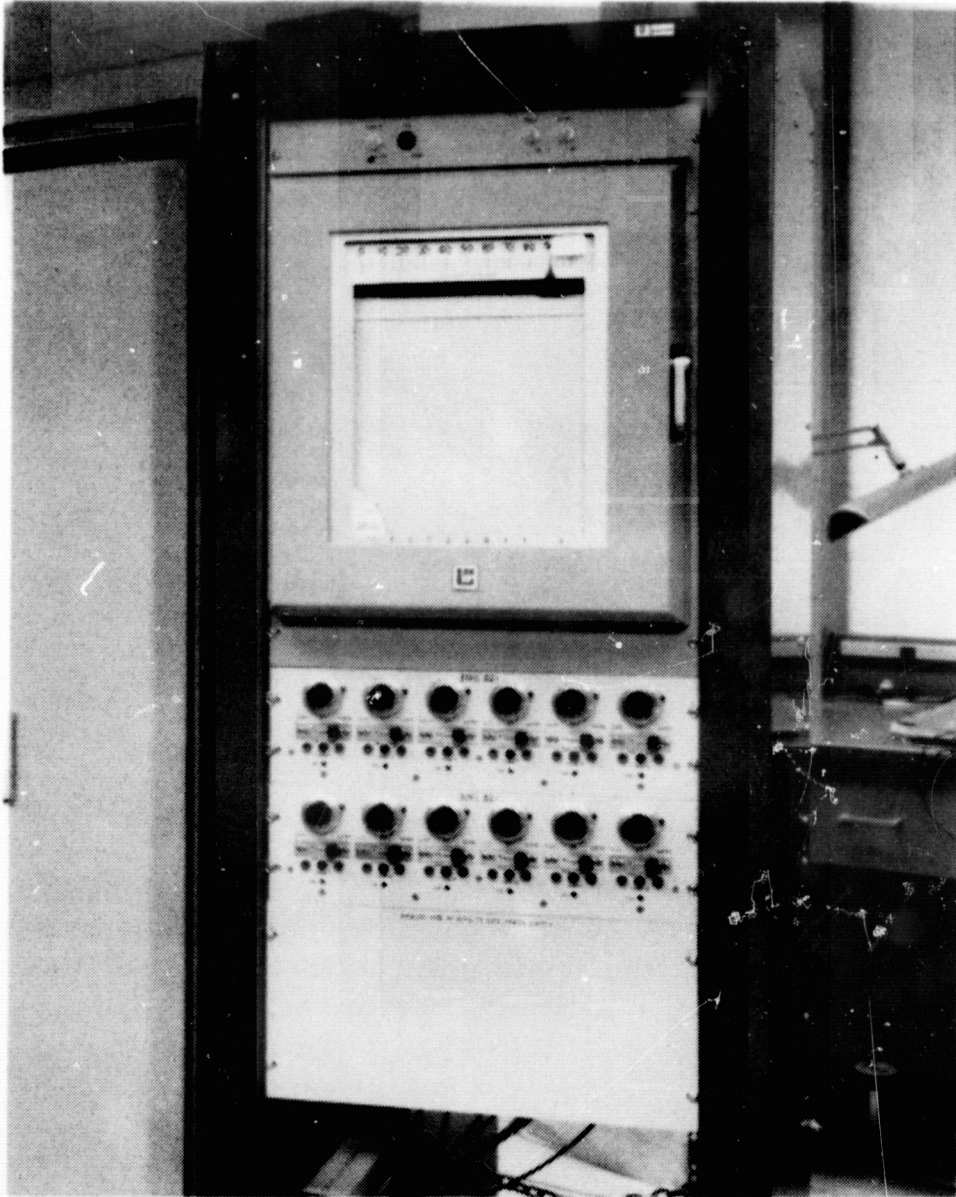


Figure 15. Multipoint Strip-chart Data Recorder

Figure 16 shows the bank of eight Bristol strip-chart recorders used in addition to the multipoint to record data such as tube temperatures, water temperature, liner temperature, helium ullage pressure, and water pressure.

Strip-chart recorders were calibrated before each experiment with a Leeds and Northrup Type 8690 precision potentiometer.

INLET TEMPERATURE CONTROL SYSTEM

Consisting of a heating chamber and an electronic temperature controller, the temperature control system was essentially an oil bath used to calibrate resistance thermometers. The system, a Rosemount Thermotrol Model 910A Variable Temperature Oil Bath, was modified for use in this application and was capable of control over a range from -70 to +500 F. The heating chamber was an insulated dewar filled with Dow Corning DC-200 silicone oil. A coil consisting of 12 turns of 0.50-inch O.D. copper tubing was placed inside the heating chamber to serve as a heat exchanger for the working fluid. The proportional controller sensed the bath temperature with a resistance thermometer and varied the on-time of electric cartridge heaters that offset the cooling effect of a separate reservoir at the top of the chamber which was filled with ice. An electric stirrer maintained good circulation within the heating chamber. Ice water was removed from the ice reservoir by means of a small hand pump. The ice reservoir and the top of the chamber were completely insulated with glass wool. The system was used to control the inlet fluid temperature to 75 ± 0.5 F (Figure 17). Components of the system are displayed in Figure 18.

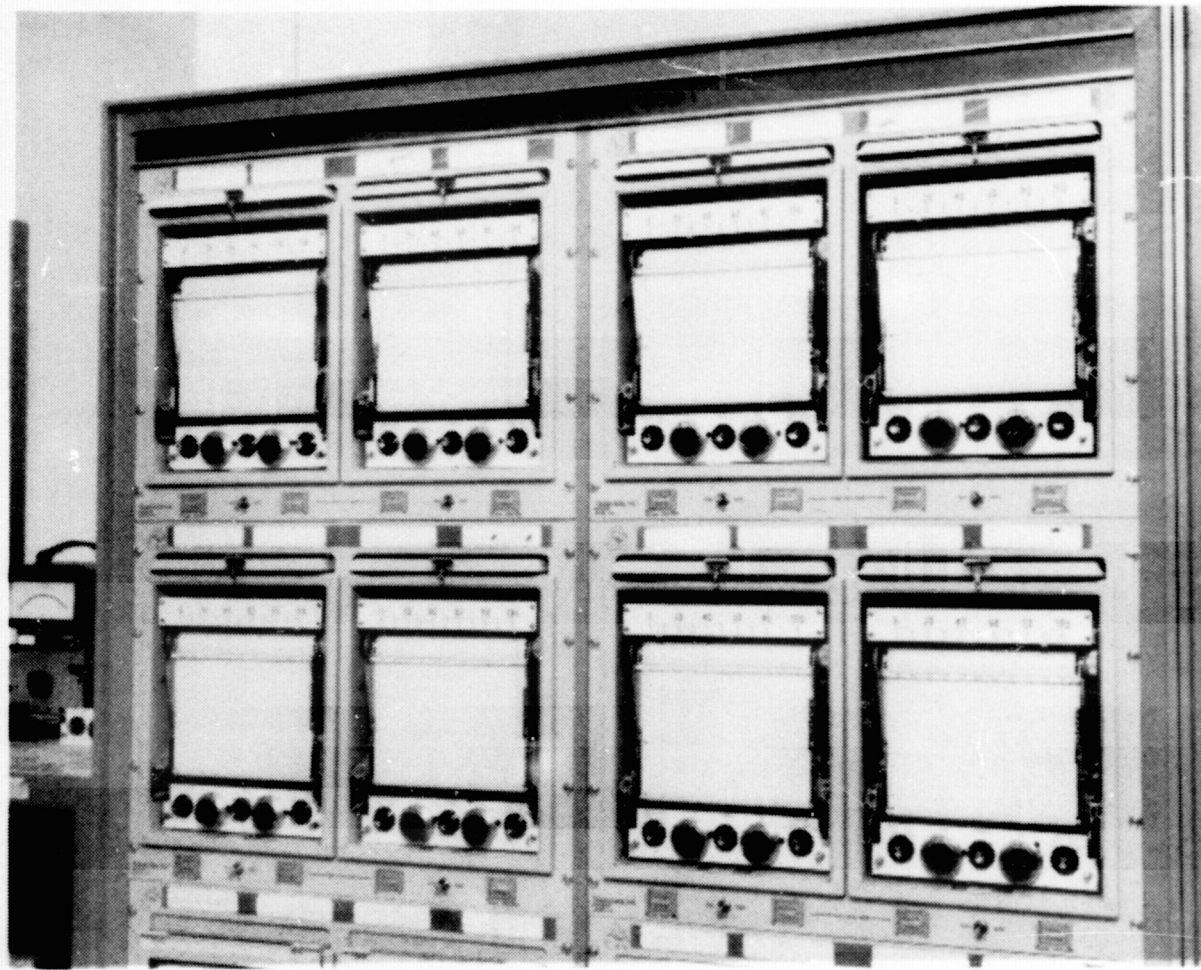


Figure 16. Strip-chart Recorders



Figure 17. Inlet Fluid Temperature Control System

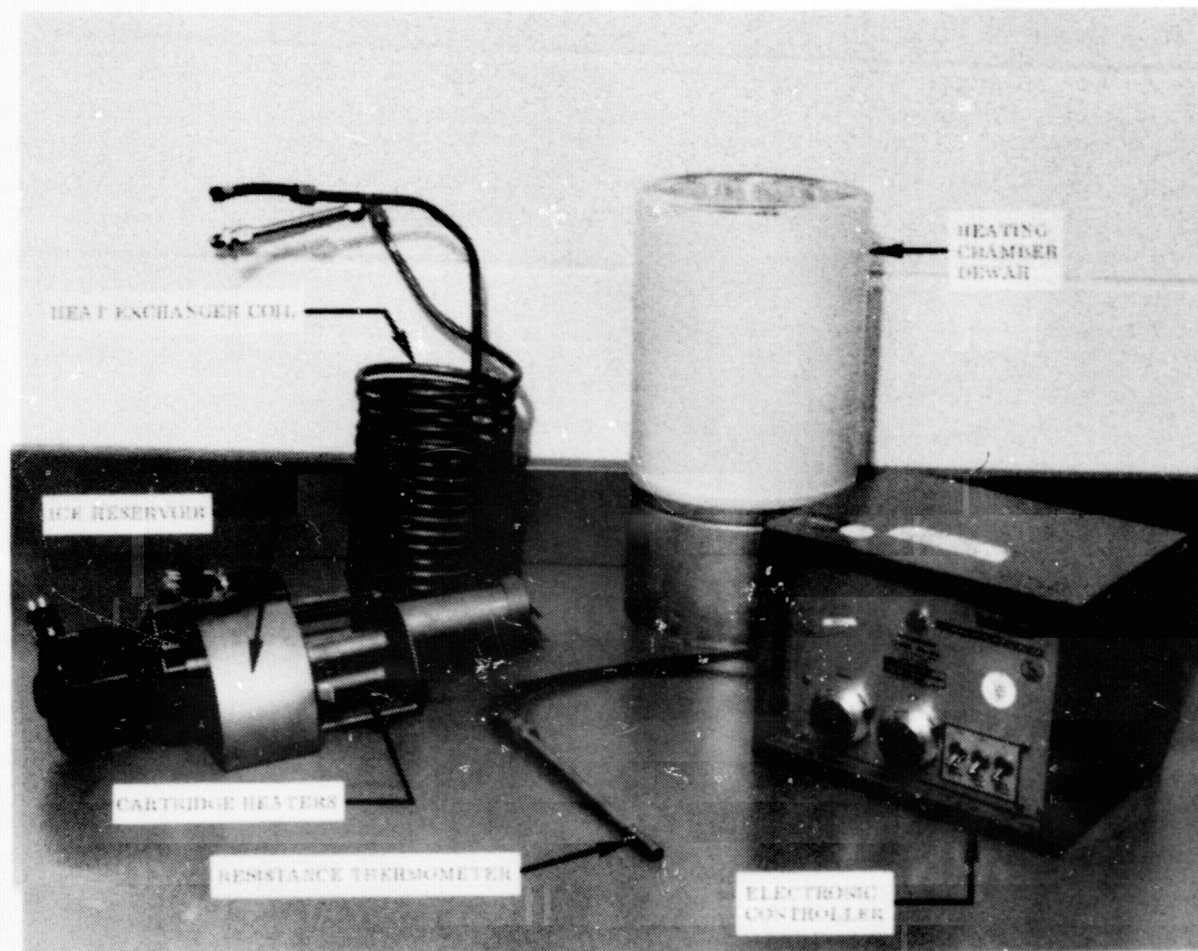


Figure 18. Temperature Control System Components

FLOW PRESSURIZATION SYSTEM

A source of pressurized gas, a pressure regulator, and a water reservoir made up the flow pressurization system (Figure 19). Because of its high insolubility in water, helium gas, stored in cylinders, was used to provide ullage pressure at the top of the reservoir; thus forcing the water through the bottom drain and a 10-micron filter, and into the temperature control system.

An open-system arrangement was preferred to a closed system to maintain a constant and known water inlet temperature to the specimen tube within the vacuum chamber.

Distilled water was used as the working fluid for this thermal modeling investigation. Eighty-two gallons were stored in a glass-lined water heater reservoir. The large capacity of this reservoir provided an adequate volume for a complete experiment, yet yielded a very slow change in head pressure due to the falling level of the water in the water tank. This slow change in head pressure reduced the need for adjustment of the ullage pressure while awaiting stabilization of a steady-state temperature distribution down the specimen tube.

A pressure regulating valve was used to control ullage pressure of a gaseous helium at 20 psig, and a pressure relief valve provided safety. A strain-gage type pressure transducer was used to sense ullage pressure.

FLOW EVACUATION SYSTEM

To insure that no air was in the entrance and specimen tubes of the tubular system (Figure 20), water was forced to flow down to the entrance tube and up from the specimen tube inside the vacuum chamber. Moreover, a vacuum pump was used to evacuate the tubular system prior

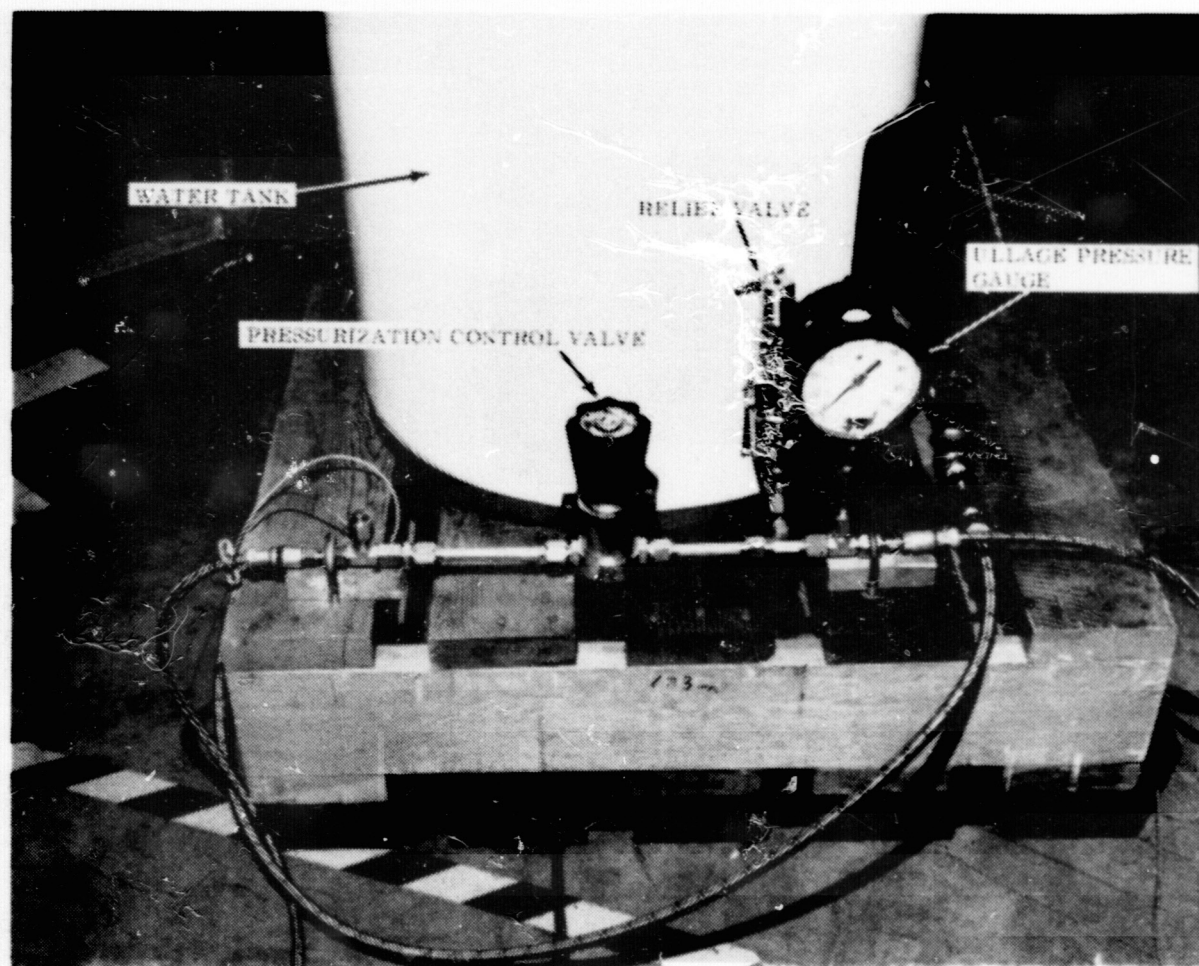


Figure 19. Pressurization Control System

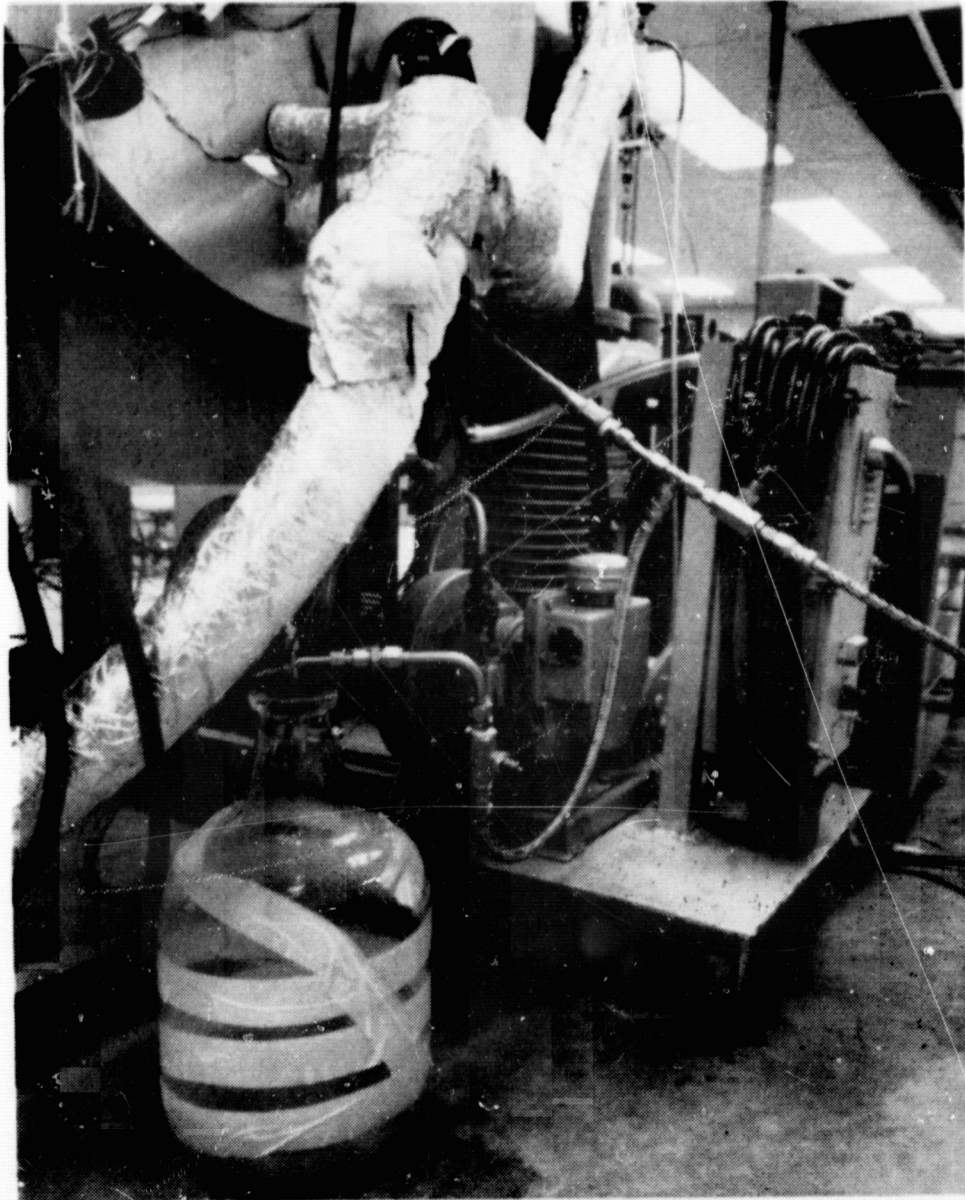


Figure 20. Flow Evacuation System

to water introduction and then to draw the water through the tubular system and into the fluid collection system. After valving off the flow measuring and collecting systems, this pump pulled a high vacuum on the tubular system at the exit tube and then drew the water from the water tank through the entrance and specimen tubes. A five-gallon, vacuum-transfer safety bottle prevented the introduction of water into the vacuum pump. A valve was used to close off this suction system when smooth and airless flow of water was obtained.

The effectiveness of this air-bleeding operation could be determined by comparing the two sets of thermocouples located the same distance down the specimen tube as shown in Chapter V. One set in the middle of the tube was located at the top and bottom surfaces, while the other set near the exit end of the tube was located on the top and side surfaces. These two sets of thermocouples were used to indicate the peripheral heat flux about the tube and were invaluable in indicating the presence of entrapped air within the specimen tube.

FLOW MEASURING AND CONTROL SYSTEM

It was important that similar flows be used in each tube so that the effectiveness of the modeling criteria could be studied. The Reynolds number, a dimensionless flow parameter, was selected as the criteria for flow similarity. Calculations of Reynolds number versus flow rate were made for each specimen tube and are presented in Appendix C. For a given fluid and tube inside diameter (I.D.), the Reynolds number is related to the volume flow rate in gallons per minute or grams of water per minute. This fact provided a simple means of flow rate calibration. Water was collected in a beaker for one minute and weighed on a set of Ohaus Triple-beam laboratory balance scales accurate to 0.1

gram. Balance was calibrated against a set of standard weights whose accuracy was certified by NASA. This calibration is given in Appendix D. Timing was accomplished with a stopwatch whose accuracy was also certified by NASA.

The flow control system is shown in Figure 21. The upstream or head pressure was held at 20.0 ± 0.05 psig by means of a Heise pressure measuring gage and a strain-gage type pressure transducer. The flow was then passed through a 10-inch Brooks rotameter modified to have a range capability of from 0.00003 to 0.04 gallons per minute of water. This was accomplished by using a rotameter that had a very low flow rate capability and shunting the rotameter with a fine micrometer needle valve. This is the same principle as that used in the conversion of a microammeter to a multimeter for electrical measurements. The rotameter had two indicating balls of different materials, thus giving it a dual range capability at a single setting of the needle shunt valve. One indicating ball was steel; the other was lighter and made of glass. To obtain the multirange capability of the flow meter, the shunt valve was first closed and the flow rate was increased until the steel ball was at its upper limit on the scale. The shunt valve was then opened to a setting which permitted the glass ball to indicate approximately 10 percent of its range, and a new calibration was made. It was found that only two settings of the control valve were necessary to cover the necessary range for the flows used in the experiment. Calibration curves for the rotameter are given in Appendix E. It should be pointed out that the calibration curves were used merely as a guide and that an on-line measurement of flow rate was made during each run of the experiments. This

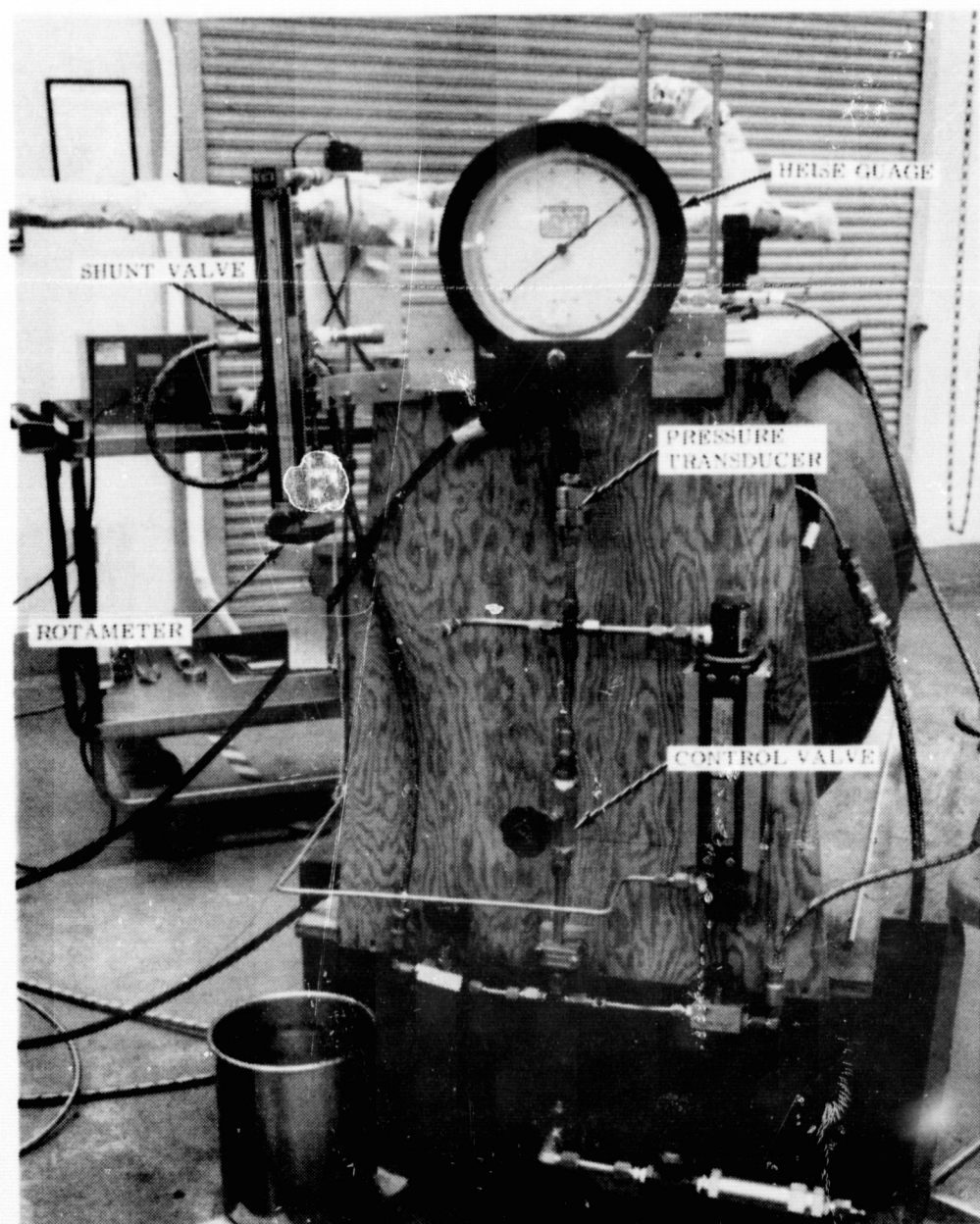


Figure 21. Flow Control System

insured an accuracy of flow rate measurement which exceeded the repeatability of the rotameter.

A 16-turn needle valve was used to control the flow and provided a sufficient fine adjustment to this critical parameter. The flow then passed through a tee that provided a choice of two paths, each of which could be shut off with a valve. One path was to the top of the two spherical storage containers of the flow collection system. The other path was to a height identical to that of the former path to the collection system and then to an open tube which permitted collection of the water in the beaker for a flow rate determination. The same height for each flex hose path was important to give the same back pressure during either the flow measurement or collection in the storage spheres.

FLOW COLLECTION SYSTEM

The flow collection system consisted of two 40-gallon spherical tanks manifolded together to provide adequate storage for the water during an experiment (Figure 22). Water flowed into the top of each sphere rather than the bottom to provide a constant back pressure. Two tubes extended above the tanks provided venting of the displaced air.

Use of a closed collection reservoir system also permitted its pressurization to cycle the water back into the water tank at the conclusion of a day's run. Vent tubes were capped, the valve on the control system was closed, the helium pressurization system was connected to the collection system, and the resulting pressurization of the spherical tanks forced the water through the manifolded bottom of the spheres. From this point, the water flowed through a 40-micron filter and returned to the water tank reservoir.

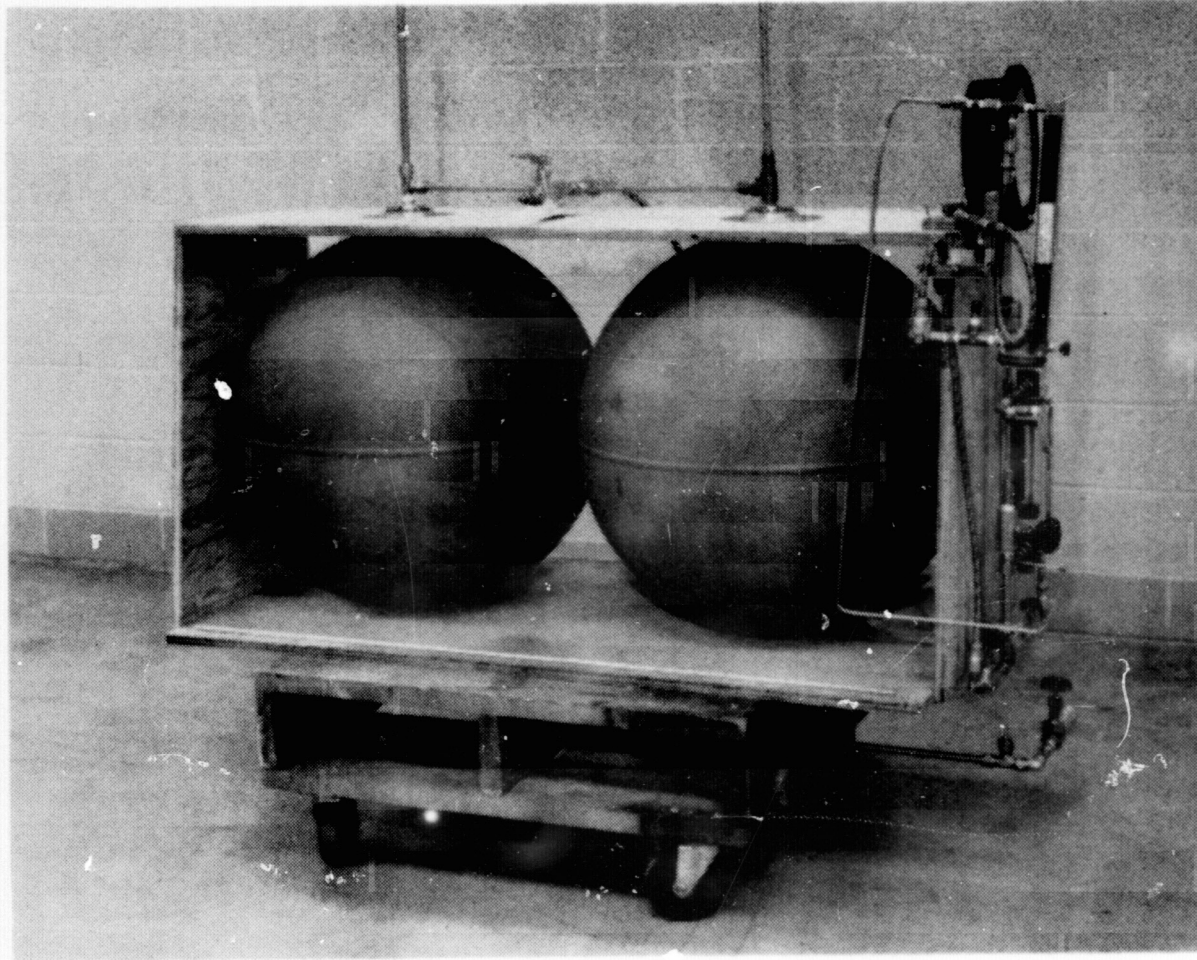


Figure 22. Flow Collection System

CHAPTER VII.

EXPERIMENTAL PROCEDURE

The experimental procedure can be divided into two parts: the preparation for the experiment on a tube, and the experiment itself. The preparation took approximately eight hours, while the experiment required about 20 hours.

PREPARATION

The specimen tube was placed on a rolling table in front of the vacuum chamber while the transition junctions for the 16 thermocouples were made. The transition junctions were connected by wrapping the smaller 30-gage wire around the larger 12-gage wire to make a good mechanical junction. Constantan wires were spot welded with an energy level of approximately nine watt-seconds. Copper wires were first coated with Telkem 350 flux and then soldered with Kirkson K-703 low thermal EMF solder. Heat-shrinkable tubing was applied to the junction with a heat gun, and the junctions were clamped between two copper bars to insure temperature similarity and stability.

After the transition junctions were connected, thermocouple identity and continuity were checked by placing one's finger upon the measuring junction and noting the corresponding indication on the strip-chart recorders. The specimen was then suspended within the chamber and the plumbing was attached to its exit end. After wrapping the exit plumbing with radiation shielding as previously described, the tube was aligned and leveled.

It was necessary to insure the alignment of the entrance and specimen tubes because the liner cover had to be bolted onto the liner after the specimen was suspended within the chamber. This was accomplished with the aid of a plug gage--a solid rod whose outside diameter permitted a snug fit within the tubes and tube fittings. Plug gages for the stainless steel tubes were made of brass, whereas the gages for the aluminum tubes were made from nylon. The gage was inserted through the entrance tube, by means of a long handle, until it was positioned equally within both entrance and specimen tubes as well as the nylon union fitting that was used to connect them. The fitting was then tightened and the gage was carefully extracted through the entrance tube. It was found that the use of vacuum grease on the teflon front ferrules, which were used within the nylon fittings, greatly improved the sealing properties of the tubular system. The disassembled nylon fitting with the inserted plug gage is shown in Figure 23. The entrance tube rested on a stand, the height of which could be adjusted to level the tubular system.

Water from the flow pressurization system was introduced into the tubular system at a pressure of 50 psig for five minutes to facilitate checking for leaks before the liner cover was set in place. Figures 24 and 25 show the assembled tubular system during this operation. The copper heat sink which clamped the transition junctions can be seen on the liner floor. If no leaks were present, the entrance and specimen tubes were disconnected and the liner cover was bolted to the liner shell. Figure 26 shows the tubular system after the liner cover has been attached to the liner shell. The chamber door was then held

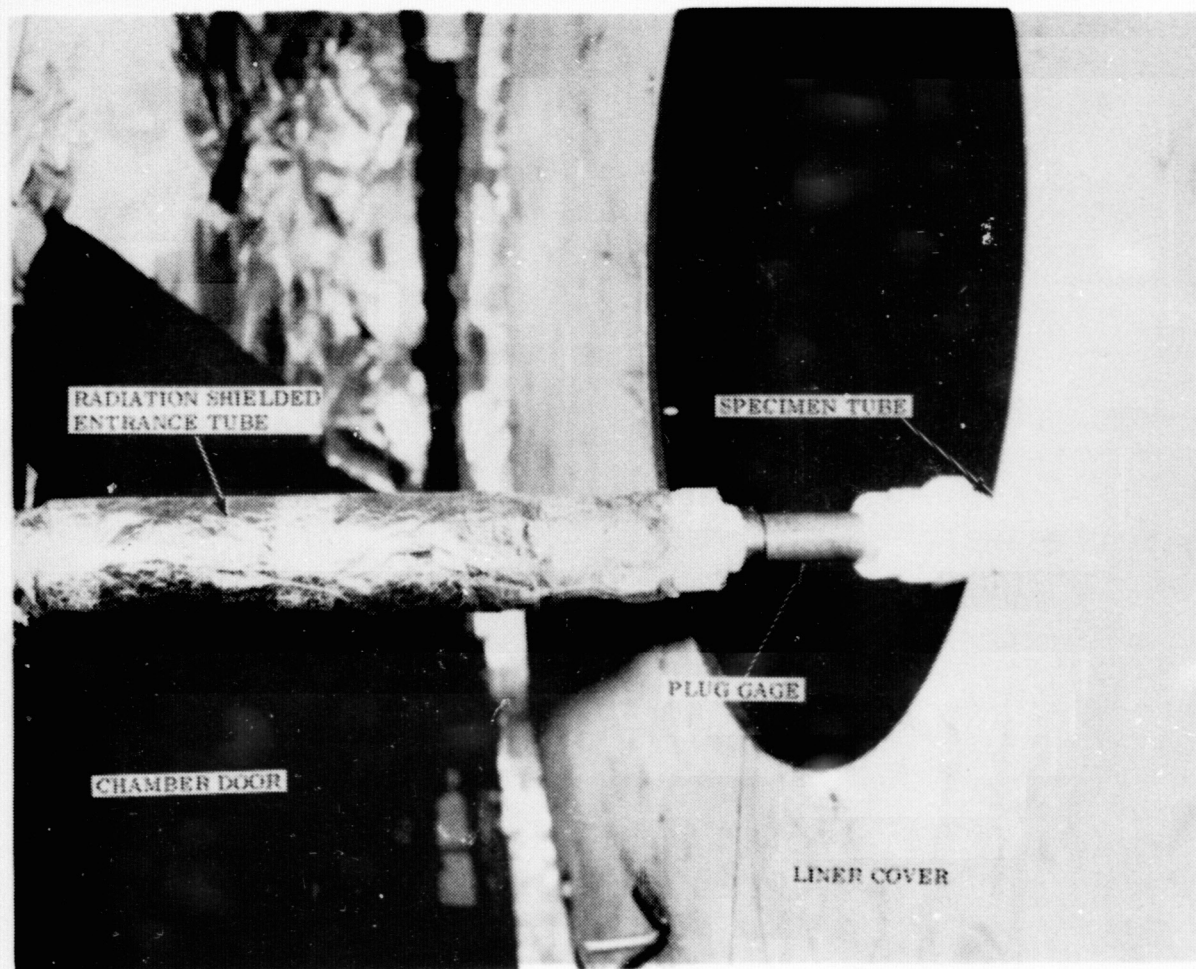


Figure 23. Entrance Tube to Specimen Tube Connection

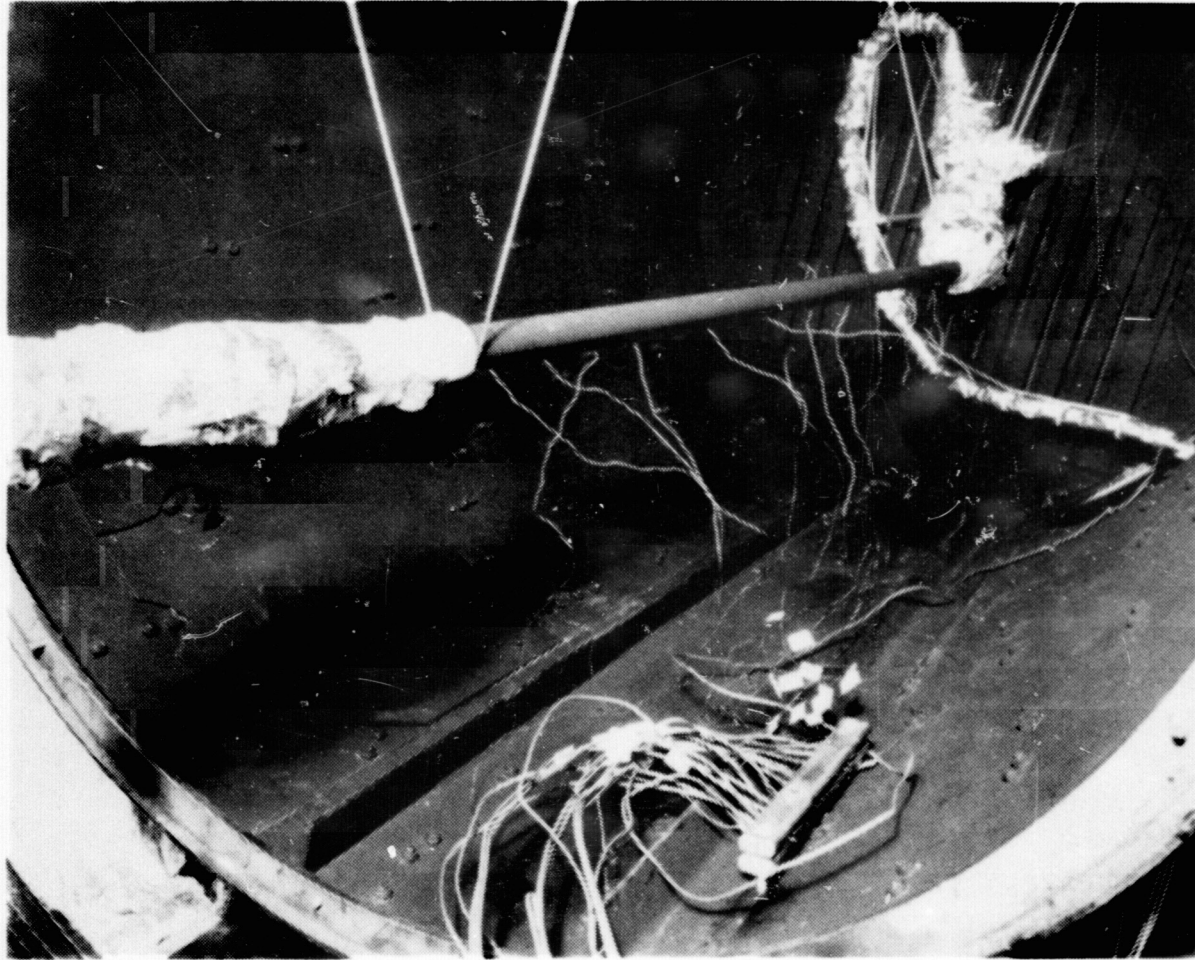


Figure 24. Assembled Tubular System and Transition
Junction Heat Sink

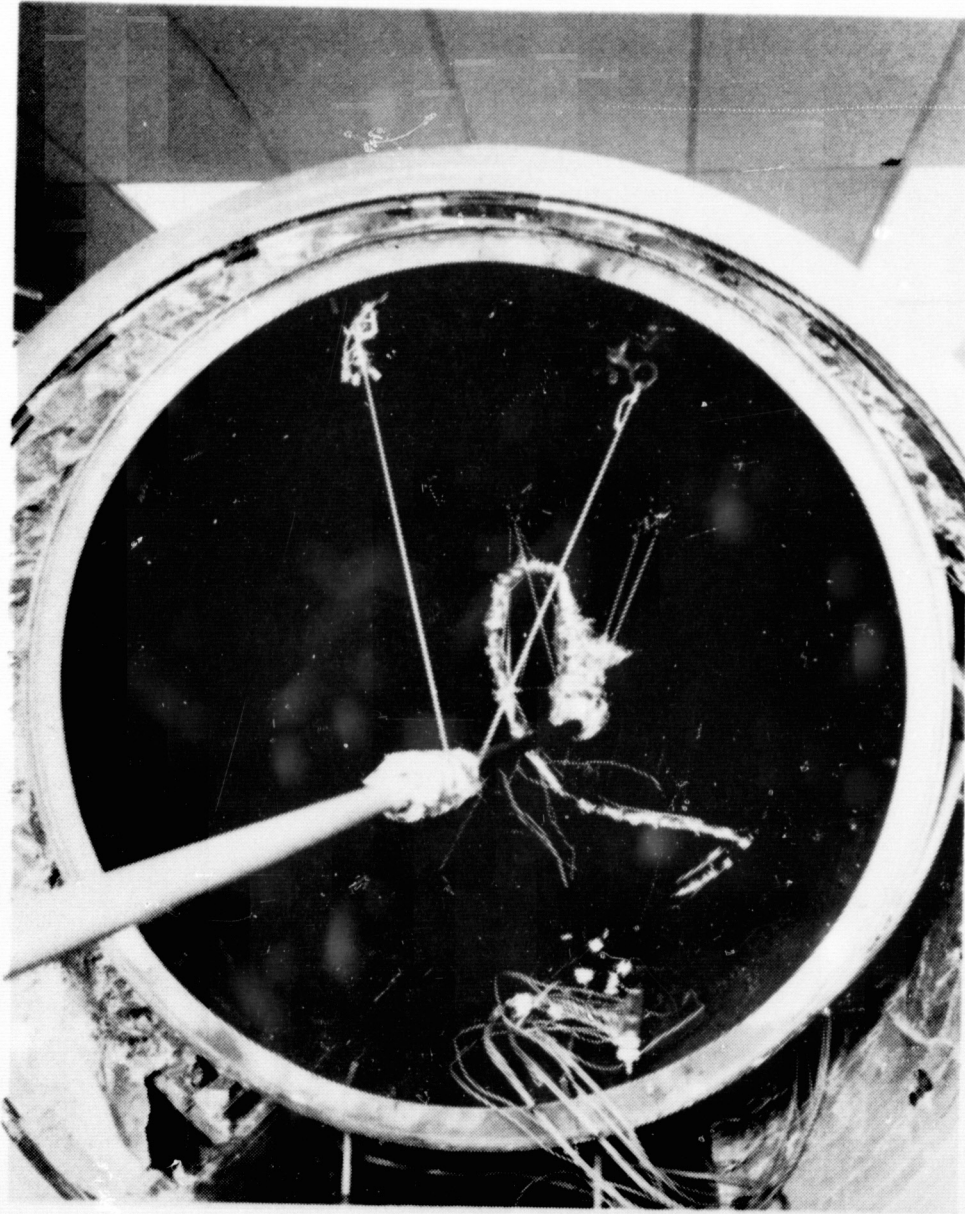


Figure 25. Tubular System in Vacuum Chamber

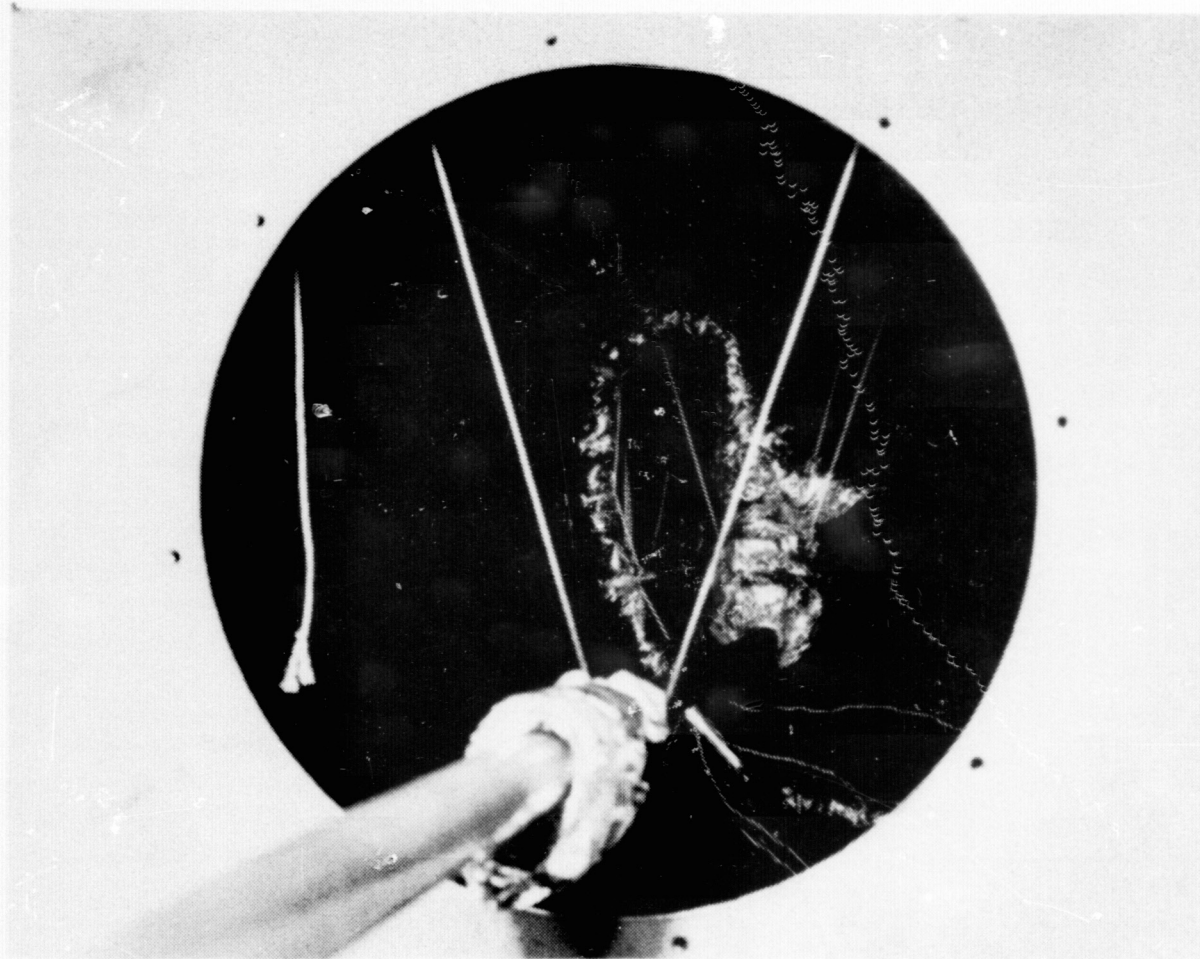


Figure 26. Tubular System Viewed Through Cryogenic Liner Cover

slightly open while the entrance and specimen tubes were reassembled with the plug gage.

The door flange was slipped over the entrance tube and suspended from a portable lift crane, thus preventing an excessive load on the leveled entrance tube. The attached entrance tube, inserted through the door flange, can be seen through the opening in the chamber door (Figure 27). Figure 28 depicts the nylon cords supporting the door flange being removed prior to attachment of the flange to the chamber door. The chamber door was then closed and latched.

The entire system was checked for leaks by starting the vacuum system while the tubular system was pressurized with water at 20 psig. The vacuum system was then pumped down with just the holding pump, the roughing pump, and the blower. If the system could attain a vacuum of 100 torr in 15 minutes, it was assumed that no leaks were present. If a leak in the system was noted, it was sometimes necessary to use the helium leak detector to find the problem. This equipment is described in Appendix F.

Two 100-gallon liquid nitrogen dewars were filled at the outside storage facility in preparation for the experiment. One dewar was connected to the system, and the volume of gaseous helium for the flow pressurization system was checked. The entrance tube and flexible hose which connected the tube to the temperature control system were wrapped with fiber glass insulation to reduce heat loss from the water as it flowed down the tube. Figures 29 and 30 show the test equipment in preparation for the experiment.

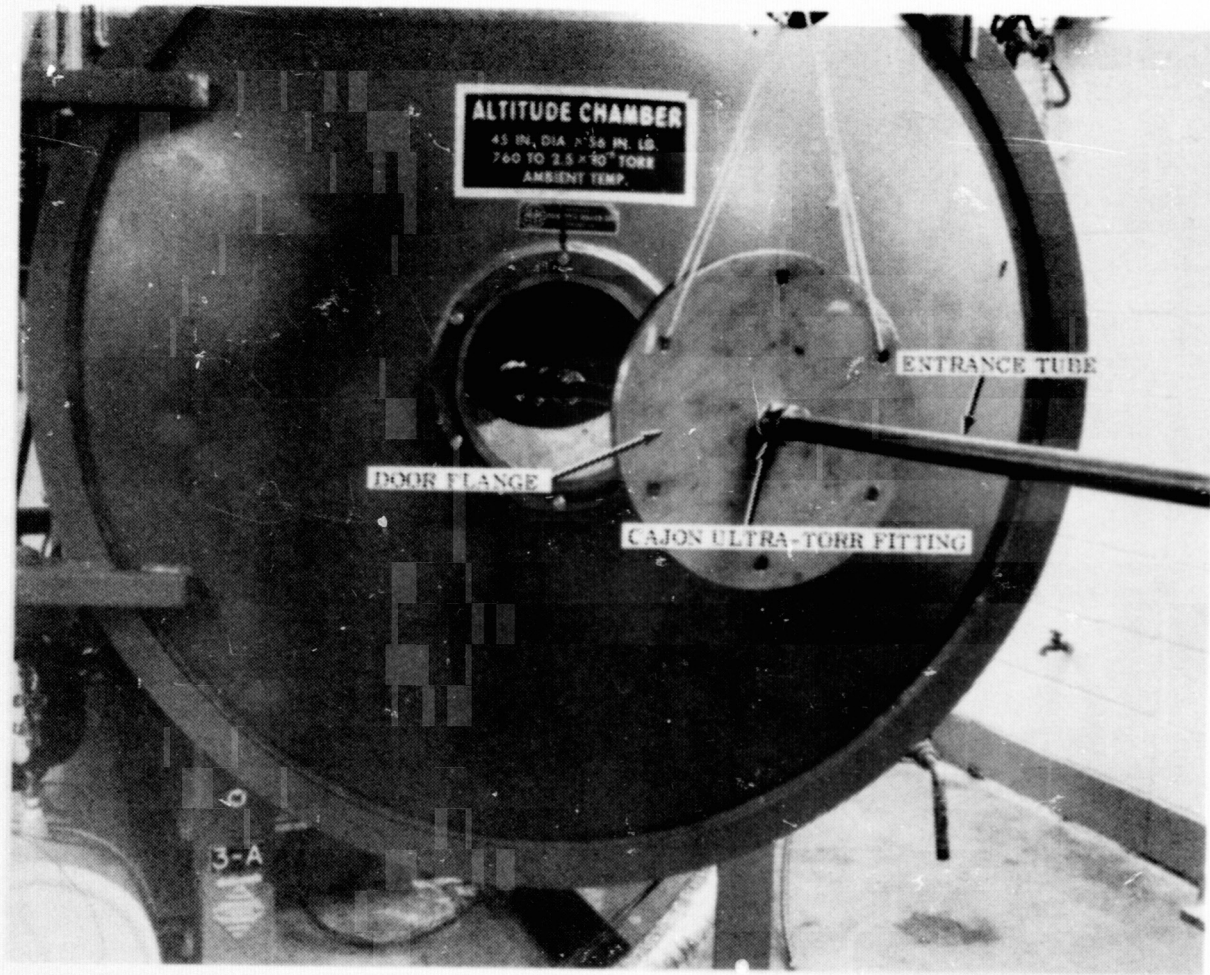


Figure 27. Suspended Entrance Tube with Door Flange

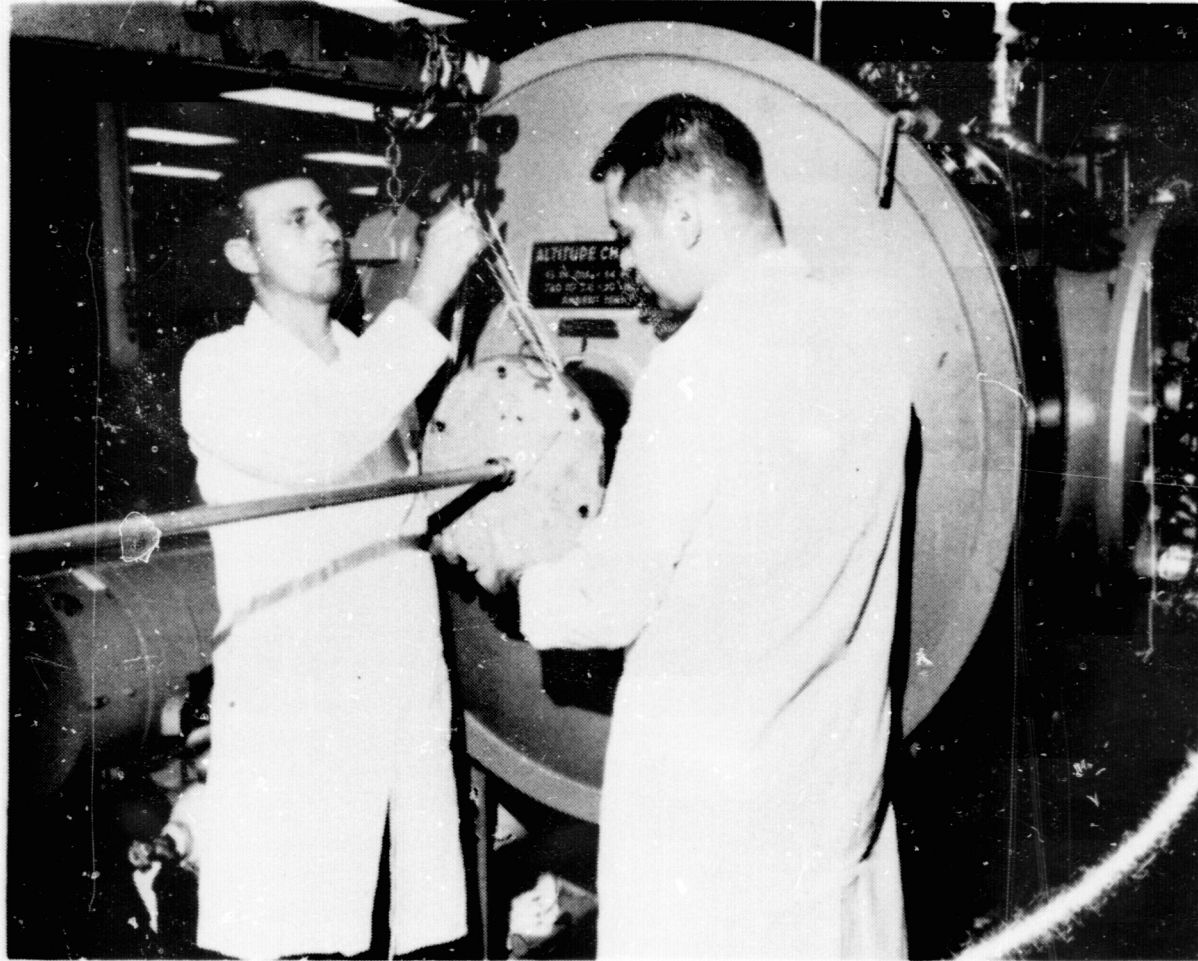


Figure 28. Attachment of Flange to Chamber Door

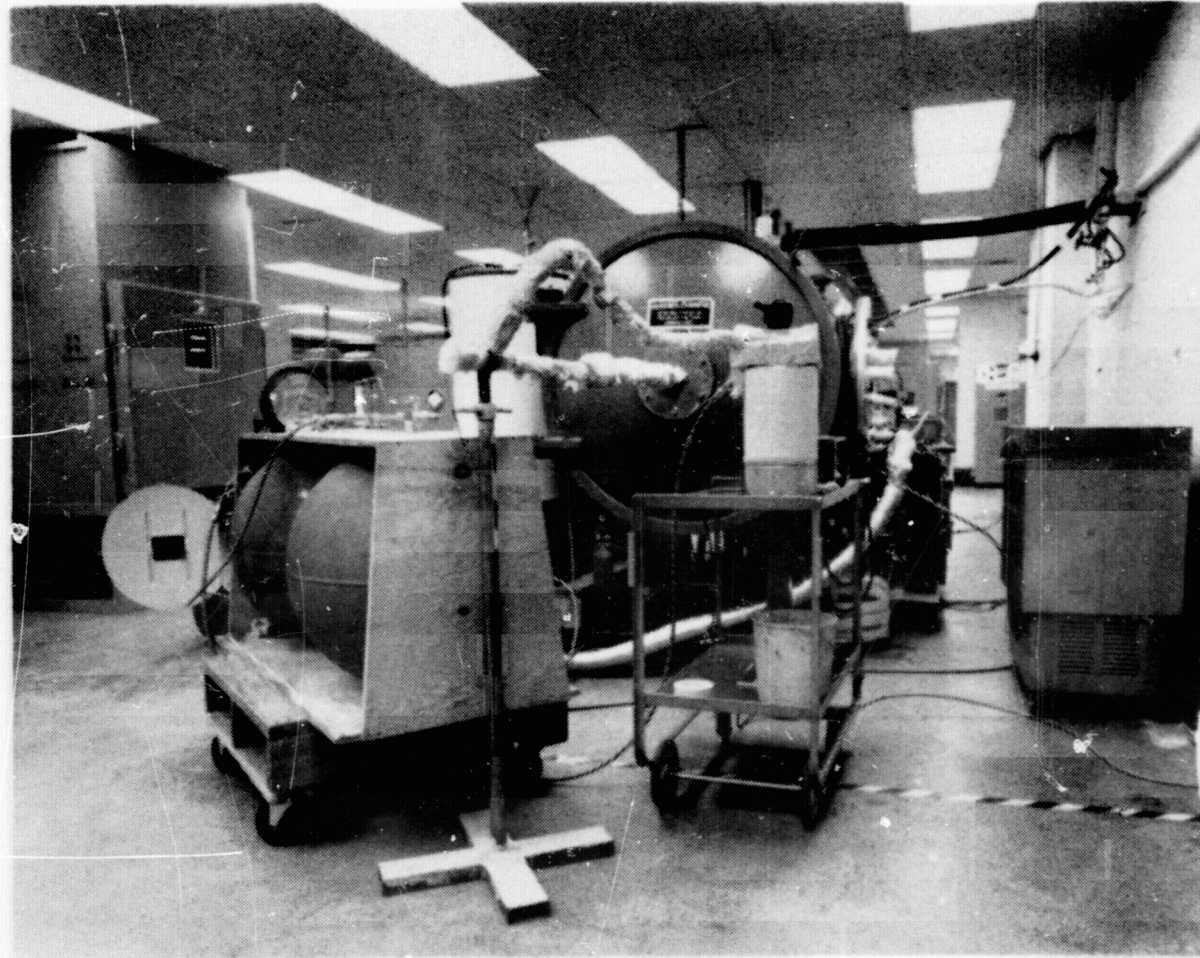


Figure 29. Experimental Test Setup (Right Side View)

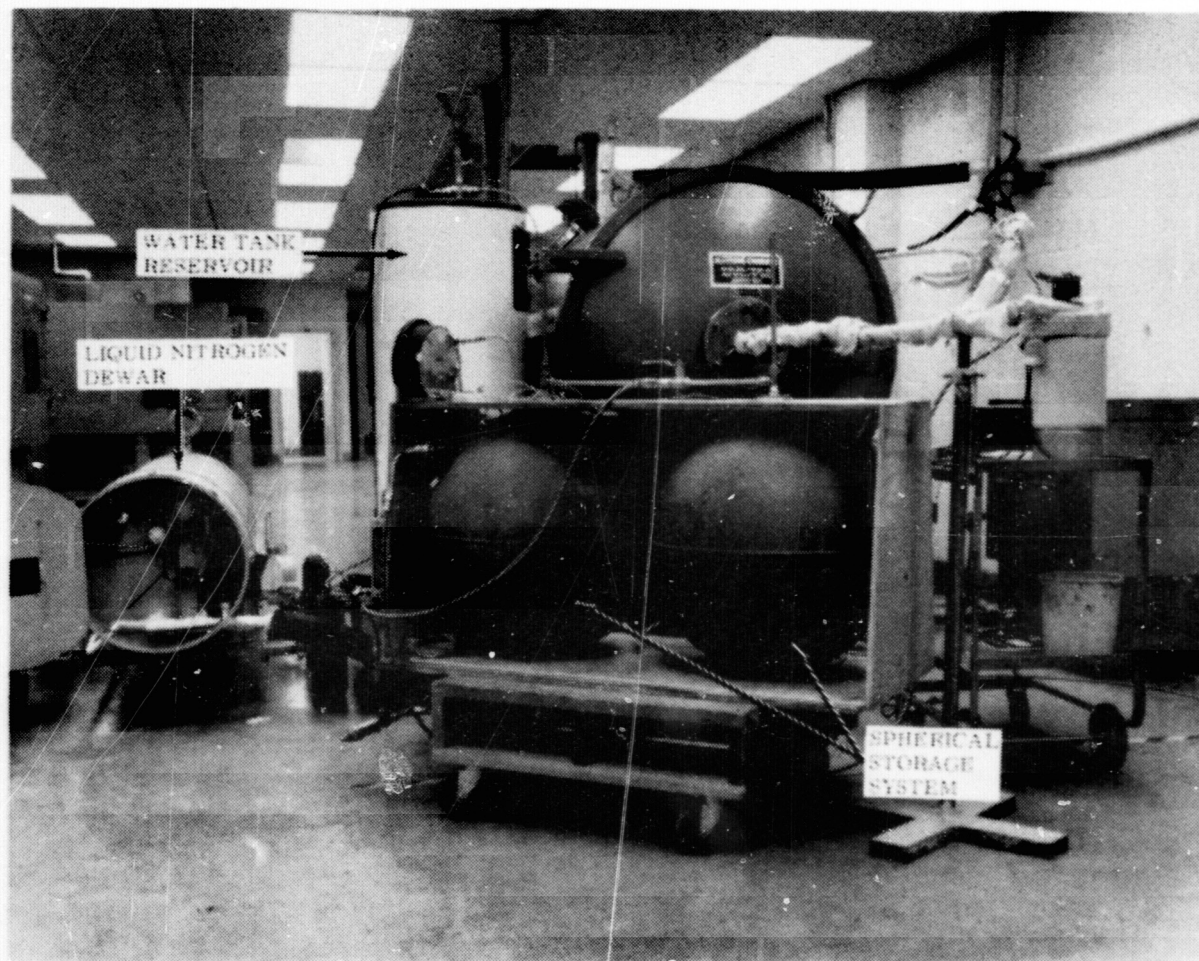


Figure 30. Experimental Test Setup (Left Side View)

EXPERIMENT

The vacuum system was turned on according to the pump-down procedure given in Appendix B. Before liquid nitrogen was introduced to the liner, the continuity and temperatures of the thermocouples were monitored on the strip-chart recorders. If the indicated temperatures of all the thermocouples on the specimen tube were within 1 F, the liquid nitrogen was introduced to the cryogenic liner. Approximately six hours were required for the liner to chill down to a temperature of -290 F.

During liner chill-down, the recorders were calibrated and the tubular system was momentarily evacuated to assure an air-free system as discussed in Chapter VI. The temperature control system was then turned on and the controls were set to maintain a water inlet temperature of 75 ± 0.5 F at the front of the entrance tube. It was necessary to replenish the supply of ice in the ice reservoir every 30 minutes and drain the accumulated water with a hand pump. A supply of cubed ice was kept in a nearby chest freezer.

Water flow was set at the rate corresponding to the desired Reynolds number after the necessary liner temperature was attained. These rates are given in Appendix C. The flow rate was determined by setting the Heise pressure gage to 20.0 psig and then collecting the water in a beaker for one minute after it had flowed through the tubular system (Figure 31). The time interval was monitored with an accurate stopwatch. The beaker and its contents were then weighed (Figure 32), and the weight of the empty beaker was subtracted to determine the number of grams of water that were collected during one minute. The flow control valve was adjusted until the desired flow rate was obtained (Figure 33).

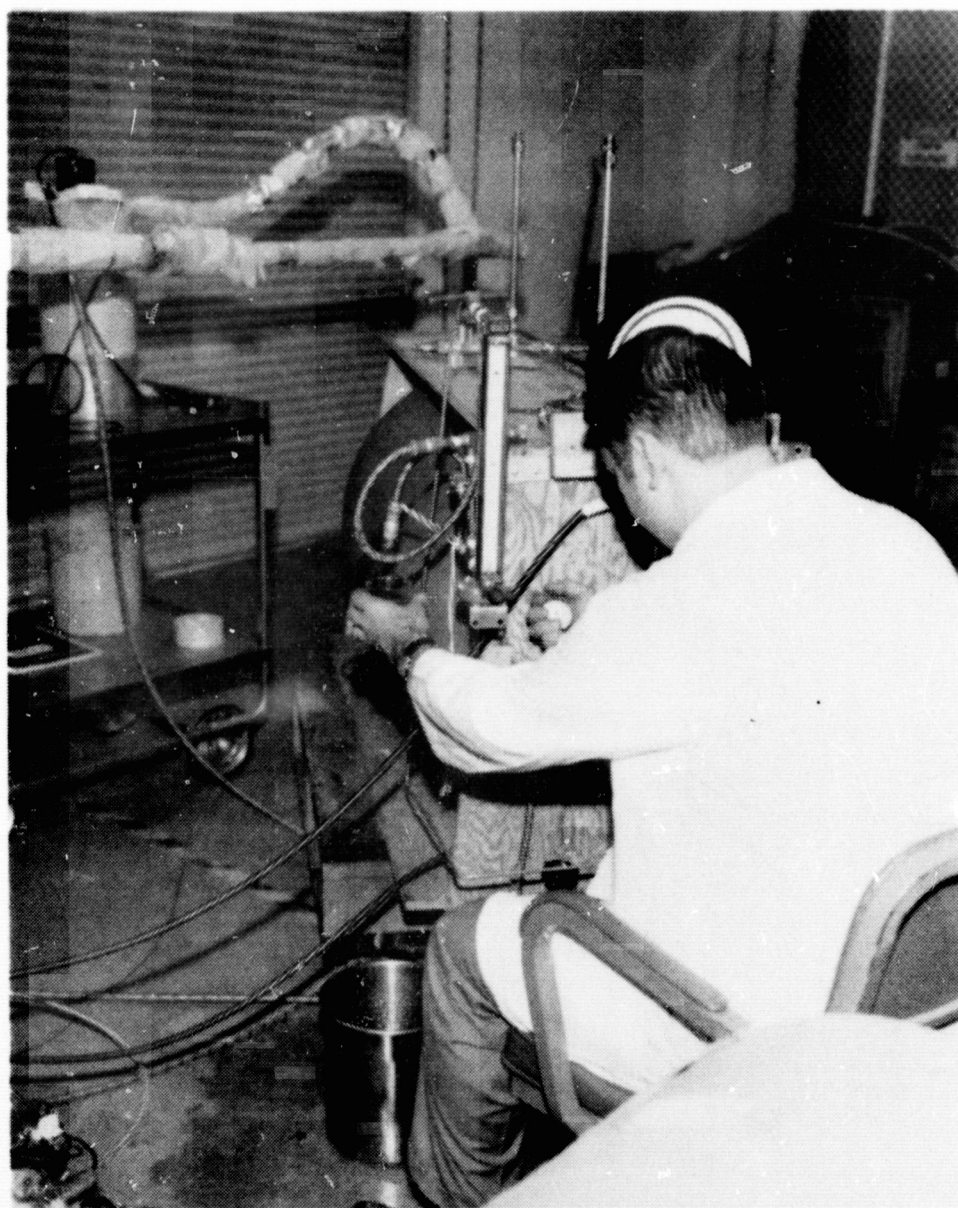


Figure 31. Water Collection for Flow Rate Determination

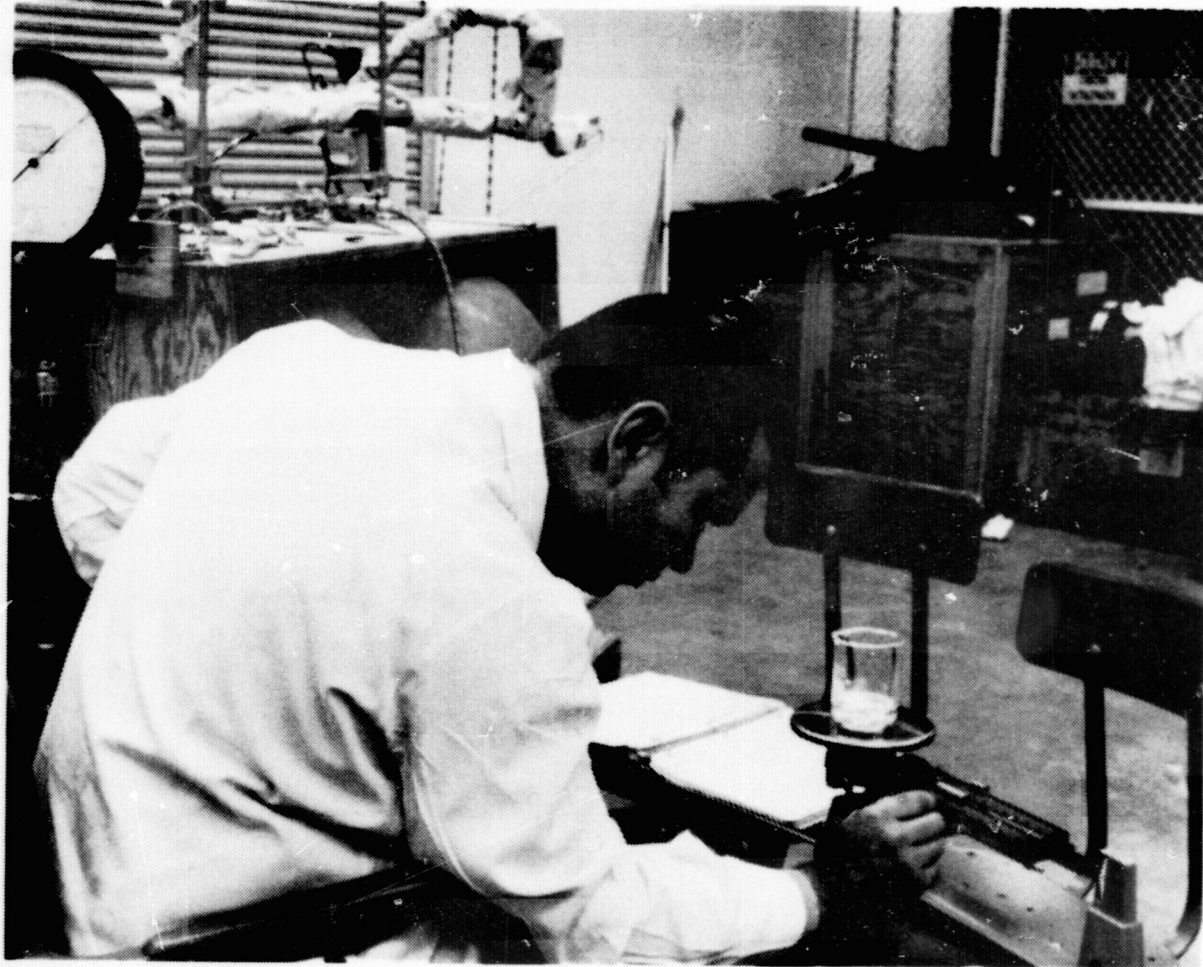


Figure 32. Weighing of Water for Flow Rate Determination

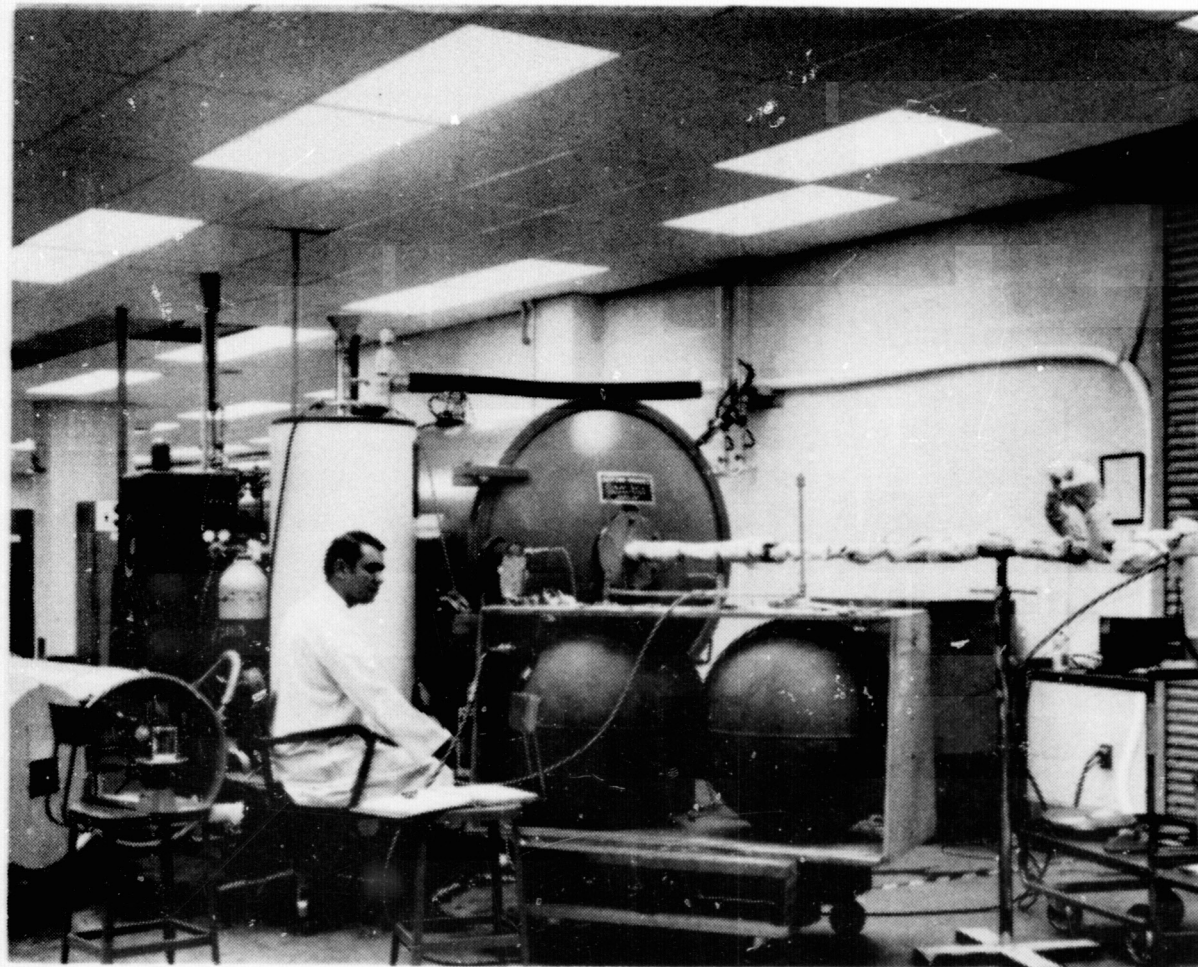


Figure 33. Flow Control Adjustment by Author During Experiment

Recorders were monitored to determine when the system had achieved steady-state conditions. The strip charts were marked when equilibrium was reached. The flow control valve was readjusted to give each desired flow rate until completion of the experiment. The recording system normally required 30 to 45 minutes to achieve equilibrium. Upon completion of all runs, the vacuum system was brought to atmospheric conditions as described in the pump-up procedure given in Appendix B.

Water level in the storage spheres was monitored with a long dowel that served as a dipstick and could be inserted into either sphere through the vent tubes atop the flow collection system. Water was allowed to flow until the liner temperature was above 32 F to prevent freezing of the water in the tubular system. Calibration curves for the strip-chart recorders were used to reduce the resulting experimental data and are given in Appendix G.

CHAPTER VIII

RESULTS AND DISCUSSION

Experimental test data for the four stainless steel and four aluminum specimen tubes are presented in Tables 5 through 22, and Figures 35 through 44. Data for each tube is presented on three sheets: an experimental sheet describing the conditions under which the test was run, a temperature sheet showing the temperatures at designated locations along the tube for various Reynolds numbers, and a graph illustrating the results of the temperature sheet. Inconsistencies in the data caused some runs to be repeated; e.g., the 1.0-inch O.D. and 0.25-inch O.D. stainless steel tubes.

The correct results were then analyzed further. Although fluid inlet temperature to the entrance tube was held to 75 ± 0.5 F, the different lengths of entrance tube along with the different flow rates contributed to a varying degree of heat loss prior to fluid introduction to the specimen tube. Temperature measurement of fluid temperature at the specimen tube entrance was not possible without disturbing the established hydrodynamic boundary layer. Because of this variation it was necessary to normalize the data graphically to a consistent temperature of 65 F at thermocouple number 1 located at $z^* = 0.05$. The selection of this temperature required the least shift of fluid temperature at this location. The associated difference in thermal radiation is negligible. Results of this normalization are presented in Figures 45 through 56. These results are presented for different Reynolds number and material as a function of tube diameter.

Comparison of the normalized data shows that the same temperature distribution down the tube occurs at $Re = 45$ for the 1.0-inch O.D. tube, $Re = 40$ for the 0.75-inch O.D. tube, $Re = 35$ for the 0.5-inch O.D. tube, and $Re = 25$ for the 0.25-inch O.D. tube. Furthermore, the distributions and flow rates correspond well for both stainless steel and aluminum tubes. These results are shown in Tables 25, 26, and 27. The Reynolds numbers mentioned above gave a temperature difference less than 1 F for the stainless steel tubes and less than 2 F for the aluminum tubes. Consistency between both materials for the same Reynolds numbers was within 3 F. These temperature differences are also presented as percent error in terms of absolute temperature and percentage of total temperature difference down the tube in the Table 3 below.

TABLE 3

MODELING ERROR

<u>Tube Combination</u>	<u>Temperature Difference</u>	<u>% Error Abs. Temp.</u>	<u>% Total Temp. Difference</u>
Stainless Steel	1 F	0.196	5.88
Aluminum	2 F	0.392	11.75
S. Steel & Aluminum	3 F	0.588	17.65

The slight dispersion of data for the aluminum tubes is probably due to a larger conduction error resulting from the tube's higher thermal conductivity. An indication of the conduction error for the 0.75-inch O.D. and 1.0-inch O.D. aluminum tubes is presented in Appendix H. Heat conduction is seen to be minimal at $z^* = 0.7$. Conduction error at this location is calculated to be 3.2% for the 1.0-inch O.D. tube and 6.45% for the 0.75-inch tube.

The thermal distribution around the cryogenic liner showed marked differences in temperature between the cylindrical shell and the uncooled end plates. Porthole and porthole covers, which were warmer than the surrounding shell, also contributed to the elevated temperature of the surroundings. The effect of this raised surroundings temperature introduced an error of 2.5% to the 1-inch O.D. tube radiating at 50 F.

Calculation of Grashof number requires the knowledge of temperature difference in the fluid at the top and bottom of the tube. This was not measured because of the disturbing effect of an instrument on the hydrodynamic boundary layer. Temperature differences between top and bottom on the exterior of the tube never exceeded 2 F, and an assumed $\Delta T = 1$ F across the fluid gave Grashof numbers ranging from $Gr = 7$ in the 0.24-inch O.D. tube at 40 F to $Gr = 8850$ in the 1.0-inch O.D. tube at 70 F. This range extends from the laminar into a region that is possible to have mixed flow (free and forced convection). Very little investigation has been made in this area, and no work has been published for mixed flow in horizontal tubes. It is difficult, however, to see where free convection can play a major role in the heat transfer within the tube.

Experimental verification of the modeling criteria for Nusselt number, $Nu^* = D^* = L^{*2}$ was not attempted since lack of fluid temperature data prevented the determination of h , the convective heat transfer coefficient. It may be pointed out, however, that $Nu^* = D^*$ requires that $h^* = 1$ for the same fluid.

The thermal entry length was calculated from equation (44) to range from $z = 1.6$ inches in the 0.25-inch O.D. tube at $Re = 25$ to $z = 12.8$ inches in the 1.0-inch O.D. tube at $Re = 45$.

The relationship between $Re^* = Re_m/Re_p$ and D^* may be determined from the experimental data presented in Figures 57, 58, and 59. Values for these parameters are given in Table 4 below.

TABLE 4
CALCULATION OF Re^* AND D^*

<u>D_o (in.)</u>	<u>D_i (in.)</u>	<u>D_i^*</u>	<u>Re</u>	<u>Re^*</u>
1.0	0.7629	1.0	45	1.0000
0.75	0.5625	0.73732	40	0.88889
0.50	0.3852	0.50492	35	0.77778
0.25	0.1913	0.25075	25	0.55556

These values are presented graphically in Figure 34.

A least-square curve fitting routine for a parabolic distribution was programmed on a Hewlett-Packard 9100B desk computer. The resulting equation was found to be $Re^* = 0.29909 + 1.15314D^* - 0.45605D^{*2}$ over the range from $D^* = 0.25$ to $D^* = 1.0$. This resulting curve is also given in Figure 34.

An analysis of experimental errors for instrumentation, measuring systems, and experimental apparatus is presented in Appendix I. The overall estimated error was $-8.3 \pm 5.3\%$.

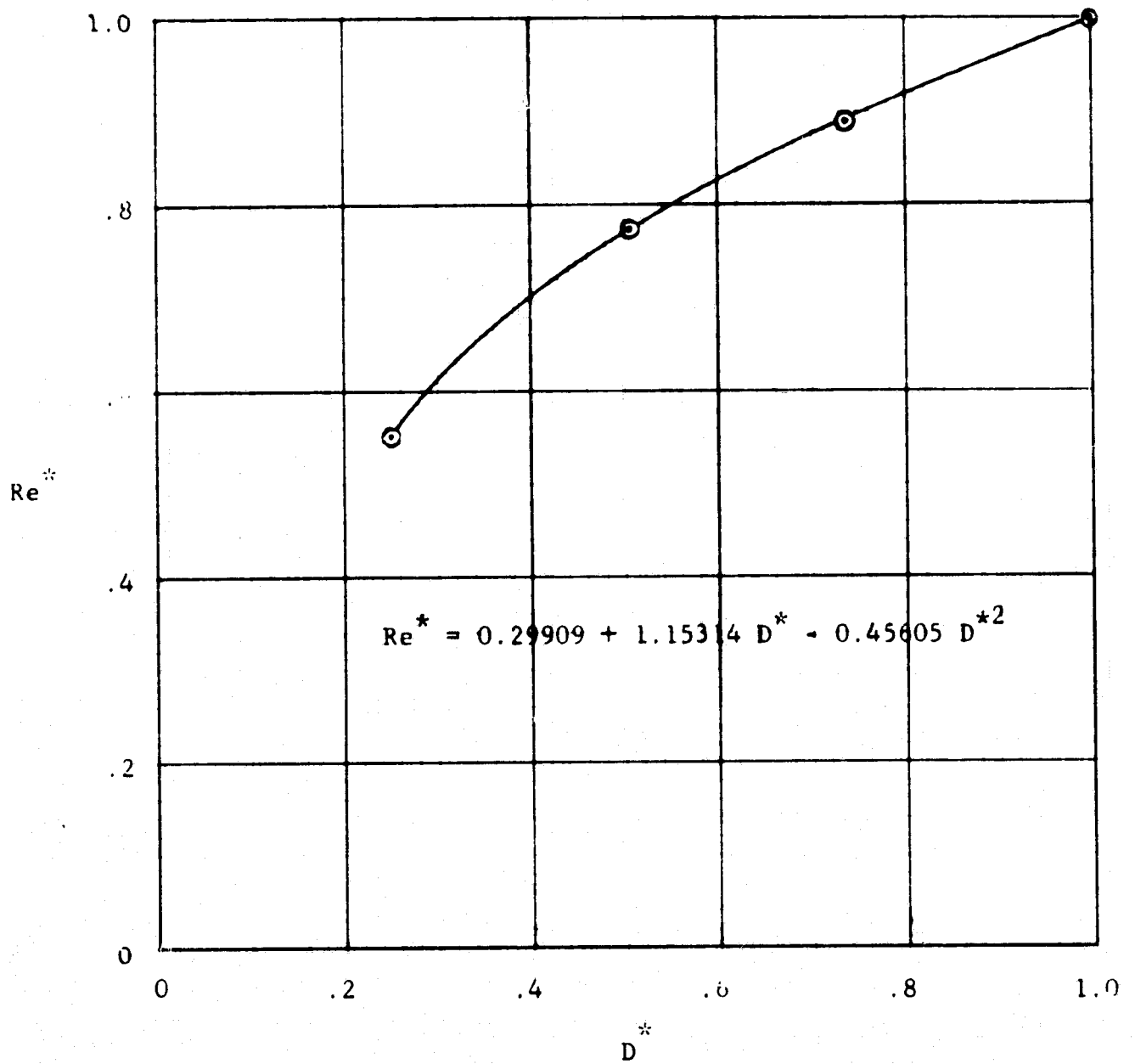


Figure 34. Graphical Relationship Between Re^* and D^*

TABLE 5
EXPERIMENT SHEET

SPECIMEN: 1" Stainless Steel Tube

DATE: January 8, 1971

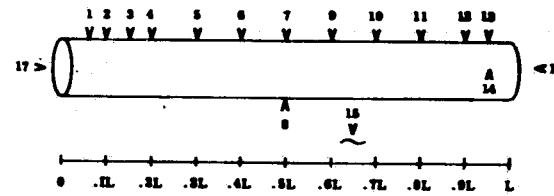
RUN	Re	HEAD PRESSURE	SHUNT VALVE	GLASS BEAD	STEEL BEAD	GRAMS H ₂ O	GPM	VACUUM
1	20	20.0	1.07	--	24	20.82	.00474	1x10 ⁻⁴
2	23.4	20.0	1.07	--	26.2	26.01	.00592	1x10 ⁻⁴
3	30	20.0	1.07	--	38	31.23	.007108	9x10 ⁻⁵
4	35	20.0	1.07	--	46	36.30	.008293	2x10 ⁻⁴
5	38.4	20.0	1.07	--	57	41.64	.009478	1x10 ⁻⁴
6	43.1	20.0	1.30	--	32	46.84	.010662	6x10 ⁻⁵
7	48.1	20.0	1.30	--	39	52.05	.011847	3x10 ⁻⁴
8	52.9	20.0	1.30	--	46	57.25	.013032	1x10 ⁻⁴
9	57.5	20.0	1.30	--	51	62.45	.014216	1x10 ⁻⁴

TABLE 6

MEASURED TEMPERATURES AT DESIGNATED LOCATIONS

1" Stainless Steel Tube

January 8, 1971



THERMOCOUPLE NUMBER

<u>RUN</u>	<u>Re</u>	<u>1</u>	<u>2</u>	<u>3</u>	<u>4</u>	<u>5</u>	<u>6</u>	<u>7</u>	<u>8</u>	<u>9</u>	<u>10</u>	<u>11</u>	<u>12</u>	<u>13</u>	<u>14</u>	<u>15</u>	<u>16</u>	<u>17</u>
1	20	65.0	63.1	61.0	58.5	55.0	50.7	46.8	44.4	43.0	39.5	35.5	32.0	30.3	30.6	-305	31.2	74.7
2	23.4	65.6	64.1	62.0	59.9	56.5	52.6	48.8	46.6	45.4	41.9	38.4	35.3	33.3	32.5	-302	32.9	74.8
3	30	66.8	65.3	63.6	61.3	58.8	55.7	52.3	49.9	49.2	46.3	43.5	41.5	40.3	39	-300	37.5	74.8
4	35	67.3	66.3	64.9	62.9	60.7	58.0	55.1	52.8	52.5	49.9	47.1	45.5	44.3	43.2	-297	41.3	74.7
5	38.4	67.6	66.9	65.6	63.8	62.0	59.7	57.0	54.8	54.9	52.5	50.2	48.8	47.8	46.5	-306	43	75.4
6	43.1	68.8	68.1	66.9	65.3	63.8	61.6	59.4	57.2	57.5	55.3	53.3	52.0	51.1	50	-304	47.5	75.5
7	48.1	69.0	68.3	67.3	65.8	64.5	62.5	60.5	58.3	58.8	57.0	55.1	53.9	53	51.9	-306	50	75.4
8	52.9	69.1	68.7	67.3	66.3	65.1	63.4	61.5	59.3	59.9	58.2	56.5	55.3	54.6	53.5	-306	51.9	75.3
9	57.5	69.3	68.8	67.9	66.5	65.5	63.9	62.1	60.0	60.7	59.2	57.5	56.7	56	54.5	-308	53.6	75.1

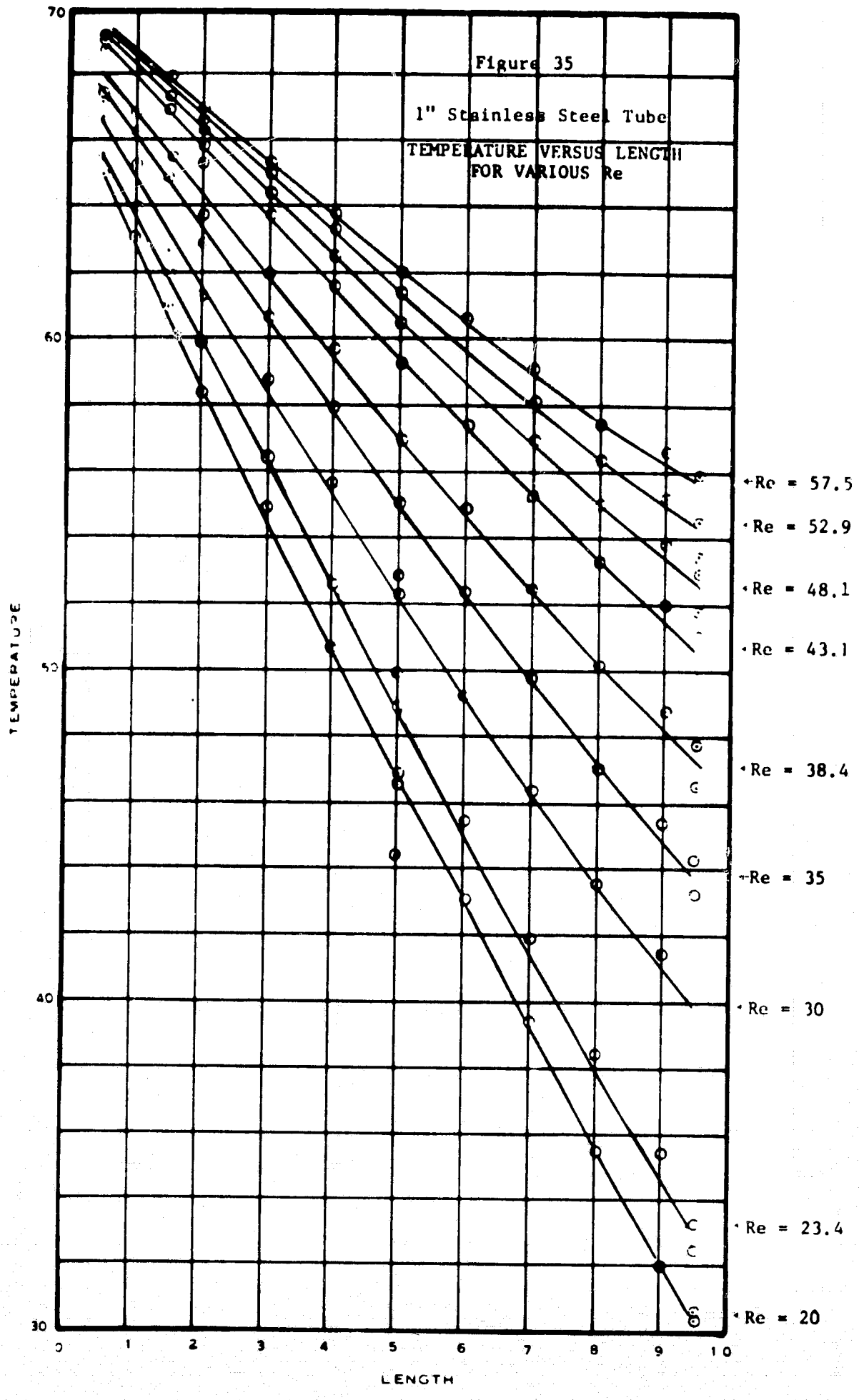


TABLE 7
EXPERIMENT SHEET

SPECIMEN: 1" Stainless Steel Tube

DATE: January 11, 1971

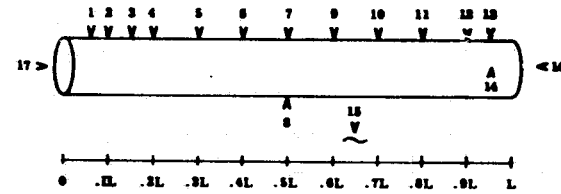
RUN	Re	HEAD PRESSURE	SHUNT VALVE	GLASS BEAD	STEEL BEAD	GRAMS H ₂ O	GPM	VACUUM
1	25.17	20.0	1.07	--	29.3	26.2	.00596	5×10^{-4}
2	30	20.0	1.07	--	38.3	31.2	.00710	5×10^{-4}
3	35	20.0	1.07	--	47.5	36.4	.00828	4×10^{-4}
4	40	20.0	1.07	--	53	41.7	.00949	5×10^{-4}

TABLE 8

MEASURED TEMPERATURES AT DESIGNATED LOCATIONS

1" Stainless Steel Tube

January 11, 1971



THERMOCOUPLE NUMBER

RUN	Re	1	2	3	4	5	6	7	8	9	10	11	12	13	14	15	16	17
1	25.17	66.3	64.8	62.8	60.5	57.5	53.8	49.9	47.6	46.7	43.3	40.0	37.2	35.3	34.2	-298	33.8	75.1
2	30	67.2	66.1	64.3	62.3	59.9	56.8	53.3	50.9	50.2	47.5	44.7	42.6	41.8	40.7	-297	39.1	75.3
3	35	68.2	67.2	65.8	63.8	61.7	59.2	56.2	53.8	53.7	51.0	48.6	47.1	46.0	44.9	-294	42.7	75.4
4	40	69.0	68.1	66.9	65.1	63.3	61.0	58.3	56.0	56.2	53.8	51.2	49.9	49.2	47.9	-294	45.5	75.5

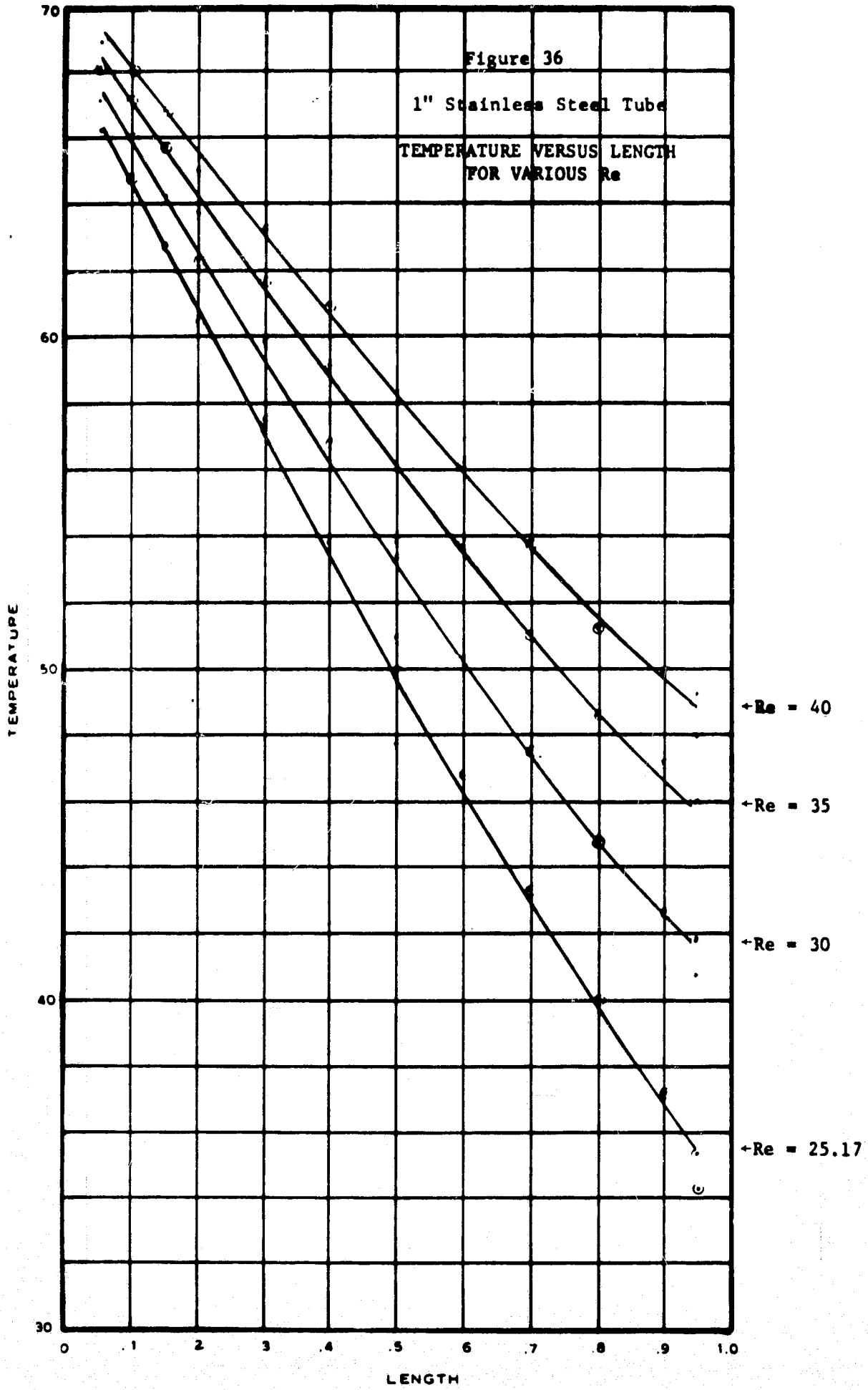


TABLE 9
EXPERIMENT SHEET

SPECIMEN: 3/4" Stainless Steel Tube

DATE: February 8, 1971

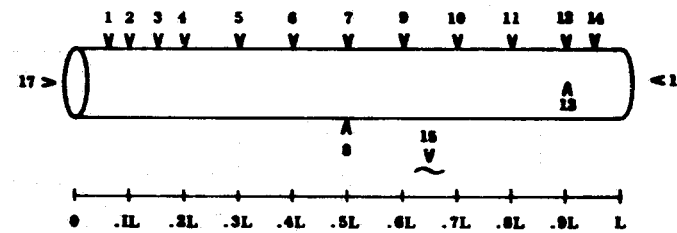
RUN	Re	HEAD PRESSURE	SHUNT VALVE	GLASS BEAD	STEEL BEAD	GRAMS H ₂ O	GPM	VACUUM
1	20	20.0	0.0	--	84	15.368	.003498	6x10 ⁻⁴
2	25	20.0	0.0	--	98	19.212	.004373	6x10 ⁻⁴
3	30	20.0	.75	--	49	23.052	.005247	8x10 ⁻⁴
4	35	20.0	.75	--	57	26.896	.006122	7x10 ⁻⁵
5	40	20.0	.75	--	63	30.735	.006996	1x10 ⁻⁴
6	45	20.0	.75	--	70.5	34.580	.007871	8x10 ⁻⁵
7	50	20.0	.75	--	75.7	38.419	.008745	1x10 ⁻⁴

TABLE 10

MEASURED TEMPERATURES AT DESIGNATED LOCATIONS

3/4" Stainless Steel Tube

February 8, 1971



THERMOCOUPLE NUMBER

<u>RUN</u>	<u>Re</u>	<u>1</u>	<u>2</u>	<u>3</u>	<u>4</u>	<u>5</u>	<u>6</u>	<u>7</u>	<u>8</u>	<u>9</u>	<u>10</u>	<u>11</u>	<u>12</u>	<u>13</u>	<u>14</u>	<u>15</u>	<u>16</u>	<u>17</u>
1	20	66.0	64.4	62.2	60.2	56.5	52.2	48.6	46.5	44.5	40.8	35.4	33.2	32.2	B	-290	33.0	75.0
2	25	66.9	65.8	64.0	62.3	59.7	56.1	53.0	50.9	49.5	46.3	42.2	41.6	40.2	39.2	-290	40.5	75.0
3	30	67.2	66.4	64.7	63.3	61.0	58.0	55.5	53.1	52.2	49.5	45.7	45.0	43.7	43.5	-294	44.7	75.0
4	35	67.4	66.9	65.6	64.5	62.6	60.2	58.2	56.1	55.9	53.5	47.8	49.8	48.1	48.5	-288	49.8	75.0
5	40	67.8	67.2	66.2	65.1	63.3	61.3	59.8	57.5	57.5	55.5	49.8	52.0	50.4	50.9	-292	52.4	75.0
6	45	68.0	67.7	66.8	65.8	64.5	62.5	61.1	58.9	59.2	57.3	51.8	54.5	53.0	53.4	-298	54.8	75.0
7	50	68.1	67.9	67.1	66.2	65.0	63.2	62.0	59.9	60.2	58.5	53.1	55.8	54.3	55.0	-298	56.2	75.0

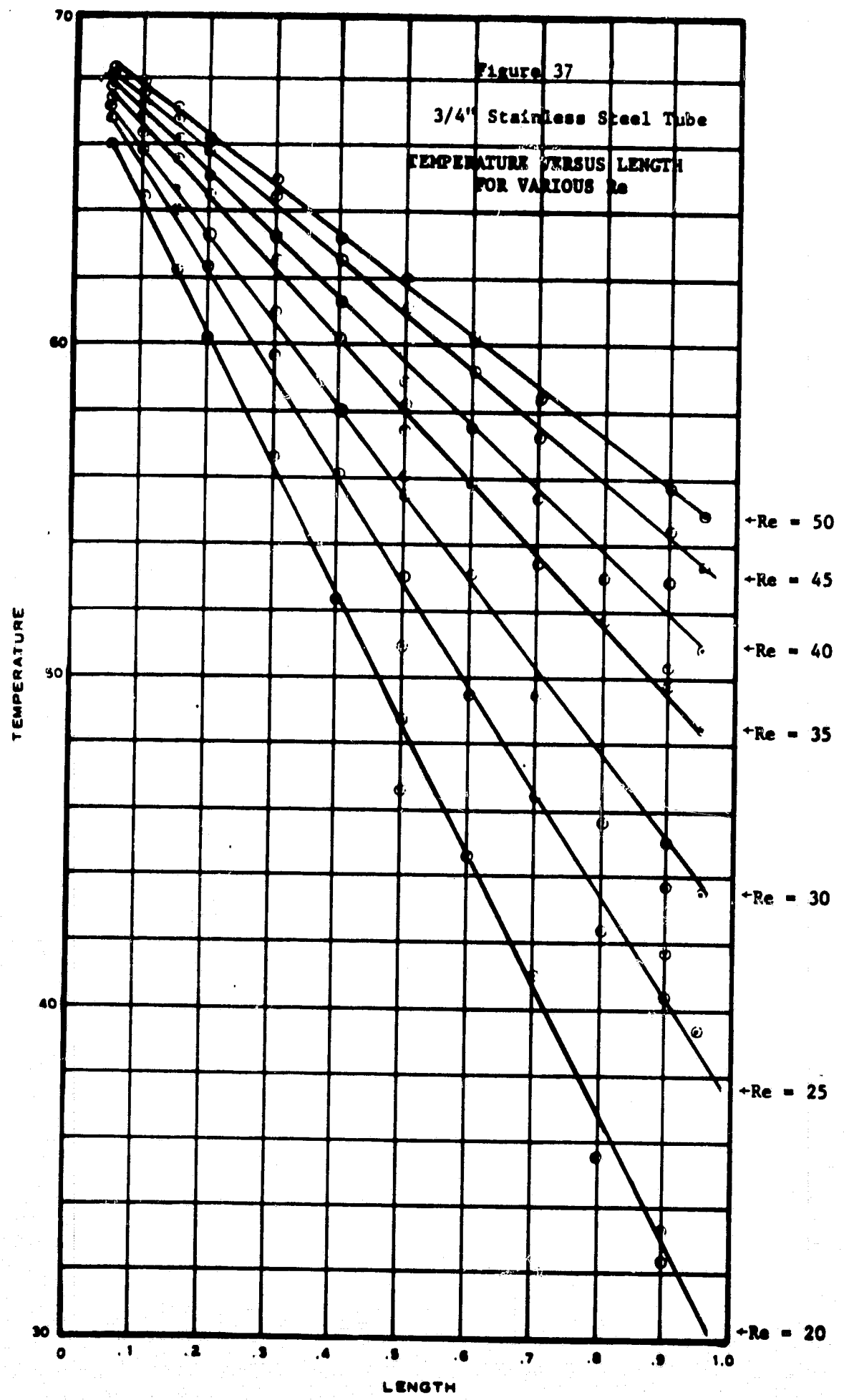


TABLE 11
EXPERIMENT SHEET

SPECIMEN: 1/2" Stainless Steel Tube

DATE: December 15, 1970

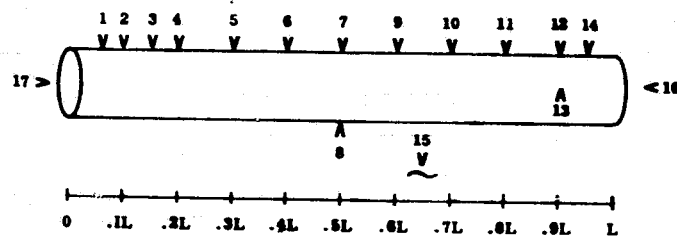
RUN	Re	HEAD PRESSURE	SHUNT VALVE	GLASS BEAD	STEEL BEAD	GRAMS H ₂ O	GPM	VACUUM
1	17.5	20.0	0.0	--	60	8.96	.00204	2x10 ⁻⁴
2	20	20.0	0.0	--	66	10.54	.00240	9x10 ⁻⁵
3	25	20.0	0.0	--	75	13.14	.00299	5x10 ⁻⁵
4	30	20.0	0.0	--	85	15.77	.00359	2x10 ⁻⁴
5	35	20.0	0.0	--	95	18.41	.00419	3x10 ⁻⁴
6	40	20.0	1.30	6	--	21.04	.00479	2x10 ⁻⁴
7	45	20.0	1.30	8	--	23.68	.00539	2x10 ⁻⁴
8	50	20.0	1.30	10	--	26.32	.00599	2x10 ⁻⁵
9	55	20.0	1.30	12.5	--	28.95	.00659	2x10 ⁻⁵

TABLE 12

MEASURED TEMPERATURES AT DESIGNATED LOCATIONS

1/2" Stainless Steel Tube

December 15, 1970



RUN	Re	1	2	3	4	5	6	7	8	9	10	11	12	13	14	15	16	17
1	17.5	62.3	60.6	58.3	B	52.0	48.3	44.4	44.5	41.2	37.0	33.8	31.2	31.5	B	-282	30	74.6
2	20	63.3	61.8	59.8	B	54.2	50.8	47.6	47.6	45.0	41.3	38.3	35.5	35.5	33.9	-283	34.1	74.5
3	25	65.3	63.9	62.3	60.8	58.0	55.0	52.3	52.2	50.3	47.3	45.0	42.8	42.5	41.0	-295	41.5	74.5
4	30	66.5	65.7	63.8	62.3	60.7	58.3	55.8	55.5	54.0	51.6	49.6	48.1	48.0	46.6	-294	46.2	74.8
5	35	67.5	66.8	65.1	63.8	62.3	60.5	58.3	58.4	56.8	54.5	53.0	51.8	51.1	50.3	-292	48.2	75.1
6	40	68.3	68.0	66.7	64.8	64.2	62.5	61.0	60.8	59.9	58.0	56.6	55.6	55.2	54.6	-290	52.9	75.5
7	45	69.2	69.0	67.8	B	65.5	64.2	62.8	62.6	62.0	60.5	59.2	58.5	58.0	57.4	-285	55.0	75.5
8	50	69.2	69.0	68.0	B	65.9	64.6	63.1	63.0	62.5	61.0	59.9	59.3	58.8	58.3	-270	56.5	75.3
9	55	69.3	69.2	68.3	B	66.5	65.3	64.0	63.8	63.3	62.1	61.1	60.6	60.2	59.9	-276	58.3	75.3

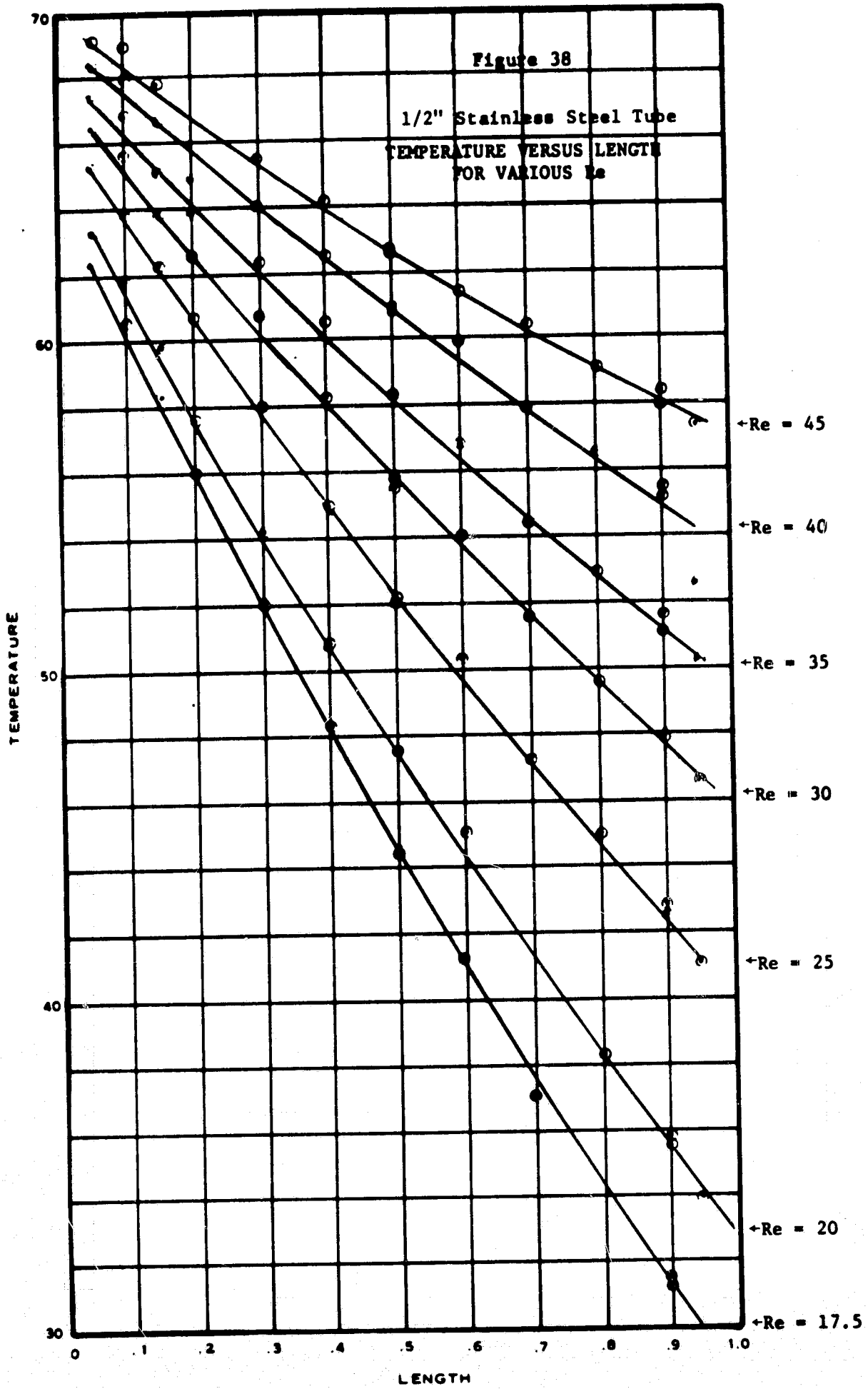


TABLE 13
EXPERIMENT SHEET

SPECIMEN: 1/4" Stainless Steel Tube

DATE: January 14, 1971

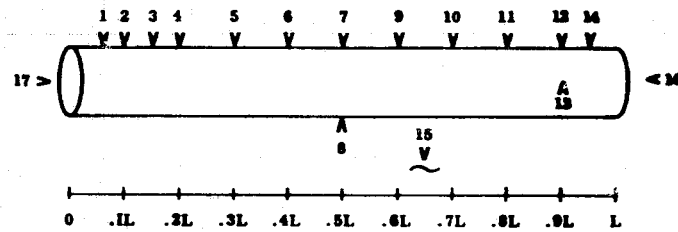
RUN	Re	HEAD PRESSURE	SHUNT VALVE	GLASS BEAD	STEEL BEAD	GRAMS H ₂ O	GPM	VACUUM
1	12.94	20.0	0.0	79	30.5	186.28	.000769	4x10 ⁻⁵
2	15	20.0	0.0	87	35	186.82	.000892	1x10 ⁻⁴
3	20	20.0	0.0	--	42.0	5.22	.001189	4x10 ⁻⁴
4	25	20.0	0.0	--	48.5	6.53	.001486	2x10 ⁻⁴
5	30	20.0	0.0	--	54	190.73	.001783	1x10 ⁻⁴
6	35	20.0	0.0	--	59.6	192.04	.002080	1x10 ⁻⁴
7	40	20.0	0.0	--	65	193.34	.002377	2x10 ⁻⁴
8	45	20.0	0.0	--	70	194.65	.002675	9x10 ⁻⁵
9	50	20.0	0.0	--	75	195.95	.002972	9x10 ⁻⁵

TABLE 14

MEASURED TEMPERATURES AT DESIGNATED LOCATIONS

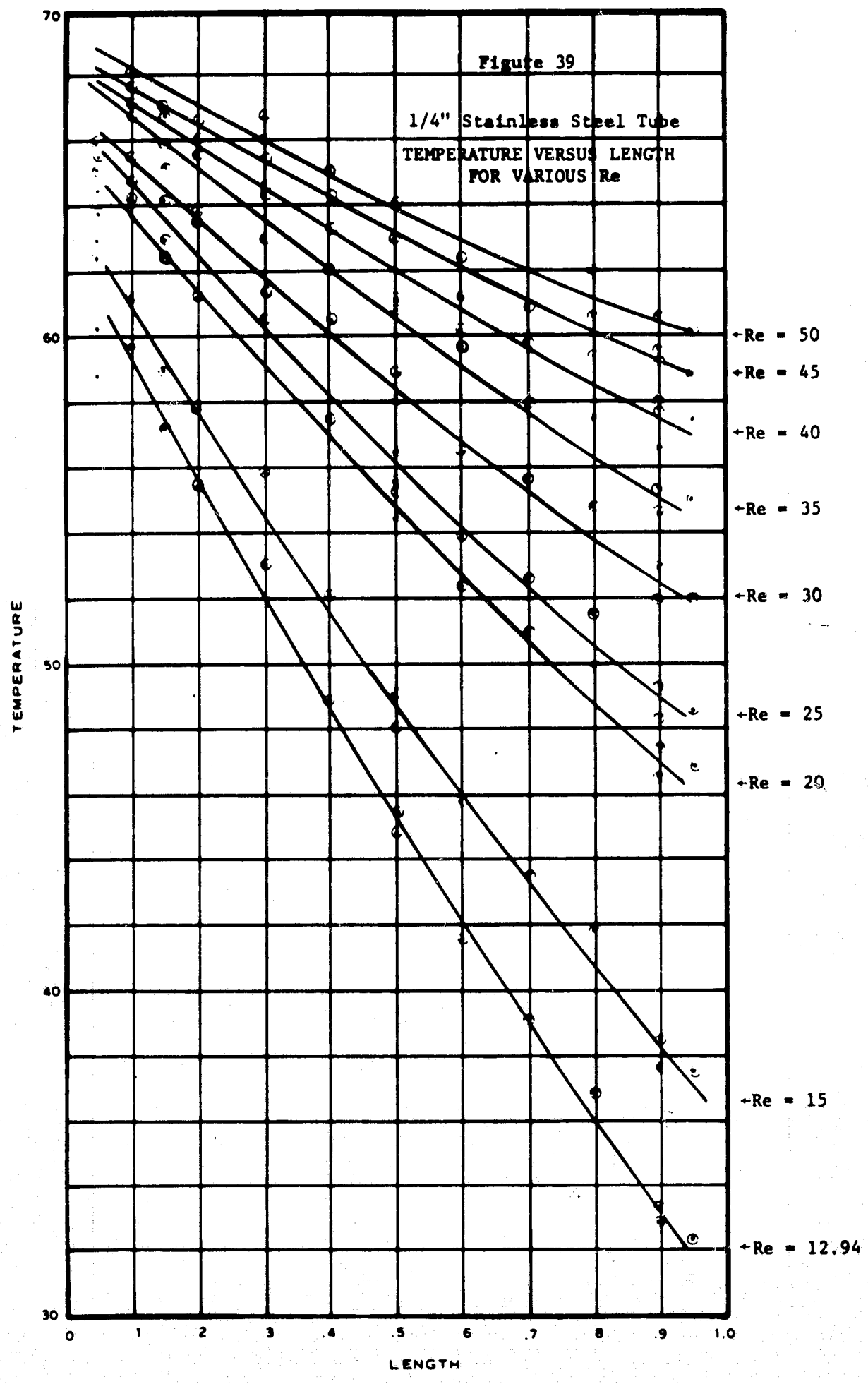
1/4" Stainless Steel Tube

January 14, 1971



THERMOCOUPLE NUMBER

RUN	Re	1	2	3	4	5	6	7	8	9	10	11	12	13	14	15	16	17
1	12.94	58.9	59.8	57.2	55.4	53.0	48.8	45.4	44.8	41.5	39.1	36.8	33.3	32.8	32.3	-295	B	74.5
2	15	60.3	61.3	59.0	57.8	55.8	52.0	49.0	48.0	45.7	43.5	41.8	38.5	37.6	37.5	-305	B	74.7
3	20	61.0	62.8	60.7	59.7	58.4	55.1	52.5	51.6	49.3	48.0	46.4	43.9	43.0	43.1	-300	B	74.0
4	25	62.9	65.0	63.0	62.3	61.3	58.8	56.6	55.8	54.0	53.0	51.8	49.3	48.5	48.6	-294	B	74.5
5	30	63.8	65.5	64.2	63.5	63.0	60.5	58.9	58.0	56.5	55.7	54.8	53.0	51.9	52.0	-302	B	74.9
6	35	64.5	66.8	65.2	63.8	64.3	62.1	60.8	60.0	58.5	58.0	57.5	55.4	54.6	55.0	-300	B	75.0
7	40	65.2	67.2	66.0	65.6	65.5	63.3	62.1	61.2	60.2	59.9	59.4	57.8	56.6	57.5	-300	B	75.2
8	45	65.6	67.8	66.8	66.1	66.1	64.3	63.0	62.0	61.2	61.0	60.7	59.2	58.0	58.9	-298	B	75.2
9	50	66.0	68.2	67.1	66.7	66.8	65.1	64.1	63.0	62.4	62.1	62.0	60.7	59.6	60.2	-295	B	75.3



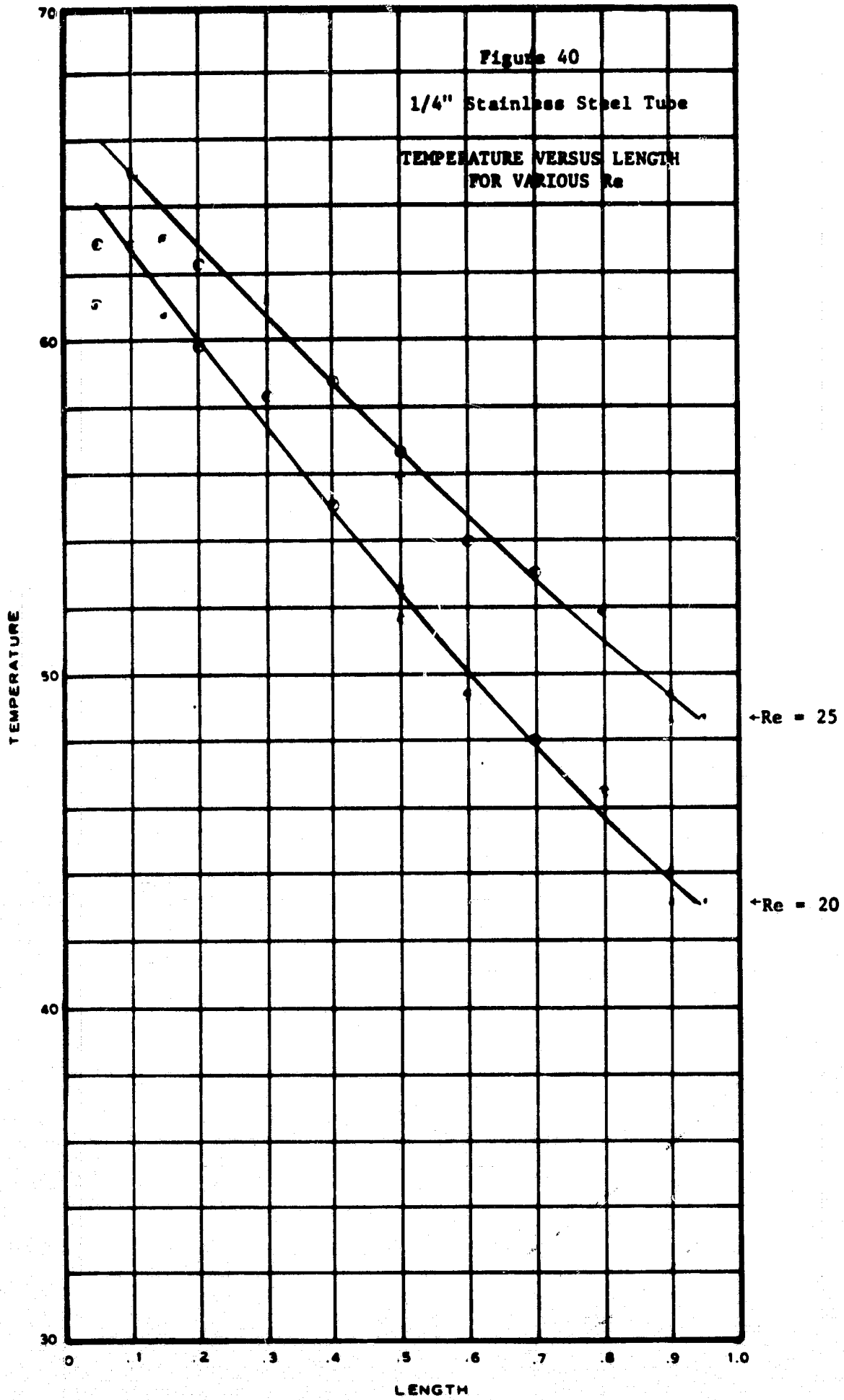


TABLE 15
EXPERIMENT SHEET

SPECIMEN: 1" Aluminum

DATE: February 26, 1971

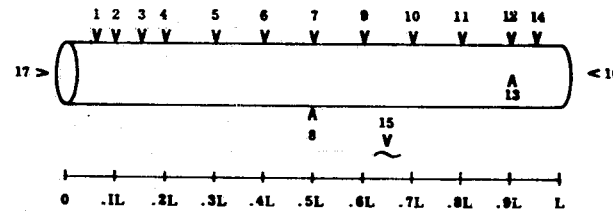
RUN	Re	HEAD PRESSURE	SHUNT VALVE	GLASS BEAD	STEEL BEAD	GRAMS H ₂ O	GPM	VACUUM
1	20	20.0	1.00	--	20.0	22.854	.005202	1x10 ⁻⁴
2	25	20.0	1.00	--	27.8	28.569	.006503	1x10 ⁻⁴
3	30	20.0	1.00	--	37.0	34.281	.007803	1x10 ⁻⁴
4	35	20.0	1.00	--	44.0	39.996	.009104	7x10 ⁻⁵
5	40	20.0	1.00	--	50.0	45.708	.0104	2x10 ⁻⁴
6	45	20.0	1.00	--	55.5	51.42	.011705	1x10 ⁻⁴
7	50	20.0	1.00	--	57.6	57.135	.013005	1x10 ⁻⁴

TABLE 16

MEASURED TEMPERATURES AT DESIGNATED LOCATIONS

1" Aluminum Tube

February 26, 1971



THERMOCOUPLE NUMBER

RUN	Re	1	2	3	4	5	6	7	8	9	10	11	12	13	14	15	16	17
1	20	64.0	62.4	60.1	58.4	55.0	51.0	47.1	46.9	43.8	40.6	36.5	33.7	33.9	32.6	-305	B	74.5
2	25	65.5	64.1	62.1	60.7	58.0	54.6	50.9	50.8	48.3	45.4	42.4	40.3	40.3	39.3	-302	B	74.5
3	30	66.3	65.4	63.8	62.5	60.1	57.4	54.3	54.1	51.9	49.5	46.7	44.8	44.8	44.2	-296	B	74.5
4	35	67.3	66.4	65.0	63.9	62.0	59.6	56.7	56.6	55.0	52.6	50.1	48.5	48.3	48.0	-290	B	74.5
5	40	67.8	67.0	65.8	65.0	63.1	61.0	58.7	58.4	57.0	55.1	52.6	51.3	51.3	50.8	-291	B	74.7
6	45	67.9	67.3	66.0	65.2	63.7	61.8	59.6	59.4	58.3	56.3	54.2	52.9	52.4	52.5	-288	B	74.8
7	50	67.6	66.7	65.5	64.8	63.0	61.1	58.8	58.5	57.3	55.3	53.0	51.7	51.4	51.3	-288	B	74.5

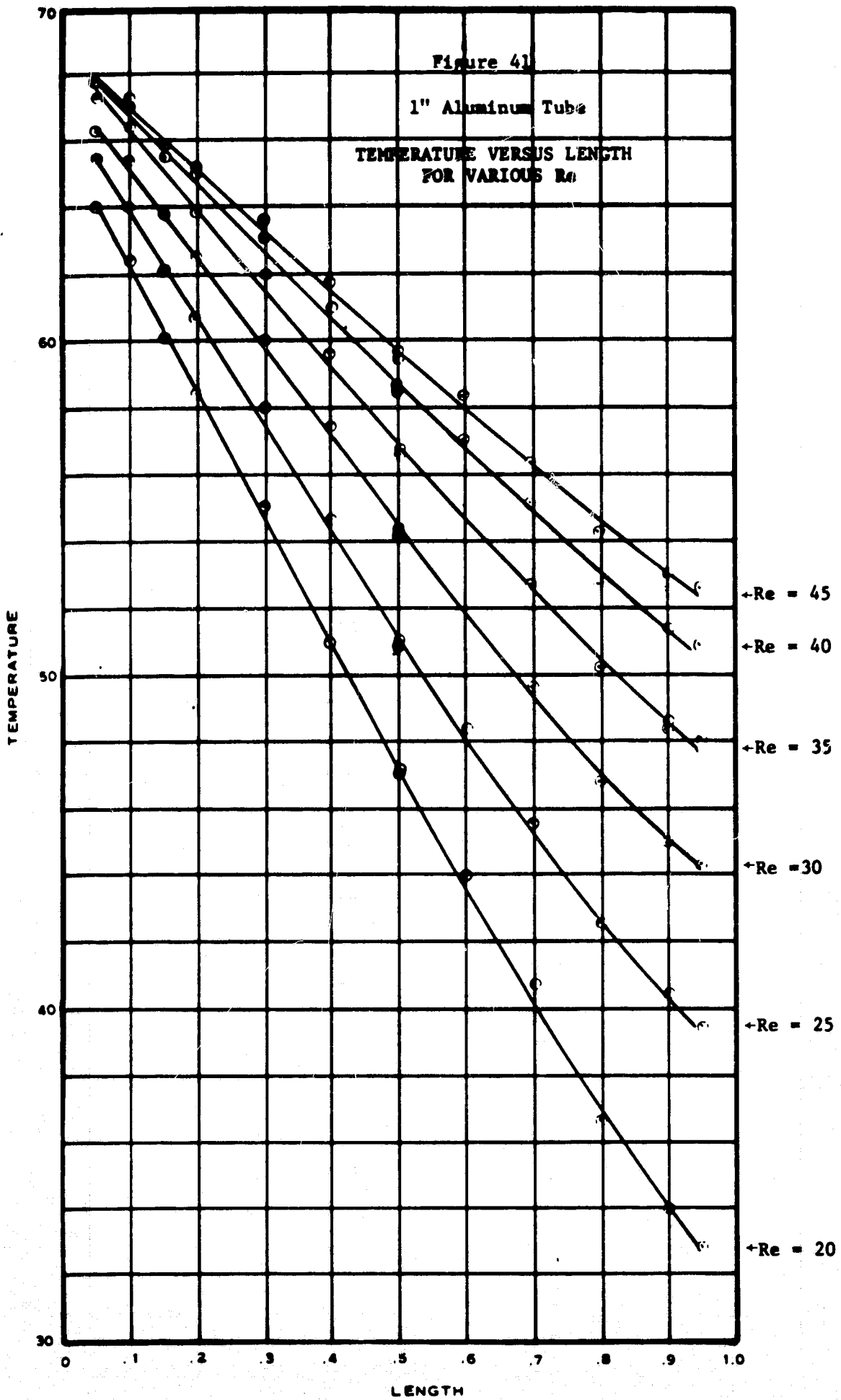


TABLE 17
EXPERIMENT SHEET

SPECIMEN: 3/4" Aluminum Tube

DATE: February 12, 1971

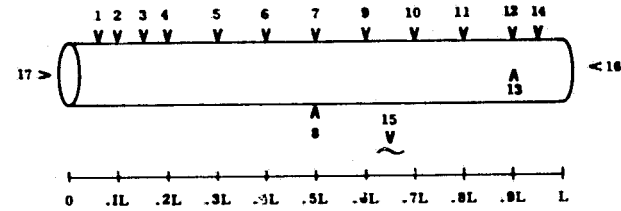
RUN	Re	HEAD PRESSURE	SHUNT VALVE	GLASS BEAD	STEEL BEAD	GRAMS H ₂ O	GPM	VACUUM
1	20	20.0	0.0	--	88.5	112.09	.003868	4x10 ⁻⁴
2	25.18	20.0	1.0	--	14.0	116.5	.004871	3x10 ⁻⁴
3	30	20.0	1.0	--	25.4	120.59	.005802	2x10 ⁻⁴
4	35	20.0	1.0	--	36.2	124.84	.006769	1x10 ⁻⁴
5	40	20.0	1.0	--	43.6	129.08	.007736	1x10 ⁻⁴
6	45	20.0	1.0	--	51.0	133.33	.008703	1x10 ⁻⁴
7	50	20.0	1.0	--	56.0	137.58	.009671	1x10 ⁻⁴

TABLE 18

MEASURED TEMPERATURES AT DESIGNATED LOCATIONS

3/4" Aluminum Tube

February 12, 1971



THERMOCOUPLE NUMBER

RUN	Re	1	2	3	4	5	6	7	8	9	10	11	12	13	14	15	16	17
1	20	66.3	64.4	62.6	60.8	57.5	53.8	50.2	50.2	46.9	43.6	40.6	37.8	37.8	35.9	-298	37.2	74.5
2	25	68.0	66.2	64.8	63.3	60.8	57.5	54.8	54.9	51.8	49.0	46.7	44.6	44.5	43.1	-300	43.9	75.2
3	30	68.3	66.9	65.9	64.8	62.5	59.8	57.4	57.4	54.8	52.5	50.2	48.8	48.3	47.3	-301	48.1	75.1
4	35	68.8	67.3	66.5	65.6	63.8	61.2	59.3	59.3	57.1	55.2	53.2	51.7	51.5	50.5	-300	51.7	75.0
5	40	69.2	68.0	67.2	66.3	64.7	62.5	60.8	60.8	58.8	57.0	55.3	54.3	54.1	53.0	-283	54.3	75.1
6	45	69.4	68.3	67.7	66.9	65.3	63.4	61.9	62.0	60.1	58.5	57.1	56.1	55.8	55.2	-290	56.3	75.1
7	50	69.6	68.7	68.1	67.3	66.0	64.4	62.9	62.9	61.3	60.0	58.8	57.5	57.2	57.0	-286	58.0	75.2

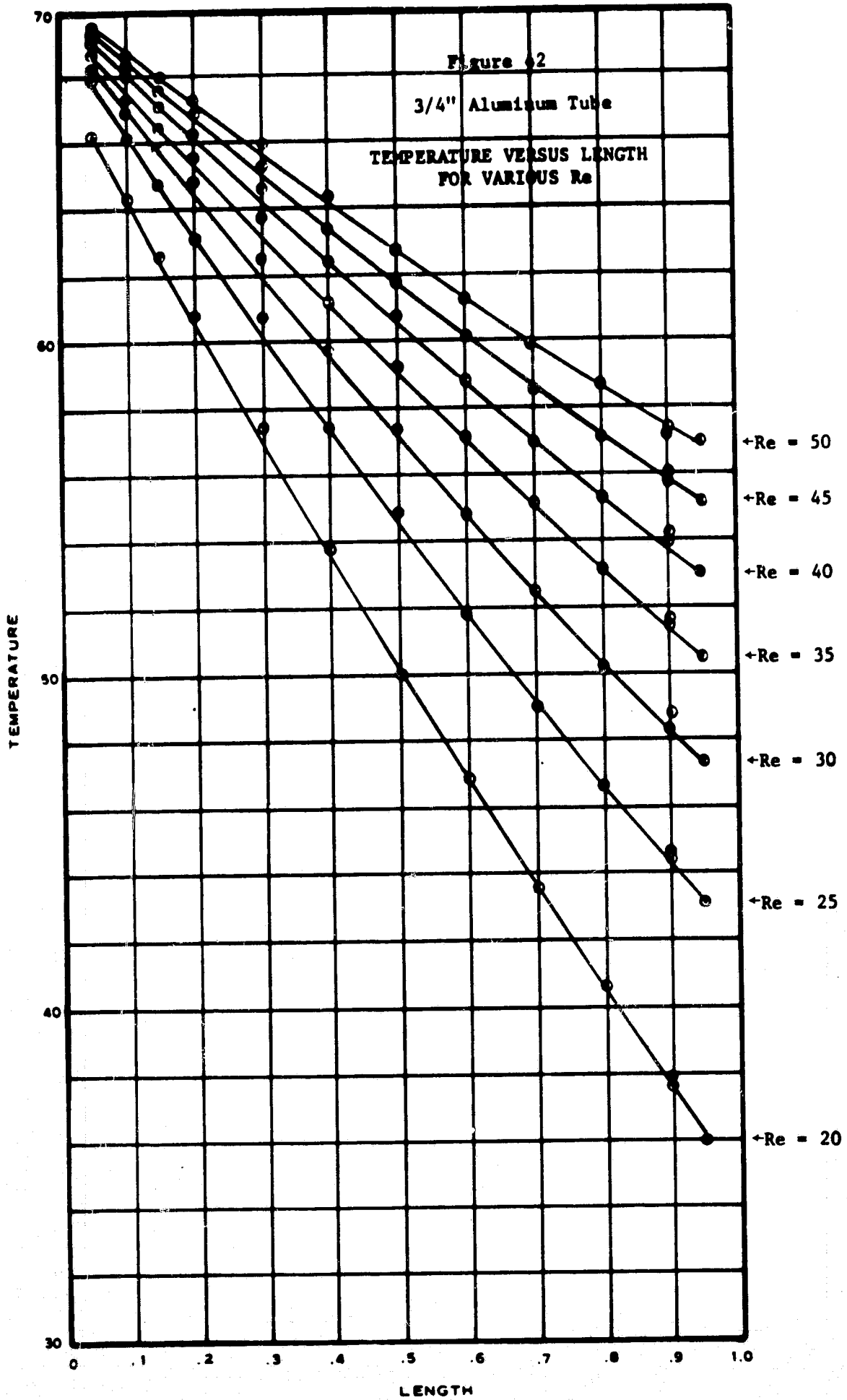


TABLE 19
EXPERIMENT SHEET

SPECIMEN: 1/2" Aluminum Tube

DATE: February 2, 1971

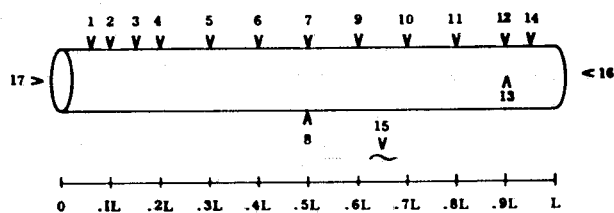
RUN	Re	HEAD PRESSURE	SHUNT VALVE	GLASS BEAD	STEEL BEAD	GRAMS H ₂ O	GPM	VACUUM
1	15	20.0	0.0	--	57.3	8.29	.001886	2x10 ⁻⁴
2	20	20.0	0.0	--	68.8	11.05	.002516	1x10 ⁻⁴
3	25	20.0	0.0	--	79	13.81	.003144	1x10 ⁻⁴
4	30	20.0	0.0	--	89	16.56	.003773	1x10 ⁻⁴
5	35	20.0	0.0	--	99.5	19.34	.004402	2x10 ⁻⁴
6	40	20.0	0.75	--	53	22.10	.005031	2x10 ⁻⁴
7	45	20.0	0.75	--	55	24.87	.00566	1x10 ⁻⁴
8	50	20.0	0.75	--	57	27.63	.006289	3x10 ⁻⁴

TABLE 20

MEASURED TEMPERATURES AT DESIGNATED LOCATIONS

1/2" Aluminum Tube

February 2, 1971



THERMOCOUPLE NUMBER

RUN	Re	1	2	3	4	5	6	7	8	9	10	11	12	13	14	15	16	17
1	15	64.0	62.0	59.9	58.1	54.3	50.5	46.9	46.9	43.5	40.1	36.5	34.1	33.7	32.5	-297	31.8	74.5
2	20	65.9	64.1	62.5	61.3	58.4	55.6	52.6	52.6	49.9	47.1	44.4	42.7	42.2	41.2	-295	40.5	74.7
3	25	66.8	65.6	64.2	63.3	61.1	58.7	56.3	56.3	54.1	51.7	49.3	47.8	47.5	46.9	-295	45.9	74.8
4	30	67.9	66.7	65.6	65.0	62.9	61.0	59.1	59.1	57.3	55.5	53.4	52.1	52.0	51.1	-293	50.8	74.8
5	35	68.9	67.9	66.9	66.2	64.7	62.9	61.1	61.1	59.7	58.0	56.3	55.1	55.1	54.5	-290	53.9	75.0
6	40	68.8	67.9	67.0	66.5	65.0	63.6	61.9	62.0	60.6	59.2	57.7	56.7	56.5	56.0	-299	56.0	75.0
7	45	69.2	68.7	67.6	67.2	65.9	64.8	63.2	63.2	62.0	60.6	59.3	57.7	58.2	58.0	-298	57.9	75.2
8	50	69.6	69.0	68.2	67.6	66.5	65.5	64.1	64.1	63.1	62.0	60.6	59.2	59.6	59.5	-299	59.5	75.2

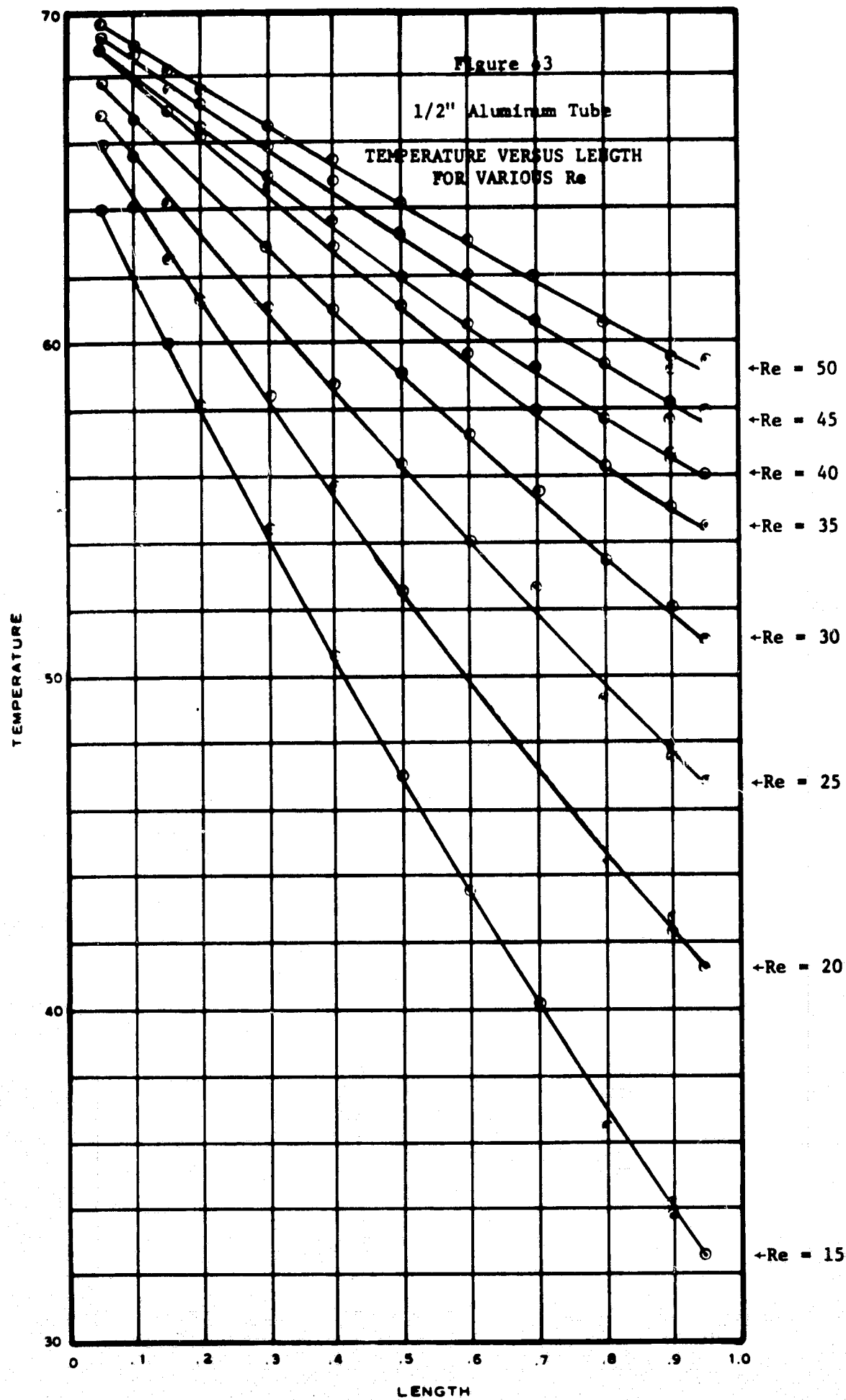


TABLE 21
EXPERIMENT SHEET

SPECIMEN: 1/4" Aluminum Tube

DATE: January 27, 1971

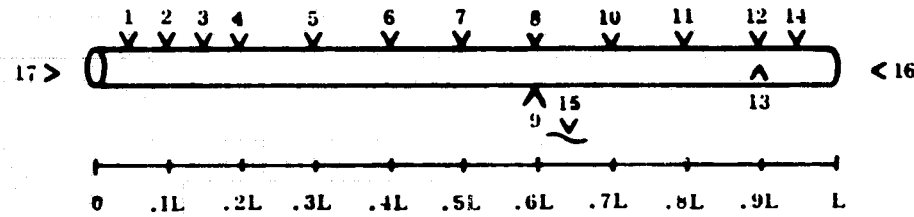
RUN	Re	HEAD PRESSURE	SHUNT VALVE	GLASS BEAD	STEEL BEAD	GRAMS H ₂ O	GPM	VACUUM
1	15	20.0	0.0	86	--	3.98	.000907	8×10^{-5}
2	20	20.0	0.0	--	42.5	5.32	.001210	1×10^{-4}
3	25	20.0	0.0	--	50.0	6.64	.001512	1×10^{-4}
4	30	20.0	0.0	--	56.1	7.97	.001814	1×10^{-4}
5	35	20.0	0.0	--	61.9	9.30	.002117	3×10^{-4}
6	40	20.0	0.0	--	67.2	10.63	.002419	1×10^{-4}
7	45 ⁺	20.0	0.0	--	72.1	11.96	.002722	1×10^{-4}
8	50.62	20.0	0.0	--	77	13.45	.00306	7×10^{-5}

TABLE 22

MEASURED TEMPERATURES AT DESIGNATED LOCATIONS

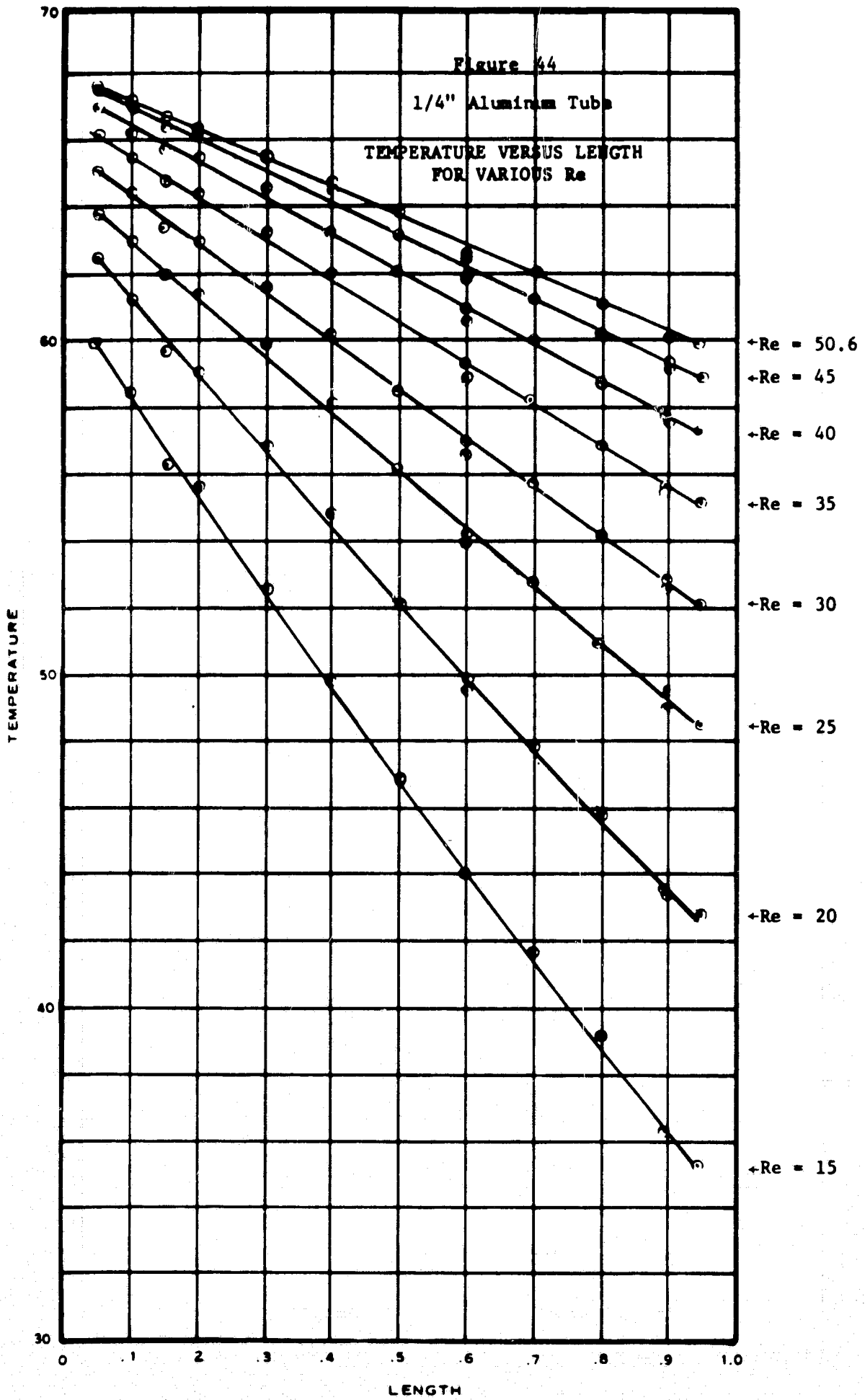
1/4" Aluminum Tube

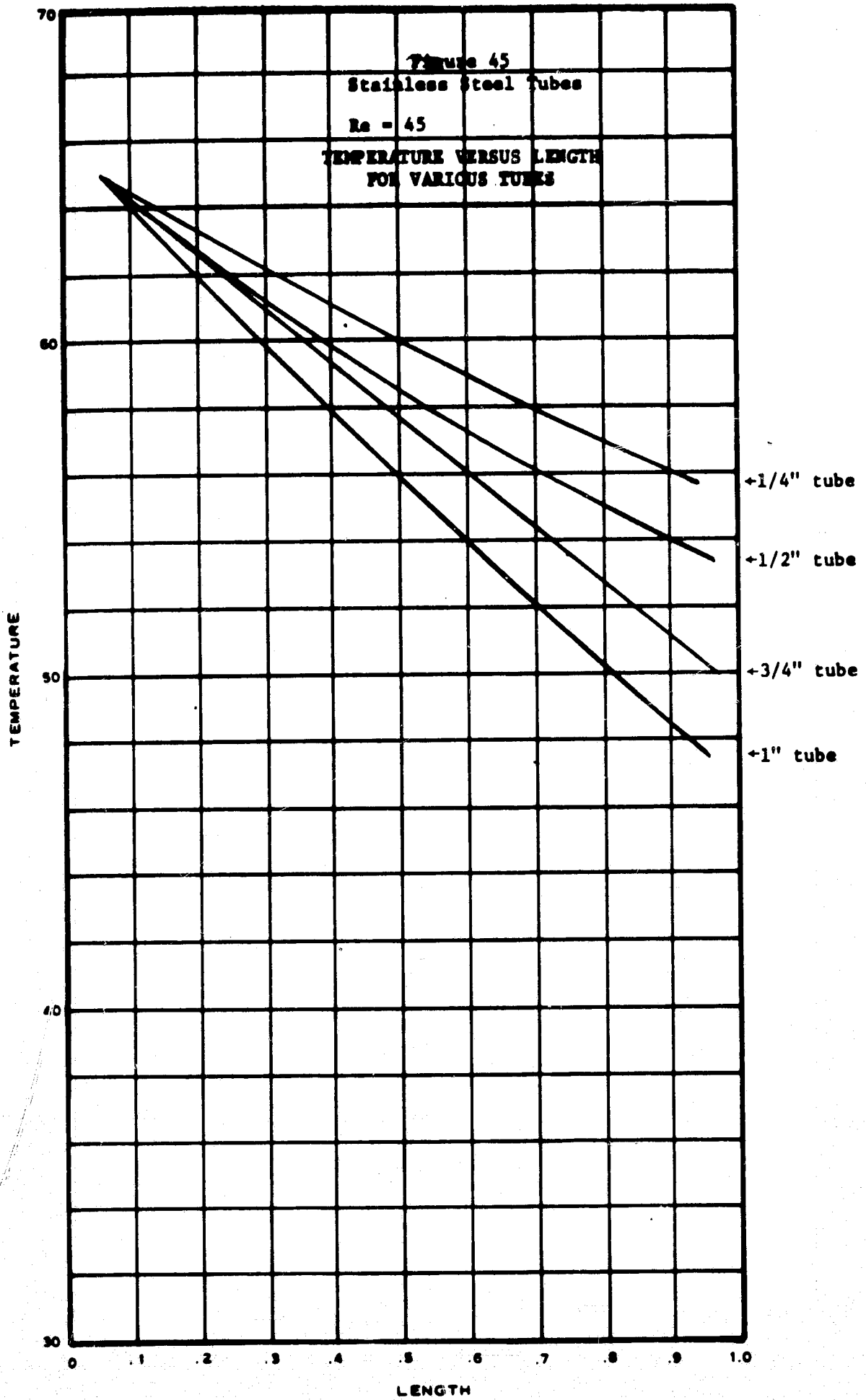
January 27, 1971

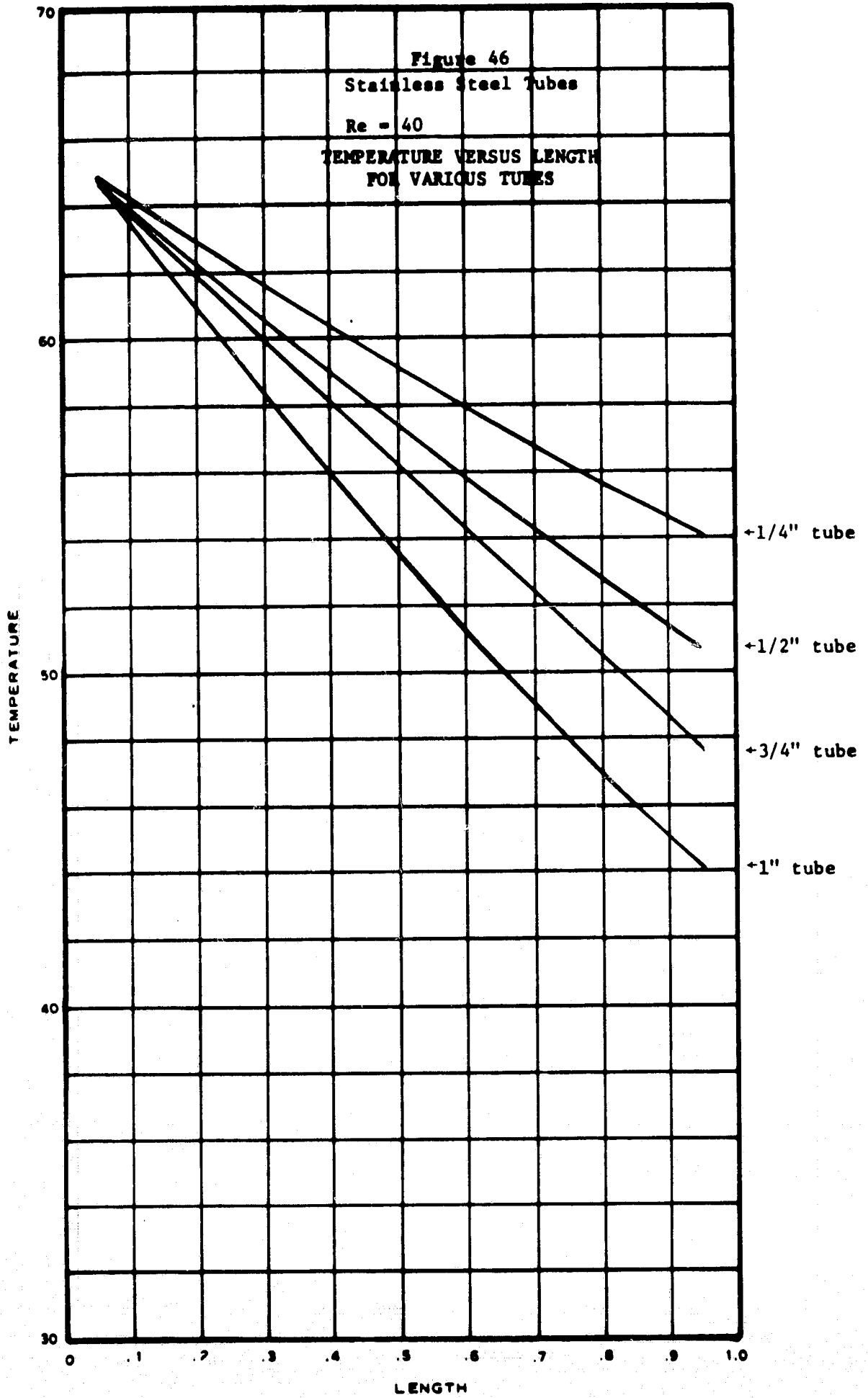


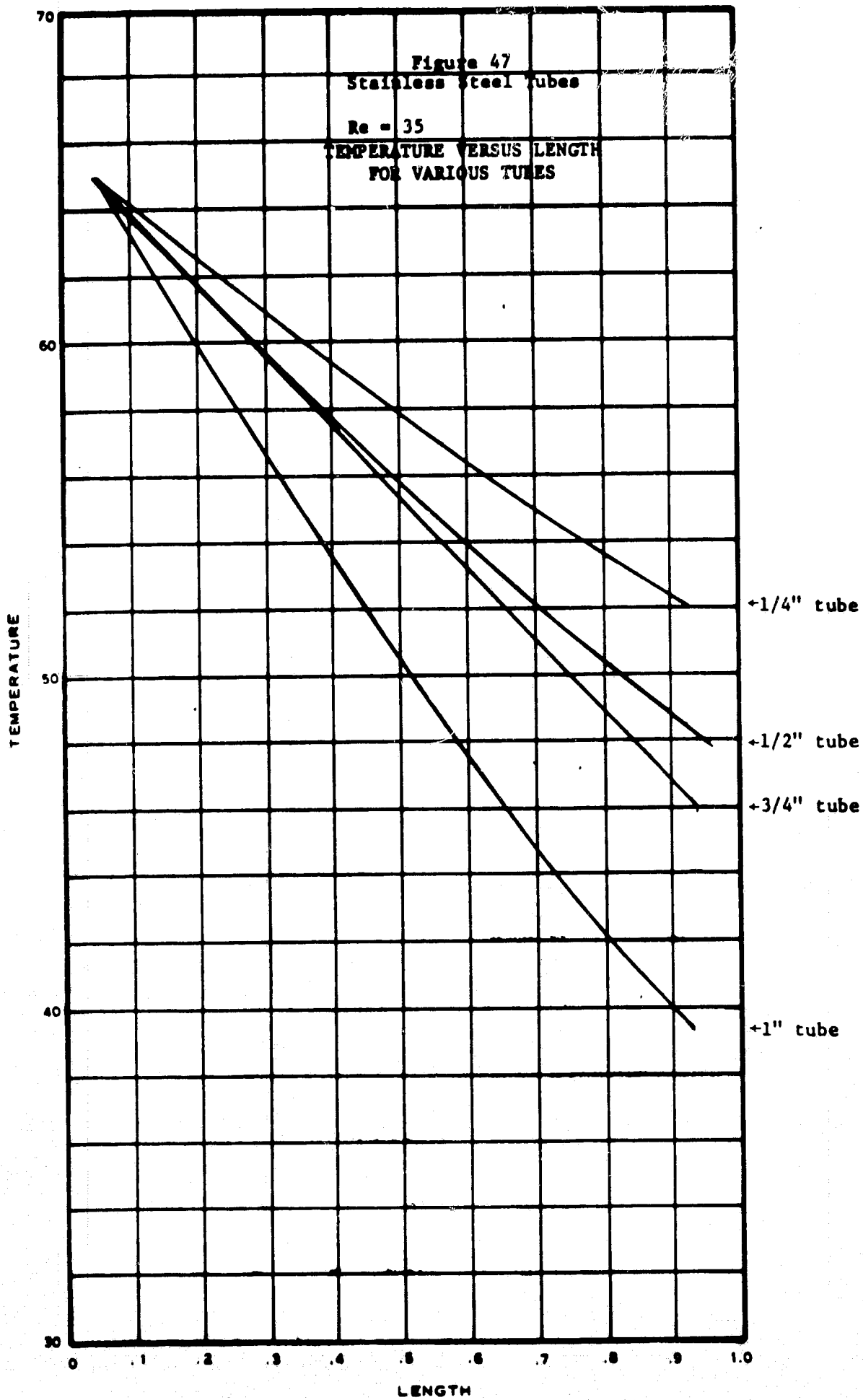
THERMOCOUPLE NUMBER

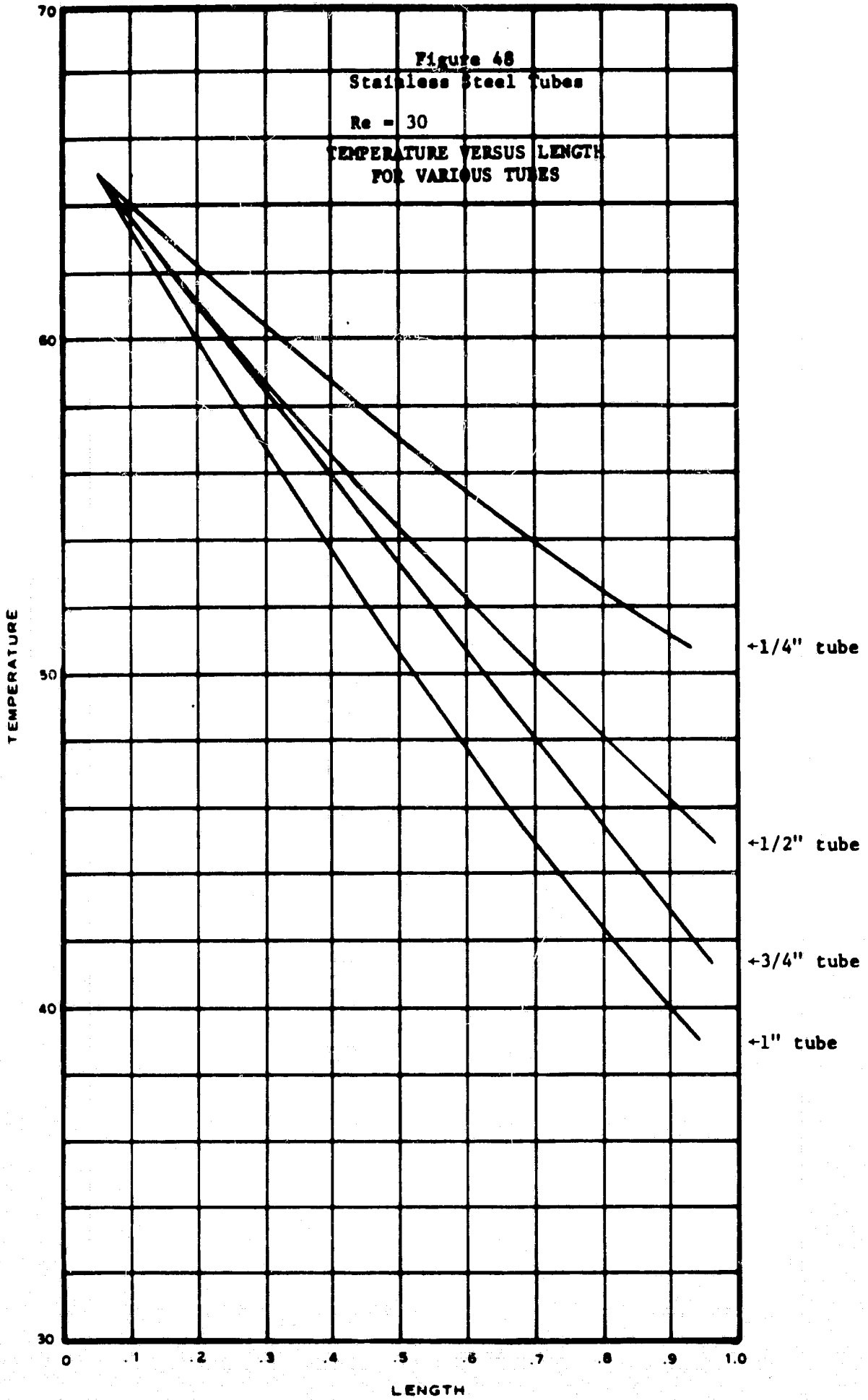
RUN	Re	1	2	3	4	5	6	7	8	9	10	11	12	13	14	15	16	17
1	15	59.9	58.4	56.3	55.6	52.6	49.8	46.8	44.0	43.9	41.6	39.1	36.3	36.2	35.2	-305	33.1	74.5
2	20	62.5	61.2	59.7	59.0	56.9	54.8	52.1	49.8	49.5	47.9	45.8	43.5	43.4	42.8	-302	40.9	75.0
3	25	63.8	63.0	62.0	61.4	59.9	58.1	56.1	54.2	54.0	52.8	50.9	49.5	49.0	48.5	-303	46.5	74.5
4	30	65.1	64.5	63.4	63.0	61.6	60.2	58.5	57.0	56.6	55.8	54.2	52.9	52.6	52.1	-301	50.8	74.5
5	35	66.2	65.5	64.8	64.5	63.3	62.1	60.6	59.3	58.9	58.2	56.9	55.6	55.4	55.2	-300	53.9	74.8
6	40	67.0	66.2	65.8	65.5	64.6	63.3	62.1	61.0	60.6	60.0	58.9	57.8	57.6	57.3	-300	56.6	75.0
7	45	67.5	67.2	66.4	66.2	65.5	64.5	63.2	62.1	61.9	61.3	60.3	59.4	59.2	59.0	-300	58.0	75.0
8	50.6	67.6	67.3	66.7	66.4	65.6	64.8	63.9	62.6	62.5	62.0	61.1	60.2	60.1	60.0	-300	59.0	74.7

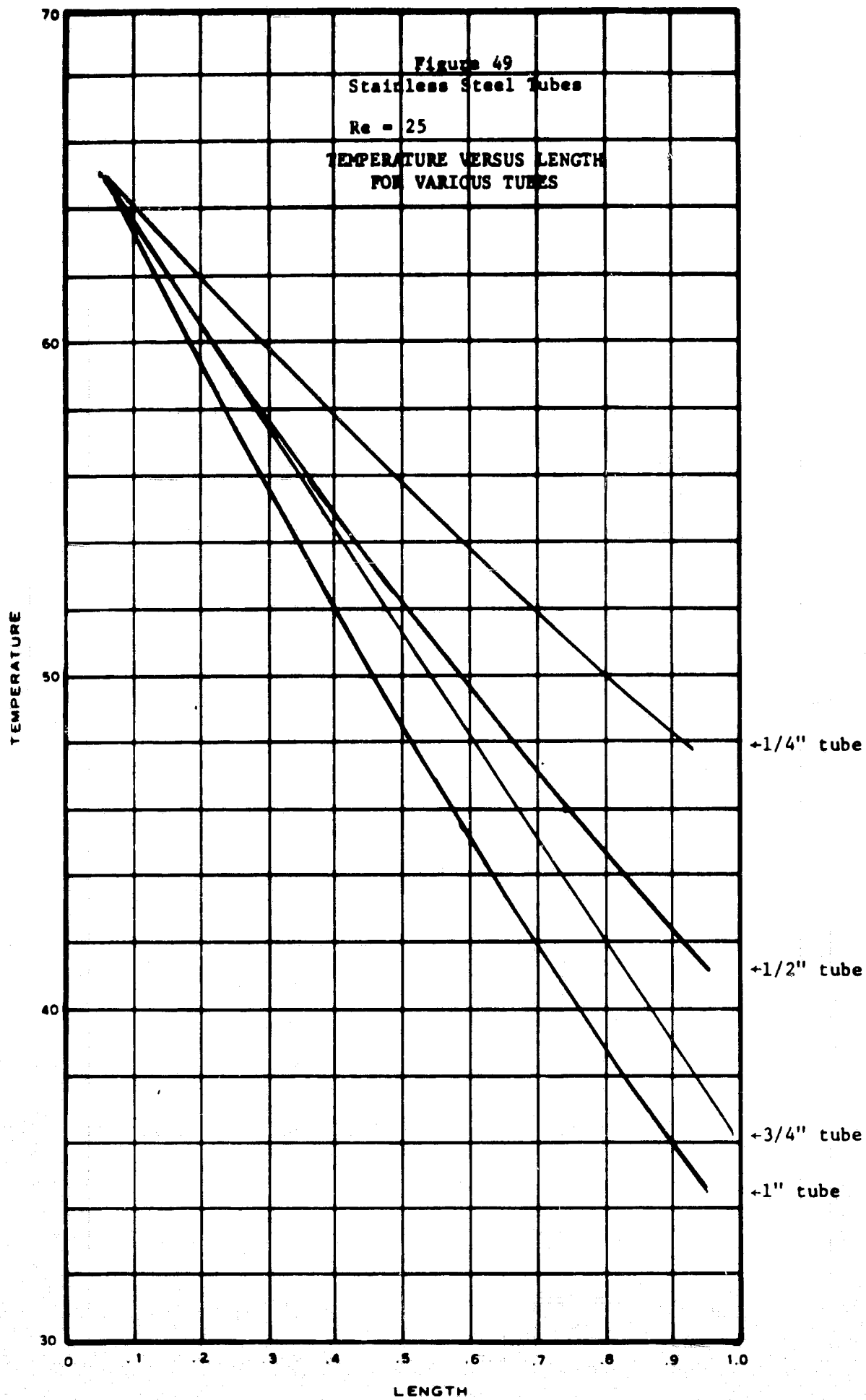


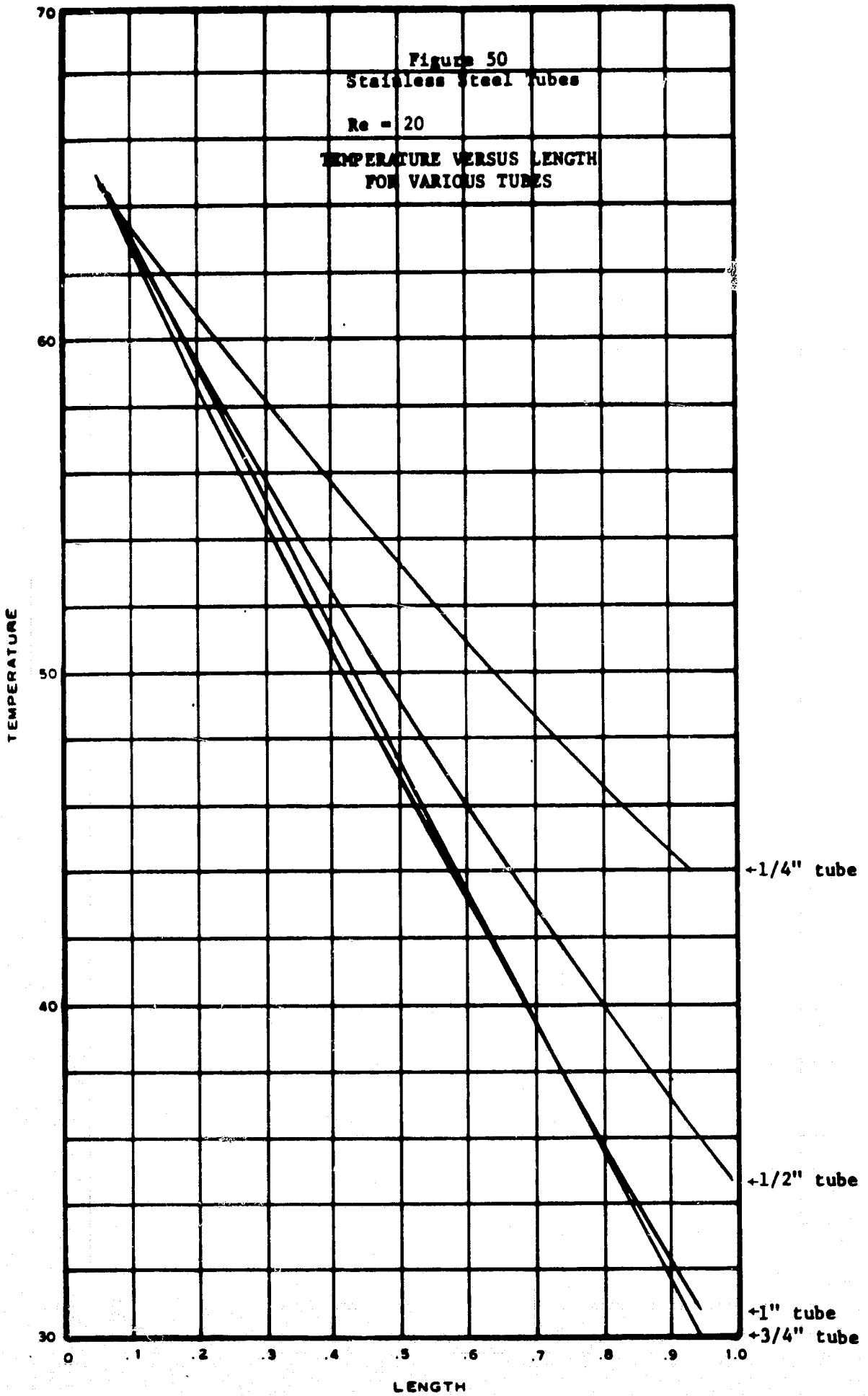


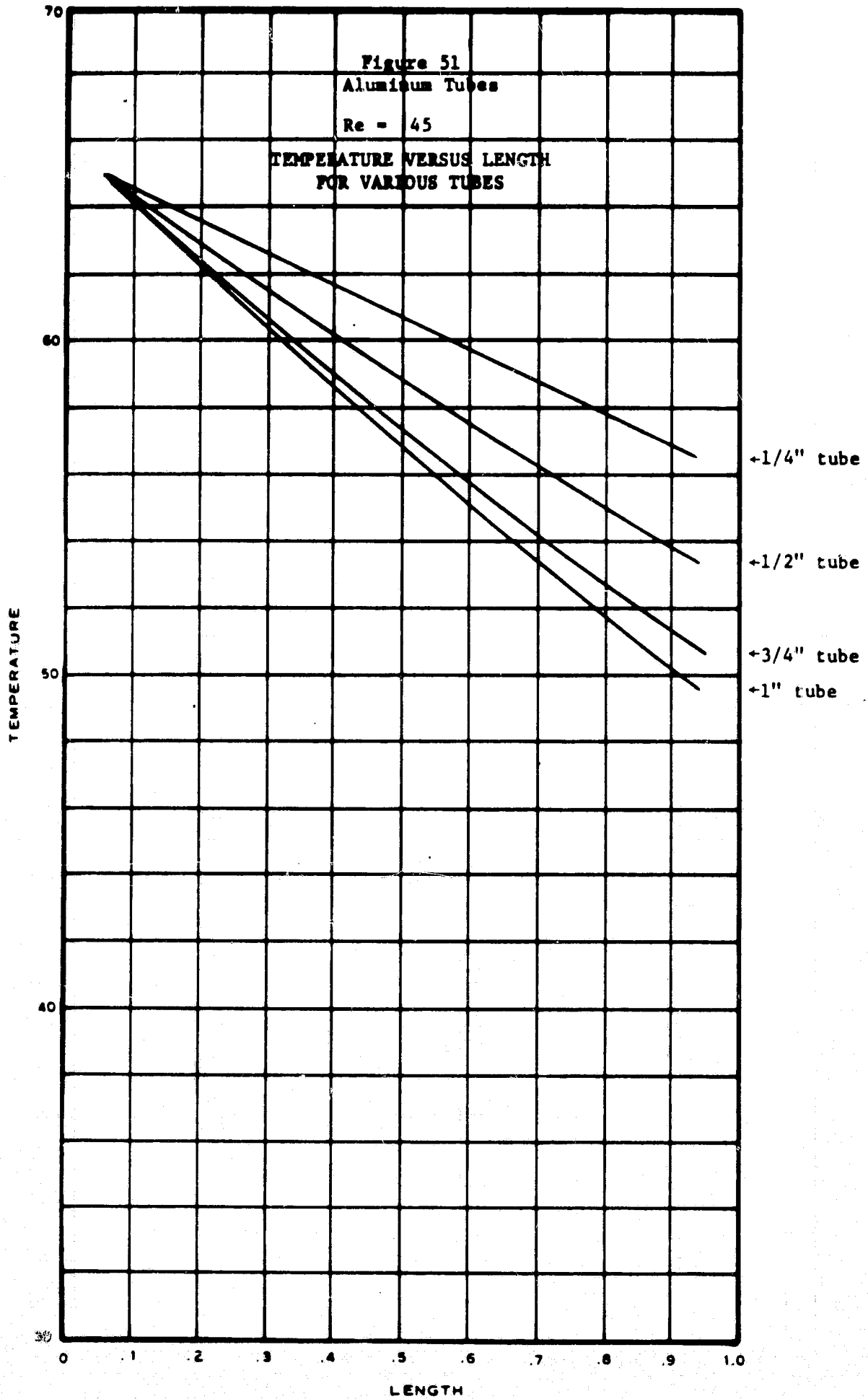


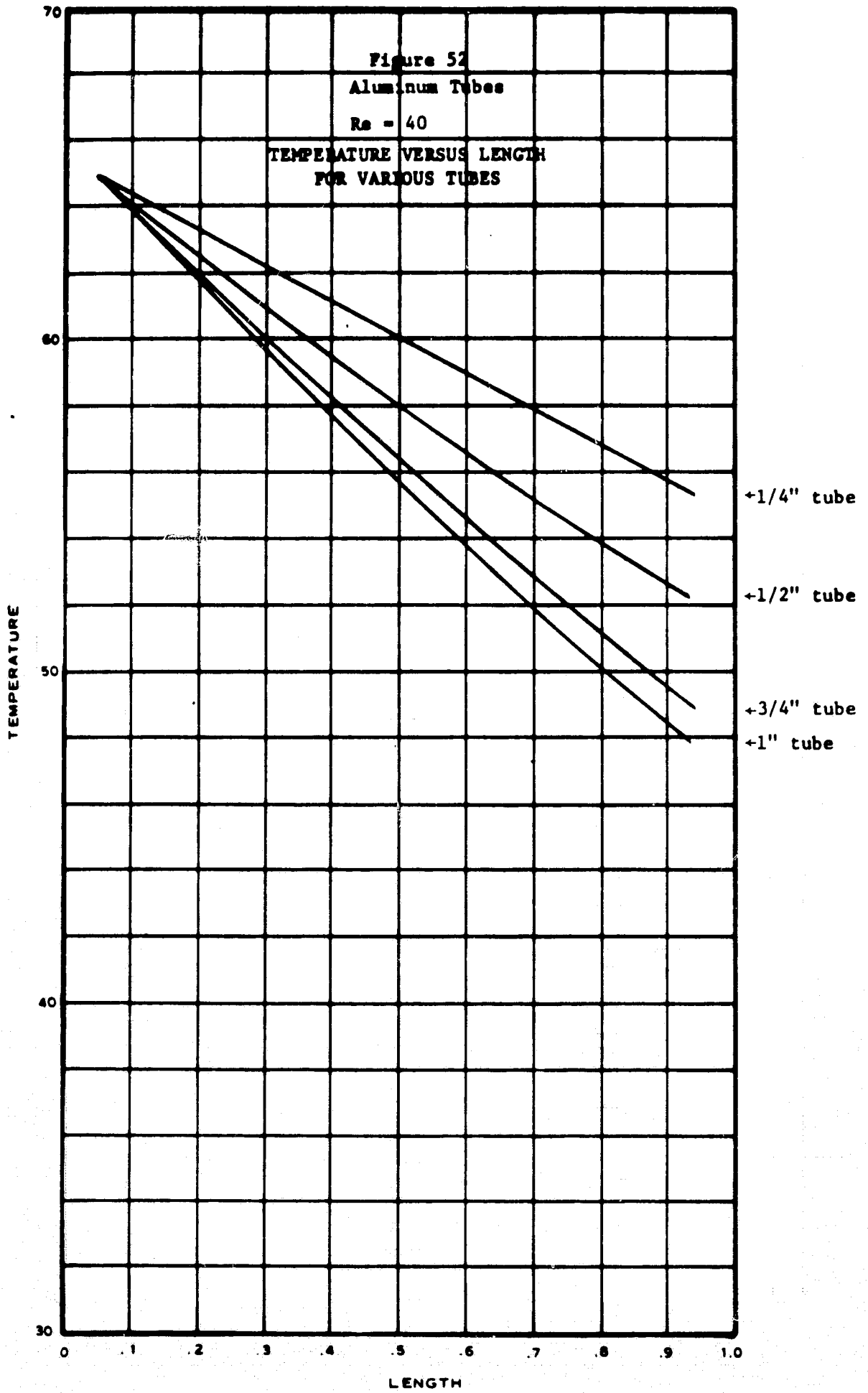


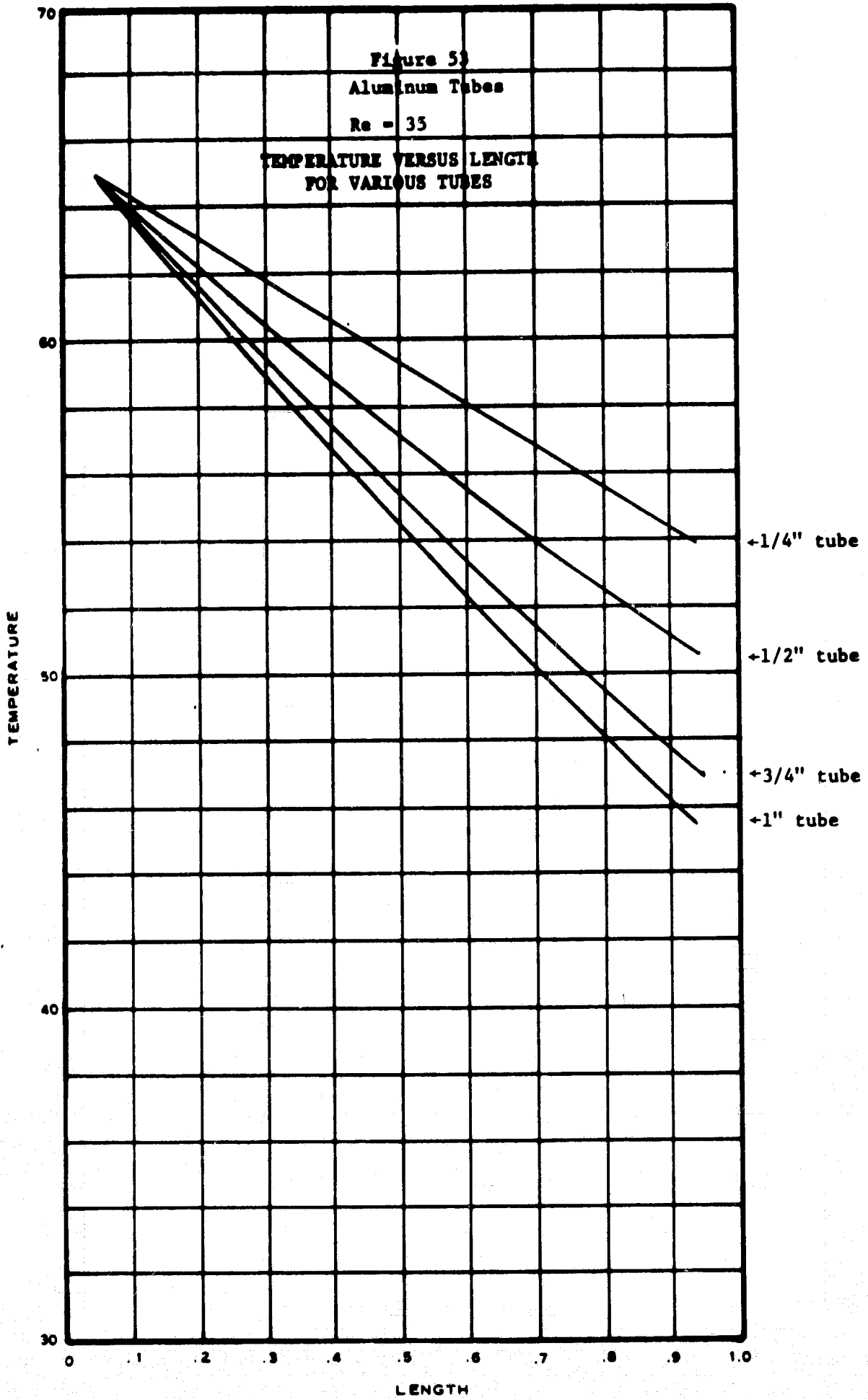


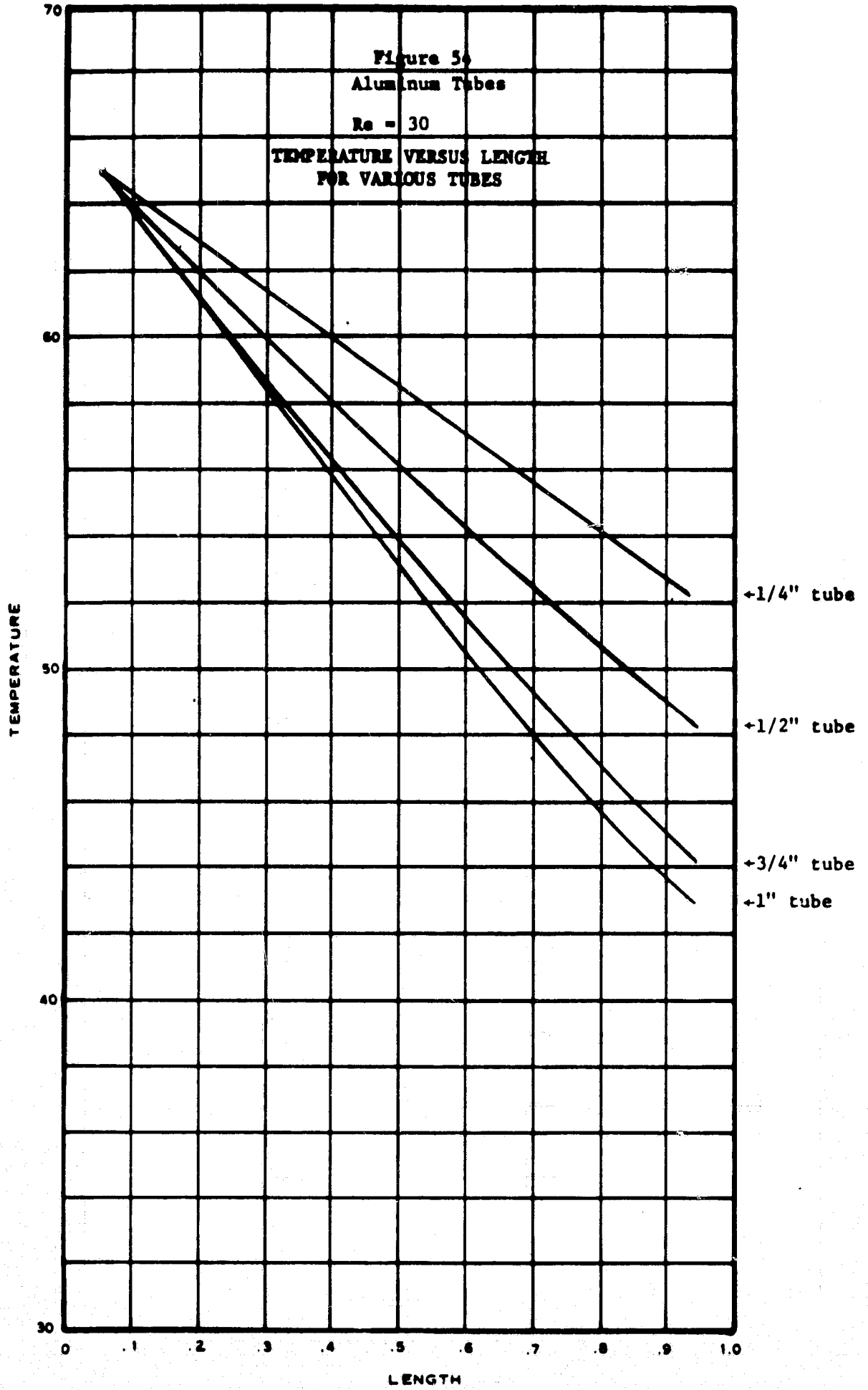


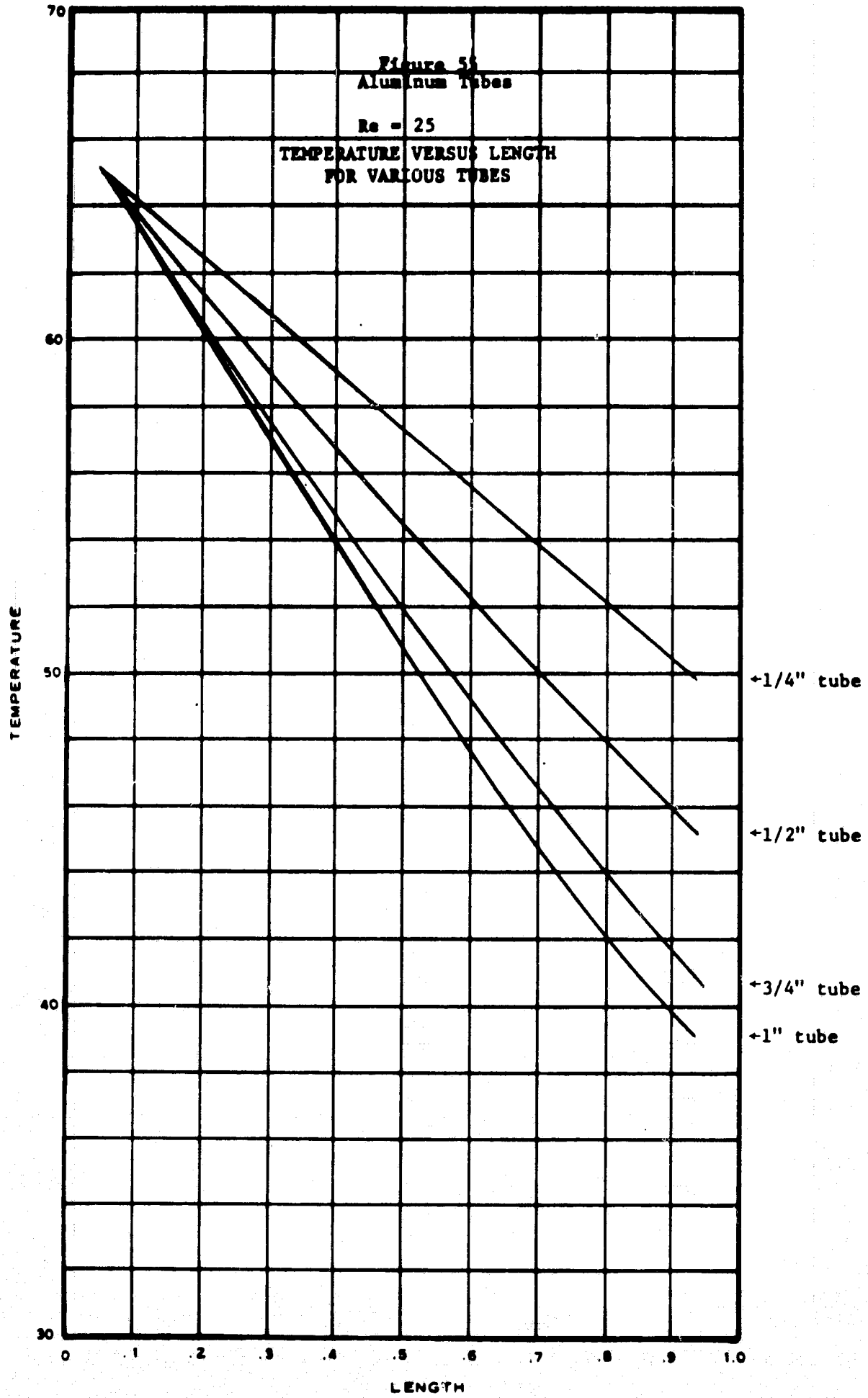


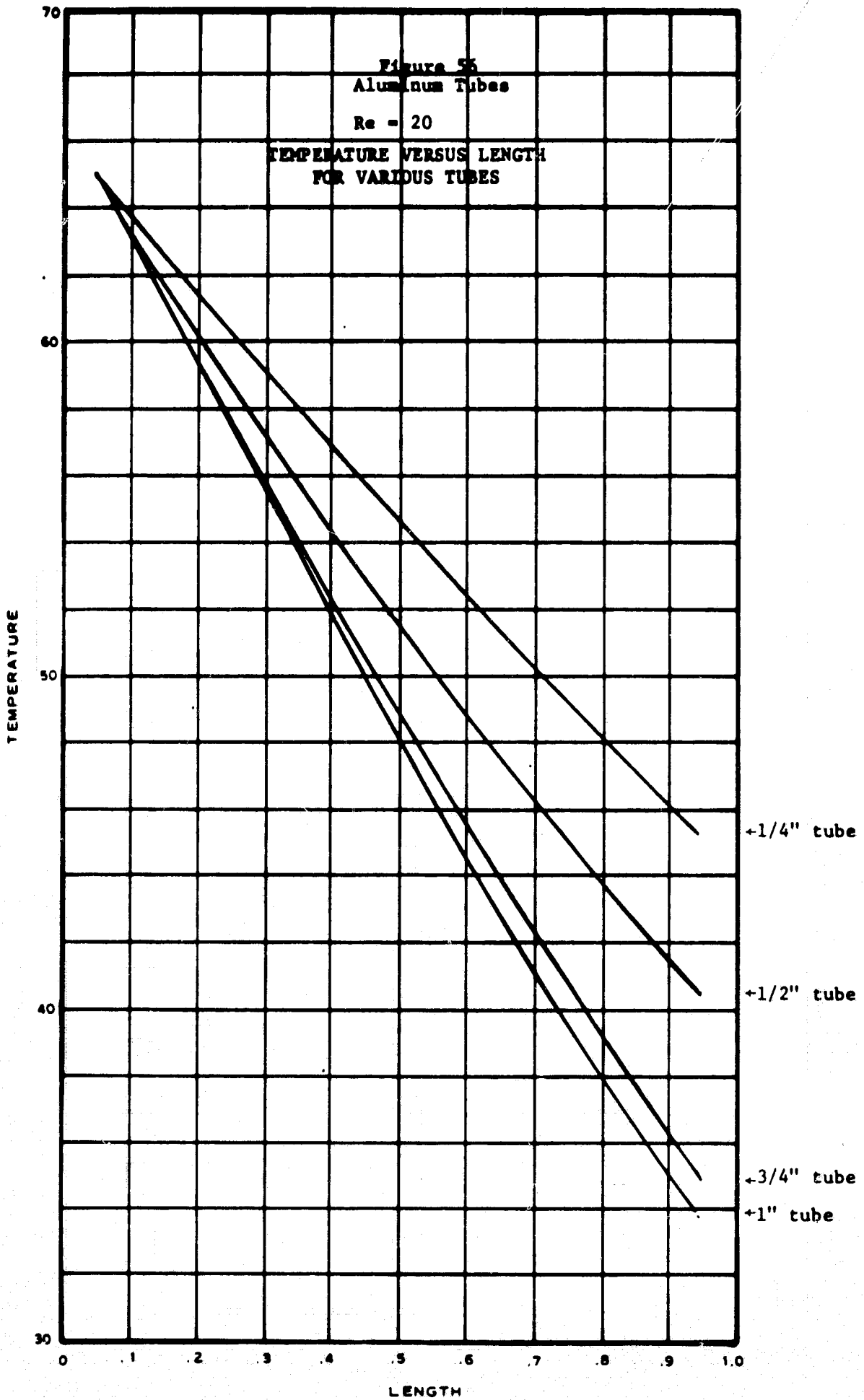


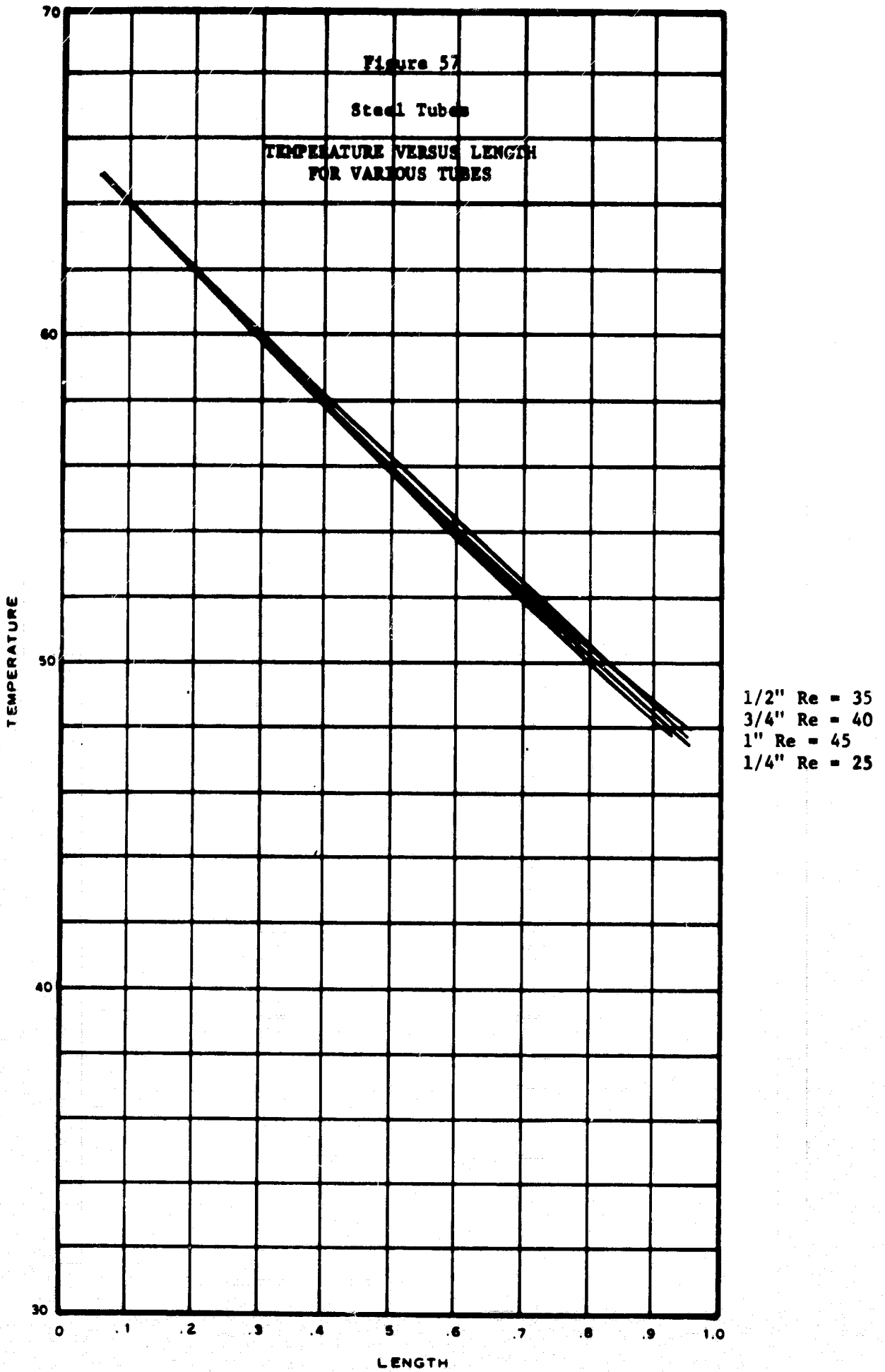


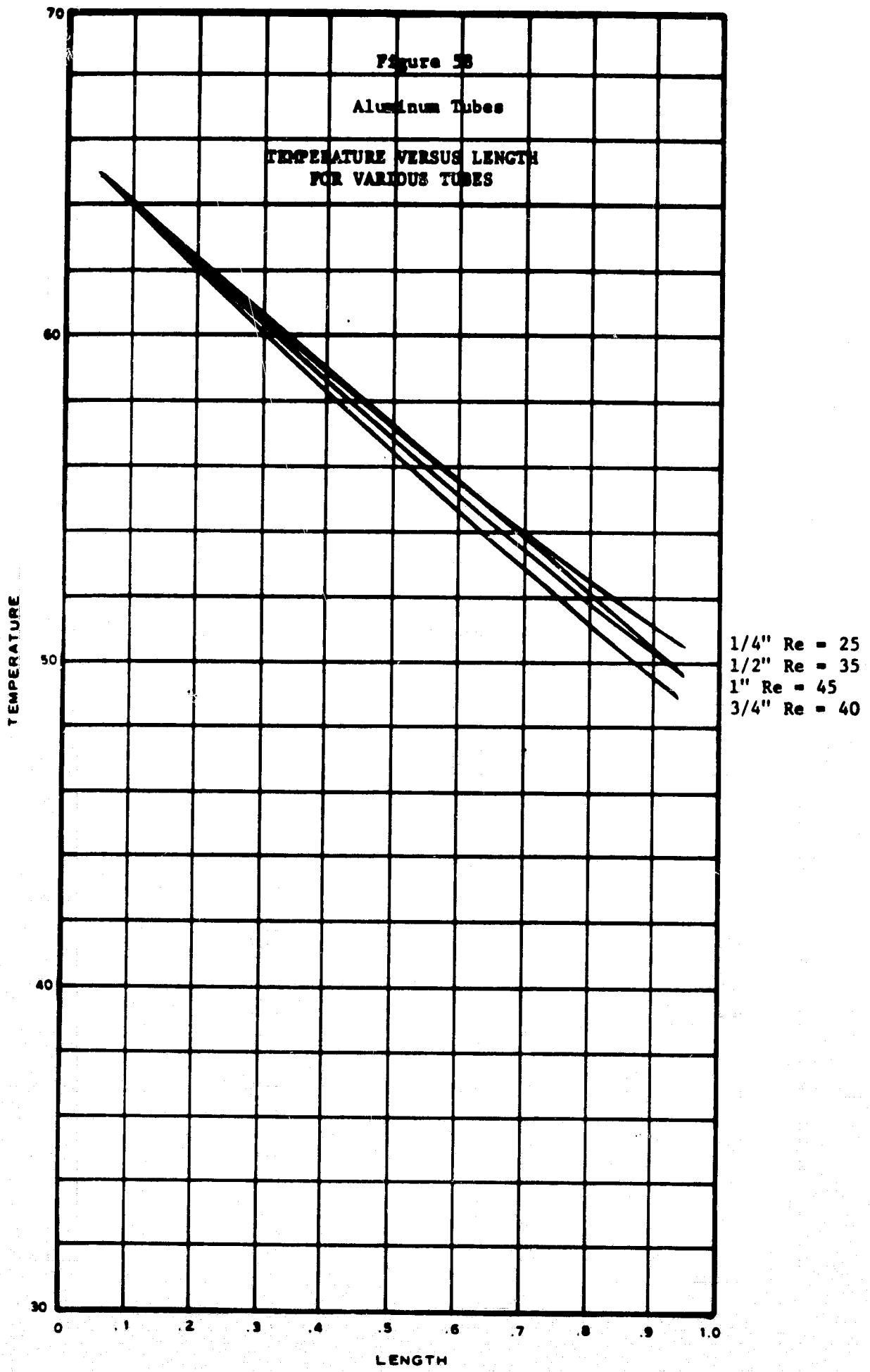


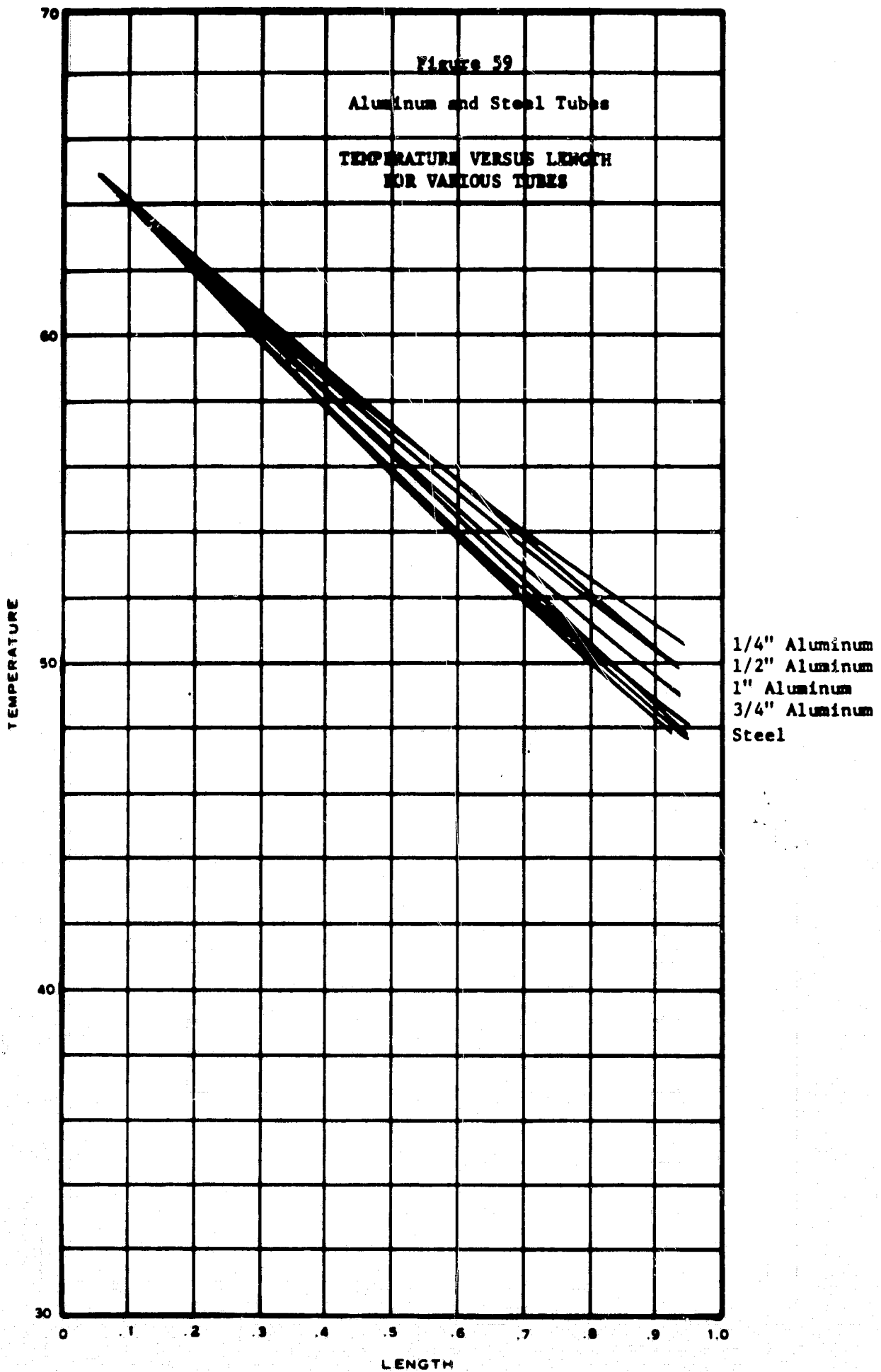












CHAPTER IX

CONCLUSIONS AND RECOMMENDATIONS

The object of this investigation was to study the applicability of thermal modeling under steady-state conditions for a single material system using forced convection from a flowing fluid in a tube, conduction through and down the tube, and radiation to a cryogenic vacuum environment. Temperature and materials preservation techniques together with the modeling criteria $D^* = t^* = L^{*2}$ were used to fabricate a prototype and three models from two materials with different thermal conductivities. The effect of fluid flow rate upon thermal modeling was a secondary object of the experimental investigation.

Conclusions

Fluid flow rate was found to have a large effect upon thermal modeling, and its measurement at very low Reynolds numbers presented difficulties. With regard to Reynolds number criteria, no other investigations have been published in this area, therefore a comparison of results is not possible.

The experiment and its analysis was complex. In order to obtain a sufficient temperature distribution along the tube to allow thermal modeling, the flow rate had to be reduced to a point where the presence of mixed flow was possible. Complete thermal isolation of the specimen tube was impractical due to end connections which permitted some conduction error, particularly in the aluminum tubes. Fluid temperature measurements within the tube could not be made without disturbing the hydrodynamic boundary layer; hence, a complete analysis of convective heat transfer was not possible. The temperature distribution within the

cryogenic liner was not close to being isothermal and low. This problem would have been minimized by fabrication of the cryogenic liner from a material with a high thermal conductivity such as brass or aluminum rather than stainless steel.

In spite of these problems it is felt that the investigation provided meaningful results which were previously unavailable and represents an initial inquiry into thermal modeling with three-mode heat transfer including forced convection.

Recommendations

Recommendations for further investigations include the study of mixed flow in a simulated space environment and its effect upon thermal modeling, thermal modeling with forced convection at higher flow rates, and further definition of the modeling criteria for the Reynolds number.

The study of mixed flow in a simulated space environment could be accomplished in a setup similar to the one used for this investigation. A thin-walled tube of low thermal conductivity could be thermally instrumented along its upper and lower surfaces and the temperature distributions could be studied for various tube orientations and flow rates.

Thermal modeling with forced convection at higher flow rates may be possible by using higher inlet fluid temperatures. Increased radiation heat transfer at higher temperatures may yield a sufficient temperature drop along the tube to permit modeling evaluation. Although tube length in this experiment was limited to 48 inches by the chamber dimensions, the use of a coiled tube may provide an effective extended length. Painting such a coil's inner surface with a low emittance coating and its outer surface with a high emittance coating should enhance the effective length.

The modeling criteria for Reynolds number should be evaluated under test conditions which preclude the possible effects of mixed flow. Conduction error can also be reduced by use of teflon union fittings or similar devices for connection of the specimen tube to the adjacent plumbing.

SELECTED BIBLIOGRAPHY

1. Langhaar, H. L. *Dimensional Analysis and Theory of Models*. John Wiley and Sons, Inc., New York, 1951.
2. Gabron, F., and A. A. Fowle. "Thermal Modeling of a Simulated JPL Spacecraft--Phase I Results." NASA Report No. CR-53455, September 1962.
3. Clark, L. G., and K. A. Laband. "Orbital Station Temperature Control." Astronautics, :40-43, September 1962.
4. Katz, A. J. "Thermal Testing." Space/Aeronautics, :30-34, October 1962.
5. Katzoff, S. "Similitude in Thermal Models of Spacecraft." NASA Report No. TN-D-1631, April 1963.
6. Wainwright, J. B., L. R. Kelly, and T. H. Keese. "Modeling Criteria and Testing Techniques for the Simulation of Space Environments." Space Environment Simulation Symposium, Los Angeles, California, May 1963.
7. Vickers, J. M. F. "A Study of Thermal Scale Modeling Techniques." JPL Technical Memorandum No. 33-153, September 1963.
8. Jones, B. P. "Thermal Similitude Studies." J. Spacecraft, 1(4): 364-369, July-August 1964.
9. Chao, B. T., and G. L. Wedekind. "Similarity Criteria for Thermal Modeling of Spacecraft." J. Spacecraft, 2(2):146-152, March-April 1965.
10. Vickers, J. M. F. "Thermal Scale Modeling." Astronautics and Aeronautics, :34-39, May 1965.
11. Matheny, J. D. "Thermal Design Studies." Final Report, Contract NAS8-5270, September 1965.
12. Folkman, N. R., F. L. Baldwin, and J. B. Wainwright. "Tests on a Thermally Scaled Model Space Station in a Simulated Solar Environment." AIAA Thermophysics Specialist Conference, Monterey, California, Paper No. 65-658, September 1965.
13. Rolling, R. E. "Results of Transient Thermal Modeling in a Simulated Space Environment." AIAA Thermophysics Specialist Conference, Monterey, California, Paper No. 65-659, September 1965.

14. Adkins, D. L. "Scaling of Transient Temperature Distributions of Simple Bodies in a Space Chamber." AIAA Thermophysics Specialist Conference, Monterey, California, Paper No. 65-660, September 1965.
15. Jones, B. P., and J. K. Harrison. "A Set of Experiments in Thermal Similitude." NASA Report No. TMX-53346, October 1965.
16. Gabron, F., R. W. Johnson, J. M. F. Vickers, and J. W. Lucas. "Thermal Scale Modeling of the Mariner IV Spacecraft." AIAA Aerospace Sciences Meeting, New York, Paper No. 66-23, January 1966.
17. Shih, C. "Thermal Similitude of Manned Spacecraft." AIAA Aerospace Sciences Meeting, New York, Paper No. 66-22, January 1966.
18. Barcus, Paul W. "Models of Thermal Behavior of Radiative Surfaces." Ph.D. Dissertation, Iowa State University, 1966.
19. Young, R. L., and R. V. Shanklin. "Thermal Similarity Study of a Typical Space Vehicle Element." AIAA Aerospace Science Meeting, Los Angeles, California, Paper No. 66-460, June 1966.
20. Miller, P. L. "Thermal Modeling in a Simulated Space Environment." Ph.D. Dissertation, Oklahoma State University, July 1966.
21. Watkins, J. R. "Sets of Similarity Ratios for Thermal Modeling." NASA Report No. TND-3452, 1966.
22. Hsia, H. M., and J. A. van der Blik. "Internal Convection Effects in Thermal Models of Space Vehicles." Arnold Engineering Development Center Report No. AEDC-TR-66-257, February 1967.
23. Doenecke, J. "Thermal Scale Modelling Without Thermal Similitude." Paris ESRO, Paper No. ESRO-TN-19 (ESTEC), November 1967.
24. Buna, Tibor. "Matched Techniques of Thermal Scale Modeling." Space Simulation Conference, Seattle, Washington, Paper No. A68-42609, September 1968.
25. Rolling, R. E., K. N. Marshall, and D. O. Murray. "Thermal and Structural Modeling of a Large Aperture Space Telescope." Lockheed Technical Report No. NAS8-20411, September 1968.
26. Maples, Dago. "A Study of Spacecraft Temperature Prediction by Thermal Modeling." Ph.D. Dissertation, Oklahoma State University, November 1968.
27. Klockzien, V. G., and R. L. Shannon. "Thermal Scale Modeling of Spacecraft." International Automotive Engineering Congress, Detroit, Michigan, Paper No. 690196, January 1969.

28. MacGregor, R. K. "Limitations in Thermal Similitude." Boeing Report, Contract NAS8-21422, December 1969.
29. Rolling, R. E., D. O. Murray, and K. N. Marshall. "Limitations in Thermal Modeling." Lockheed Report, Contract NAS8-21153, December 1969.
30. Holm, F. W., and P. L. Miller. "Thermal Scale Modeling of a Heat Pipe." ASME Space Technology and Heat Transfer Conference, Los Angeles, California, June 1970.
31. Giedt, Warren H. *Principles of Engineering Heat Transfer*. McGraw-Hill Book Co., D. Van Nostrand Co., Inc., Princeton, New Jersey, 1961.
32. Langhaar, H. L. J. Appl. Mech., 9, June 1942.
33. Kays, W. M. *Convective Heat and Mass Transfer*. McGraw-Hill Book Co., New York, 1966.
34. Singh, S. N. Appl. Sci. Res. Ser. A, 7:325, 1958.
35. Yang, K. T. Trans. ASME (C), J. Heat Transfer, 84:353-362, 1962.
36. Jakob, M. *Heat Transfer*, 1. John Wiley & Sons, Inc., New York, 1962.
37. Eckert, R. G., and A. J. Diaguila. "Convective Heat Transfer for Mixed Free and Forced Flow Through Tubes." Trans. ASME, 76:497-504, 1954.
38. Kreith, F. *Principles of Heat Transfer*. International Textbook Co., Scranton, Pennsylvania, 1964.
39. Wiebelt, J. A. *Engineering Radiation Heat Transfer*. Holt, Rinehart and Winston, Inc., New York, 1966.
40. Hottel, H. C., and A. F. Sarofim. *Radiative Transfer*. McGraw Hill Book Co., New York, 1967.
41. Lion, Kurt S. *Instrumentation in Scientific Research*. McGraw-Hill Book Co., New York, 1959.
42. Lafferty, J. M. "Techniques of High Vacuum." General Electric Report No. 64-RL-3791 G, November 1964.
43. Leak Detector Operation and Maintenance Manual for Type 24-120B. Consolidated Electrodynamics Corp., Pasadena, California, Manual No. 992231-0008, 1964.

APPENDIX A

Equipment used for this research is recorded in the following list. Reference may be made to Figure A-1 to show the location of the parts in the experimental arrangement. Support equipment that was used, but not shown in Figure A-1, is also listed.

<u>ITEM</u>	<u>DESCRIPTION</u>
He	Helium K-bottle
V1	K-bottle Regulator Valve Victor Equipment Company 0-100 psig and 0-4000 psig
V2	Gas Pressure Control Valve Grove Valve & Regulator Company Model 15-LK, Range: 0-150 psig
P1	Gas Pressure Meter Weksler Instruments Corporation Type P1-FL, Range: 0-100 psig
V3	Pressure Relief Valve Ladewig Model 1190-HL Set at 140 psig
V4	Ball Valve Pacific Valves, Inc. Model K225, 1000 psig pressure
P2	Pressure Transducer Strain-gage type Model 151-HAC-124, Ser. No. EP3731 Range: 0-100 psig
WT	Water Tank - Water Heater Sears Model 153.32440 82 gallon capacity - glass lined
V5	Gate Valve Integral with Water Tank (WT)
V6	Needle Valve APCO Accessory Products Company Part No. 506 3CK-80P

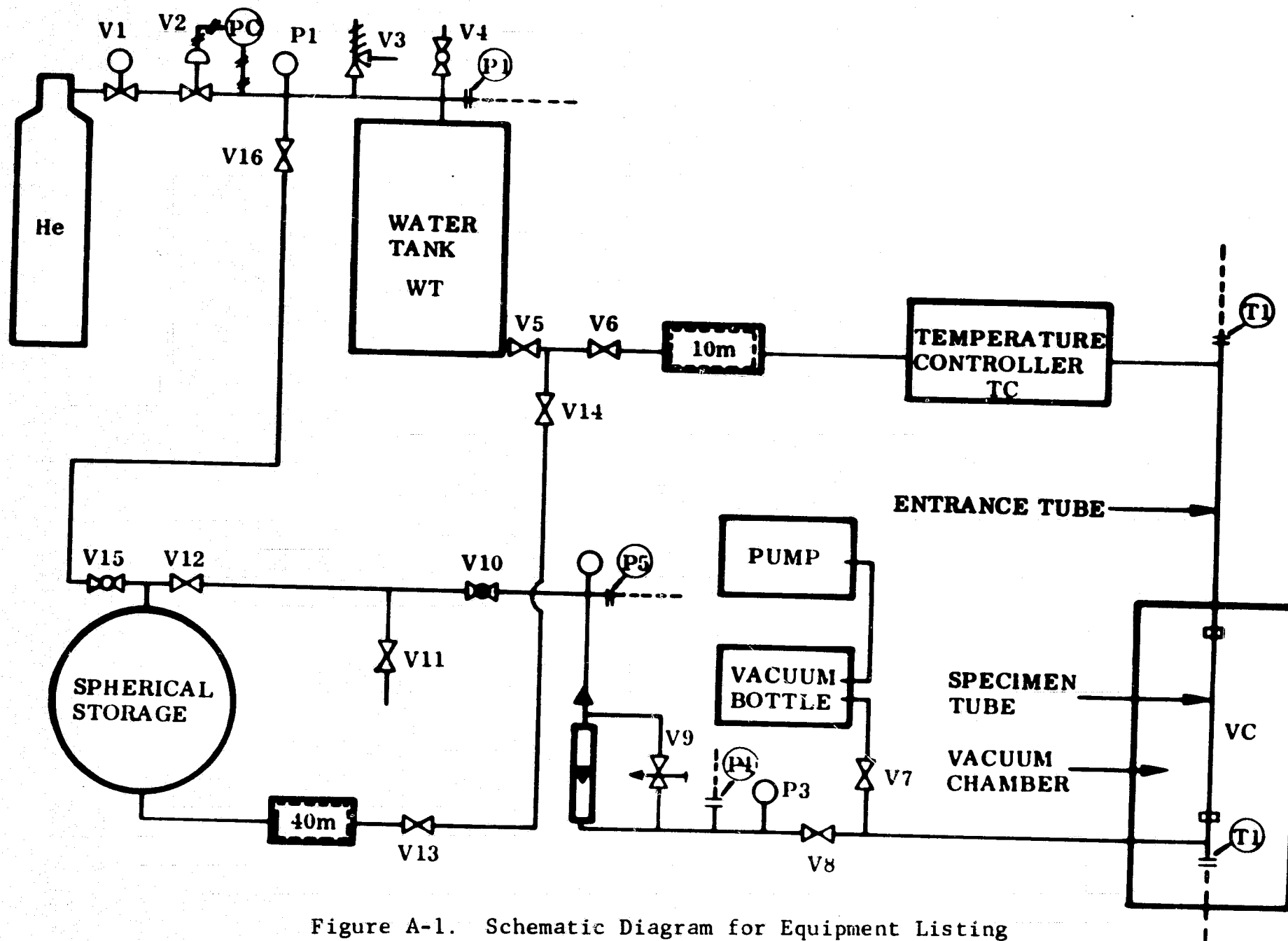


Figure A-1. Schematic Diagram for Equipment Listing

<u>ITEM</u>	<u>DESCRIPTION</u>
10M	Microporous Filter Assembly No. 4313G-10CM 10 Micron - Stainless Steel
TC	Temperature Controller Rosemount Engineering Company Model 910-508 Variable Temperature Oil Bath Range: -70 F to + 500 F
T1	Temperature Transducer The OmniRad Corporation Model 3004-CA Copper-constantan
VC	Vacuum Chamber Murphy & Miller, Inc. 45 in. dia. x 56 in. lg. 760 to 2.5×10^{-5} torr
T2	Temperature Transducer Type GE-100 Copper-constantan
V7	Needle Valve APCO Accessory Products Company Type 5063CK-80P
VB	Vacuum Bottle Corning Glass Works Model 1595, 5 gallons
PU	Evacuation Pump NASA ID No. 34044 Range: ATM to 1 micron
V8	Needle Valve APCO Accessory Products Company Type 5063CK-80P
P3	Pressure Indicating Gage Heise Bourdon Tube Company, Inc. Model C-56489 NASA ID No. BA-1071 Calibrated November 3, 1970 Range: 0-30 psig (0.05 increments)
P4	Pressure Transducer Strain-gage type Model 151-HAC-124 Ser. No. EP-3548, Range: 0-100 psig

<u>ITEM</u>	<u>DESCRIPTION</u>
V9	Micrometer Needle Valve Whitey Research Tool Company Model 3RF2-A
F	Rotameter Brooks Instrument Company Type 1357-23F1AAE Ser. No. 6907-70962 Air Range: 0.00015 GPM to 0.0053 GPM
P5	Pressure Transducer Strain-gage type Model 151-HAC-134 Ser. No. EP-4421 Range: 0-100 psig
P6	Pressure Indicating Gage Heise Bourdon Tube Company, Inc. Model H-45229, NASA ID No. BA-0058 Calibrated November 3, 1970 Range: 0-30 psig (0.05 increments)
V10	Throttling Needle Valve APCO Accessory Products Company Model 5063CK-08P (16 turn)
V11	Needle Valve APCO Accessory Products Company Model 5063CK-80P
V12	Needle Valve Robbins Aviation, Inc. Model AK6250-4T
SS	Spherican Storage Spheres Quantity: 2, Capacity: 40 gallons ea., Model: NASA ID No. 37144 - Titanium
40M	Microporous Filter Circle-Seal Development Corporation Model 43136-40EL 40 micron - stainless steel
V13	Gate Valve Jenkins Bros. Valve Company Model 106-A
V14	Gate Valve Jenkins Bros. Valve Company Model 106-A

<u>ITEM</u>	<u>DESCRIPTION</u>
V15	Ball Valve Pacific Valve Company Model G-227
V16	Needle Valve APCO Accessory Products Company Model 5063CK-80P

ADDITIONAL EQUIPMENT USED BUT NOT
SHOWN IN FIGURE A-1

<u>QUANTITY</u>	<u>DESCRIPTION</u>
1	Leak Detector Consolidated Electrodynamics Corp. Model 24-120B NASA ID No. CS-0236
1	Liquid Nitrogen Level Controller Central Scientific Company Catalog No. 94011
1	Freezer Storage Container Star Cooler Company NASA ID No. 15412 Range: Ambient to -60 F
2	Liquid Nitrogen Dewar Cosmodyne Corporation Model CML105F Capacity: 100 gallons
1	Multipoint Multirange Strip-Chart Recorder Leeds & Northrup Company Speedomax G, Model S, 60,000 series 12 Point, Adjustable Range, Adjustable zero
8	Strip-Chart Recorder Bristol Company - Model 64A-1PH1X761 Two Speed - Adjustable zero Adjustable Range
1	Triple Beam Balance Ohaus Scale Corporation Capacity: 2,610 grams (0.1 gram increments), Ser. No. M5-838 Permanent Magnetically Damped

<u>QUANTITY</u>	<u>DESCRIPTION</u>
1	Electric Vacuum-Pressure Pump Millipore Filter Corporation Model XX6000000 Range: 0 - 25 psig pressure, 0 - 27 in. Hg. vacuum
1	Hand Pump W. T. Grants Company Nylon baster type Range: 0 - 1.5 oz.
1	Calculator Friden, Inc. Model STW10
1	Heat Gun Master Appliance Corporation Model HG501LD
1	Millivolt Potentiometer Leeds & Northrup Company Model 8690
1	Spotwelder Weldmatic Unitek Model 1045 Range: 0 - 200 watt-seconds

APPENDIX B

VACUUM SYSTEM DESCRIPTION AND OPERATION

The high vacuum system consisted of a cryopump within a test chamber that was connected to a diffusion pump augmented by a roughing pump and high volume blower. A holding pump was used in conjunction with the diffusion pump for the purpose of maintaining a vacuum on the diffusion pump while the chamber was above a pressure of 200 microns. The vacuum system is shown in Figures B-1, B-2, and B-3; and normally attained a vacuum of 10^{-4} to 10^{-5} torr.

The Murphy-Miller high vacuum altitude test chamber was comprised of two skids and a separate control cabinet. The largest of the skids formed a base for the vacuum chamber, diffusion pump, holding pump, and main electrical breaker panel. The smaller skid mounted the roughing pump and blower assemblies. The two skids interconnected upstream of the blower and downstream of the vacuum chamber and diffusion pump by a flexible duct. All controls and switches were mounted in a separate control panel interconnected to the appropriate mechanical and electrical components that comprised the Murphy-Miller vacuum chamber by pneumatic and electrical umbilicals.

In studying vacuum facilities, it is important to realize that no vacuum pump can reach into a vessel and pull out the gas molecules; all any pump can do is act as a sink or hole into which the molecules diffuse and never return. As long as the gas diffuses out of the vessel faster than it leaks in, the pressure will continue to decrease. The low pressure limit is reached when these two flows reach equilibrium; thus,

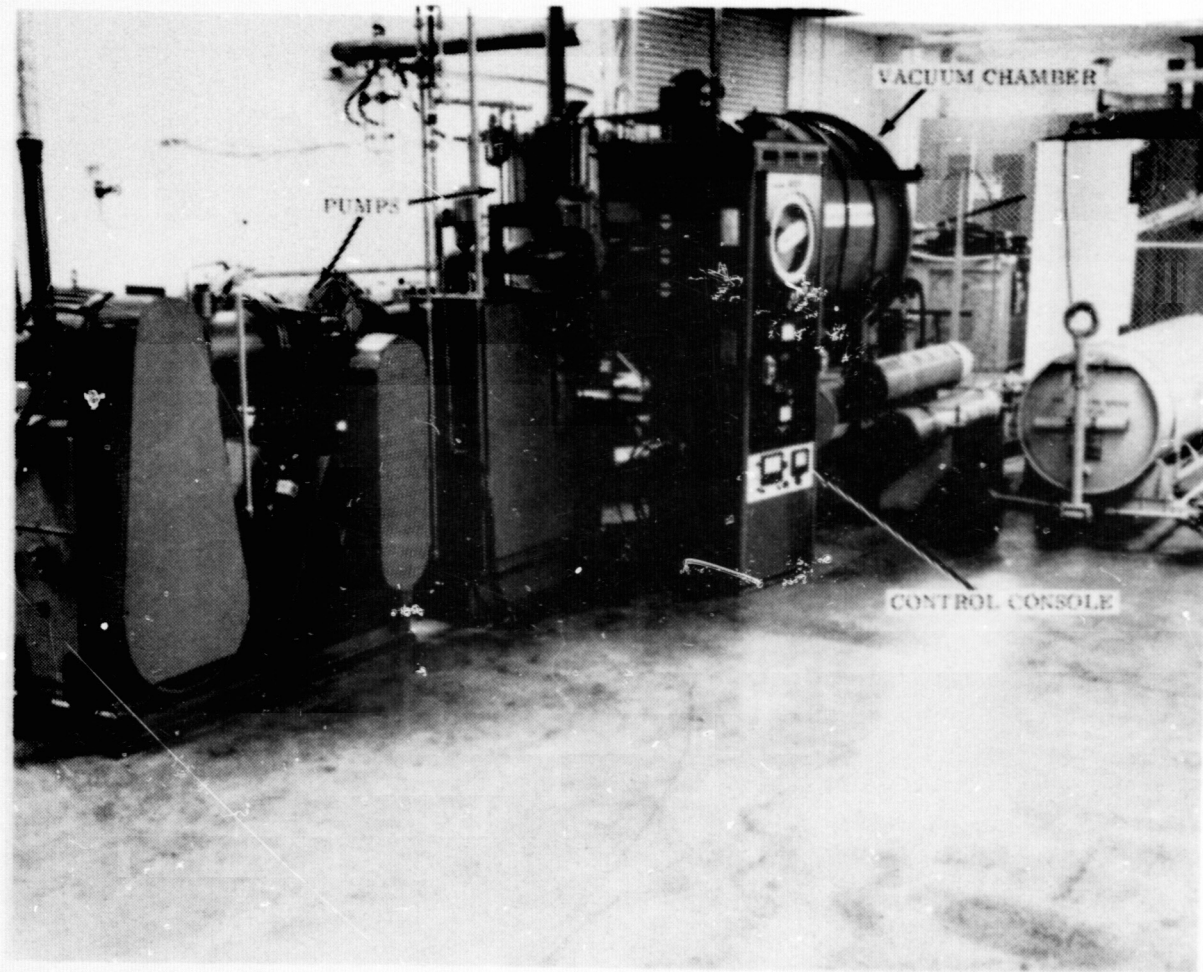


Figure B-1. Overall View of Vacuum System

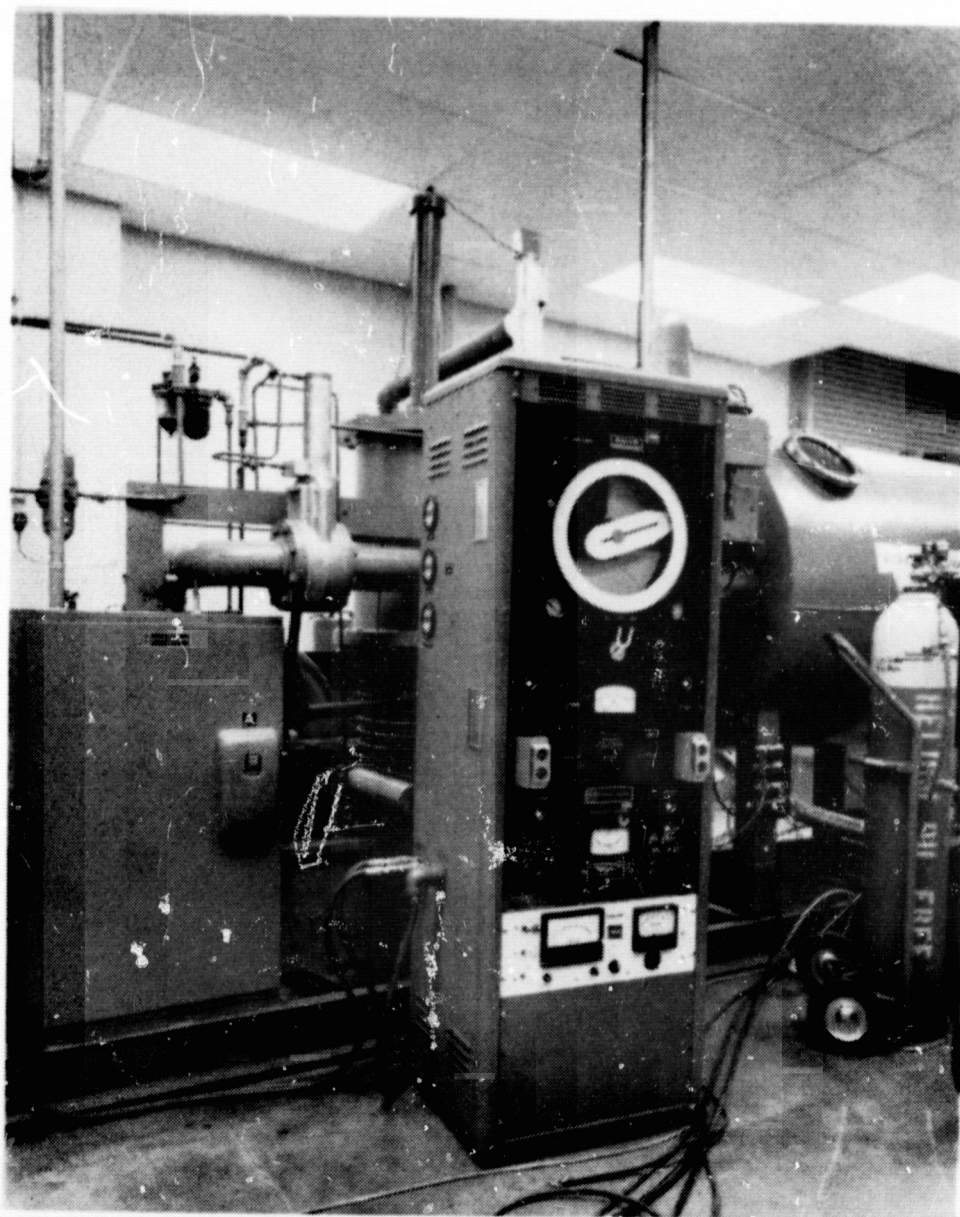


Figure B-2. Vacuum System Control Console

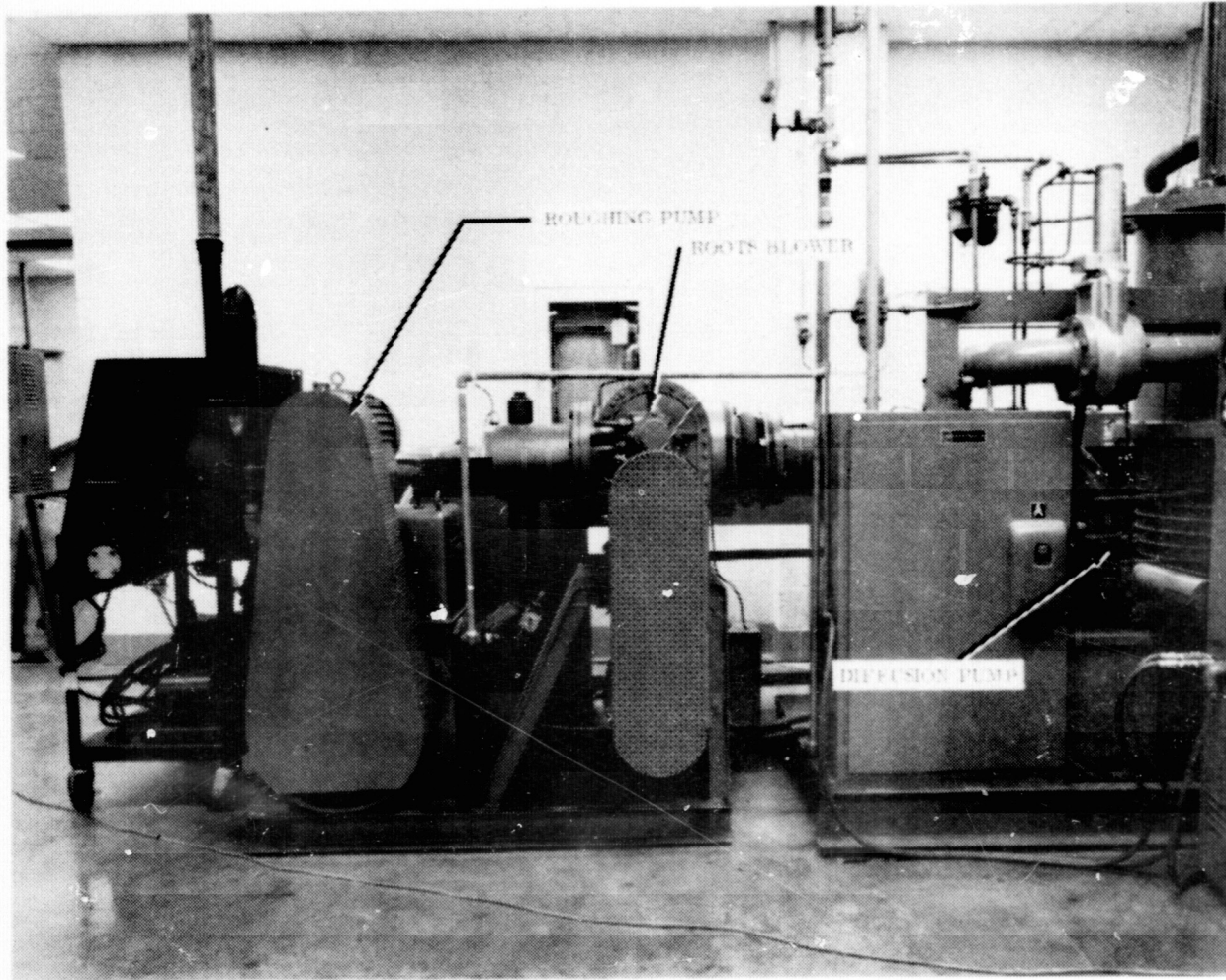


Figure B-3. Vacuum Pumping System

the permeation and outgassing rates of the materials used in a vacuum system are as important as the path over which the gas must diffuse to reach the pumps.

A Stokes roughing pump in series with a Roots high volume blower connected directly to the chamber by means of a bypass line around the diffusion pump. The Stokes unit is a rotary, oil-sealed, vane-type pump which utilizes an eccentric roter with sliding vanes or valves that use oil as a sealant and lubricant between closely fitted parts. When the chamber pressure decreased to 350 microns, a Hastings control activated the Roots high volume blower. The Roots blower utilized two figure-eight-shaped rotors that counter-rotated in a chamber without touching each other or the chamber wall. Roots pumps operate efficiently in the pressure range that lies below the efficient operating range of oil-sealed mechanical pumps and above the efficient range of diffusion pumps.

The diffusion pump was placed on the line when its oil was sufficiently heated and the chamber pressure reached 100 microns. Pneumatic valves closed the bypass line and placed the diffusion pump in series with the roughing pump and blower.

In the diffusion pump, fluid vaporized in a boiler located in the lower section was carried to the nozzle where it ejected in the form of a high-velocity jet (Figure B-4). This vapor jet was directed away from the incoming gas toward the cool walls of the pump where it condensed and returned to the boiler by gravity. The gas to be pumped flows into the annular space around the nozzle by molecular diffusion. Because of the high density and velocity of the vapor in the jet, the gas molecules that diffuse into it will be entrained by it and driven downstream with

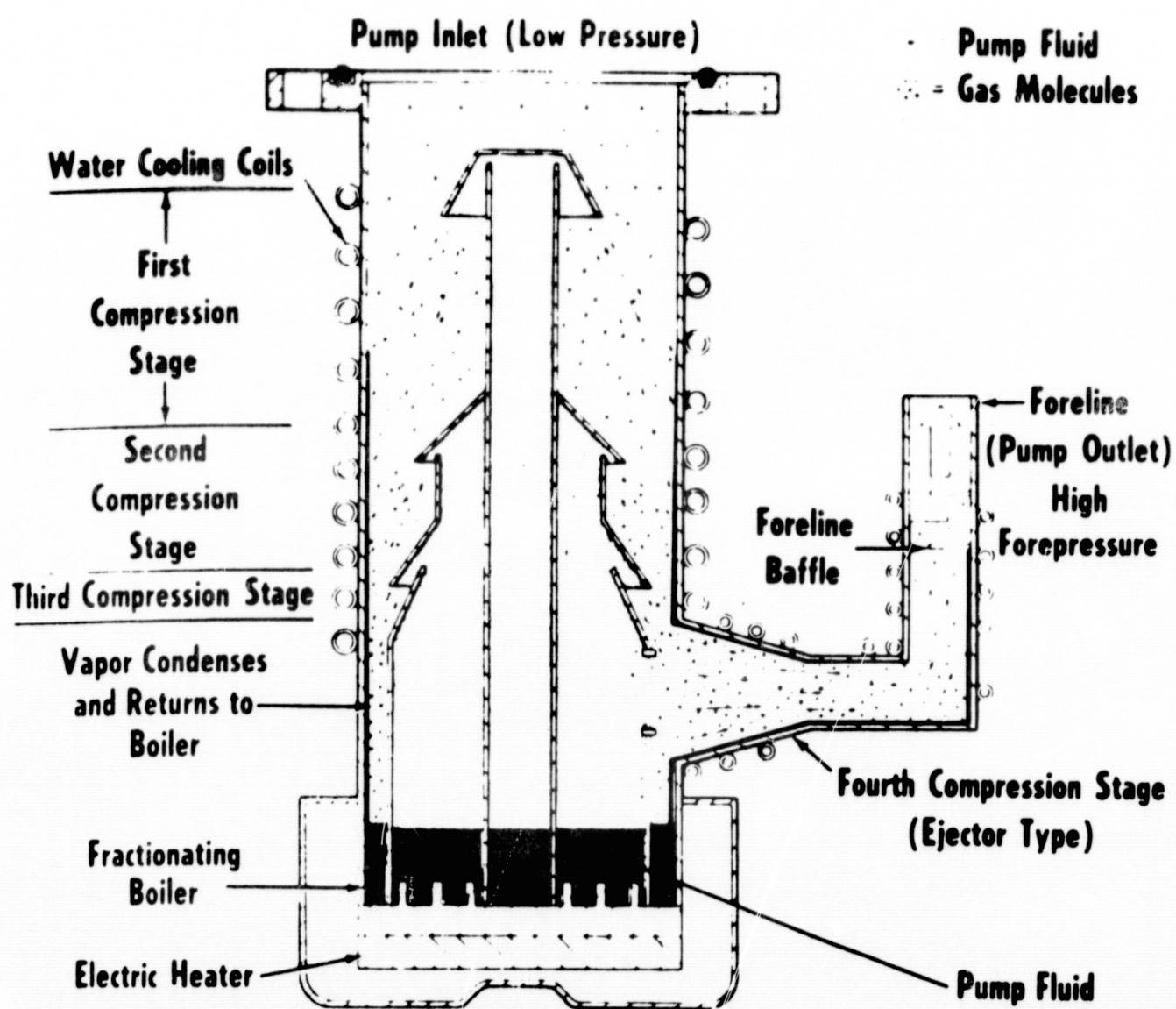


Figure B-4. Multiple-jet Metal-diffusion Pump With Ejector Stage

velocities greater than those which correspond to the temperature of the gas. In order to increase the pump speed and compression ratio, the diffusion pump used several jets which operated in series. Cooling

water was circulated through coils on the pump's upper exterior wall and emptied in a floor drain.

After the diffusion pump had reduced the chamber pressure below 40 microns, nitrogen was introduced to the cryogenic liner and chamber cold trap. Cryopumping or cryogenic pumping usually refers to the removal of gas or vapor from the gas phase by condensation or adsorption on a surface at ultralow temperatures: that is, near the boiling point of liquid H_2 or He. This surface is frequently called a cryopanel. Liquid nitrogen was used to cryogenically cool the cold trap and liner which served as cryopanel. Liquid was supplied in 100-gallon dewars which used an external heat exchanger to provide pressurization. A Cenco liquid level controller atop the chamber was used in conjunction with a solenoid valve to maintain the necessary amount of nitrogen within the cryopanel.

A thermionic ionization gage was used to measure the pressure within the chamber. The gage system was constructed like a triode vacuum tube; i.e., it contained in a glass vessel a heated electron-emitting cathode, a grid surrounding the cathode, and a plate surrounding the grid. The grid was maintained at a positive potential with respect to the cathode while the plate was kept at a negative potential. Electrons emitted from the cathode were accelerated by the grid and collided with the gas molecules in the vessel. Positive ions formed in the space between the grid and plate and were collected by the negative plate. Ions formed in the space between cathode and grid migrated toward the cathode. Electrons and negative ions will be collected by the positive grid.

The rate of ion production is proportional to the amount of gas present and to the number of electrons available to ionize the gas. The

ratio of plate current to the grid current is then a measure of the pressure P within the tube. The ionization gage measures the total pressure of all gases present. Thermionic ionization gages are used for pressure measurements in the range between 10^{-3} and 10^{-8} mm Hg. The output varies almost linearly from 10^{-4} to 10^{-9} amperes (41) within this range. Pressure within the chamber during the experiments was typically 1×10^{-4} torr to 5×10^{-5} torr.

The mean free path is defined as the average distance traveled by the gas molecules between successive collisions with one another. It varies inversely with the pressure of the gas. For air at 25 C,

$$\lambda = \frac{5 \times 10^{-3} \text{ cm}}{P}$$

where P is the pressure in torr (Reference 42). For the thermal modeling experiment, the mean free path was on the order of the interior dimensions of the cryogenic liner.

The pumpdown and shutdown procedures are given on the following page.

PUMPDOWN PROCEDURE

1. Latch chamber door.
2. Drain water from pump and cold trap drains.
3. Close valve D and turn off vacuum break V_L .
4. Turn on power switch A (upper left of console).
5. Start holding pump (on console).
6. Open valve W (below and on back side of system) and confirm 30-inch vacuum on gage. Also check to see that water supply to diffusion pump is on.
7. If gage reads okay, turn on diffusion pump heater switch.
8. Turn on blower switch.
9. Turn on roughing pump.
10. Turn on vacuum gage power switch.
11. After diffusion pump heater has been on for 30 minutes, and if pressure is below 100 microns, put the diffusion pump on line by shorting the center and right terminal on the strip behind the console with a clip lead. Pump on diffusion pump about 30 minutes, or until pressure goes under 40 microns.
12. Turn on Cenco LN_2 level controller to automatic.
13. Turn on nitrogen as follows:
 - a. Open dewar door and close relief valve V_2 .
 - b. Open pressurization valve V_3 to pressurize dewar to 20 psig.
 - c. Open valve V_1 to permit liquid nitrogen to flow into the cryogenic liner.

SHUTDOWN PROCEDURE

1. Close valve V1 to cryoliner.
2. Close pressurization valve V3.
3. Open relief valve V2 immediately.
4. Cycle diffusion pump off line (remove clip lead and strike pneumatic valve if necessary).
5. Turn off diffusion pump heater switch.
6. Turn off Roots blow switch.
7. Turn off roughing pump.
8. Turn off Cenco LN₂ level controller (after 10 minutes).
9. When the bottom of the diffusion pump is not too hot to touch (approximately two hours after diffusion pump is shut off), close valve W between holding pump and diffusion pump.
10. Turn off holding pump.
11. Turn off power switch A.
12. When liner temperature approaches ambient conditions, open valve D and vacuum break V_L.
13. Unlatch chamber door.

APPENDIX C

CALCULATION OF FLOW RATES VERSUS REYNOLDS NUMBERS

Calculations were made for flow rates of water through the specimen tubes as a function of the Reynolds number, the inside diameter of the tube, and the properties of distilled water.

Flow rate, v , in gallons per minute (GPM) can be determined from

$$v = 7.481 VA \quad (C-1)$$

where V = fluid velocity

A = cross-sectional area for flow

and $7.481 \text{ gallons/ft.}^3$ is a conversion factor for distilled water.

Fluid velocity is expressed in the definition of Reynolds number as

$$v = \frac{Re\mu}{\rho D} \quad (C-2)$$

Substitution of (C-2) into (C-1) gives

$$v = 7.481 \frac{Re\mu\pi D}{4\rho} \quad (C-3)$$

upon substitution for the cross-sectional area. Equation (C-3) can be simplified to

$$v = (5.875765 \frac{\mu D}{\rho}) Re \quad (C-4)$$

where μ = fluid viscosity

D = tube inside diameter

ρ = fluid density

Re = Reynolds number

Calculations were made for each of the eight specimen tubes using water property data at 70 F. Gallons of water per minute were converted to grams of water collected in one minute by dividing GPM by 2.2762×10^{-4} .

SPECIMEN: 1" Stainless Steel Tube

$$v = (5.875765 \frac{\mu D}{\rho}) Re$$

$$\frac{\mu D}{\rho} = \frac{(2.37 \text{ lbm/ft.-hr.}) (0.7629 \text{ in.})}{(62.2 \text{ lbm/ft.}^3) (12 \text{ in./ft.}) (60 \text{ min./hr.})} = \frac{1.805946}{44784}$$

$$\frac{\mu D}{\rho} = 4.0325 \times 10^{-5} \text{ ft}^3/\text{min}$$

$$v = (4.0325 \times 10^{-5}) (5.875765) Re$$

$$v = 2.369402 \times 10^{-4} Re \quad \text{GPM}$$

<u>Re</u>	<u>v(GPM)</u>	<u>v(grams/min.)</u>
20	.00474	20.82
23.4	.00592	26.01
25.17	.00596	26.20
30	.007108	31.23
35	.008293	36.30
38.4	.009478	41.64
40	.00949	41.70
43.1	.010662	46.84
48.1	.011847	52.05
52.9	.013032	57.25
57.5	.014216	62.45

SPECIMEN: 3/4" Stainless Steel Tube

$$v = (5.875765 \frac{\mu D}{\rho}) Re$$

$$\frac{\mu D}{\rho} = \frac{(2.37 \text{ lbm/ft.-hr.}) (0.5625 \text{ in.})}{(62.2 \text{ lbm/ft.}^3) (12 \text{ in./ft.}) (60 \text{ min./hr.})} = \frac{1.333125}{44784}$$

$$\frac{\mu D}{\rho} = 2.9767885 \times 10^{-5} \text{ ft}^3/\text{min}$$

$$v = (2.9767886 \times 10^{-5}) (5.875765) Re$$

$$v = 1.749091 \times 10^{-4} Re \quad \text{GPM}$$

<u>Re</u>	<u>v(GPM)</u>	<u>v(grams/min.)</u>
10	.001749	7.684
15	.002624	11.528
20	.003498	15.368
25	.004373	19.212
30	.005247	23.052
35	.006122	26.896
40	.006996	30.735
45	.007871	34.580
50	.008745	38.419

SPECIMEN: 1/2" Stainless Steel Tube

$$v = (5.875765 \frac{\mu D}{\rho}) Re$$

$$\frac{\mu D}{\rho} = \frac{(2.37 \text{ lbm/ft.-hr.}) (0.3852 \text{ in.})}{(62.2 \text{ lbm/ft.}^3) (12. \text{ in./ft.}) (60 \text{ min./hr.})} = \frac{0.91292}{44784}$$

$$\frac{\mu D}{\rho} = 2.0384 \times 10^{-5} \text{ ft}^3/\text{min}$$

$$v = (2.0384 \times 10^{-5}) (5.875765) Re$$

$$v = 1.1977159 \times 10^{-4} Re \quad \text{GPM}$$

<u>Re</u>	<u>v(GPM)</u>	<u>v(grams/min.)</u>
15	.00180	7.91
17.5	.00204	8.96
20	.00240	10.54
25	.00299	13.14
30	.00359	15.77
35	.00419	18.41
40	.00479	21.04
45	.00539	23.68
50	.00599	26.32
55	.00659	28.95
60	.00719	31.59

SPECIMEN: 1/4" Stainless Steel Tube

$$v = (5.875765 \frac{\mu D}{\rho}) Re$$

$$\frac{\mu D}{\rho} = \frac{(2.37 \text{ lbm/ft.-hr.}) (0.1913 \text{ in.})}{(62.2 \text{ lbm/ft.}^3) (12 \text{ in./ft.}) (60 \text{ min./hr.})} = \frac{0.453}{44784}$$

$$\frac{\mu D}{\rho} = 1.011522 \times 10^{-5} \text{ ft}^3/\text{min}$$

$$v = (1.011522 \times 10^{-5}) (5.875765) Re$$

$$v = 5.9434656 \times 10^{-5} Re \quad \text{GPM}$$

<u>Re</u>	<u>v(GPM)</u>	<u>v(grams/min.)</u>
10	.000594	2.61
15	.000892	3.92
20	.001189	5.22
25	.001486	6.53
30	.001783	7.83
35	.002080	9.14
40	.002377	10.44
45	.002675	11.75
50	.002972	13.06
55	.003269	14.36
60	.003466	15.67

SPECIMEN: 1" Aluminum Tube

$$v = (5.875765 \frac{\mu D}{\rho}) Re$$

$$\frac{\mu D}{\rho} = \frac{(2.37 \text{ lbm/ft.-hr.}) (0.8365 \text{ in.})}{(62.2 \text{ lbm/ft.}^3) (12 \text{ in./ft.}) (60 \text{ min./hr.})} = \frac{1.982505}{44784}$$

$$\frac{\mu D}{\rho} = 4.426815 \times 10^{-5}$$

$$v = (4.426815 \times 10^{-5}) (5.875765) Re$$

$$v = 2.601092687 \times 10^{-4} Re \quad \text{GPM}$$

<u>Re</u>	<u>v(GPM)</u>	<u>v(grams/min.)</u>
10	.002601	11.427
20	.005202	22.854
25	.0065003	28.569
30	.007803	34.281
35	.009104	39.996
40	.010404	45.708
45	.011705	51.423
50	.013005	57.135

SPECIMEN: 3/4" Aluminum Tube

$$v = (5.875765 \frac{\mu D}{\rho}) Re$$

$$\frac{\mu D}{\rho} = \frac{(2.37 \text{ lbm/ft.} \cdot \text{hr.})(0.6220 \text{ in.})}{(62.2 \text{ lbm/ft.}^3)(12 \text{ in./ft.})(60 \text{ min./hr.})} = \frac{1.47414}{44784}$$

$$\frac{\mu D}{\rho} = 3.2916667 \times 10^{-5} \text{ ft}^3/\text{min}$$

$$v = (3.2916667 \times 10^{-5})(5.875765) Re$$

$$v = 1.934105975 \times 10^{-4} Re \quad \text{GPM}$$

<u>Re</u>	<u>v(GPM)</u>	<u>v(grams/min.)</u>
10	.001934	8.497
15	.002901	12.745
20	.003868	16.993
25	.004835	21.242
30	.005802	25.490
35	.006769	29.738
40	.007736	33.986
45	.008703	38.234
50	.009671	42.487

SPECIMEN: 1/2" Aluminum Tube

$$v = (5.875765 \frac{\mu D}{\rho}) Re$$

$$\frac{\mu D}{\rho} = \frac{(2.37 \text{ lbm/ft.} \cdot \text{hr.}) (0.4045 \text{ in.})}{(62.2 \text{ lbm/ft.}^3) (12 \text{ in./ft.}) (60 \text{ min./hr.})} = \frac{0.958665}{44784}$$

$$\frac{\mu D}{\rho} = 2.140642 \times 10^{-5} \text{ ft}^3/\text{min}$$

$$v = (2.140642 \times 10^{-5}) (5.875765) Re$$

$$v = 1.257791 \times 10^{-4} Re \quad \text{GPM}$$

<u>Re</u>	<u>v(GPM)</u>	<u>v(grams/min.)</u>
10	.0012577	5.53
15	.001886	8.29
20	.002516	11.05
25	.0031444	13.81
30	.003773	16.56
35	.004402	19.34
40	.005031	22.10
45	.005660	24.87
50	.006289	27.63

SPECIMEN: 1/4" Aluminum Tube

$$v = (5.875765 \frac{\mu D}{\rho}) Re$$

$$\frac{\mu D}{\rho} = \frac{(2.37 \text{ lbm/ft.-hr.}) (0.1945 \text{ in.})}{(62.2 \text{ lbm/ft.}^3) (12 \text{ in./ft.}) (60 \text{ min./hr.})} = \frac{0.460965}{44784}$$

$$\frac{\mu D}{\rho} = 1.02931 \times 10^{-5} \text{ ft}^3/\text{min}$$

$$v = (1.02931 \times 10^{-5}) (5.875765) Re$$

$$v = 6.047984 \times 10^{-5} Re \quad \text{GPM}$$

<u>Re</u>	<u>v(GPM)</u>	<u>v(grams/min.)</u>
10	.000605	2.66
15	.000907	3.98
20	.001210	5.32
25	.001512	6.64
30	.001814	7.97
35	.002117	9.30
40	.002419	10.63
45	.002722	11.96
50	.003024	13.29
55	.003326	14.61
60	.003629	15.94

APPENDIX D

LEAK DETECTOR DESCRIPTION

The Consolidated Electrodynamics Corporation Leak Detector (Figure D-1) was essentially a mass spectrometer used to locate small leaks in the vacuum facility. This was a significant problem with the number of thermocouple feedthroughs and tube fittings which passed through the chamber wall. Sensitivity was such that the instrument could detect one part of helium in 10 million parts of air at a manifold pressure of 0.2 micron. Response time of the detector was less than one second.

The mass spectrometer is generally used for analysis of complex mixtures of gases. The mass spectrometer leak detector is specifically designed for the detection of one gas, helium. Briefly, the instrument draws in a small amount of gas, ionizes it, and sorts the ions according to their mass. Only one of the masses is brought into register. Referring to Figure D-2, the detector can be divided into three major sections for purposes of description: the vacuum system, the Diatron (CEC trade name for the mass spectrometer ion source), and the ion current amplifier.

A high vacuum is required for proper operation of the Diatron. Tracing through the vacuum system diagram, the inspected gas is drawn in through the sample inlet flange, travels through the protection-throttle valve, cold trap, pump isolation valve, diffusion pump, and finally out through the mechanical forepump. A side tube off the cold trap contains the vacuum gage and Diatron. The vacuum system was normally operated at 1×10^{-5} torr.

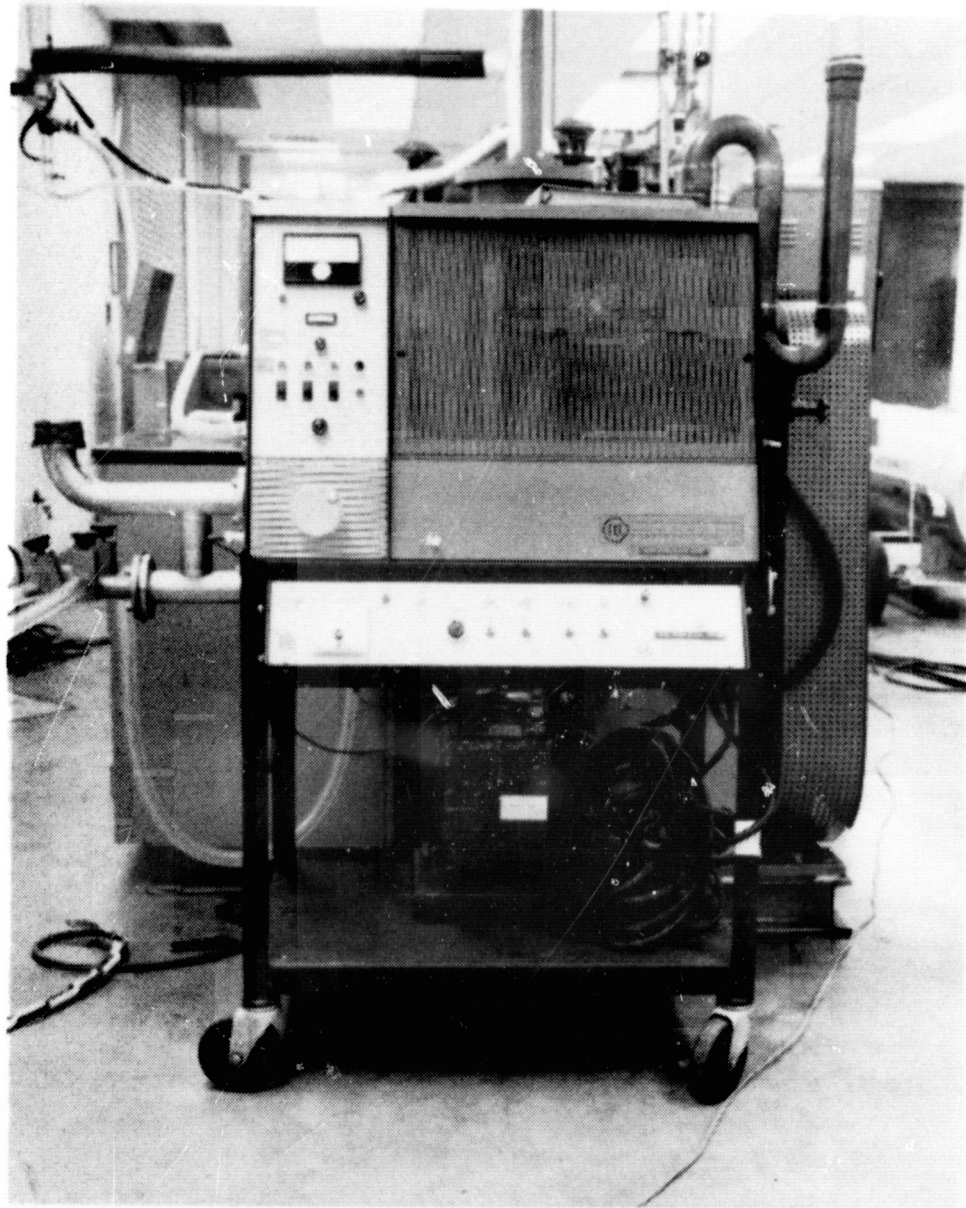


Figure D-1. CEC Vacuum Leak Detector

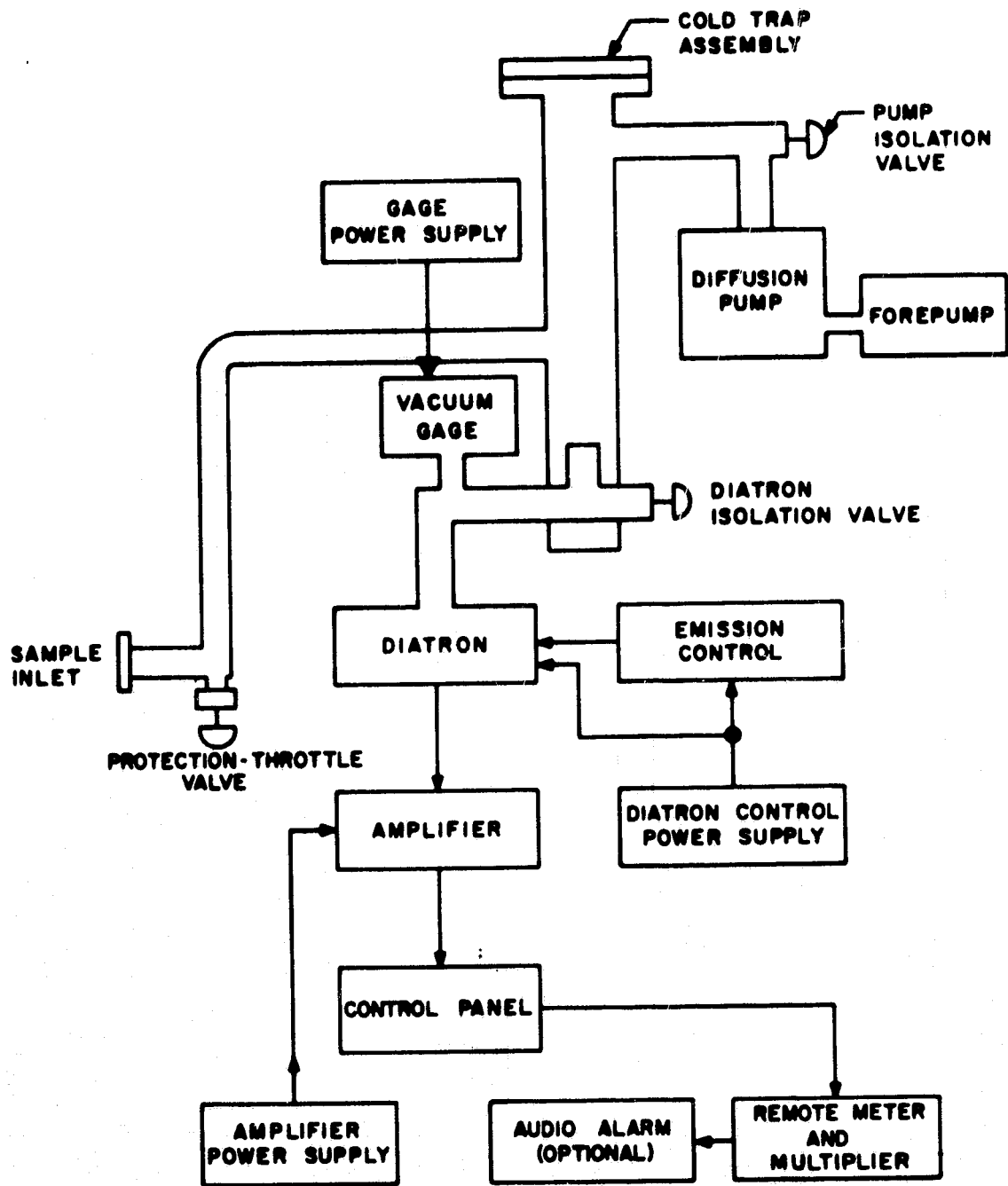


Figure D-2. Leak Detector Block Diagram

Gas molecules entering the leak detector inlet quickly diffuse throughout the system. Those that enter the ionizing chamber of the Diatron are subjected to bombardment by a beam of electrons (Figure D-3)

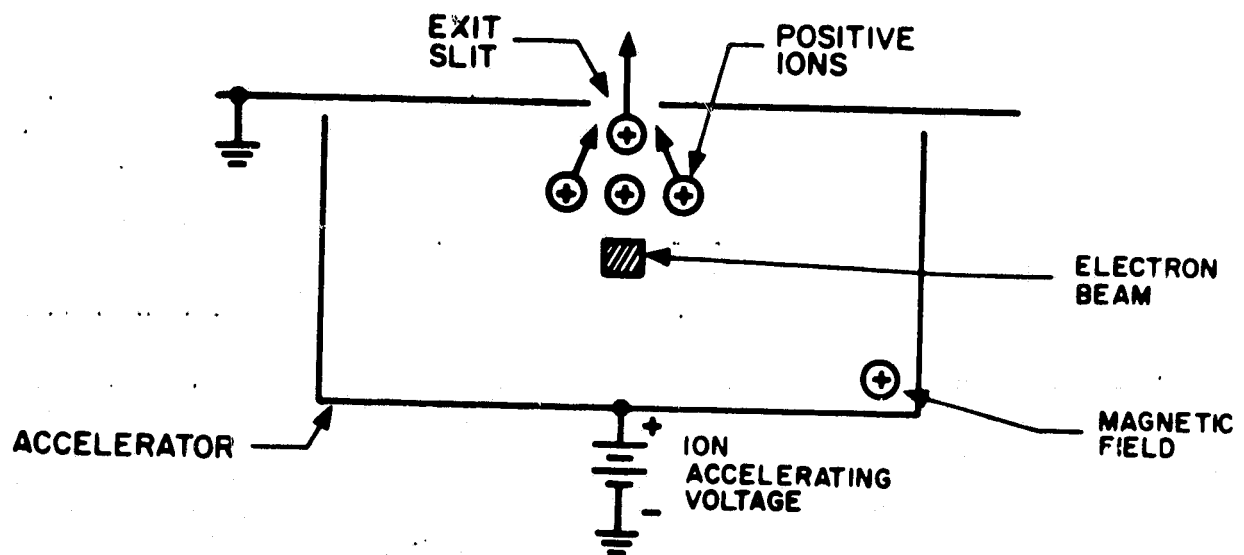


Figure D-3. Diatron Ionization Chamber

where they are struck by electrons and ionized. Along the top of the ionizing chamber (accelerator), and running parallel to the ionizing current beam, is the grounded exit slit. A potential difference called the ion accelerating voltage forces all positively charged ions from the positively charged ionizing chamber toward the slit. Some, having the proper direction of travel, will pass through the slit; while negative ions will be attracted to the accelerator wall and be eliminated.

A magnetic field is imposed on the positive ions and forces them to travel in a circular path with a radius, r , as expressed by the formula

$$r = \frac{K}{B} \sqrt{\frac{mV}{e}}$$

where r = radius of curvature
 K = units conversion constant
 B = magnetic field
 m = ion mass (amu)
 v = accelerator voltage
 e = charge of electron

Figure D-4 shows the paths of three different ions leaving the exit slit where mass 1 is greater than mass 2 which is greater than mass 3. The ions that were bunched together at the exit slit are now separated from each other.

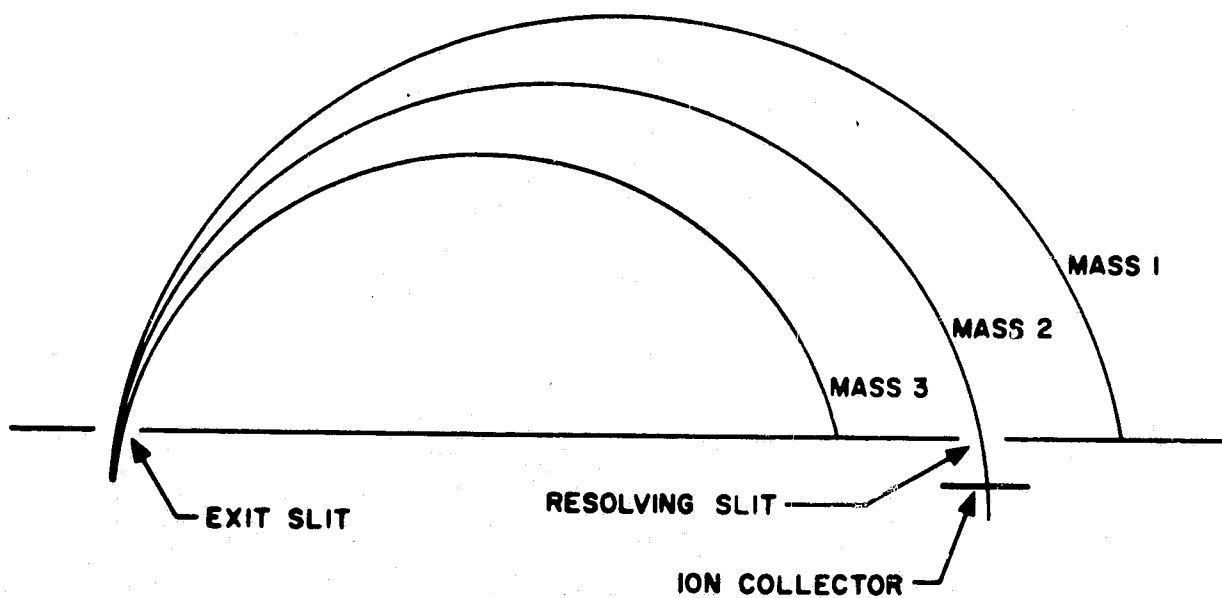


Figure D-4. Ion Paths from Exit Slit

The radius of curvature and magnetic field are both fixed in the leak detector. This leaves the only variable acceleration, which is a function of the accelerator voltage. As can be seen in Figure D-5, the

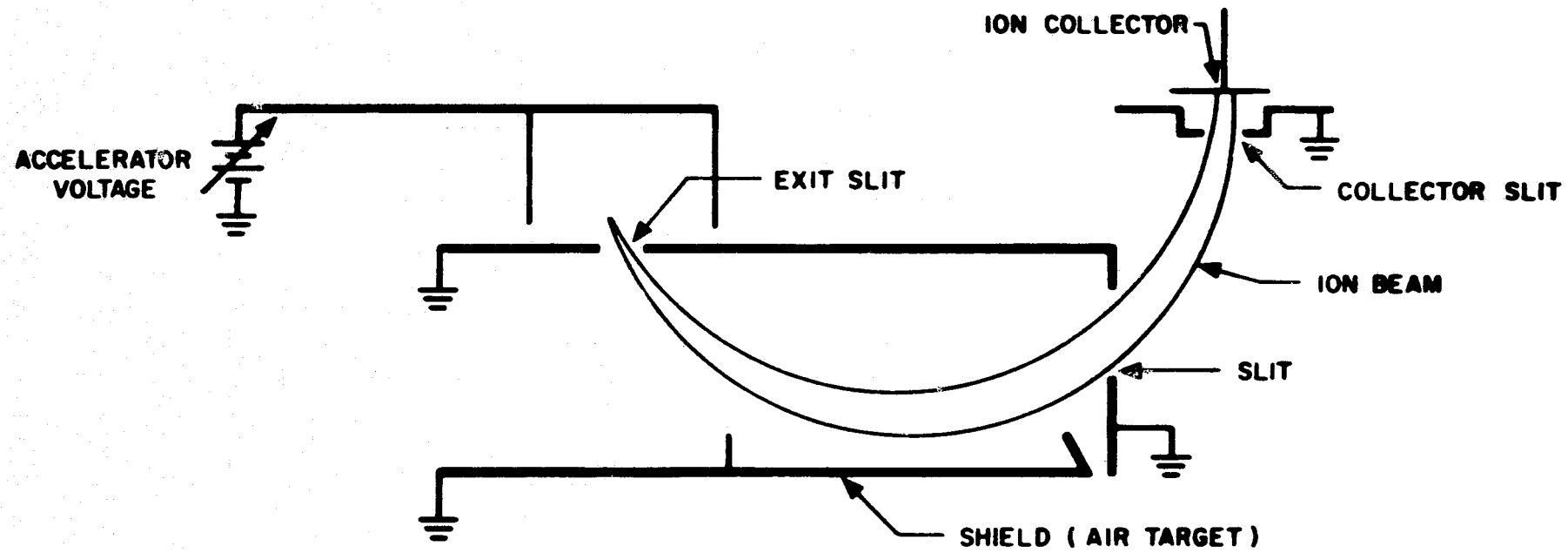


Figure D-5. Diatron Ion Path

ion collector had a grounded slit in front of it. This slit was wide enough to let ions through, but grounded out all others. Mass 1, mass 2, or mass 3 may be separately placed on the collector by adjusting the accelerator voltage. The relationship of the charge to mass registered on the collector to the accelerator voltage may more easily be seen by rewriting the formula given previously to read:

$$\frac{e}{m} = \frac{K^2 V}{B^2 r^2} = \frac{V}{K^1}$$

since B and r are fixed. The accelerator voltage can then be adjusted to collect only helium ions which have a specific value of e/m . The positive helium ions striking the collector are neutralized by a flow of electrons through the DC amplifier input resistor. Measurement of ion current is done by the amplifying system. The first stage of the amplifier is an electrometer tube which is sensitive to the minute (electron) current flow to the collector. This output is amplified by two stages that provide the additional gain necessary to operate the indicating meter.

In order to use the leak detector, it was first necessary to connect the instrument to the vacuum system by means of a flexible hose attached to a valve at the rear of the chamber. The leak detector system was then activated and evacuated. Helium was then sprayed in minute quantities at suspected locations using a small probe attached to a standard gas cylinder. Deflection of the leak detector indicating meter determined the location of the leak, which was then sealed with glyptol or vacuum grease.

Operation of the leak detector is more fully described in reference

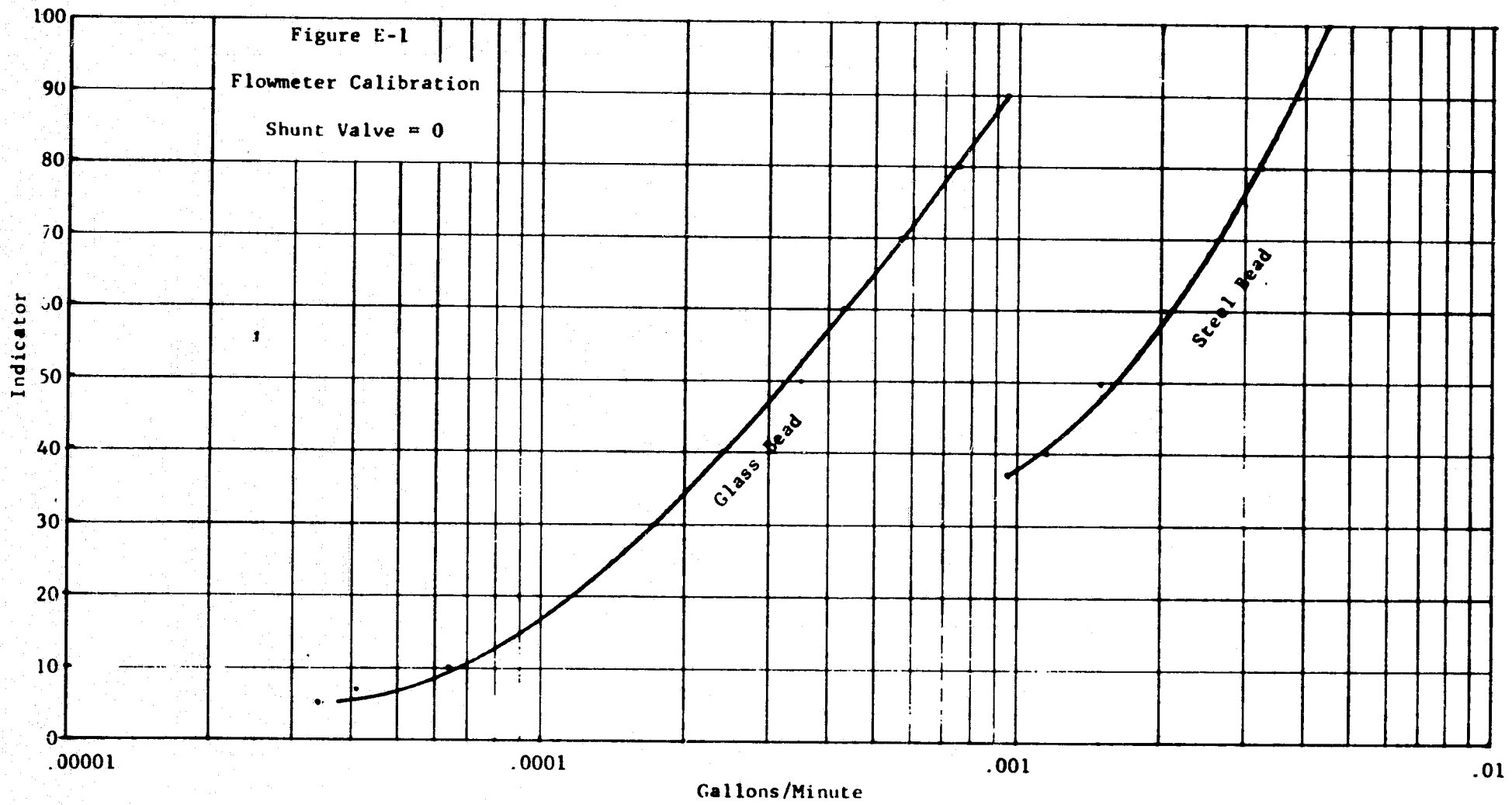
APPENDIX E

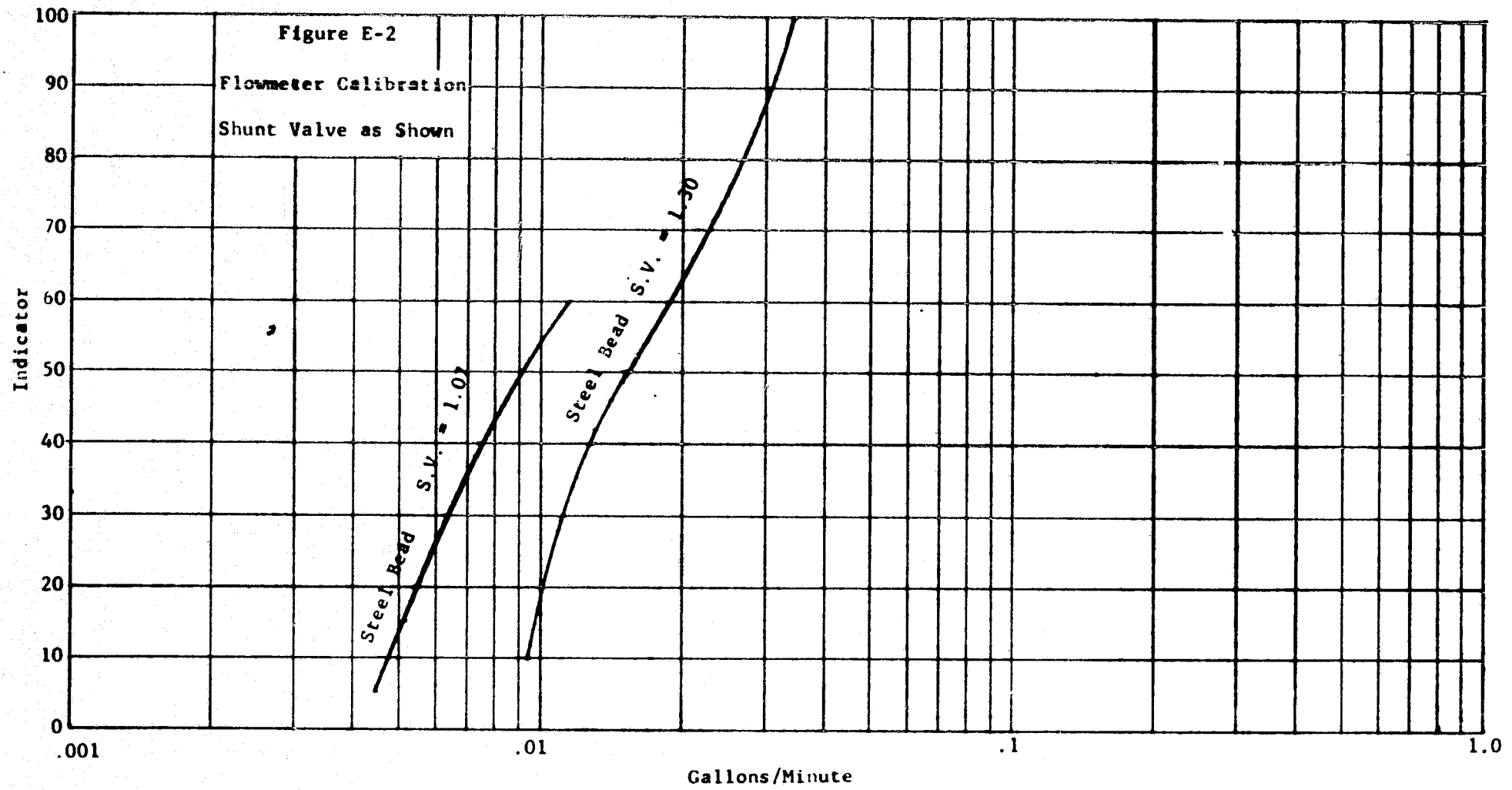
CALIBRATION OF FLOW METER AND BALANCE SCALE

Maintenance of a constant water flow rate within the tube was necessary for the system to achieve thermal equilibrium. A sensitive flow meter that spanned a range of 0.00004 GPM to 0.035 GPM was developed for this purpose from a dual-range, glass-tube rotameter which was originally used for measurement of gas flow. A pressure regulator on the unit's inlet was removed and a parallel or shunt path around the device was provided with a needle valve which had a micrometer indicator on its handle (Figures 10 and 21). The pressure at the flow meter was maintained by the pressure control system at 20.0 ± 0.05 psig with the aid of a Heise indicating pressure gage. The flow rate was regulated with the control valve located between the flowmeter and the collection system.

With the shunt valve closed, the rotameter could measure from 0.00004 GPM to 0.0045 GPM by means of the two indicating floats which were made of glass and steel. At the upper limit of this range the shunt valve was opened to allow water flow to bypass the rotameter and the float indicators to return to a lower value. The position of the micrometer handle was recorded, and the control valve was adjusted to cover the new range of the flow meter indicator.

The flow meter was calibrated with the water weighing technique as described in Chapter VII. Calibration curves for the device are presented in Figures E-1 and E-2 for the steel and glass indicators in the





rotameter. Shunt valve (S.V.) settings necessary for range extension are given in Figure E-2.

An earlier attempt at flow measurement using orifices calibrated as a function of pressure head was abandoned because of accumulated trash congestion within the microminiature openings in the orifices.

The shunted rotameter was used as a flow rate monitor because the repeatability of the device was not considered to be high enough to warrant its use as a primary determination of flow rate. Flow rate was determined for each data point by collection of the water during one minute, weighing it on a balance, and comparing the result with the previously calculated value given in Appendix C.

Ohaus Triple-Beam Balance Calculation

<u>Indicated Weight (grams)</u>	<u>True Weight (grams)</u>
0.0	0.0
1.0	1.0
2.0	2.0
3.0	3.0
4.0	4.0
5.0	5.0
6.0	6.0
10.0	10.0
20.0	20.0
30.0	30.0
50.0	50.0
70.0	70.0
100.0	100.0
200.0	200.0
300.0	300.0
500.0	500.0

Balance was checked with MTF Ohaus weight set No. NA2483, calibrated
August 10, 1970.

APPENDIX F

THERMOCOUPLE LEAD WIRE TEST

Initial tests on the 0.5-inch O.D. steel specimen indicated discontinuous results as well as marked differences in temperature between the top and bottom of the tube. Thermocouples 1 through 7 (Figure 2) indicated a substantially higher temperature than thermocouples 8 through 14; and thermocouples 7 and 8, which should have read the same value, indicated a large temperature difference. Using the heat gun, which forced air at a high temperature on the desired location, the problem was traced to the transition junctions and the thermocouple feedthroughs on the chamber wall. Further investigation revealed that the common tin-lead electrical solder used at the transition junctions and thermocouple feedthroughs introduced an undesired thermal EMF into the circuit when the junction is heated or cooled. It is believed that the electrical conductivity of constantan wire is less than the solder, thus introducing two thermocouple junctions in series with the two lengths of constantan wire. The copper wires were soldered with a low thermal EMF solder (Kirkson-703), and the constantan wires were spot welded to correct this problem.

In addition, it was found that thermocouple lead wire from a different spool had been used for thermocouples 1 through 7 than had been used for thermocouples 8 through 14. Although the two spools of lead wire were manufactured by the same company and had identical stock numbers, the dates of manufacture were different; thus indicating a difference in batch. A test using the heat gun on the transition junctions of

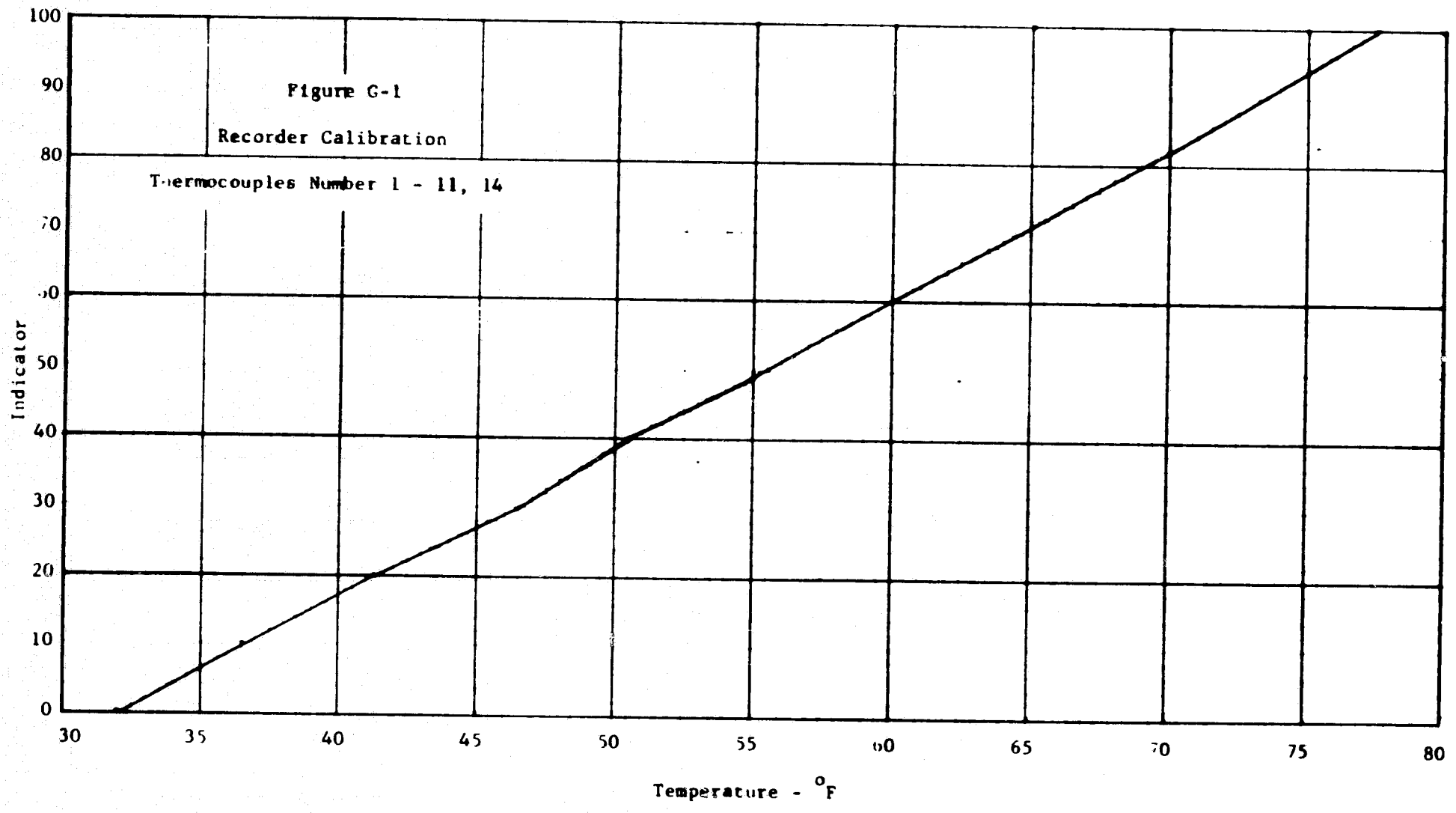
two identical thermocouples measuring the same temperature, but with the two different lead wires, showed the output from one thermocouple to increase while the other thermocouple's output decreased. As a solution, the lead wire for thermocouples 1 through 7 was changed to match that for thermocouples 8 through 14. A heat sink made of two large copper wires was also used to clamp the thermocouple transition junctions on the liner floor, thus insuring a constant and stable transition temperature.

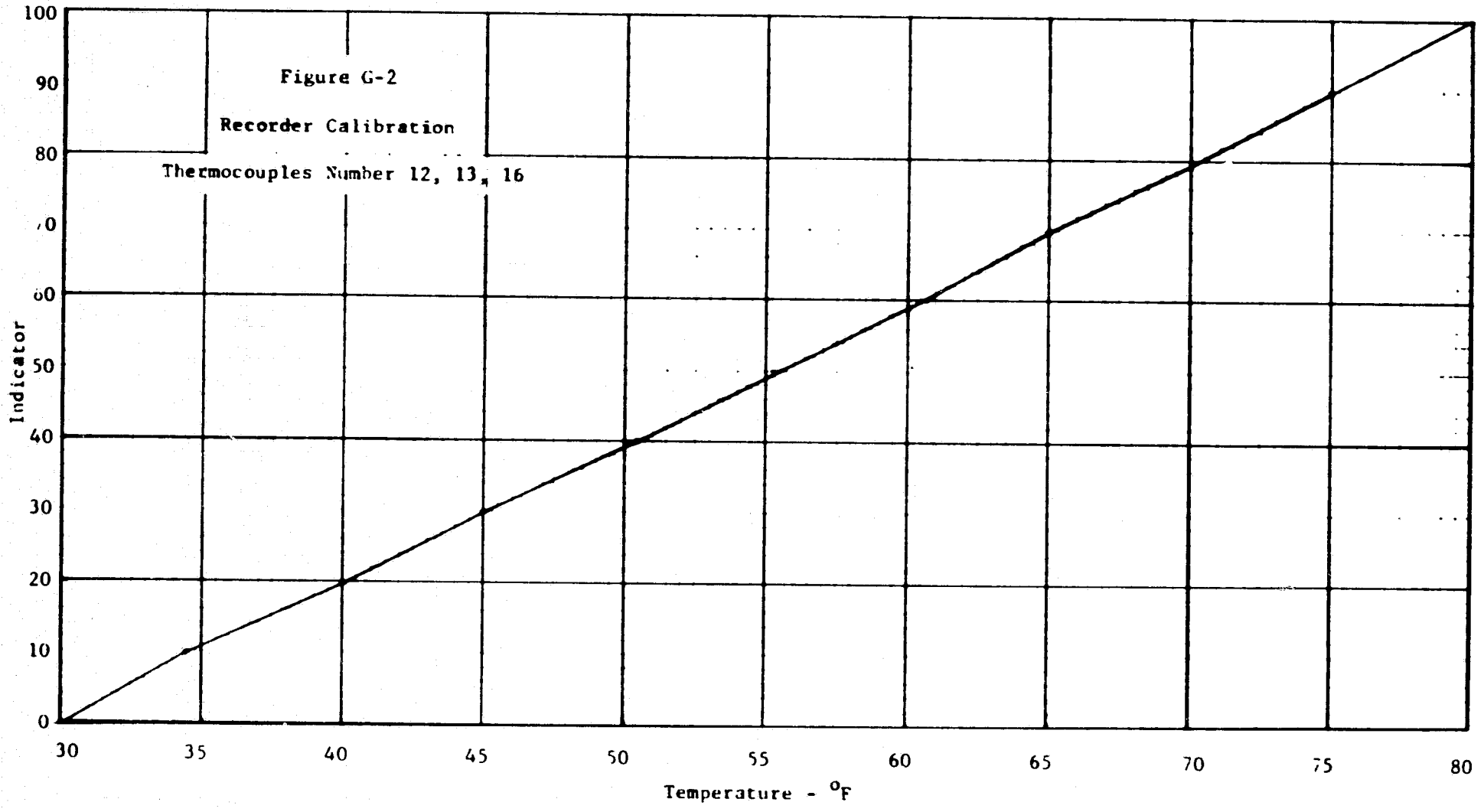
As a result of these solutions, the temperatures along the tube in an open chamber were constant within 0.5 F.

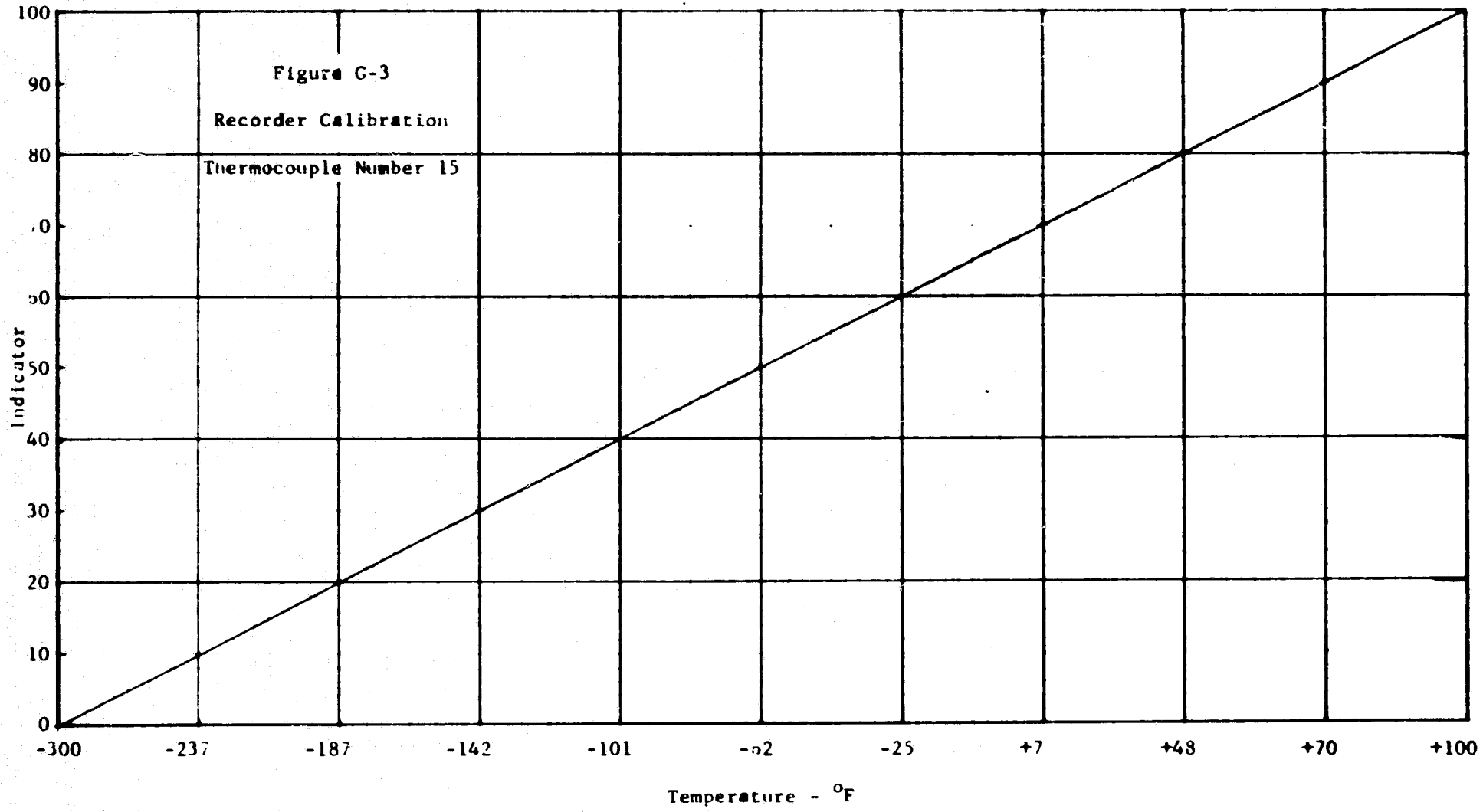
APPENDIX G

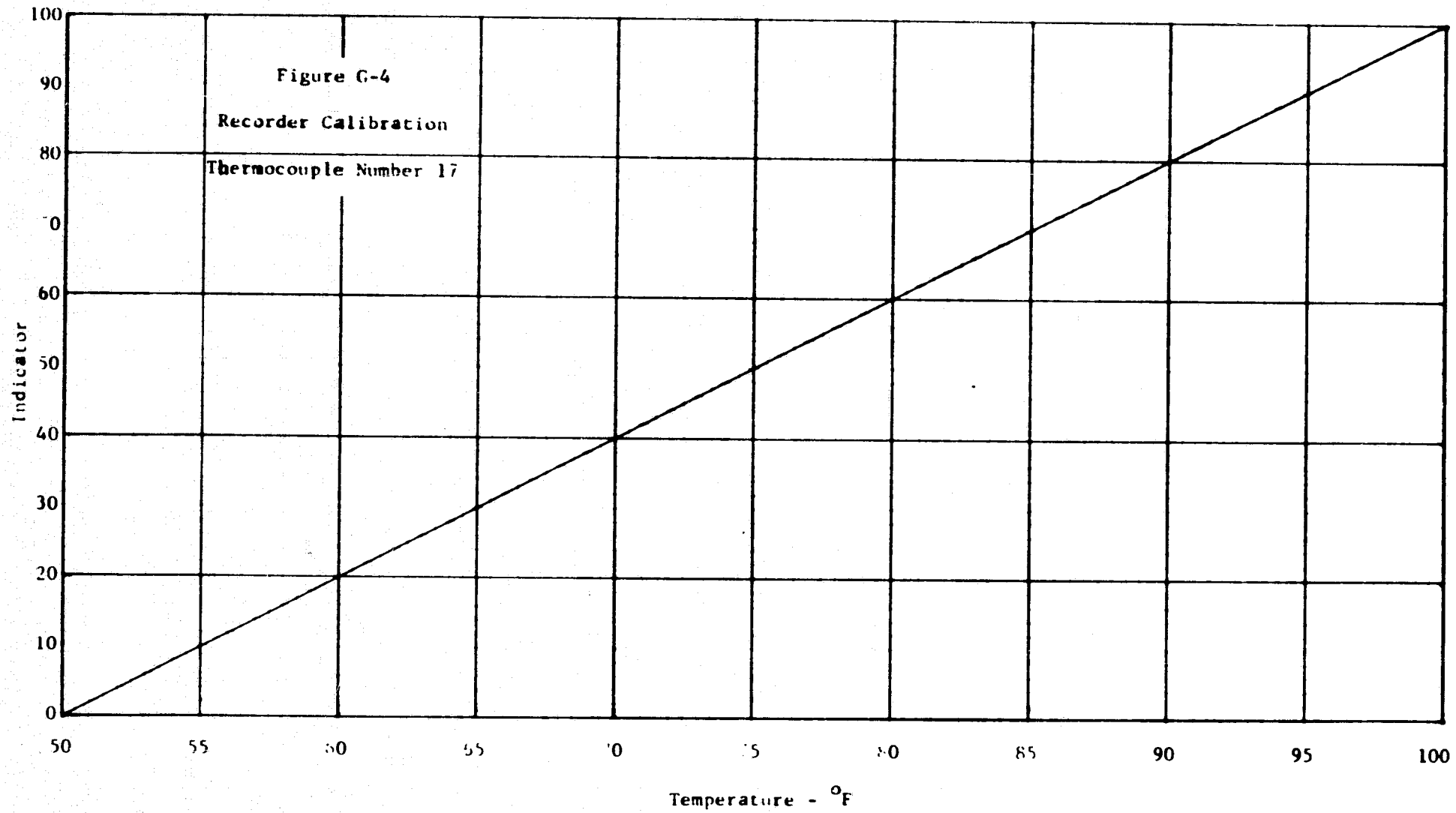
STRIP-CHART RECORDER CALIBRATION

The Leeds and Northrup multipoint, and the Bristol strip-chart recorders (Figures 15 and 16) were calibrated prior to each experiment with a Leeds and Northrup Type 8690 precision potentiometer. The calibration curves for the thermocouple recorders are given in Figures G-1, G-2, G-3, and G-4.









APPENDIX H

CONDUCTION ERROR TEST

Tests to determine the degree of thermal conduction in the two largest aluminum tubes were run. It was believed that these tubes, which have the highest thermal conductivity and cross-sectional area, would indicate the largest conduction error. The tubes were run in two conditions: ends connected and ends disconnected. No water was introduced so that energy input was only by conduction. The tubes were suspended within the chamber in their normal configuration and allowed to reach thermal equilibrium. Results of the tests are presented and are shown in Figure H-1.

TABLE H-1
EXPERIMENT SHEET

SPECIMEN: 3/4" & 1" Aluminum Tubes

DATE: SEE BELOW

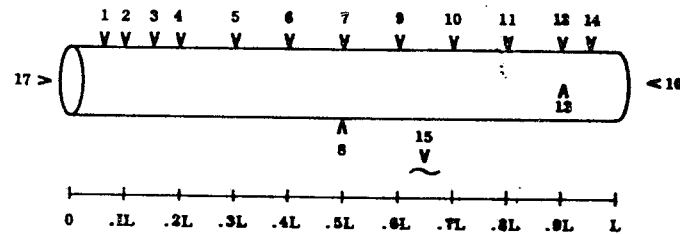
CONDUCTION ERROR TESTS

<u>RUN</u>	<u>DATE</u>	<u>TUBE</u>	<u>END CONDITION</u>	<u>VACUUM(μ)</u>
1	2/17/71	3/4"	Ends Connected	1×10^{-4}
2	2/18/71	3/4"	Ends Disconnected	2×10^{-4}
3	2/22/71	1"	Ends Disconnected	2×10^{-4}
4	2/23/71	1"	Ends Connected	2×10^{-4}

TABLE H-2

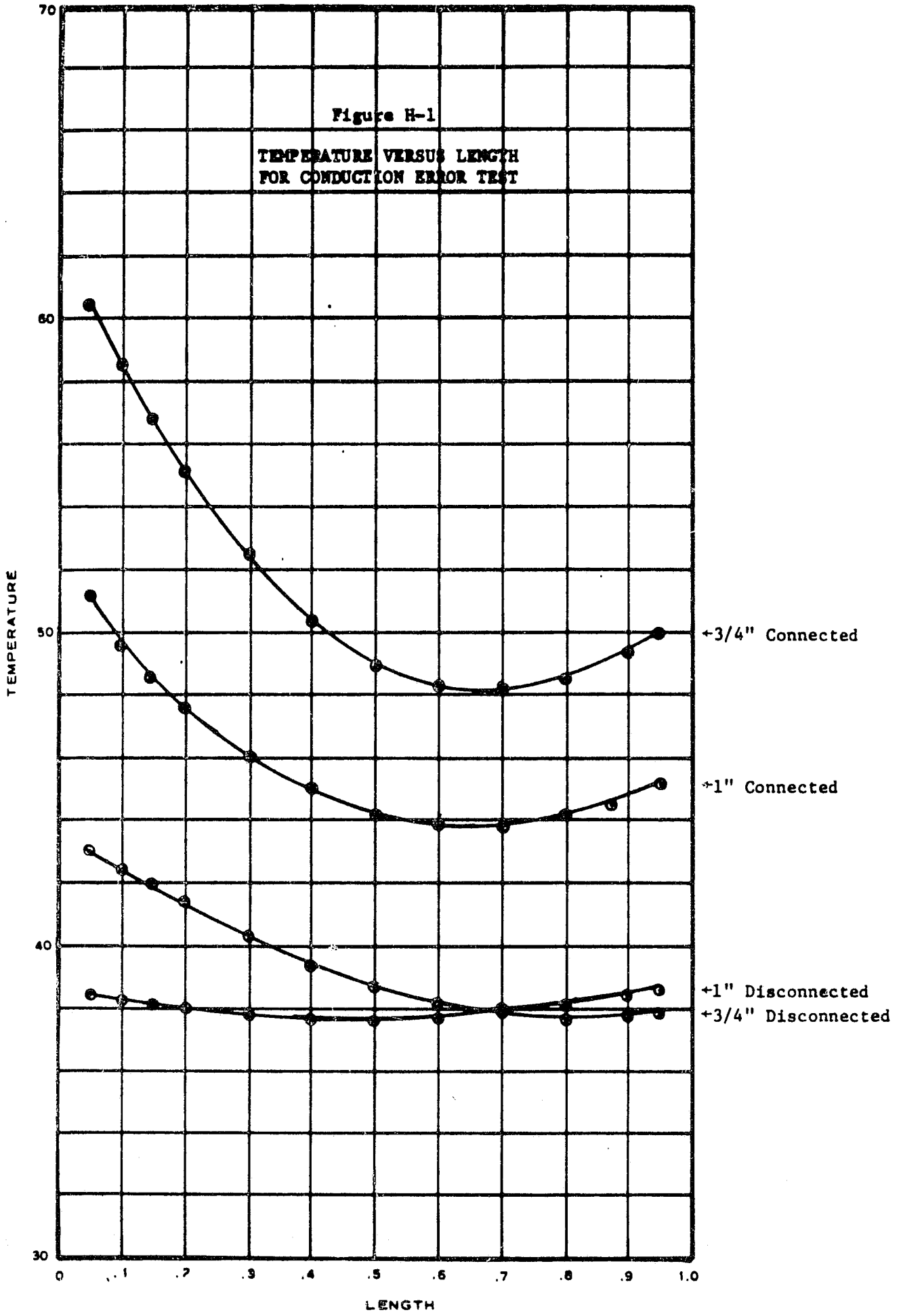
MEASURED TEMPERATURES AT DESIGNATED LOCATIONS

3/4" & 1" Aluminum Conduction Tests



ALL TEMPERATURES IN °F BELOW ZERO

RUN	SPECIMEN	1	2	3	4	5	6	7	8	9	10	11	14	15	END CONDITION
1	3/4"	97.5	107.0	116	124	137.5	148	155.5	155.5	158.5	159.5	157	150	305	Connected
2	3/4"	185	188	190	193	199	203	206.5	206.5	209	211	211.5	211	304	Disconnected
3	1"	208	209	209.5	210	211	212	212	212	211	210.5	209	207	304	Disconnected
4	1"	144	152	157	162	169.5	175	179	179	181	181	179	174	305	Connected



APPENDIX I
ERROR ANALYSIS

An analysis of possible errors during this investigation may be divided into two categories: (a) instrumentation and measurement errors which were, for the most part, low and random; and (b) experimental and equipment errors which were larger and systematic in nature. These two areas will be considered separately, and their effects will be added later. Random errors will be summed by a RSS (square root of the sum of the squares) technique and presented together with the algebraic sum of the systematic errors as the overall experimental error. Possible errors for which there is no supporting evidence will also be pointed out, but they will not be included in the final evaluation.

INSTRUMENTATION AND MEASURING SYSTEMS

Temperature Measuring System

Temperature measurement using copper-constantan thermocouples was considered to be accurate within ± 0.5 F over a span of 45 F, or a random error of $\pm 1.11\%$.

Flow Pressurization System

The flow pressurization was accurate to ± 0.1 psig, which is equivalent to a random error of $\pm 0.5\%$ at 20 psig.

Flow Measuring System

This system was considered to be sufficiently accurate to determine the Reynolds number within ± 1 , or a random error of $\pm 5\%$ at $RE = 20$.

Property Variation of Re with Temperature

Using equation (45), the change in Re with decreasing temperature is a systematic error of -3.85%.

Fluid Inlet Temperature

The inlet temperature of the fluid was held at 75 ± 0.5 F, which corresponded to a random error of ± 1.25%.

EXPERIMENTAL AND EQUIPMENT ERRORS

Thermocouple Wire and Support Losses

Losses from the thermocouple locations and ends of the tube due to heat conduction down the leads and the supporting strings may be estimated by considering the leads to be infinitely long pin fins with a known base temperature and radiation from the fin surface. The calculated systematic errors were less than -0.5%.

Conduction Error Through Tube Fittings

Conduction error through tube fittings for the 0.75-inch aluminum tube was a systematic -6.45% at $z = 0.7$, and increased somewhat toward the tube ends. Conduction error for the stainless steel tubes can be expected to be substantially less.

Liner Temperature Distribution

The liner temperature distribution as measured in Appendix J constituted a systematic error of + 2.5% for the 1.0-inch O.D. tube.

The preceding errors may be totaled by adding the systematic errors and computing a random error figure by RSS technique. The resulting

error was $-8.3 \pm 5.3\%$. It should be pointed out that this error does not include the possible effects of mixed flow (free and forced convection), or variations in the tube surface emittance due to handling.

APPENDIX J

LINER TEMPERATURE DISTRIBUTION

Cryogenic liner steady-state temperature distribution was determined by instrumenting the interior of the vacuum chamber and liner with thermocouples and allowing them to approach equilibrium conditions as the vacuum and cryogenic systems were in operation. The test specimen tube was removed, but the exit plumbing remained suspended within the chamber in its normal position.

Thermocouple locations can be determined from Figures J-1 and J-2. Figure J-1 denotes the sectional views shown in Figure J-2. Section A-A denotes the interior of the cryogenic liner, while section B-B shows the inside surfaces of the liner cover and door flange.

Fourteen 30-gage copper-constantan thermocouples were attached to the surfaces with a small piece of aluminum-backed adhesive tape. The installation was then spray-painted with 3M (101-C10) velvet black paint to provide a highly emissive surface. The interior surface of the aluminum door flange was not painted, thus corresponding to its normal state.

Sufficient steady-state conditions were achieved after approximately eight hours of operation. The vacuum was 1×10^{-4} torr and the temperature readings were:

<u>Thermocouple No.</u>	<u>Temperature (F)</u>
1	-266
2	-286
3	-262

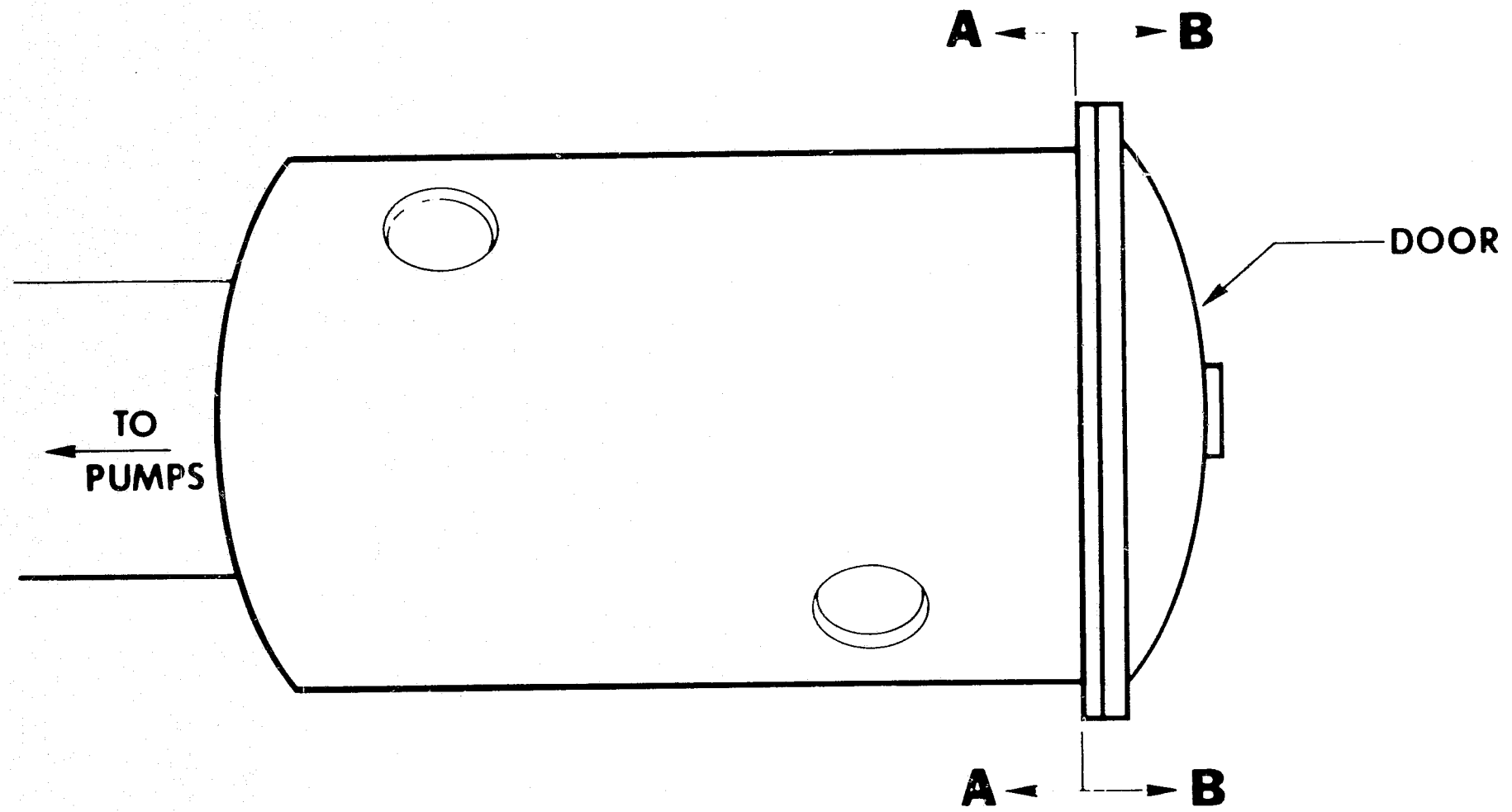


Figure J-1. Liner Section Key

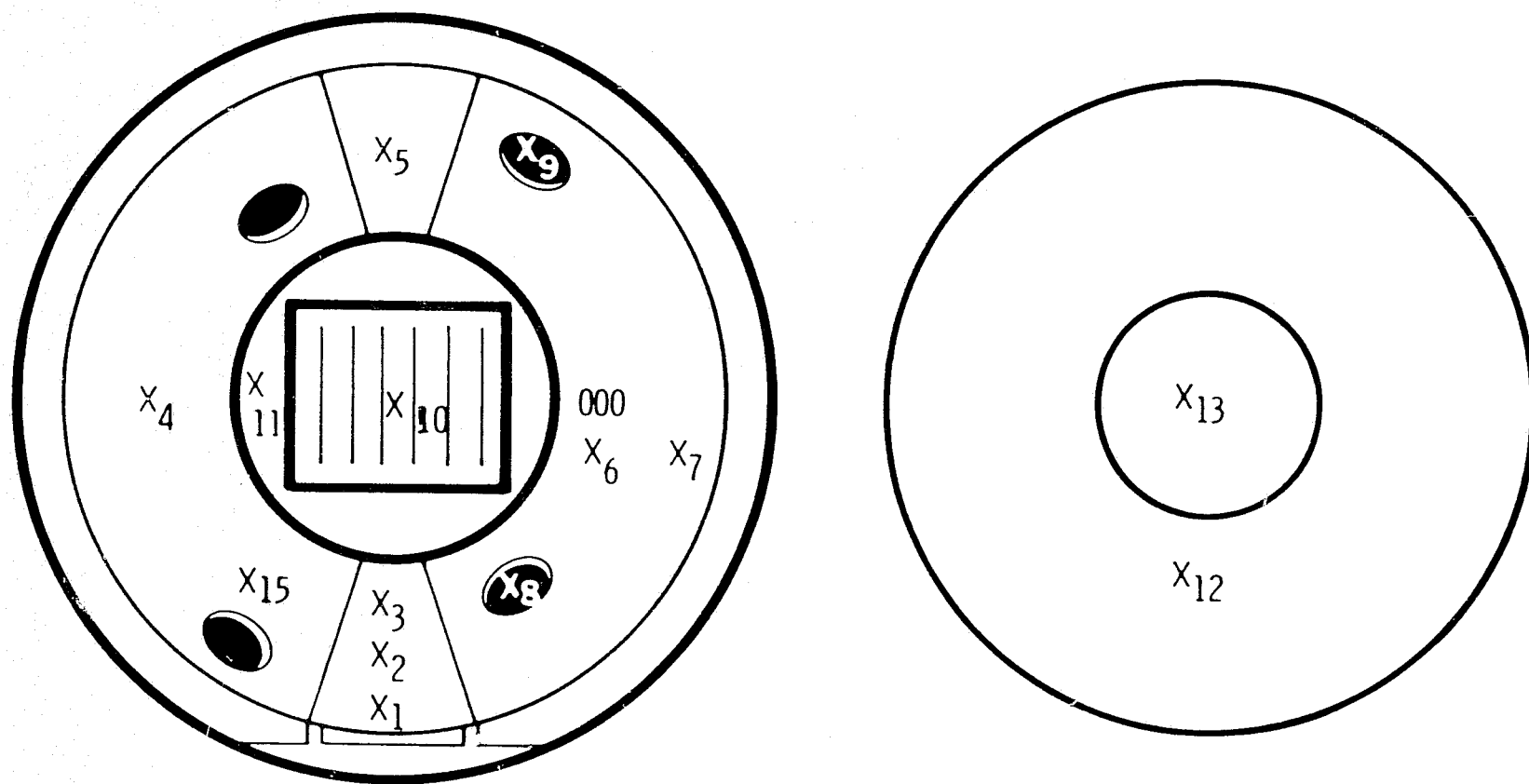


Figure J-2. Liner Temperature Distribution Layout

<u>Thermocouple No.</u>	<u>Temperature (F)</u>
4	-302
5	-298
6	-188
7	-293
8	+40
9	-204
10	-149
11	-254
12	-170
13	+54
14	+9
15	-303

VITA

David Payne Colvin

Candidate for the Degree of

Doctor of Philosophy

Dissertation: THERMAL SCALE MODELING OF A SPACECRAFT RADIATOR WITH
COUPLED FORCED CONVECTION - CONDUCTION - RADIATION
HEAT TRANSFER

Major Field: Mechanical Engineering

Biographical:

Personal Data:

the son of Thomas Henry and Eva B Colvin.

Education: Received the Bachelor of Science degree and Master of Science degree from Louisiana Tech University, with a major in Physics, in May, 1961 and August, 1962, respectively. Completed the requirements for the degree of Doctor of Philosophy in May, 1971.

Professional Experience: Employed by Gravier & Harper General Contractors in Alexandria, Louisiana as an Engineering Aide from June, 1959 to August, 1959. Employed by the Department of Physics at Louisiana Tech University as an Undergraduate Assistant from September, 1959 to May, 1960 and September, 1960 to May, 1961. Employed by Argonne National Laboratory as a Research Aide from June, 1960 to August, 1960 and June, 1961 to August, 1961. Employed by the Department of Physics at Louisiana Tech University as a Graduate Assistant from September, 1961 to August, 1962. Employed by the Saturn V Instrumentation Technology and Heat Transfer Analysis Departments at The Boeing Company in New Orleans as a Research and Design Engineer from September, 1962 to September, 1967. Employed by the Biocommunications Department of the Louisiana State University Medical School in New Orleans as a Research Engineer and Instructor from October, 1967 to August, 1969. Recipient of a National Defense Education Association Fellowship from September, 1969 to August, 1970. Recipient of a National Science Foundation Fellowship from September, 1970 to May, 1971. Employed by the Department of Engineering Research at Louisiana State University as a Research Assistant from June, 1970 to May, 1971.

Professional Organizations: Member of the American Society of Mechanical Engineers, the American Institute of Aeronautics and Astronautics, and Phi Kappa Phi.

Colvin, David Payne, B.S. Louisiana Tech University, 1961
M.S., Louisiana Tech University, 1962
Doctor of Philosophy, Spring Commencement, 1971
Major: Mechanical Engineering; Minor: Physics
Thermal Scale Modeling of a Spacecraft Radiator With Coupled Forced
Convection-Conduction-Radiation Heat Transfer
Dissertation directed by Dr. Dupree Maples
Pages in Dissertation, 225. Words in Abstract, 205.

A thermal model of a spacecraft radiator has been designed and tested at the National Aeronautics and Space Administration's Mississippi Test Facility. The unique feature of this model is that all three modes of heat transfer---forced convection, conduction, and radiation--are utilized simultaneously under steady-state conditions. A fluid is forced under pressure using similar flow conditions through both prototype and model which are suspended within a cryogenic vacuum chamber. Heat is transferred from the fluid to the tube's inside wall, which then conducts the energy to its outer surface where it is radiated to the surrounding shell that is maintained at a cryogenic temperature with liquid nitrogen. A high vacuum chamber at the facility is used to house the experiment. Both prototypes and models take the form of long tubes with thermocouples welded to the exterior surface to determine the effectiveness of the modeling criteria. Special precautions have been taken to isolate thermally the specimen and to establish a hydrodynamic boundary layer before specimen entry. The wall thickness of the models has been sized to permit both temperature and material preservation. The effects of physical size and fluid flow parameters on the modeling criteria for both low and high thermal conductivity materials are presented.